uOttawa

L'Université canadienne
Canada's university

FACULTÉ DES ÉTUDES SUPÉRIEURES ET POSTOCTORALES

uOttawa

L'Université canadienne
Canada's university

FACULTY OF GRADUATE AND POSDOCTORAL STUDIES

Adel Abdulmola Bugaldian
AUTEUR DE LA THÈSE / AUTHOR OF THESIS

Ph.D. (Civil Engineering)
GRADE / DEGREE

School of Information Technology and Engineering
FACULTÉ, ÉCOLE, DÉPARTEMENT / FACULTY, SCHOOL, DEPARTMENT

Performance of Reinforced Concrete Columns with Steel-Belted Tires as Transverse Reinforcement
TITRE DE LA THÈSE / TITLE OF THESIS

Murat Saatcioglu
DIRECTEUR (DIRECTRICE) DE LA THÈSE / THESIS SUPERVISOR

CO-DIRECTEUR (CO-DIRECTRICE) DE LA THÈSE / THESIS CO-SUPERVISOR

Burkan Isgor

Bruno Massicotte (École Polytechnique)

Nove Naumoksi

Dan Palermo

Gary W. Slater
Le Doyen de la Faculté des études supérieures et postdoctorales / Dean of the Faculty of Graduate and Postdoctoral Studies

Performance of Reinforced Concrete Columns with Steel-Belted Tires as Transverse Reinforcement

by

Adel Abdulmoula Bugaldian

A thesis Submitted to the Faculty of Graduate Studies and Research
In Partial Fulfillment of the Requirements for the Degree of

Doctorate of Philosophy
in
Civil Engineering*

Department of Civil Engineering
University of Ottawa
Ottawa, Canada
May 2009

*The Doctorate of Philosophy Program in Civil Engineering
Is a Joint Program with the Carleton University,
Administrated by the Ottawa-Carleton Institute for Civil Engineering

Your file Votre référence
ISBN: 978-0-494-65583-2
Our file Notre référence
ISBN: 978-0-494-65583-2

IN THE NAME OF GOD, THE BENEFICENT, THE MERCIFUL.

TO WHOM

WHO TAUGHT ME AND LOVED ME

TO MY MOTHER

AND

TO MY WIFE

WHO HAS ALWAYS BEEN BESIDE ME

Abstract

The majority of column failures observed during recent earthquakes were attributed to poor column behaviour caused by lack of inelastic deformability. The deformability of reinforced concrete columns can be improved through the confinement of potential plastic hinge regions by properly designed transverse reinforcement. The conventional reinforcement used for confinement consists of closely spaced perimeter hoops, overlapping hoops, cross-ties and circular spirals. One possible alternative for column confinement is to use steel-belted tires. Scrap automotive tires may provide an environmentally friendly alternative to conventional transverse reinforcement in circular concrete columns, especially for bridge and parking structures.

Steel-belted radial tires contain sufficiently high percentage of high-grade embedded steel that can be effective in confining column concrete. Tires can be assembled on top of each other, clamped by longitudinal reinforcement inserted through their sidewalls, and function as stay-in-place formwork. The same assembly can confine the compression concrete and provide shear resistance while also protecting the column against corrosion and chemical attacks. They also provide energy absorption under impact loads.

The effectiveness of steel–belted tires as transverse column reinforcement was investigated experimentally by testing six full size circular concrete columns encased in either 550 mm or 700 mm diameter tires. Columns were tested under constant axial compression and incrementally increasing lateral deformation reversals. The results indicate that reinforced concrete columns, cast in steel-belted radial tires perform favorably well into the inelastic range of deformations, exhibiting drift capacities of 4% to 8%, providing superior concrete confinement. The results also indicate that the concrete between the longitudinal reinforcement and tires are able to restrain the compression bars against buckling. The results further indicate that column flexural capacity can be computed through conventional plane-section analysis when appropriate concrete models are incorporated, accounting for concrete confinement and the presence of rubber sidewalls between the layers of

compression concrete. Moment-curvature relationships generated by such analysis can be used to construct the variation of curvatures along the column height. The curvature variation can be used to compute force-deformation relationships under monotonically increasing loads. These relationships are shown to provide very good agreement with experimentally recorded hysteretic relationships, further verifying the applicability of conventional techniques to tire-confined columns.

The experimental results provided invaluable information on the contribution of steel-belted radial tries to shear resistance while also providing knowledge on shear capacity of concrete enchased in tires. It is shown that the General Design Method for shear, specified in CSA A23.3-2004, can be employed to compute column shear capacity with a limit of 0.4% on transverse steel strains in tire rubber. A design approach is developed for reinforced concrete columns transversely reinforced with steel-belted tires. Design for flexure and shear under earthquake loads are illustrated.

Acknowledgments

First of all, thanks to Almighty God for giving me the opportunity, courage, strength and support to undertake this research. The author wishes to express his sincere appreciation and gratitude to his thesis supervisor, Dr. Murat Saatcioglu for his continued guidance, advice, encouragement, and stimulating discussions during the period in which this study was carried out. His inspiring ideas and positive feedback have been invaluable for the progress of this research.

Technical supports, suggestions and help received from Mr. Muslim Majeed during the constructions and testing of column specimens as the laboratory technician, are highly appreciated. Thanks are also extended to the technical staff of the Department of Civil Engineering and the Machine Shop at the University of Ottawa for their services and help during the experimental research.

My sincere appreciation and thanks are extended to my mother, my wife and my children for their patience, advice, support, encouragement and continuous prayers. Their patience, sacrifices, encouragements, supports and continuous prayers throughout the many years of this study deserve my deepest gratitude.

Many special thanks are extended to Derna University, Derna, Libya for awarding me the scholarship that enabled me to pursue a PhD degree.

I also wish to thanks my fellow graduate student friends for their valuable help during this research project.

Table of Contents

List of Tables

List of Figures

Notations

A_{st} = area of steel in tire tread

A_{sr} = area of steel in each rim of tire

A_v = area of shear reinforcement within a distance s

A_{vtr} = total area of transverse reinforcement embedded in tire

b_w = web width of a section

c = neutral axis depth

d = distance from extreme compression fiber to the centroid of tension reinforcement

D = diameter of column cross-section

d_b = nominal diameter of bar

D_r = diameter of the rim of a tire

D_t = diameter of column enclosed by tread ($D_t = D$ for columns cast in tires)

D_{st} = diameter of a steel wire in tread

D_{sr} = diameter of a steel wire in rim

d_v = effective shear depth, taken as the greater of $0.9d$ or $0.72h$

E_s = modulus of elasticity of steel

f_c' = specified compressive cylinder strength of concrete

f_{cc}' = specified compressive strength of confined concrete

f_{fr} = maximum stress in transverse FRP reinforcement

f_{cr}' = specified compressive strength of concrete with rubber layers

f_{co}' = in-place strength of unconfined concrete

f_ℓ = average lateral confinement pressure

$f_{\ell t}$ = uniform confinement pressure applied by the treaded segment of tire

$f_{\ell r}$ = uniform confinement pressure applied by the rims of a tire

$f_{\ell e}$ = equivalent uniform confinement pressure

f_{st} = stress in tread steel embedded in tire

f_{sr} = stress in rim steel embedded in tire

f_{str} = stress in steel embedded in tire

f_{yt} = specified yield strength of transverse reinforcement

f_{ytr} = yield strength of steel embedded in tire

f_y = yield strength of steel

h = cross-sectional diameter of column

K = coefficient that relates in-place unconfined and confined strength of concrete

k_1 = coefficient that relates confinement pressure to strength enhancement

ℓ_p = plastic hinge length

M_{cr} = cracking moment

M_n = nominal moment

M_u = ultimate moment capacity of a section

P = axial load applied to a column section

P_o = concentric capacity of an unconfined column

$P_{o,r}$ = concentric capacity of column with rubber sidewalls

s = width of the treaded portion of tire defining the spacing of transverse reinforcement

V_n = nominal shear stress resistance

V_c = shear stress resistance provided by concrete

V_s = shear stress resistance provided by shear reinforcement

V_r = shear stress resistance

V_{str} = shear stress resistance provided by steel-belted tires.

Δ = lateral displacement

ε_c = strain in concrete

ε_{cu} = ultimate axial strain in concrete

ε_{01} = axial strain corresponding to peak stress of unconfined concrete

ε_1 = axial strain corresponding to peak stress of confined concrete

ε_{085} = strain at 85% of peak unconfined stress

ε_{85} = strain at 85% of peak confined stress

δ = lateral drift ratio

λ = mass density factor

θ_t = total rotation

$\theta_{a.s}$ = rotation due to anchorage slip

θ_f = rotation due to flexure

ϕ = capacity reduction factor

ϕ_c = resistance factor for concrete

ϕ_s = resistance factor for reinforcement

ρ_{fv} = area ratio of transverse FRP reinforcement

ρ_t = percentage of steel in tread

ρ_r = percentage of steel in rim

ρ = area ratio of transverse steel

CHAPTER 1

INTRODUCTION

1.1 General

The majority of column failures observed during recent earthquakes were attributed to poor column behaviour caused by lack of inelastic deformability (Saatcioglu and Bruneau 1994, Mitchell et al. 1995, Saatcioglu et al. 2001). Lack of column ductility is a source of concern among structural engineers for seismic applications. It is therefore recommended to design columns to withstand cycles of inelastic deformations without a significant loss of strength. These deformations take place at the ends of columns where plastic hinges may form, creating critical areas which are sensitive to rapid degradation of strength. Ductility and energy absorption capacities of these critical regions are of paramount importance for seismic resistance of structures. Ductility is defined as the ability to deform beyond the elastic range of deformations without significant strength decay. This can be achieved through the confinement of compression concrete by properly designed transverse reinforcement. It is usually not possible to prevent yielding and plastic hinging of columns, especially at the first storey level. These regions are particularly susceptible to damage caused by the crushing of brittle concrete and hence require to be confined by transverse reinforcement for improved inelastic deformability.

Earthquake resistant reinforced concrete columns are typically confined by conventional hoops, overlapping hoops, FRP jackets, crossties and spirals. However, the required reinforcement often creates congestion of column cage, resulting in concrete placement problems. New and innovative approaches are always sought for column confinement to improve structural performance and ease of construction. An environmentally friendly alternative to conventional transverse reinforcement for circular columns may be the use of scrap tires, when suitable for a specific application. The use of steel belted tires may offer

the required properties for concrete confinement, though at first it is not obvious. The first attempt to explore this possibility was made by Bugaldian and Saatcioglu (2008). Their experimental research demonstrated that tires can be used as column confinement reinforcement in flexure dominant columns. However, more research is needed to ensure the development of design procedures, not only for column confinement but also for shear, since shear resistance is another important aspect of transverse reinforcement in columns. The current research project is devoted to this topic, with the objective of generating more data on the use of automobile tires as column transverse reinforcement for both concrete confinement and shear resistance.

1.2 Research Objectives

The primary objective of the current research program is to generate experimental and analytical data on performance of circular columns reinforced with steel belted radial automobile tires as column transverse reinforcement. The objective also includes the development of design procedures for confinement and shear resistance of such columns.

1.3 Scope of Research

The research program consists of experimental and analytical investigations, and includes the following scope:

- Review of previous research on column confinement under simulated seismic loading.
- Design and assembly of an experimental set-up suitable for testing full scale columns under constant axial compression and incrementally increasing lateral deformation reversals.
- Design, construction and instrumentation of six full-scale circular columns with conventional longitudinal reinforcement and steel-belted radial tires as transverse reinforcement.

- Testing of six columns under combined axial compression and incrementally increasing lateral deformation reversals, while recording the relevant test data by means of two data acquisition systems.
- Evaluation of test data and investigation of the effects of test parameters that consist of; cross-sectional dimension (tire sizes), splicing of longitudinal bars, level of axial load, and column height (shear span).
- Development of analytical models for stress-strain relationships for concrete with embedded tire layers, as well as core concrete confined with radial tires.
- Analytical predictions of column behaviour and computation of inelastic force-displacement relationships for comparison with experimental results.
- Generation of design guidelines for circular columns confined with scrap tires.
- Preparation of thesis and presentation of results.

1.4 Previous Research on Column Confinement

Confinement of reinforced concrete columns with scrap tires is a new concept with no previously reported research in the literature, with the exception of the results of an earlier phase of the proposed investigation by the author (Bugaldian and Saatcioglu 2008). The research reported in the literature on scrap tires as reinforcement material is limited to geotechnical engineering applications. Some research has been conducted on transportation applications involving tire chips as replacement for aggregates in pavements. There is no data available on structural engineering applications with the exception of research involving tire chips in concrete (Eldin and Senouci 1993). Therefore, the literature review presented in this section consists of previous research on column confinement by conventional steel reinforcement, transverse prestressing and column wrapping by fiber reinforced polymers (FRP).

The pioneering work on concrete confinement was conducted by Richart et al. (1928). The researchers tested specimens subjected to different levels of hydrostatic pressure. The results helped establish basic parameters of concrete confinement by transverse reinforcement. They established a relationship between lateral confinement pressure and strength enhancement.

The researchers subsequently tested a large number of concrete cylinders confined by spiral reinforcement (Richart et al. 1929). Their research led to the development of concrete confinement requirements in the American Concrete Institute, ACI 318 Building Code, which have been used up till today (ACI-38 2008). Balmer (1949); and Sato and Ibushi (1988) also generated data that shed light on the relationship between lateral confinement pressure and concrete strength enhancement due to confinement.

Additional pioneering research on concrete confinement was conducted by Chan (1955), Roy and Sozen (1964), and Kent and Park (1971). These researchers conducted experimental investigations to study the behaviour of concrete confined by transverse reinforcement. They proposed analytical models to describe stress-strain relationships for confined concrete. The main variables considered in these investigations were the spacing and amount of lateral reinforcement, strength, cross-sectional size and shape, and the rate of loading. Before 1975, researchers did not consider the distribution of longitudinal reinforcement and the tie arrangement as confinement parameter (Bresler and Gilbert 1961, Pfister 1964, Hudson 1966, Somes 1970, Burdette and Hilsdorf 1971).

Sheikh and Uzumeri were the first to demonstrate the effectiveness of closely spaced longitudinal reinforcement on concrete confinement. They tested twenty-four tied columns under monotonic axial compression at the University of Toronto (Sheikh and Uzumeri 1980). The specimens had a square cross-section, with 305 mm sectional dimension and 1960 mm high. Column reinforcement included four different tie configurations and eight to sixteen longitudinal bars. The main variables considered in this investigation were tie arrangement, volumetric ratio, spacing and characteristics of lateral steel, and distribution and amount of longitudinal steel around the core perimeter. From this investigation, it was concluded that;

- Strength and ductility were improved by increasing the amount of lateral steel.
- The amount of longitudinal steel, within the range of 1.7% to 3.7%, had small effect on concrete confinement.

- The strength of concrete increased up to 70%, and significant improvement in ductility was observed when concrete was confined with rectangular ties and well distributed longitudinal steel.
- Enhancement of strength and ductility was observed when tie spacing was reduced, even if the same volumetric ratio was used.

Scott, Park and Priestley (1982) tested twenty-five square columns under high and low strain rates at the University of Canterbury in New Zealand. The cross-sectional dimension was 450 mm and the column height was 1200 mm. Each column contained either eight or twelve longitudinal steel bars and different arrangements of square or octagonal steel hoops. The variables considered included the effect of longitudinal steel distribution on enhancement of concrete strength and ductility. The following conclusions were reported from this investigation:

- By increasing the spacing of lateral reinforcement, the confinement efficiency decreased in columns with the same amount of lateral reinforcement.
- Concrete showed significant improvement in compressive strength by proper confinement.
- Increasing the number of longitudinal reinforcing bars while maintaining a constant longitudinal reinforcement area showed good improvement in confinement. This was shown by reducing the longitudinal bar spacing.
- By increasing the amount of lateral reinforcement, the peak stress for concrete core increased and the slope of falling branch of the stress-strain relationship for concrete core decreased.

Mugumura, Watanabe, Iwashimizu, and Mitsueda (1983) tested eighteen square columns with concrete strength ranging between 34 MPa and 89 MPa. The specimens had a 147 mm square cross section, 400 mm height, and no longitudinal reinforcement. Fourteen columns were laterally reinforced with circular spirals, having 50 mm spacing and 1390 MPa yield strength. Two columns had a volumetric transverse reinforcement ratio of 4.26%, and the remaining specimens had 2.13%. The main variables considered in this investigation were concrete strength and volumetric ratio of lateral reinforcement. It was concluded that the

ductility of high-strength concrete (HSC) could be significantly improved by using sufficient amounts of confinement reinforcement, having high yield strength. The researches used the same stress-strain relationship originally proposed by them for normal–strength concrete, with some modifications based on this study.

Fafitis and Shah (1985) developed simple equations to predict the stress-strain relationship of confined concrete for circular columns. By using these equations they compared the predicted behaviour of confined columns with the available experimental data. Distribution of longitudinal steel, tie spacing and tie configuration were not included in their equation.

Basset and Uzumeri (1986) conducted an experimental investigation on fifteen reinforced and three unreinforced square columns to determine the behaviour of confined high-strength light-weight aggregate concrete (HSLWAC). The concrete strength varied between 37 MPa and 40 MPa and the yield strength of the steel ties ranged between 530 MPa and 600 MPa. The specimens had a cross-sectional core dimension of 305 mm and a height of 1956 mm. They were tested under monotonically increasing axial compression. The researchers concluded that the ductility of columns improved with the increased amount of longitudinal reinforcement and the brittle behaviour of HSC columns improved by using a large amount of transverse reinforcement with well distributed longitudinal reinforcement. It was also reported in this investigation that the existing concrete confinement models gave unconservative results for HSLWAC, overestimating column ductility.

Ozcebe and Saatcioglu (1987, 1989) tested sixteen full size columns with different confinement configurations under constant axial compression and incrementally increasing lateral deformation reversals. All the columns were tested under 600 kN of constant compressive axial load. The specimens had 350 mm square cross sections and 900 mm height. The main variables considered in this investigation were the effectiveness of arrangement, spacing and volumetric ratio of transverse reinforcement. It was concluded that inelastic response of columns improved very significantly by proper confinement of core concrete. Crossties supporting the longitudinal bars had high efficiency in providing confinement only if they were properly supported by lateral reinforcement.

Mander, Priestley and Park (1988) tested thirty-one circular, rectangular and square columns with different arrangements of reinforcement under low and high strain rates with different volumetric ratios and spacing of confinement reinforcement. It was observed that the concrete strength increased due to the increase in the volumetric ratio of confinement reinforcement.

Razvi and Saatcioglu (1989) tested thirty-four small scale columns confined with different combinations of welded-wire fabric as confinement reinforcement under monotonic axial compression. The results of this investigation showed a significant improvement in strength and ductility of columns. This indicated that welded-wire fabric could be effective in confining the core concrete.

Rangan, Saunders, and Seng (1991) did an experimental investigation to study the effects of the amount and type of transverse reinforcement. Sixteen small scale HSC columns with a compressive strength of 65 MPa were tested under concentric and eccentric loadings. Ten columns had a cross sectional dimension of 160 mm and a height of 800 mm. They were tested under concentric loading. The rest of the columns were slender columns with 100 x 100 x 2000 mm dimensions, and were tested under eccentric loading. They concluded that the confinement reinforcement did not have any significant effect on load-strain curves, even though yielding and rupturing of confinement reinforcement were observed. This could be attributed to the low amount of confinement reinforcement used in this investigation.

Saatcioglu and Razvi (1992) developed an analytical model for confined concrete. The model was compared with different shapes of cross sections and different confinement configurations (spirals, cross ties, welded wire fabric, and rectilinear hoops). This model produces good predictions of concrete behaviour under concentric and eccentric loadings, as well as slow and fast strain rates.

Itakura and Yagenji (1992) tested 24 HSC square columns. The cross sectional dimension of the columns was 218 mm and the height was 500 mm. The specimens had no concrete cover.

The concrete strength was 74 MPa. The test variables included longitudinal reinforcement; and the configuration, amount, and hook length of confinement reinforcement. Test results showed that the concrete strength was enhanced greatly by the confinement steel. Ties with 10-bar diameter hooks were more effective than those with a hook length of 6 bar diameter.

Sheikh and Khoury (1993) tested six square columns under cyclic lateral loading, accompanied by simultaneously applied axial compression. The cross-sectional dimension was 305 mm, and the column height was 1473 mm. The columns were cast integrally with a stub. The main variables in this investigation were the level of axial load, amount of lateral steel, configurations of lateral steel, and the stub effect. The researchers concluded that the increase in the amount of lateral steel, the effectiveness of confinement reinforcement, and reduction in axial load, increased the ductility and energy-absorbing capacity of the columns. It was also observed that the stub effect was to enhance the strength of the adjacent section by 20%.

Sheikh, Shah, and Khoury (1994) tested four square HSC columns with a cross-sectional dimension of 305 mm and a height of 2.3 m under axial compression and cyclic displacements to simulate seismic loading. The main test variable was the volumetric ratio of the transverse steel which ranged from 1.7% to 4.3%. The columns were tested under different levels of axial load, ranging from 59% to 63% of their concentric capacity. The test results were compared with those for normal strength concrete columns. The comparison indicated that the required amount of confinement reinforcement was proportional to concrete strength.

The mechanism of concrete confinement was discussed by Razvi (1995). The researcher explained that lateral reinforcement reduces the internal cracking associated with lateral expansion of concrete under axial compression. The main variables affecting concrete confinement include spacing of confinement reinforcement, concrete strength and type, percentage and distribution of longitudinal reinforcement, tie arrangement, rate of loading, level of axial compression, size and section geometry, and the volumetric ratio or ratio of lateral steel volume to the volume of concrete core.

Baingo and Saatcioglu (1995) conducted an experimental investigation on nine high-strength concrete circular columns to evaluate deformability of confined HSC columns. The columns had 250 mm circular cross-section and 1640 mm column height. The columns were tested under constant axial compression and incrementally increasing lateral deformation reversals. The columns had two different concrete strengths of 90 MPa and 60 MPa. They were tested under different levels of axial load compression, ranging between 22% and 43% of their concentric capacity. The transverse reinforcement used in this investigation were either circular hoops or circular spirals with a volumetric ratio ranging between 1.59% and 3.67% and a yield strength ranging between 400 MPa and 1000 MPa. The test variables included concrete strength, concrete cover, axial load level, yield strength, volumetric ratio and spacing of transverse reinforcement. Test results showed superior performance of columns confined with high-strength transverse reinforcement compared with those confined with normal-strength reinforcement. The beneficial effects of high-strength transverse steel were more obvious for columns subjected to high axial load level. The results also indicated that the concrete cover did not affect the deformability of the test columns.

Razvi and Saatcioglu (1996) tested 26 square and 20 circular HSC columns to determine the effect of test parameters on circular and square columns. Test variables were concrete strength; cross-sectional dimension; longitudinal reinforcement arrangement; and volumetric ratio, spacing, and yield strength of transverse reinforcement. The columns had a cross-sectional dimension of 250 mm and a height of 1500 mm. The concrete strength ranged between 60MPa and 124 MPa. The yield strength of transverse reinforcement ranged between 400 MPa and 1000 MPa and the volumetric ratio ranged 0.41% to 4.59% with a transverse reinforcement spacing of 40mm to 135mm. All specimens used in this investigation were tested under monotonically increasing concentric compression. They concluded that high confinement pressure could be provided either by increasing the volumetric ratio of transverse reinforcement and/or by using high-strength transverse reinforcement. Longitudinal reinforcement in circular sections had an effect on concrete confinement. Confined HSC columns with closely spaced transverse reinforcement exhibited early spalling of cover concrete. The test results also indicated that HSC columns behave in an extremely brittle manner under monotonically increasing concentric compression.

Grira and Saatcioglu (1996) conducted an experimental investigation to study the structural performance of concrete columns reinforced with welded grids. They tested ten large scale columns under simulated seismic loading. The main variables considered in this investigation were volumetric ratio, spacing and arrangement of welded reinforcement grids. From this investigation, it was concluded that:

- Columns confined with reinforcement grids showed ductile response, developing lateral drifts equal to or greater than those expected in columns confined with conventional ties of equal volumetric ratio.
- Welded reinforcement grids can be used effectively as confinement reinforcement.
- The transverse reinforcement employed had 7% to 10% strain elongation prior to failure.
- The grids improved structural performance of columns which developed lateral drift ratios in excess of 3% with transverse reinforcements less than or approximately equal to that required by the AC1 318-95 Building Code.
- The drift capacity increased when grids with smaller cells were used.
- The cage assembly became easier and faster as compared to columns with conventional tie reinforcement.

The use of transverse prestressing as column confinement reinforcement was suggested by Saatcioglu and Yalcin (2003). The researchers tested shear-deficient square and circular columns, prestressed in the transverse direction. The prestressing provided active lateral pressure, not only prevented shear failures, but also confined compression concrete, increasing column deformability very significantly. Mes and Saatcioglu (1999) tested six flexure dominant, large-scale columns under constant axial compression and incrementally increasing lateral load reversals. Four of them were circular with a diameter of 508 mm and two short columns with a diameter of 610 mm. The remaining two were square with a cross-sectional dimension of 500 mm. Twelve No. 20 longitudinal bars were used for longitudinal reinforcement. The transverse reinforcement for the circular columns consisted of No. 10 hoops at different spacing. All columns were retrofitted with the same prestressing strands used by Yalcin (1997). The results showed that transverse prestressing could improve column deformability in excess of 4% lateral drift ratio.

Bugaldian (1999) conducted an experimental investigation to explore the possibility of using steel-belted-radial tires for column confinement. The investigation included six full-scale circular columns confined with scrap tires and tested under simulated seismic loading. Three different arrangements of tires and two different levels of axial load were used as test variables. The results indicated that the columns behaved in a ductile manner, developing lateral drifts comparable to those expected in conventionally confined columns. It was concluded that steel-belted tires could be used effectively to confine concrete in reinforced concrete columns thus leading to potentially significant reductions in tire waste and its negative impact on the environment, as well as construction cost.

Liu, Foster, and Attard (2000) tested twelve circular columns with 250 mm cross-section and eight number 12 mm longitudinal reinforcement bars under concentric compression. The concrete strength ranged between 60 MPa and 96 MPa. The purpose of the experimental program was to investigate the ultimate strength and ductility of high strength concrete circular columns confined with steel ties and spirals. The effect of concrete cover on concrete strength was also studied. The main test variables were concrete strength, the diameter and spacing of the tie and spiral reinforcement, and concrete cover. From the results of this investigation, it was concluded that the capacity of columns increases with an increase in effective confinement stress for well confined high strength concrete columns with covers of 0 to 15 mm. For specimens with 25 mm cover, the highest load was carried by the specimen with the lowest quantity of confining reinforcement steel. Also the results indicated that the first peak load can be taken 0.85 times the capacity of the concrete section based on in-place strength of concrete plus the capacity of longitudinal reinforcement.

Xiao and Yun (2002) carried out an experimental investigation on six full-scale square HSC columns with concrete strengths ranging between 62.1 MPa and 64.1 MPa. The column cross-section was square with a sectional dimension of 510 mm. The column height was 1778 mm. They were confined with conventional ties at a vertical spacing of 100 mm to 150 mm, and yield strength of 445 MPa and 525 MPa. The specimens were tested under constant axial compression and incremental increasing lateral deformation reversal. The level of axial load used was 20% to 34% of concentric capacity. The test variables were the level of axial

load; and volumetric ratio, yield strength and spacing of transverse reinforcement. The researchers concluded that columns under a low axial load of 20% of concentric capacity with a transverse reinforcement ratio of higher than 82% of that required by ACI 318 Building Code (2002) showed a ductile behaviour of 6% lateral drift and higher. On the other hand, columns which were tested under higher axial load of 30% of concentric capacity showed a lower drift ratio of 3%. However, the column behaviour improved for columns confined with high-strength transverse reinforcement.

Tan and Nguyen (2005) conducted an experimental investigation on 30 plain and reinforced concrete columns with a 200 mm square cross-section to investigate the effects of confinement on flexural capacity of high strength concrete and the applicability of the rectangular stress block recommended by the ACI code to high strength concrete sections. The specimens had different volumetric ratios of transverse reinforcement ranging between 0.7% and 2.4%, and different concrete strengths varying between 46 MPa and 101 MPa. The columns were tested under either concentric or eccentric compression. The main test variables considered in this investigation were the amount and the arrangement of transverse reinforcement, the eccentricity of axial load, and concrete compressive strength. The test results indicated that the flexural strength and ductility of improved by confinement. They also found that the confinement of HSC columns can be enhanced by using high-strength reinforcement rather than using normal-strength reinforcement. The researcher proposed a new set of rectangular stress block parameters.

Ozbakkaloglu and Saatcioglu (2006) did a comprehensive experimental investigation on circular stay-in-place FRP formwork for high-strength and normal strength concrete columns. The researchers also developed a displacement based design approach for normal and high-strength concrete columns encased in FRP stay-in-place formwork. They tested circular columns with concrete strengths ranging between 50 and 90 MPa, cast in carbon FRP tubes. The columns had a 270 mm circular cross section and either a 2.0 or 1.2 m cantilever length. The test results showed that the inelastic deformability of high-strength and normal strength concrete columns can be improved significantly by using FRP tubes. Ozbakkaloglu and Saatcioglu (2007) further tested large-scale square columns with a 270

mm cross-sectional dimension. The columns were 1720 mm high. The researchers studied the effectiveness of square stay-in-place FRP formwork for HSC columns subjected to simulated seismic loading. Three of the columns had a FRP tube with internal FRP crossties. One of the columns had 12 longitudinal bars and two crossties in each cross sectional direction. The other two columns had 8 longitudinal bars and one internal crosstie in each cross sectional direction. Two types of concrete strength were used; 75 and 90 MPa. The concrete cover used was 25 mm, measured to the outside of longitudinal reinforcement. Three different longitudinal reinforcement arrangements were used. It was concluded that the deformation capacity of HSC columns can be improved significantly by using FRP casings. The columns developed inelastic drift capacities of up to 11%. Also the confinement efficiency improved with the use of FRP crossties. Other researchers also investigated the performance of concrete-filled circular and rectangular FRP tubes under combined bending and axial load (Seible et al. 1996; Mirmiran et al. 1999, 2000; Fam and Rizkalla 2002; Fam et al. 2003, 2005; Zhu 2004; Shao and Mirmiran 2005). Further, FRP wrapping of concrete columns as a seismic retrofit strategy has been studied by researchers in the past (Saadatmanesh et al. 1996, 1997; Xiao and Ma 1997; Seible et al. 1997; Sheikh and Yau 2002; Iacobucci et al. 2002, Elnabelsy and Saatcioglu 2004). It has been reported that the effectiveness of externally applied FRP jackets is higher in circular columns than square columns (Rochette and Labossiere 2000; Mirmiran et al. 1998b; Pessiki et al. 2001).

In addition to the above mentioned experimental and analytical research on column confinement, a number of researchers have proposed mathematical and numerical models for concrete confinement (Kupfer et al. 1969, Chen 1982, Malvar and Simons 1996, Malvar et al. 1997, Légeron and Paultre 2003). Paultre and Légeron (2008) have recently conducted a comprehensive study at the Uuniversity of Sherbrooke on column ductility to develop new equations for the design of confinement reinforcement for rectangular and circular concrete columns. The equations are applicable to concrete strength of up to 120 MPa and confinement steel strengths of up to 1400 MPa. Test variables used in this investigation were longitudinal reinforcement ratio, axial load level, effective confinement index, reinforcement yield strength and concrete compressive strength. The proposed equations then compared with experimental results of 93 square and circular columns made with normal and high

strength concrete that have been tested by different researchers. They indicated that the equations account for the influence of concrete strength, transverse reinforcement yield strength, axial load level, and the amount of transverse confinement reinforcement as the main variables.

The following conclusions can be drawn from the literature review presented in this chapter:

- The pioneering work on concrete confinement was conducted by Richart et al. (1928). Their research led to the development of concrete confinement requirements in the American Concrete Institute, ACI 318 Building Code, which have been used up till today (ACI-318 2008).
- The strength and ductility were improved by increasing the amount of lateral steel. The amount of longitudinal steel within the range of 1.7% to 3.7%, had small effects on concrete confinement.
- The strength of concrete increased up to 70% with significant improvement in ductility when concrete was confined with rectangular ties and well distributed longitudinal steel. On the other-hand the confinement efficiency decreased when the spacing of lateral reinforcement was increased. Enhancement of strength and ductility was observed when tie spacing was reduced, even if the volumetric ratio was kept constant. The increase in the amount of lateral steel, the effectiveness of confinement reinforcement, and reduction in axial load, increased the ductility and energy-absorption capacity of columns.
- Confinement reduces internal cracking associated with lateral expansion of concrete under axial compression. The main variables of confinement were found to include the spacing of confinement reinforcement, concrete strength and type, percentage and distribution of longitudinal reinforcement, tie arrangement, rate of loading, level of axial compression, size and section geometry, and the volumetric ratio of transverse steel (the ratio of lateral steel volume to the volume of concrete core).
- The ductility of high-strength concrete (HSC) could be significantly improved by using sufficient amounts of confinement reinforcement with high yield strength.

- The beneficial effects of high-strength transverse steel were more obvious for columns subjected to high axial load level.
- Columns under a low axial load of 20% of concentric capacity with a transverse reinforcement ratio of higher than 82% of that required by ACI 318 Building Code (2002) showed a ductile behaviour of 6% lateral drift and higher. On the other hand, columns which were tested under higher axial load of 30% of concentric capacity showed a lower drift ratio of 3%. However, the column behaviour improved for columns confined with high-strength transverse reinforcement.
- High confinement pressure could be provided either by increasing the volumetric ratio of transverse reinforcement and/or by using high-strength transverse reinforcement. The test results also indicated that HSC columns behave in an extremely brittle manner unless properly confined.
- The deformation capacity of HSC columns can be improved significantly by using FRP casings. These columns developed inelastic drift capacities of up to 11%. Also the confinement efficiency improved with the use of FRP crossties.
- Columns confined with reinforcement grids showed ductile response, developing lateral drifts equal to or greater than those expected in columns confined with conventional ties of equal volumetric ratio. The drift capacity increased when grids with smaller cells were used. The grids improved structural performance of columns which developed lateral drift ratios in excess of 3% with transverse reinforcements less than or approximately equal to that required by the AC1 318-08 Building Code.
- Test results showed that transverse prestressing could improve column deformability up to 4% lateral drift and higher.

CHAPTER 2

Properties of Tires as a Civil Engineering Material

2.1 Introduction

The use of recycled materials in civil engineering applications has been increasing over the past decade and the use of composite materials gaining acceptance in the construction industry. There has been a growing concern over the past twenty years regarding the volume of waste products to be disposed. Disposal of scrap tires poses a growing challenge since the accumulation of discarded automobile tires has become environmental, fire, and health hazards worldwide. They contribute to the problem of pollution when burned to dispose. Waste tires require large space for storage because of their shape, quantity and compaction resistance. Furthermore, they are non-biodegradable. Therefore, the mechanical properties of tires remain virtually unchanged even after their economic life as an automobile tire has expired (O'Shaughnessy 1997). This provides incentives to explore economically and environmentally feasible alternatives for re-using and recycling scrap tires in the construction industry in addition to their existing use in ports, as well as coastal and river structures. Indeed, scrap tires are now being used in civil engineering applications, in various forms.

It is estimated that the European Union (EU) produces over 2.5 million tones of used tire material every year, of which around 1.5 million tones are subsequently processed and the remaining portion is disposed to landfill (Khalid and Artamendi, 2004). In France, more than 450,000 tonnes of old tires are thrown away every year. Only 150,000 - 200,000 tonnes are recycled in one form or another (Long 1993). In the UK, 25-30 million tires are disposed

every year. In the United States, it is estimated that more than 200 million automobile tires and 40 million truck tires are discarded every year (Williams 1987). In the same country, more than 250 million tires are scrapped each year (South Carolina Department of Health and Environmental Control Office of Solid Waste Reduction and Recycling 1999). That's the equivalent of almost one tire for every man, woman and child in the country. Only in the State of Iowa alone 3 million waste tires are generated each year. Also, in South Carolina, the law now prohibits the storage of scrap tires without a permit, and it is illegal to dispose off whole tires in county or public landfills. In 2003, the Rubber Manufacturer's Association estimated that New York State generates between 18 and 20 million waste tires per year.

Canada generates over 28 million passenger tires per year, of which approximately 30% are disposed in landfills or tire stockpiles (Canadian Council of Ministers for the Environment (CCME 1994)). It is estimated that 41 percent are converted into crumb, 14 percent are used for molded products, 21 percent are used in tire-derived fuel, and the remaining 24% are export sales.

There are several methods used for tire disposal. Putting the scrap tires in stockpiles, as shown in Figure 2.1, is one method of disposal. Burying them or dumping in landfills as shown in Figure 2.2, is another method. These disposal techniques often require large areas. Tires are also burned, shredded, and/or reused for other purposes such as for boat fenders, children swings etc. Only 25 % or fewer are used as fuel or as raw materials for manufacturing rubber goods. Some tires are retreated and used again as automobile tires. Retreading is not a solution because the tire still has to be disposed. Furthermore, only a few tires with good sidewalls can be retreaded.

The majority of tire disposal methods used are wasteful and costly, often requiring large disposal areas and/or resulting in other environmental problems. Clearly, scrap tires are a major problem on an international scale. However, scrap tires are abundant and may be utilized economically as a civil engineering material if their mechanical properties are found to be of adequate quality for the application at hand. In 1996, an estimated 10 million scrap tires were used in civil engineering applications (STMC, 1997). In 1998, civil engineering

uses for scrap tires doubled relative to 1996. In 2005, the Rubber Manufactures Association (RMA) estimated that, of the 299 million tires that were generated in the U.S., only over 49 millions were consumed for civil engineering applications. There are several applications in which tires could be used as a structural media. These are sea defense, crash barriers, noise barriers, land terracing, bridge abutments, gravity retaining walls, facings for reinforced earth walls, and enabling embankments to be built with steeper side slopes. Moreover, tire shreds are used as backfill for retaining walls because of their lightweight. They produce low horizontal pressures on the back side of the walls and they provide drainage so that water pressure built up behind the wall can be prevented. They are also a good insulator, preventing frost related problems.

The use of tires as concrete column reinforcement, which forms the main focus of current research, requires detailed understanding of the properties of tires as a construction material. The following section of this chapter is devoted to this subject.

2.2 Tire Types and Constituent Materials

Vehicle tires are manufactures in various forms and sizes, ranging from standard automobile tires to those used for airplanes, bicycles, tractors, etc. Therefore, they encompass a wide range of designs, materials, and manufacturing processes.

Tires can be viewed under four major categories based on their use; i) passenger tires, ii) truck tires, iii) farm tires, and iv) off-road tires. The passenger tires form the most common type, representing 80% of the market (Deese et al 1981). Passenger tires come in rim sizes of 12 to 15 inches (305 mm to 381 mm). Truck tires come in rim sizes of 15 to 16 inches (381 mm to 406 mm) for lightweight vehicles, and 15 to 24 inches (381 mm to 610 mm) for heavyweight vehicles. They weigh approximately 10 kg, 13.5 to 27 kg, and 41 to 91 kg, respectively. The tire industry uses ASTM 1070 for manufacturing new tires. There are approximately 2.5 pounds of steel belts and bead wire in a typical passenger car tire (Rubber Manufacture Association (RMA). The average weight of steel used for a passenger tire is 1.14 kg per tire (2.5 lb/tire).

Three types of passenger tires are used in the automotive industry; i) radial, ii) bias-ply, and iii) bias-belted. A tire is manufactured from several separate components, such as tread, inner liner, beads, and belts (RMA 2003). Structural elements that are common to all of these tires are the casing, bead, and tread band. Table 2.1 shows which components account for the rubber used to make the tire (RMA). The most common type, which was used in the current research program, is the radial tire. The physical tire constituents consist of fabric, bed wire, and rubber compound. Radial tires are fabricated with vulcanized rubber that contains reinforcing textile cords, high-strength steel wire reinforcing bead, and high-strength steel. The major tire components by weight are given in Table 2.2.

The major classes of materials used to manufacture passenger and truck tires are given in Table 2.3. The steel typically makes up about 15 percent of total weight, the cord material another 5 percent, and the rubber compound in the carcass and tread about 80 percent (Modern Tire Dealer 2006, 51). The main chemical components for the rubber are given in Table 2.4. The most commonly used tire rubber is styrene-butadiene-copolymer (SBR), containing about 25% styrene. Other tire rubbers used are cis-polybutadiene, natural rubbers (cis-polyisoprene), and synthetic cis-polyisoprene (O'Shaughnessy 1997). Carbon black is added to strengthen rubber and increase abrasion resistance. Other constituent materials are also used for specific functions. Extender oil, which is a mixture of aromatic hydrocarbons, is used to increase the workability of the rubber while also softening it. Sulphur is used to harden rubber by cross-linking the polymer chains within the rubber to prevent deformations at high temperature (O'Shaughnessy 1997). Zinc oxide, stearic acid and organo-sulphure accelerator are used to aid in the vulcanization process and also to enhance the physical properties of rubber (Williams et al. 1990).

Tires have three main structural parts; treads, sidewalls, and rims. These parts are illustrated in Figure 2.3 (a). The tread is an important part which contains a number of strong cords coated with rubber. The steel belt or cord under the tread of a radial tire and in the rim contains high-tensile steel with high percentage of carbon. The steel in the tread and rim is well protected by a rubber coating. These cords have a high ultimate tensile strength of up to approximately 2000 MPa to 2500 MPa. Figure 2.3 (b) shows a typical cross-sectional view of a tire. The components of a radial tire are shown in Figure 2.4.

The steel belt is made by using fine wire twisted into cables as cords. Most manufacturers use typical cord diameters of 0.25, 0.22, 0.28, 0.30, and 0.32 mm. Each cord contains four wires. The diameter for each wire is 0.25 mm, resulting in an area of 0.048 mm^2. This means that the area of each cord is 0.192 mm^2/ cord (4 x 0.048 = 0.192 mm^2/ cord). Some manufactures put three to four wires per cord, while others may put up to 10 wires per cord. The commonly used wires have a diameter of 0.25 mm, (area = 0.048 mm^2), producing a cord area of 0.192 mm^2 in a 4-wire cord. However, the majority places four wires in each cord. The number of cords per tire in the tread varies among different companies. Some common figures are 14, 15, 17, 20, and 22 cords per inch (per 25.4 mm). The average weight of steel used in passenger tires is 0.7 kg/tire (1.54 lb/tire). The tire reinforcement used in this research program consists of whole scrap tires (sidewalls and tread), stacked together on top of each other continuously to resist lateral pressure due to concrete expansion, as well as diagonal tension caused by shear.

2.3 Tire as a Civil Engineering Material

Old tires have excellent mechanical properties and are readily available in large quantities as waste material. Scrap tires can be excellent substitutes for steel reinforcement and column formwork. Dealers and garages can supply them free of charge to construction sites, except for the cost of transportation. Previous applications of scrap tires in civil engineering applications include lightweight fill for retaining walls, backfill behind walls, insulation to limit frost penetration beneath roads, aggregate in leachate and gas collection systems in landfills, highway crash barriers, insulated layers in roadways, drainage materials, reinforcement for slope and river protections, sound barriers, energy dissipaters, artificial reefs, breakwaters, and rubberized asphalt. The light weight of tire shreds is an advantage that appeals to civil engineers for applications in their fields. Scrap tires have become one of the more popular recycled materials used in geotechnical engineering applications such as roadway embankment construction, landfill drainage layers, retaining wall backfill, thermal insulation, and vibration attenuation media.

The in-place unit weight of tire shreds range between 45 and 58 pcf compared to soil fill

which typically weighs 125 pcf (Humphrey 1999). Tires are used in civil engineering projects according to their material characteristics, highlighted below.

Durability: Tires are non-biodegradable elements and have long life expectancy. The deterioration of a tire is usually caused by the effects of sunlight and water. There are some tires in museums that are as much as eighty years old. However, recently manufactured tires contain antioxidants and other additives to prevent deterioration. When tires are not used as transportation elements, their life can be in excess of 100 years (O'Shaughnessy 1997). Malek and Stevenson (1986) studied physical conditions of vulcanized rubber submerged in 24 m of sea water for a period of 42 years. Their investigation showed that no serious deterioration of the rubber had occurred. Detailed laboratory investigation by (O'Shaughnessy and Garga (2000) provide further evidence on the durability of old tires.

High Radial Strength: Tires can resist very large tensile forces due to their circular geometry which enables them to develop hoop tension. Hence, they may be used as transverse reinforcement in concrete columns of buildings and bridges. When used to confine concrete against lateral expansion, they may have the ability to resist lateral pressure. This characteristic forms a significant aspect of the current study.

Handling and Transportation: Handling of tires can be done by traditional construction equipment and labor, without much difficulty. Tires can be easily transported to the construction site in loads of 600 to 1000 tires per truck. Off loading of the tires can be readily accomplished by one worker.

Economy and Availability: Scrap tires, as waste material, are readily available and may be supplied to construction site often free of charge, except for the cost of transportation.

Flexibility and Extensibility: Tires are able to extend and deform without cracking. They are very flexible and able to deform more than most other construction materials.

2.4 Previous Applications and Research on Scrap Tires as a Civil Engineering Material

Civil engineering applications are a growing market for scrap tires. A literature review was conducted on the use of scrap tires for different Civil Engineering applications. Engineers and researchers are interested in civil engineering materials that are more economical but

otherwise comparable to existing proven materials. Scrap tires have received wide acceptance for a variety of applications as soil reinforcement in geotechnical engineering. The American experience showed that the construction of reinforced earth structures using scrap tires can provide an alternative solution to many geotechnical problems. Tire reinforced soils have been achieved in many countries like Brazil, France, Germany, Switzerland, and United States, at lower costs than those that involved conventional techniques for reinforcement.

One of the first practical applications in the United States, using discarded tires, was the repair of a hillside fill instability along California Highway 236, north of Santa-Cruz, built in mid 1970s (Forsyth and Egan 1976). Research in the US concentrated on the use of shredded tires as a form of a lightweight fill in roads and retaining wall construction (Giesler et al. 1989, Eldin and Senouci 1992, and Drescher and Newcomb 1994). The results published by Giesler et al. (1989), Eldin and Senouci (1992), Drescher and Newcomb (1994), and Humphrey and Eaton (1995) indicate that shredded tires increase the shear strength of soils. Shredded tires produce a lightweight fill that reduces settlements up to 50% and increase the stability of road embankment. Shredded tires do not present any major handling and placement problems in road construction, and have good thermal properties.

There has been a lot of interest among geotechnical engineers to find out the characteristics of tire derived aggregate (TDA). Researchers focused on the study of shear strength, compressibility, and permeability of tire derived aggregate (Manion and Humphrey 1992, Edil and Bosscher 1992 & 1994, Humphrey and Sandford 1993, Ahmed and Lovell 1993, Drescher and Newcomb 1994, Cosgrove 1995, Benda 1995, Bernal et al. 1996, Tatilsoz et al. 1996, Tweedie et. al, 1998, Heimdahl 1998, Yang et al. 2002, Moo-Young et al. 2003, Youwai and Bergado 2003, and Zornberg et al. 2004). The coefficient of variation of shear strength parameters for TDA was found to be close to or slightly higher than the maximum value reported for comparable natural soil parameters (Strenk et al. 2007).

Other tire projects have also been undertaken in California (Drescher and Newcomb 1994), including the use of scrap truck tires to control shoulder erosion of an embankment on Rout

32, in Tehama County. The Minnesota Department of Natural Resources in the US studied the use of automobile tires as reinforcement to determine if roads constructed over highly compressible soils in Saint Louis County could improve subgrade performance (Drescher and Newcomb 1994). The settlements were reported to be less than those expected from a conventional soil embankment without the reinforcement. Also, on State Route 111, near Palm Springs, they used automobile tire piles and tied tire walls to supply temporary barriers against wind blown sand.

In the State almost all applications for scrap tire material replaced some other material currently used in construction such as lightweight fill materials like expanded shale, subgrade fill and embankments, backfill for retaining walls and bridge abutments, subgrade insulation for roads, landfills, drainage aggregate, or even soil or clean fill as a possible solution to the problem of scrap-tire disposal. According to the Rubber Manufacturers Association (2003), 39 states approved tire shreds for civil engineering applications.

In the United Kingdom, the first project using scarp tires was the construction of an experimental gravity wall at the mechanical engineering services at Lofthouse in West Yorkshire Metropolitan County Council (WYMCC 1977). The height of the tire wall was 3.7 m and the length was 45 m. A total of 4500 tires were used in the project, with an average tire layer thickness of 0.15m. The wall consisted of whole passenger tires having R-13 to R-15 (radius of the tire rim in inches) sizes with corresponding tire widths varying from 125 to 200 mm. It was observed that the effective interlock at the face of the tire wall was difficult for slopes steeper than 1 to 1. The cost of this project was estimated to be approximately one quarter the cost of a similar traditional retaining wall.

In 1982, Dalton and Hoban reported on another application of a tire wall. The reinforced soil structure was an anchored or tied-back tire wall. The face of the wall was constructed by placing the tires tread to tread to form a single line.

Many previous studies in geotechnical applications were conducted, included laboratory investigations, numerical and physical modelling and field investigations regarding the use

of scrap tires as whole tires, shredded or chipped tires, or mixed with soils especially as embankment materials (Ahmed and Lovell, 1993, Bernal 1996, Masad et. al 1996, Lee et. al 1999, Chu and Shakoor 1997, Tweedie et. al 1998, Bergado and Youwai 2002, Humphrey and Tweedie, 2002, and Edil 2002). Other research in the field are summarized in the following paragraphs.

Aydilek, Madden, and Demirkan (2006), reported on laboratory and field studies which were conducted to investigate the performance of tire chips as a leachate collection material in municipal solid waste landfills. Two field test cells were constructed and used, one with tire chips and another with gravel. Laboratory tests were also performed to study the compressibility and hydraulic conductivity of tire chips under different stress levels. Leachate collected from the two cells was analyzed to determine if tire chips contaminate the groundwater. They conclude that the tire chips can be safely used as part of a landfill leachate collection layer and they have adequate drainage conditions as compared to gravel.

Palit, Reddy, and Pandey (2004) conducted experimental investigations on normal and crumb rubber modified asphalt mixes. The crumb rubber used in the study was obtained from discarded truck and bus tires. The test variables considered were; fatigue and permanent deformation characteristics, temperature and moisture susceptibility, and three aggregate gradations. They concluded that the crumb rubber modified mixes were found to have improved fatigue and permanent deformation characteristics significantly, lowered temperature susceptibility, and provided greater resistance to moisture damage compared to normal mixes.

Scrap tires have been used in hot mix asphalt (HMA) for several decades in the United State. Since 1960 when Charles McDonald became the first engineer to use scrap tire rubber in asphalt mixtures to improve pavements in Phoenix, Arizona, many experimental studies and tests have been constructed and tested to explore the possibility of using the scrap tires in HMA. The mixing of crumb rubber with conventional binders resulted in an improvement in the binder's resistance to rutting, fatigue cracking and thermal cracking (Dantas Neto et al., 2003; Way, 2003). Researchers have also concluded that rubberized asphalt mixes can be

helpful in reducing the thickness of asphalt overlays and reflective cracking potential (Amirkhanian, 2003; Holleran and Van, 2000; Cano et al., 1989; Esch, 1982; Choubane et al., 1999; Sousa et al., 2002), in addition to protecting the environment and saving resources (e.g., landfill space).

Lee (2002) has introduced the concept of cementing tire rubber bits into rubber blocks using binder materials for use in geotechnical applications. Ghani et. al (2002) used shreds instead of bits in a study to improve and establish pre-determine yielding behaviour of geo-materials developed for use as retaining wall backfill layers. The researchers also conducted numerical analysis to study the pressure on walls with and without compressible layers. Their results indicated that pressure on wall with compressible layer can be reduced to about half the pressure of wall without the compressible material. This was also in agreement with full scale tests carried out by Humphrey et. al (1998) and Tweedie et. al (1998) who found out that earth pressures could be reduced to more than 45% to 50%.

Garga and O'Shaughnessy (2000a) constructed a 57 m high, 17 m wide instrumented test fill which included both retaining wall and reinforced slope sections. 10,000 whole tires and one sidewall removed tires were used in the investigation. These tires were tied together with polypropylene rope. In the reinforced fill section, the tires were tied together as a mat, followed by a compacted backfill layer of soil, 0.3m thick, followed by the next layer of tire mat. The tires were stacked on top of each other in a staggered manner. Three large plate loading tests were performed on the surface of the completed test fill to assess the load-deformation behaviour of the composite material. They concluded that this embankment proved the practical feasibility of using scrap tires as soil reinforcement technique for tire reinforced slopes and tire reinforced gravity retaining walls.

Humphrey (1999) presented special applications of using tire shreds in civil engineering and studied their properties to enable civil engineers to solve difficult design situations. He used tire shreds as lightweight fill for highway embankment construction, bridge abutment backfill, thermal insulation to limit frost penetration beneath roads, and drainage layers in landfills. Tire shreds were used as lightweight fill for construction of two 32-ft high highway

embankments in Portland, Maine (Humphrey, et al., 1998). Tire shreds were chosen in this project because they were $300,000 cheaper than the other alternatives and put some 1.2 million tires to a beneficial end use. He concluded that tire shreds have a low unit weight, high permeability, and high insulating value making them an excellent fill for embankments construction.

Eldin and Senouci (1993) performed an experimental study to examine the potential of using tire chips and crumb rubber as aggregate in Portland-Cement concrete. They used different amounts of rubber-tire particles of several sizes as aggregate to examine strength and toughness properties of concrete. More than 200 (150 mm in diameter x 300 mm high) concrete cylinders were tested. Their results showed that the concrete mixtures presented lower compressive and splitting-tensile strengths than did normal concrete. These mixtures also demonstrated a ductile plastic failure, and had the ability to absorb a large amount of plastic energy under both compression and tension. The researchers suggested the use of rubber aggregates for; i) architectural applications such as nailing concrete, stone backing, false facades, and interior construction because of its light unit weight, ii) low-strength concrete applications such as sidewalks, and driveways and iii) crash barriers around bridges because of their high ability to absorb plastic energy.

The following conclusions can be drawn from the literature review presented in this chapter:

- The shredded tires when used as lightweight fill in roads and retaining walls increase the shear strength. Shredded tires produce a lightweight fill that reduces settlements up to 50% and increase the stability of road embankment. They do not present any major handling and placement problems and have good thermal properties.
- The coefficient of variation of shear strength parameters for tire derived aggregate (TDA) was found to be close to or slightly higher than the maximum value reported for comparable natural soil parameters (Strenk et al. 2007).
- Scrap truck tires can be used to control shoulder erosion of an embankment. When the automobile tires are used to reinforce highly compressible soils, they could

improve subgrade performance. The settlements in soils were reported to be less than those expected from a conventional soil embankment without the reinforcement.

- In the U.S., 39 states approved tire shreds for civil engineering application. They replaced some of the other materials, such as lightweight fill materials like expanded shale, for stabilizing subgrades and embankments, backfilling for retaining walls and bridge abutments, insulating subgrades for roads, as well as landfills, drainage aggregates, or even soil or clean fills as a possible solution to the problem of scrap-tire disposal.
- Tire chips can be safely used as part of a landfill leachate collection layer and they have adequate drainage conditions as compared to gravel.
- The crumb rubber modified mixes were found to have improved fatigue and permanent deformation characteristics, significantly lowering temperature susceptibility and providing greater resistance to moisture damage compared to normal asphalt mixes.
- Scrap tires have been used in hot mix asphalt (HMA). The mixing of crumb rubber with conventional binders resulted in improvements in binder's resistance to rutting, fatigue cracking and thermal cracking. Researchers have also concluded that rubberized asphalt mixes can be helpful in reducing the thickness of asphalt overlays and reflective cracking potential, in addition to protecting the environment and saving resources (e.g., landfill space).
- Using tire chips and crumb rubber as aggregate in Portland-Cement concrete cylinders showed lower compressive and splitting-tensile strengths than conventional concrete. These mixtures also demonstrated ductile plastic failure, and had the ability to absorb a large amount of plastic energy under compression and tension.

Table 2.1: Percentage of Rubber by Weight in a New Radial Passenger Tire (Rubber Manufacturers Association 2003)

Type	Weight (%)
Tread	32.6
Base	1.7
Sidewall	21.9
Bead Apex	5.0
Bead Insulation	1.2
Fabric Insulation	11.8
Insulation of Steel Cord	9.5
Innerliner	12.4
Undercushion	3.9
Total	100.0

Table 2.2: Tire Constituent Materials by Weight (Humpstone et al. 1972)

Tire Constituents	Weight (kg)	Weight (%)
Fabric	1.41	10
Bead Wire	0.46	4
Rubber Compound	9.80	86
Total	11.67	100

Table 2.3: Typical Composition of Tires by Weight (Rubber Manufacturers Association 2003)

Tire Component	Passenger Tire (Weight %)	Truck Tires (Weight %)
Natural rubber	14	27
Synthetic rubber	27	14
Carbon black	28	28
Steel	14-15	14-15
Fabric, Fillers, accelerators, antiozonants, etc.	16-17	16-17
Average Weight	New 25Ibs., Scrap 20Ibs	New 120Ibs., Scrap 100Ibs.

Table 2.4: Typical composition of Tire Rubber (Williams et al. 1990)

Component	Weight (kg)	Weight (%)
Rubber Polymer (SBR)	6.088	62.1
Carbon Black	3.039	31.0
Extender Oil	0.186	1.9
Zinc Oxide	0.186	1.9
Stearic Acid	0.188	1.2
Sulphur	0.107	1.1
Accelerator	0.069	0.7
Total	≈9.80	99.9

Figure 2.1: Scrap Tires in Stockpiles

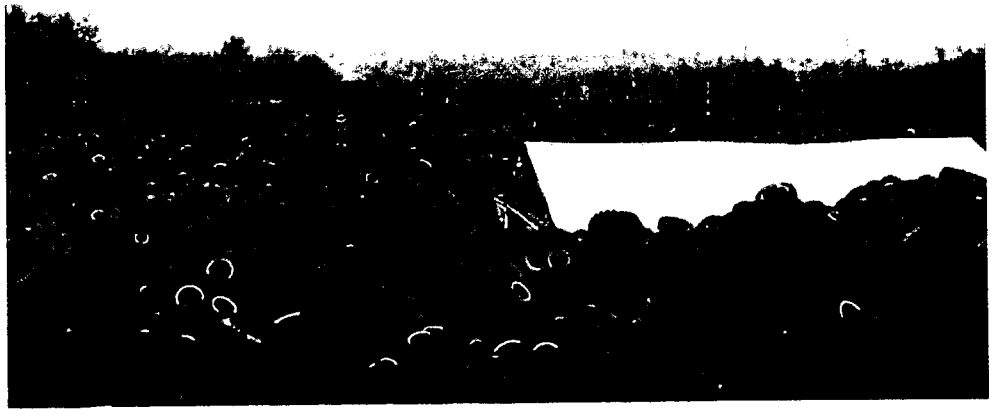

Figure 2.2: Dumped Tires in a Landfill in Oswego County, NY (Photo by Chris Glander)

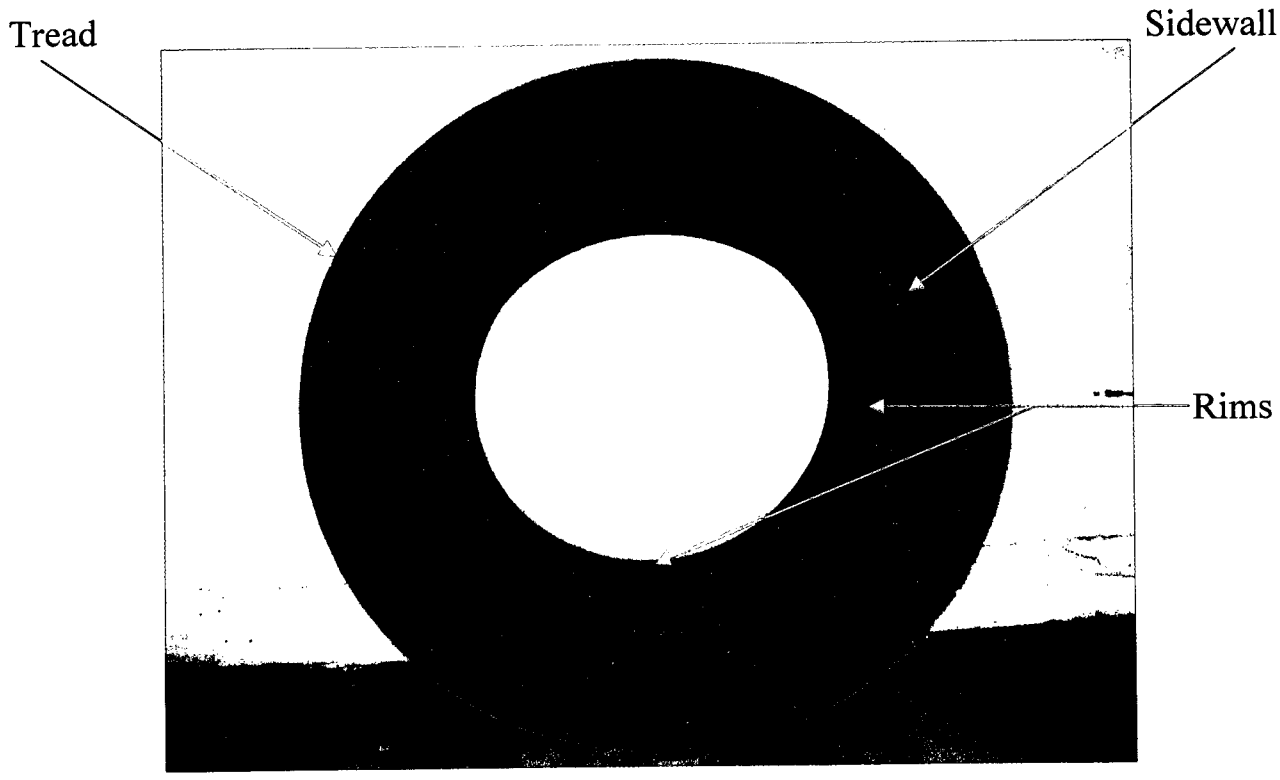

(a)

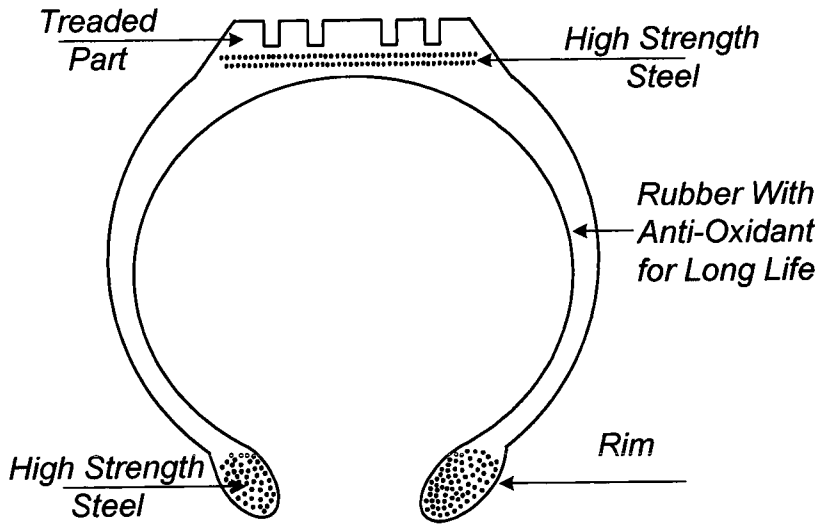

(b)

Figure 2.3 (a): Components of a Typical Tire; (b) Cross-Sectional View of a Tire

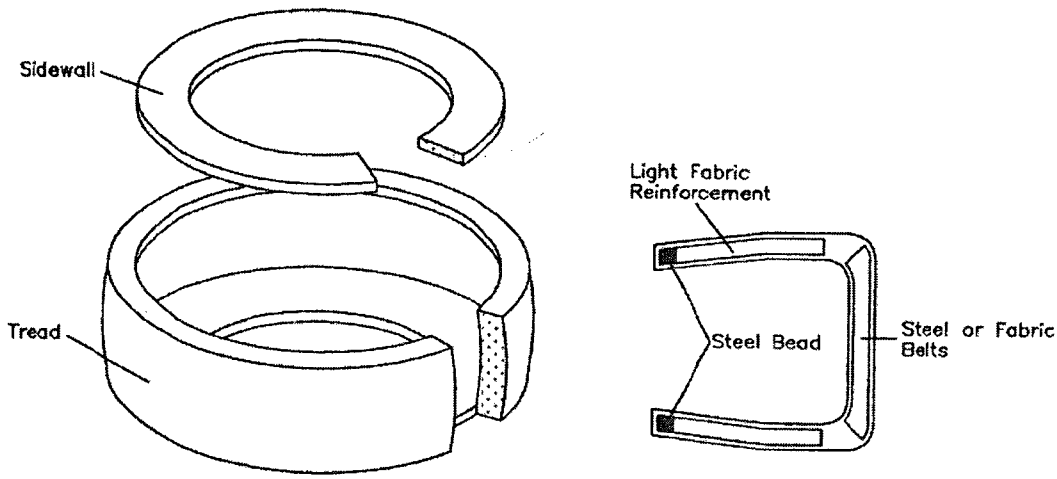

Figure 2.4: Different Components of a Radial Tire

CHAPTER 3

Experimental Research

3.1 General

The experimental program was designed to investigate the effectiveness of steel belted tires as transverse reinforcement in bridge columns. This constitutes the second phase of an ongoing research project at the University of Ottawa, where the first Phase involved tests of 6 flexure dominant columns, confined with different arrangements of scrap tires (Bugaldian 1999). The second phase, proposed as part of the current investigation, involves an additional six full-scale circular columns with different cross sectional sizes and column heights to generate flexure and shear dominant responses. The columns were designed, built, constructed and tested under constant axial compression and incrementally increasing lateral deformation reversals. The main test parameters were the tire size and column height, producing either flexure or shear dominant columns. The objective of the test program was to assess the performance of steel belted automobile tires as transverse reinforcement in resisting diagonal tension created by shear or hoop tension created by laterally expanding concrete under compression. The construction of the test specimens, material properties and instrumentation are described in this chapter. The chapter also includes discussions on test set up and test procedure. The test results, observed behaviour and evaluation of test data to date are discussed in Chapter 4.

3.2 Description of Test Specimens

The columns were designed to utilize standard tire sizes that are commonly used as automobile tires. Passenger tires with 550 mm out-to-out diameter, having either 330 mm (13 in – size 13) or 356 mm (14 in – size 14) rim diameter, or with 700 mm out-to-out diameter and either 381 mm (15 in – size 15) or 406 mm (16 in –size 16) rim diameter were

used. The columns had an aspect ratio (the ratio of column shear-span to cross-sectional diameter) of 3.6 for flexure dominant response or 2.2 for shear dominant response. This translated into column heights of either 2000 mm or 1200 mm for 550 mm diameter columns, and 2500 mm or 1500 mm for 700 mm diameter columns, where the column heights were measured to the point of inflection of cantilever specimens. They were attached to a steel loading beam of 275 mm depth for transfer of applied horizontal force. This beam formed a portion of the column top segment, leaving the concrete column portion with a height of 925 mm, 1225 mm, 1725 mm, or 2225 mm. The specimens represented part of a first storey building column or a bridge column between the footing and the point of inflection. Each specimen consisted of a column and a footing. The cantilever lengths represented prototype columns with an inter-story height of 2.4 m, 3.0 m, 4.0 m, or 5.0 m, which are representative column heights used in practice. Two of the flexure dominant columns, one with 550 mm cross-section and the other with 700 mm cross section, had spliced longitudinal reinforcement to reflect the actual construction practice. The spliced length of these re-bars was 30 bar-diameters. The specimens were labelled as TC-7 through TC-12, following the numbering scheme used earlier in Phase I of the same research program (Bugaldian 1999). Table 3.1 provides a summary of the specimens tested. Figure 3.1 shows the geometric details.

The columns were poured from the same batch of concrete, with a design strength of 30 MPa. Control cylinders were cast to monitor the strength gain with time. The 28 day cylinder strength of the concrete used in columns was established to be 45 MPa, which increased to 54 MPa during the period in which the column tests were performed.

Longitudinal column reinforcement consisted of either 12 - 19.5 mm diameter (No. 20) or 12 - 25.2 mm diameter (No. 25) deformed bars, with average yield strength of 467 MPa and 460 MPa respectively. This resulted in approximately the same percentage of longitudinal reinforcement in all columns. The longitudinal reinforcement ratio for TC-7, TC-8, and TC-11 was 1.56%, and for TC-9, TC-10, and TC-12 was 1.51%. The bars extended 405 mm into the footing, and were bent to form 90 degree hooks. The hook extension was 500 mm, which conformed to the development length requirement of CSA Standard A23.3-2004. Each

column had eight Grade 8, 19 mm diameter bolts embedded in the concrete at the top of the column, vertically protruding to facilitate the attachment of the loading beam to the top of the column. The bars were placed through the sidewall by punching through the rubber. This implies that the bars were positioned in the middle of the sidewall with some cover concrete between the steel and the tire. This is illustrated in Figure 3.2 and Figure 3.3. The column transverse reinforcement consisted of only the tires, without conventional circular steel hoops. The properties of tire reinforcement are discussed in details in the subsequent section.

The design variables considered in the test program included the cross-sectional dimension (tire size), column aspect ratio, and the level of axial load. Figure 3.2 and Figure 3.5 show the photographs of longitudinal reinforcement, including the placement of tire transverse reinforcement.

Each column had a heavily reinforced concrete footing. The dimensions of the footing were 1730 mm x 1400 mm x 520 mm. The footing concrete was cast two footings at a time using the two plywood formwork that were prepared. The 28 day concrete strength for the footings was 48 MPa. Four plastic (PVC) tubes with an outside diameter of 80.5 mm were placed near the corner of each footing to secure the specimens on to the laboratory strong floor by means of four bolts with a diameter of 70 mm and a length of 1800 mm. Eight plastic (PVC) tubes with an inside diameter of 38 mm were placed on the right and left sides of the footing for fixing the vertical actuators to apply the axial force during testing.

3.3 Material Properties

3.3.1 Properties of Concrete

The concrete used was normal density ready-mix concrete with 100-mm slump. Type I Portland cement, natural sand and 20-mm maximum size aggregate were used for a specified 28-day design concrete strength of 30 MPa, although higher strength was achieved in columns (45 MPa after 28 days and 54 MPa during the testing period). A total of 40 standard cylinders (100 x 200-mm) were cast along with the columns to establish concrete strength. All cylinders were ground at their ends by a special concrete grinder to ensure the uniform

application of load. Strength-age relationship for concrete was developed by performing standard cylinder tests according to CSA A23.2-9C at frequent intervals. Cylinders were tested using a Fourney testing machine with 2225kN capacity or a Galdabini Universal testing machine with 600kN capacity after 7, 14, 28 days, and the time of column tests. Table 3.2 illustrates concrete strength development with time. The average of at least three cylinders was used to establish concrete strength at a given time. The instrumentation and standard cylinder tests are depicted in Figure 3.6. The strength gain with time and the stress-strain relationship of concrete during the period of column tests are shown in Figure 3.7 and Figure 3.8.

3.3.2 Properties of Longitudinal Reinforcement

All longitudinal reinforcements were ordered from a local supplier. Three randomly selected coupons were tested for each bar size, using a 600 kN capacity Galdabini Universal testing machine. The coupon tests provided the stress-strain relationships as shown in Figure 3.9. Average yield strengths for No. 20 and No. 25 bars were established to be 467 MPa and 460 MPa, respectively. None of the columns had any transverse reinforcement, except for the single tie that was used at the top for the purpose bar assembly to keep the longitudinal bars in place.

3.3.3 Properties of Steel-Belted Tires

Six different brand names of tires were used in this investigation. The tires in critical regions (bottom three or six tires in each column pair) were of identical brand and type to ensure consistency. Good Year, Michelin, Firestone, Winter King, Continental, and Han Kook tires were used for TC-7, TC-8, TC-9, TC-10, TC-11, and TC-12 respectively. Starting with the forth or the seventh tire from the footing, till the top, different types of the same size tire were used.

In the absence of a standard test for tires, three coupons of arbitrary size were prepared and tested in direct tension, for each brand tire using the Galdabini Universal testing machine. Tests of these coupons provided the stress-strain relationships for each type of tire. Figure

3.10 illustrates the geometry and dimensions of the coupons tested.

The tire coupons were taken from the treaded part of the tire, which consisted of a number of strong steel cords coated with rubber of different brand names. The diameter of the cord per tire varied in size and was 0.22, 0.25, 0.28, 0.30, and 0.32 mm. Every cord contained four wires. The diameter of each wire was 0.25 mm, resulting in an area of 0.049 mm^2. The area of each cord was 4 x 0.049 = 0.196 mm^2. Some manufacturers put three or four wires per cord, and others put up to 10 wires per cord. The majority, however, used four wires per cord. The brand names of tires which were tested or used in this investigation had four wires per cord. The numbers of cords per tire in the treaded part varied among the brand names. The numbers were 14, 15, 17, 20, and 22 cords per inch (25.4 mm).

Both Good Year and the Michelin tires used in this investigation had 17 cords per inch (25.4 mm). The average of at least three coupons per brand name was tested in direct tension. The average ultimate strength was 2150 MPa, 1950 MPa, 1900 MPa, and 2000 MPa for Good Year, Michelin, Firestone, and Yokohama tires respectively. The strain measurements were established from displacement measurements obtained from the Galdabini Universal testing machine with a capacity of 600 kN. The stress-strain relationships for tires with different brand names are shown in Figure 3.11. General view, test setup and typical failure of a tire coupon are illustrated in Figure 3.12 and Figure 3.13

3.4 Preparation of Test Specimens

3.4.1 Construction of Columns

The construction of test specimens was done at the Structures Laboratory of the University of Ottawa in five stages; i) the assembly of steel reinforcement cages for footings and columns, ii) installation of strain gauges for longitudinal reinforcement of columns , iii) installation of strain gauges on the tread and rim of tires, iv) Drilling of holes through tire sidewalls using a special plywood template for insertion of longitudinal bars, v) construction of formwork for footings and columns, and vi) casting of footings, two at a time, and subsequently casting of columns all at once.

Strain gauges for longitudinal reinforcement were installed at predetermined locations and the necessary wiring was soldered to gauge terminals prior to cage assembly. Strain gauges for tires were installed after drilling the holes through sidewalls of tires. The details of strain gauge locations are described in section 3.5. The assembly of steel cages was executed in stages. First the footing cages were built without some of the footing reinforcement, then the longitudinal column bars were secured in the center of the footing, and then the remaining footing reinforcement was built around and through the column cage. Footing shear reinforcement was installed last.

A plywood formwork was prepared for two footings, and reused for the second and third pairs. The formwork was held together by a combination of screws at the joints and triangular pieces of plywood were placed all around the formwork to give lateral support. To prevent warping and bulging of the formwork due to lateral concrete pressure, threaded rods and nuts were used to tie the sides of the formwork. The steel cages for footing were placed in formwork with the aid of a 10 Ton capacity laboratory crane. The PVC tubes were fixed in the formwork. The construction process of a typical specimen cage, strain gauges, formwork and placement of reinforcement cages are seen in Figure 3.14 through Figure 3.16. Local ready mix concrete was used to cast concrete in layers and vibrated thoroughly. Figure 3.17 shows the footings before, during, and after casting.

3.4.2 Placement of Tire Reinforcement

Whole tires were stacked on top of each other in a circular manner as transverse column reinforcement. Eleven tires were used for TC-7 and TC-8, nine tires for TC-9, and five tires per column for TC-10, TC-11, and TC-12. Size 16, 15, 14, and 13 passenger tires with a designation of (P245 / 70 R 16), (P 235 / 75 R 15), (P 185 / 65 R 14), (P 175 / 65 R 14), and (P175 / 75 R 13) were used to build the columns. "P" in the designation indicates the intended use of tire as "passenger", the numerals "245, 235, 185, and 175" indicate the width of the tire in millimeters, "75, 70, and 65" indicate the height to width ratio, "R" stands for radial, and "16, 15, 14, and 13" are the diameter of the rim in inches. Tires were supplied to the lab free of charge, except for the cost of transportation. All the preparation of tires

(cleaning, drilling holes and inserting bars) was performed at the Structures Laboratory of the University of Ottawa.

The holes in the sidewalls, for insertion of longitudinal bars, were made using two different sizes of cutter steel tubes, fixed into a drill. Two special plywood templates were manufactured to align the holes, with dowels made of plywood. Both the plywood templates and the cutter steel tube were designed and prepared in the laboratory. Figure 3.18 illustrates the general view of the tire templates and cutter tubes which were used for two different sizes of reinforcement (No. 20 & 25). Figure 3.19 shows the process of drilling the holes in the sidewalls using the two template and cutter tube. The tires for all columns were inserted through longitudinal bars, on top of each other, with longitudinal bars passing through the sidewalls. Figure 3.20 depicts the procedure of positioning the tires and the longitudinal reinforcement. These columns were confined by the steel in treads, covering the entire exterior surface of column, as well as the steel in the rim, providing hoops to further confine the concrete, while also providing shear reinforcement.

There was no formwork used during column casting. A light frame was built around the columns to help maintain vertical position. A batch of concrete was prepared and delivered to the laboratory by a local ready mix company for casting all the columns at once. A team of students was available to aid in casting. Concrete was cast in layers and vibrated thoroughly to ensure proper placement. The photographs included in Figure 3.21 show column specimens before and after casting.

3.5 Instrumentation

The specimens were instrumented for strain and displacement measurements. Tokyo Sokki strain gauges, model FLA-10-11 with a gauge length of 10 mm were used on longitudinal reinforcement and tires. Each column had six strain gauges attached to the two extreme longitudinal bars (tension and compression sides). Two of the gauges on longitudinal bars were placed at the column-footing interface, one on each extreme bar. Additional two gauges were placed at h/4 distance above and below the column-footing interface (175 mm or 135

mm depending on the size of the column), as shown in Figure 3.22, except for TC-8 and TC-9 with spliced reinforcement which had an extra gauge on each extreme bar at h/2 above the interface and two gauges on each of the extreme starter bars, one at h/2 and the other at h/4. Figure 3.23 depicts the locations of strain gauges on longitudinal reinforcement for lap spliced columns.

A set of strain gauges were placed on tires (on treads and rims) to measure hoop tension. All columns had fifteen gauges attached to treads and rims of the first three tires in each column. The gauge locations on tires are shown in Figure 3.24 and Figure 3.25.

The data obtained from strain gauges were used to obtain strain profiles in longitudinal reinforcement, starter bars and tires. The gauges inside the footing indicate yield penetration into the footing, which helps identify the extension of reinforcement within the footing.

The specimens were also instrumented with transducers to measure lateral displacements and rotations of the hinging region. A total of seven Linear Variable Displacement Transducers (LVDT) and one PT 101 transducer were used in all specimens to measure elongations and/or displacements. Six of these transducers were placed vertically to measure total rotations within the assumed hinging region, as well as the anchorage slip rotation that occurs at the end of the column. The LVDTs labeled as 1 through 6. LVDTs 1 and 2 had 100 mm stroke. LVDTs 3 through 6 had a stroke of 51 mm (2 in). The seventh LVDT was manufactured by Temposonic, and had high precision. This LVDT, PT 101 and the Temposonic were used to measure column horizontal displacement at the point of application of horizontal actuator. This point corresponded to 2500 mm, 2000 mm, 1500 mm, and 1200 mm height above the footing (the shear span of column), depending on the specimen. The horizontal top displacement read during testing was used to impose the pre-determined deformation history. All LVDTs were secured with brackets on six threaded rods that had been cast in column concrete on either side. These three pairs of threaded rods were placed either at 25 mm, 350 mm (h/2), and 700 mm (h) for 700 mm diameter columns; or at 25 mm, 275 mm (h/2), and 550mm (h) for 550 mm diameter columns, above the footing for rotation measurements. LVDTs 1 and 2 were placed to measure the total rotation within the

assumed plastic hinge length (700 or 550 mm, equal to depth of the cross section). LVDTs 3 and 4 were placed at a distance of 350 or 275 mm above the surface, to measure the total rotation within these segments, while LVDTs 5 and 6 were placed only 25 mm above the footing to record the member end rotation due to anchorage slip. LVDTs 1 and 2 were positioned at approximately 50 mm away from the face of the column, LVDTs 3 and 4 were positioned at approximately 100 mm away from the face of the column, and 5 and 6 at 25 mm from column face. The difference between vertical readings of two opposite LVDTs, divided by the distance between the two, gave the rotation of that segment.

The Temposonic and PT 101 were mounted with brackets to a light steel mecano frame, which was constructed using slotted steel angles. This frame was fixed onto the footing by means of twelve screws so that all the readings of displacements were relative to the column footing. The Temposonic and PT 101 had a stroke of ± 250 mm and ± 320 mm, respectively. Figure 3.26 and Figure 3.27 illustrate the locations of LVDTs and a photographic view of instrumentation on a typical column specimen.

The loads were measured by means of load cells contained in the MTS actuators. The data were recorded using a Vishey data acquisition system which was connected to a PC, and the MTS controller which was connected to a second PC. Figure 3.28 illustrates the schematic network diagram for the data acquisition system, and the MTS controller device.

3.6 Description of Test Setup

The columns were tested under constant axial compression and incrementally increasing lateral displacement reversals, simulating seismic loading. This type of loading necessitated a loading system in which vertical and horizontal actuators could be controlled separately. Three servo-controlled MTS hydraulic actuators and a steel loading beam assembly were used to apply the loading. Each MTS actuator had a load capacity of 1000 kN in compression and tension. The hydraulic pressure for the MTS actuators was provided by a 33 GPM gear driven pump, and was controlled by an MTS servo-valve to apply the required load. The maximum stroke of the actuator was 500 mm, which allowed ± 250 mm relative to

the neutral position. The actuators were equipped with multi directional swivels at the ends. These swivels eliminated the risk of damage to the actuators due to any accidental eccentricity and/or force component that may be developed perpendicular to their axis. Figure 3.29 shows the overall geometry of a typical MTS actuator.

A single MTS actuator was used to apply the horizontal force reversals. The actuator was first positioned horizontally, and attached to the steel loading beam that had been bolted on the column. A pair of steel A-frames was used to support the horizontal actuator. The A-frames were bolted on three pairs of C-channels. These channels were placed back-to-back and secured to the laboratory strong floor by means of 1800mm long, and 64 mm diameter Grade 400 MPa bolts. The actuator ends were connected using grade 8 high-strength bolts, which were 400 mm long and 38 mm in diameter. Figure 3.30 and Figure 3.31 describe the details of the horizontal load setup. The maximum force applied by the horizontal actuator during testing was 458 kN, which was applied to Column TC-11.

The vertical load setup consisted of two MTS actuators and a steel loading beam assembly which also contained two different heights of concrete spacer blocks depending on the height of the specimen. The actuators were placed vertically on either side of the column as shown in Figure 3.32. The top ends were connected to the loading beam assembly, and the bottom ends were attached to the column footing, using high strength bolts.

The loading beam assembly consisted of two parts. The upper part was a built-up box section beam, which was attached to the vertical actuators by means of 400 mm long, 38 mm diameter Grade 8 bolts. The bottom part was a built-up I section spacer block, which was used to connect the horizontal actuator to the column specimen. Because the vertical actuators rested on top of the column footing, an additional two reinforced concrete spacer was necessary to allow for full height of actuators. The spacer block was connected to the built-up box section beam from the top, and to the built-up I section spacer block from the bottom by means of eight 25 mm diameter, 100 mm long grade 8 bolts. The details of the loading beam assembly and the concrete spacer block are illustrated in Figure 3.33.

3.6.1 *Lateral Restraints*

A pair of steel frames, made out of hollow steel sections, was positioned on either side of a test column to provide lateral bracing and additional safety against unexpected out-of -plane failure at high inelastic deformations. The frames were secured to the laboratory strong floor and connected to each other at the top by two hollow section steel box beams. Clear views of the lateral restraint frames are shown in Figure 3.34.

3.7 *Test Procedure and Loading Program*

The first step in the test procedure was to position the specimen in the test area. The 10-ton overhead crane of the Structures Laboratory was used for this purpose. The column footing was then fixed to the laboratory strong floor by means of four bolts. The vertical actuators were attached to the footing on either side of the column to apply constant axial compression throughout the test. The loading beam assembly, including the reinforced concrete spacer block, was subsequently attached to the column. The actuator ends were bolted to the bottom flange of the loading beam. The horizontal actuator was then positioned and connected to the web of the spacer block. Finally the strain gauges and LVDTs were connected to the data acquisition system, and calibrated and initialized for data collection.

Tests started by applying the required level of axial compression. Two levels of axial load were applied; 10% or 16% of column concentric capacity P_0. The axial load was kept at the same level for the entire duration of test. All Columns were tested under either 1900 kN or 1954 kN of axial compression (corresponding to 10% or 16% of P_0). This force level represents the level of axial load expected for bridge columns which usually vary between (10% to 15%) and corresponded to the maximum capacity of the actuators, where,

$$P_0 = 0.85 f_c^{'}(A_g - A_s) + f_y A_s \tag{3.1}$$

The horizontal load was then applied in displacement control mode, following a loading program that consisted of incrementally increasing inelastic displacement reversals.

Displacement levels were expressed in terms of lateral drift ratio. The drift ratio was defined as the ratio of column top deflection to column height. Figure 3.35 illustrates the loading program followed for lateral displacements. Every column was subjected to three full elastic cycles at approximately 0.5% drift ratio. The drift level was increased incrementally to 1.0%, 2.0%, 3.0%, etc. until failure. The drift level of 1% corresponded approximately to the yield displacement. Three deformation cycles were applied at each drift level. Total duration of a typical test was about three to four hours and some of the columns took five hours, depending on the deformability of the column. The duration of loading per cycle was approximately 6-8 minutes. Testing continued until the lateral load resistance of the column dropped by at least 20% of the peak load.

Table 3.1: Properties of Test Specimens

Label	Type	Shear Span (mm)	Diam. D (mm)	Tire Size (inch)	Long. Reinforcement		Axial Load	
					Reinforcement Arrangement	f_y (MPa)	P (kN)	P / P_o
TC-7	Flexure	2500	700	16	12 No. 25	460	1900	10%
TC-8	Spliced	2500	700	15	12 No. 25	460	1900	10%
TC-9	Spliced	2000	550	14	12 No. 20	467	1950	16%
TC-10	Shear	1200	550	14	12 No. 20	467	1950	16%
TC-11	Shear	1500	700	15	12 No. 25	460	1900	10%
TC-12	Shear	1200	550	13	12 No. 20	467	1950	16%

Table 3.2: Development of Concrete Compressive Strength with Time

Time (days)	Average Compressive Strength (MPa)
7	34
14	42
21	44
28	45

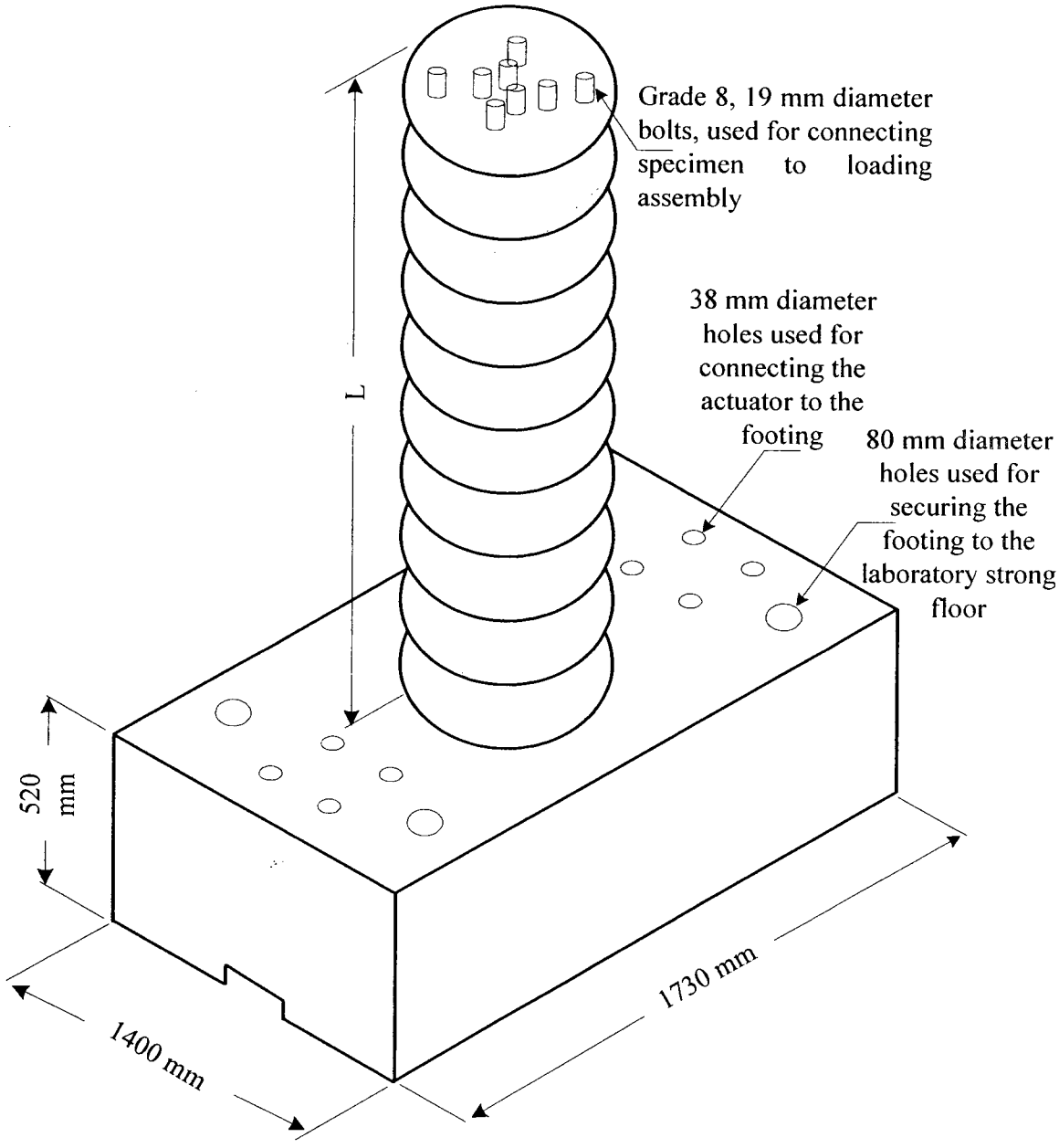

Figure 3.1: Geometry of a Typical Specimen

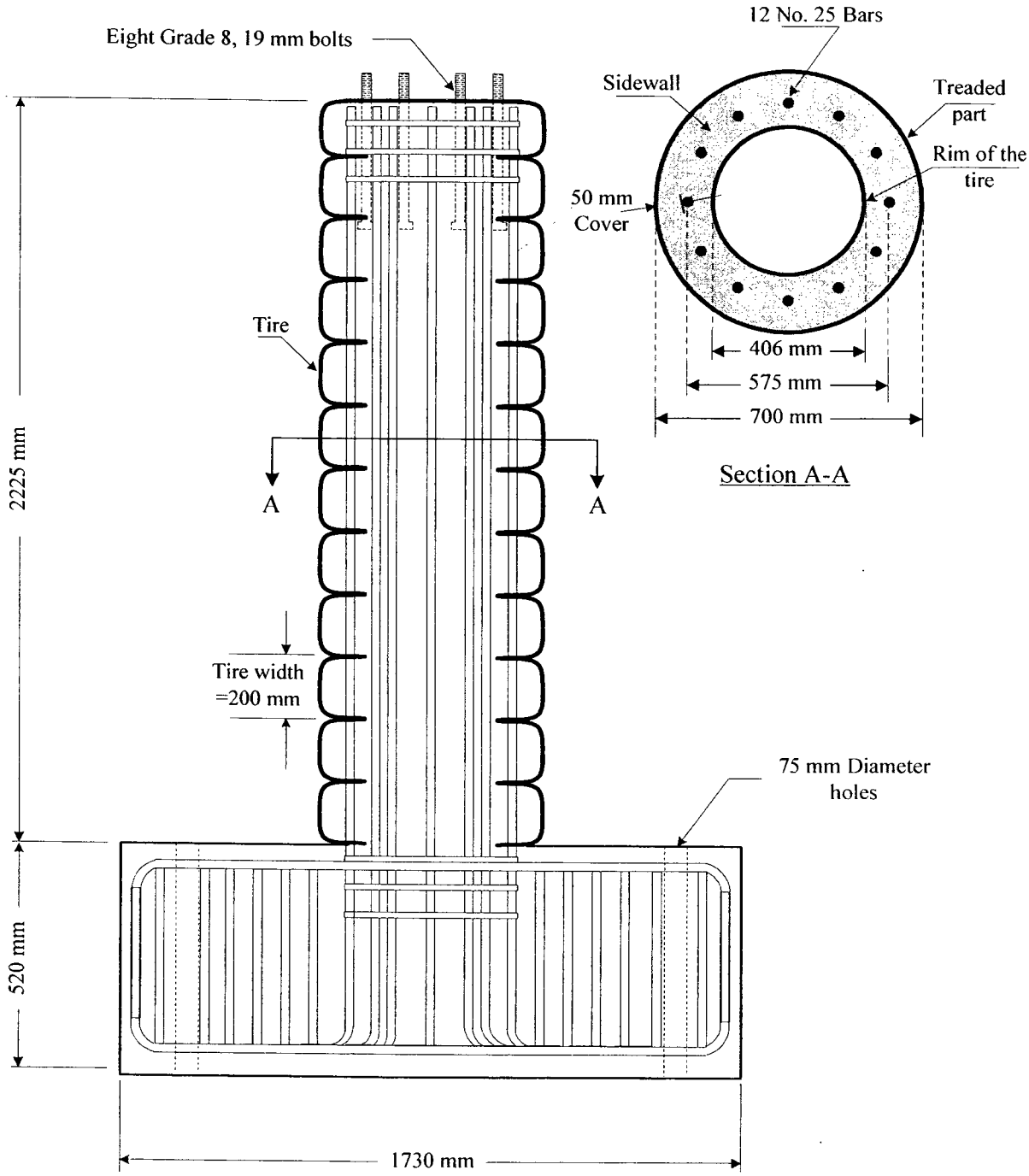

(a) Column TC-7

Figure 3.2: Reinforcement Details for Columns TC-7, TC-8, and TC-11

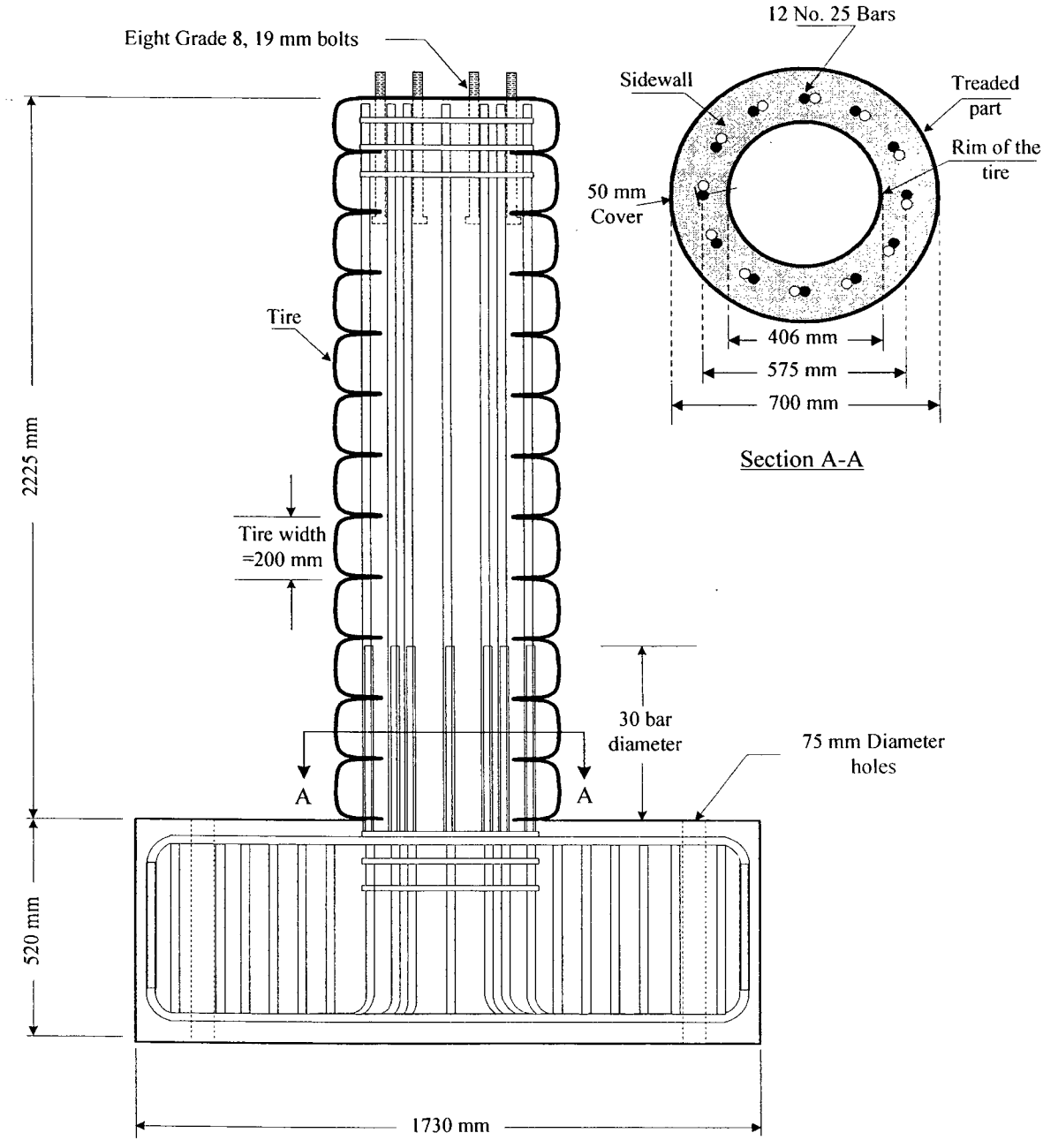

(b) Columns TC-8

Figure 3.2 (Cont'd): Reinforcement Details for Columns TC-7, TC-8, and TC-11

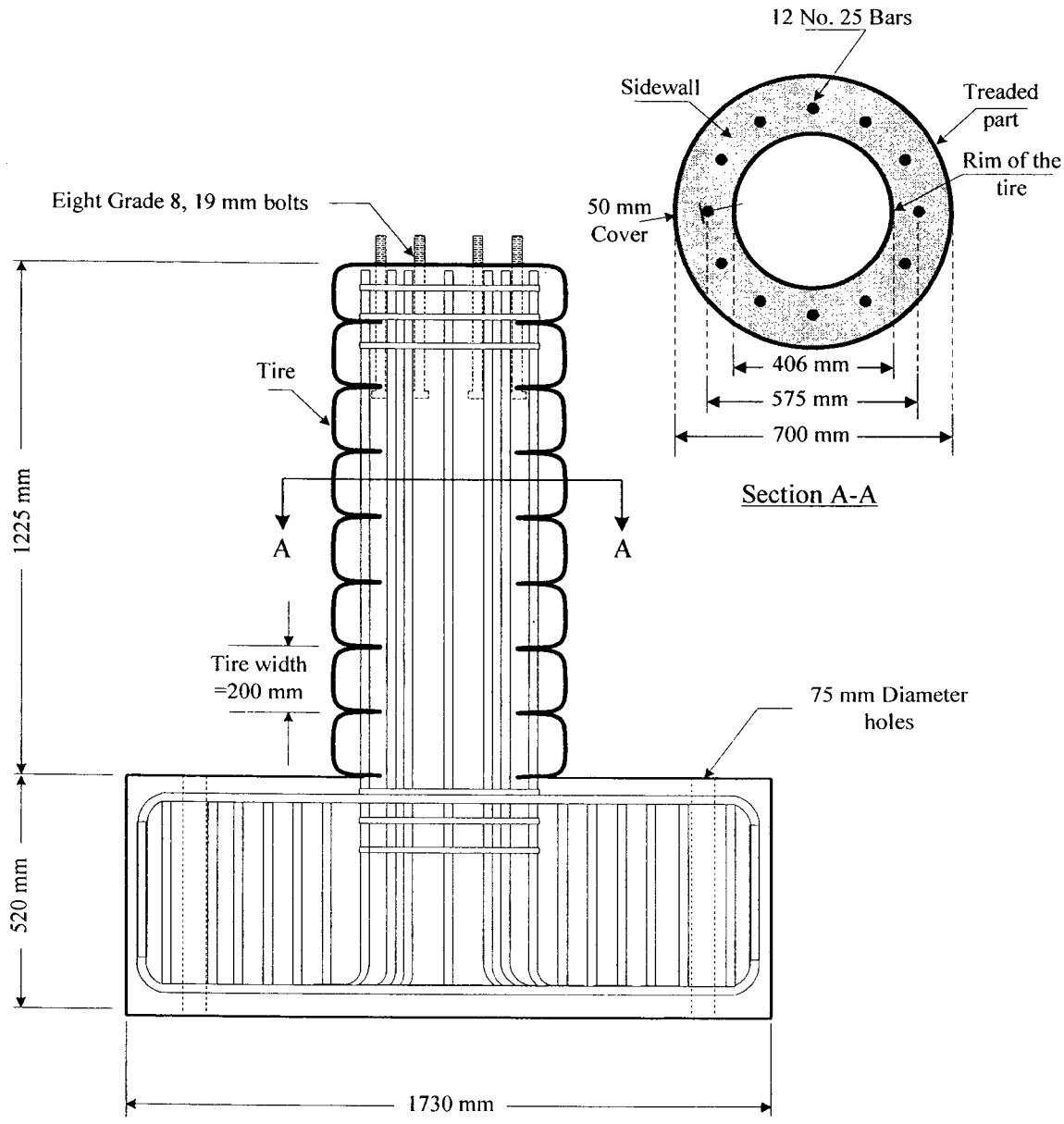

(c) Columns TC-11

Figure 3.2 (Cont'd): Reinforcement Details for Columns TC-7, TC-8, and TC-11

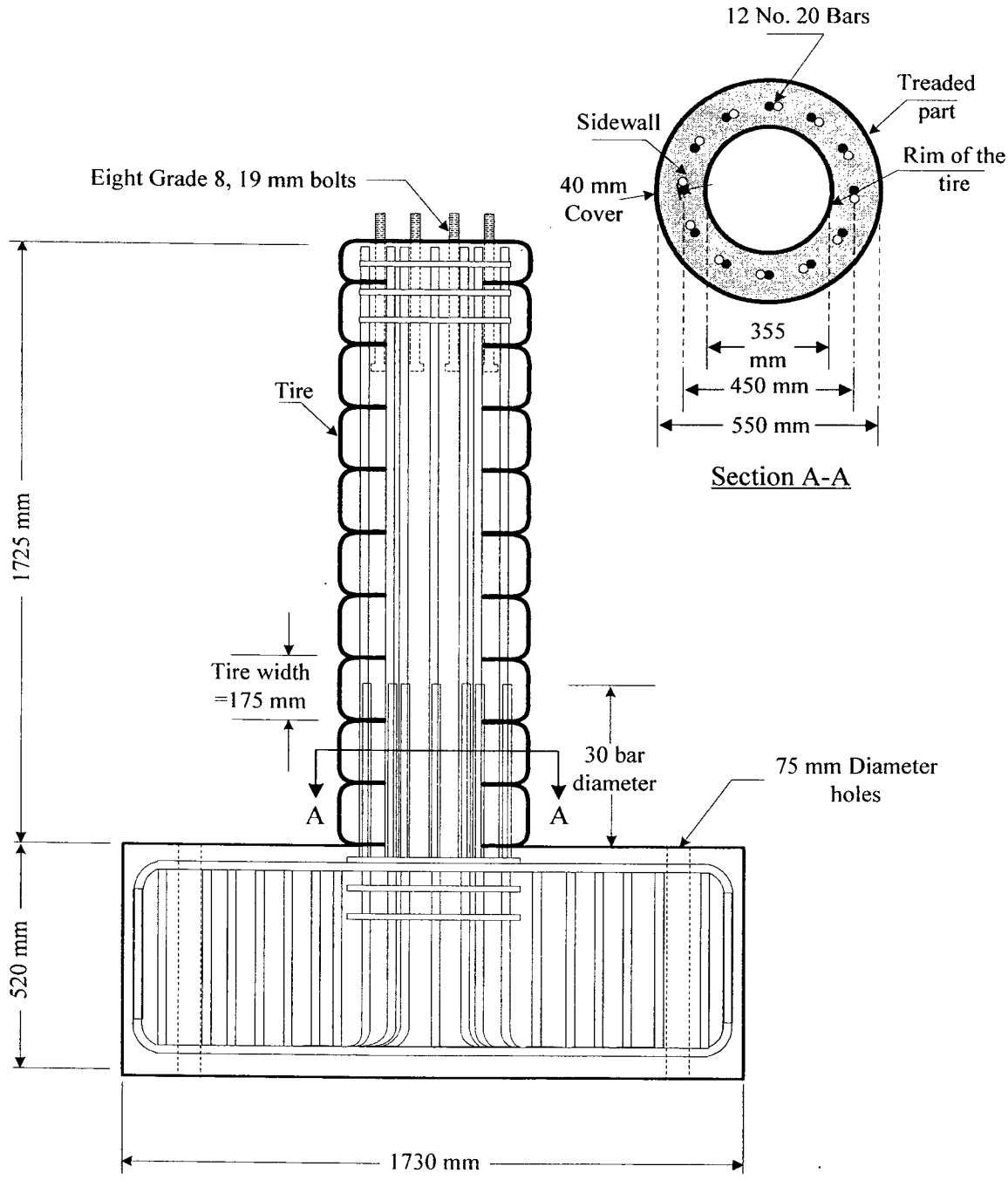

(a) Columns TC-9

Figure 3.3: Reinforcement Details for Columns TC-9, TC-10, and TC-12

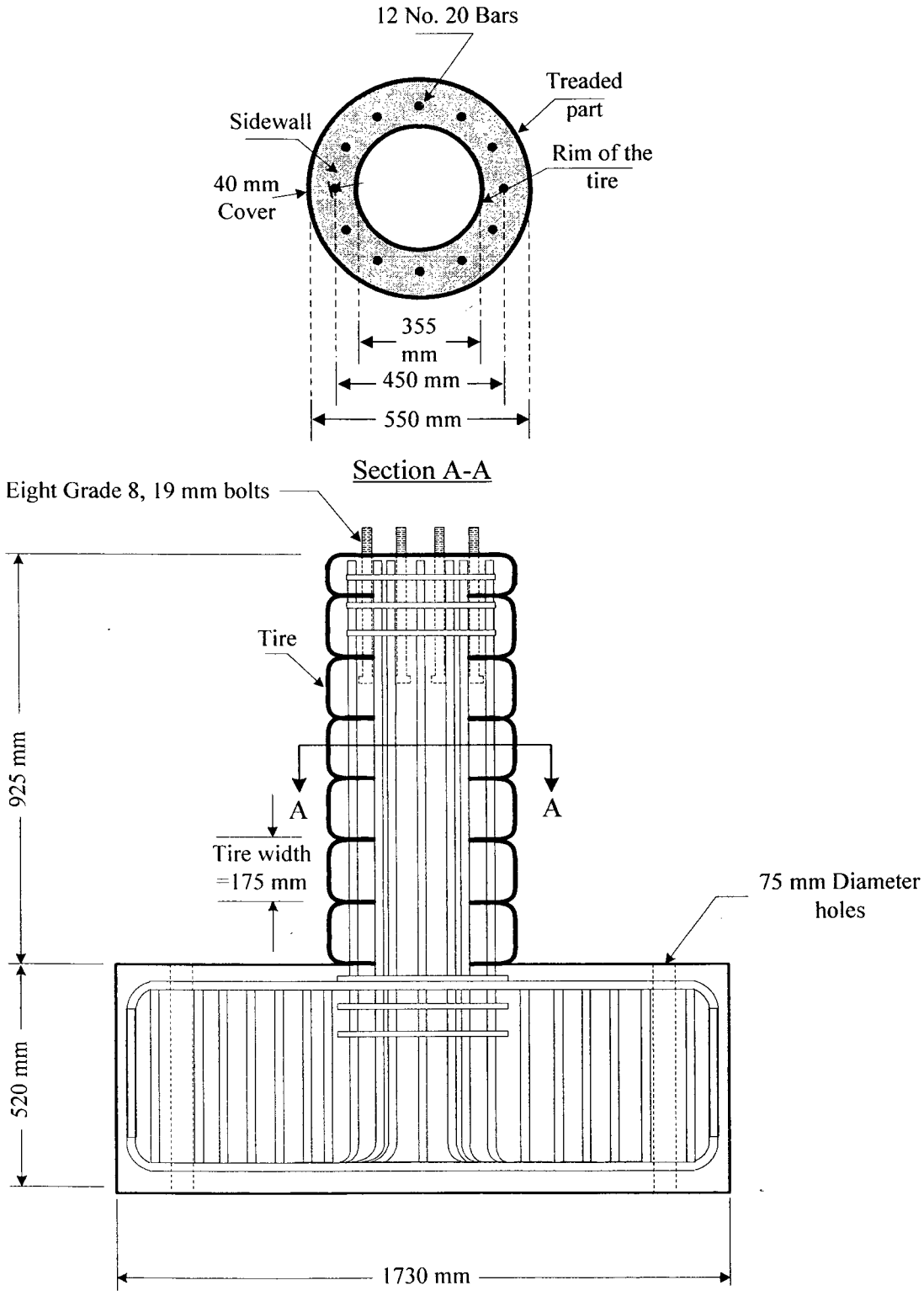

(b) Columns TC-10 and TC-12

Figure 3.3 (Cont'd): Reinforcement Details for Columns TC-9, TC-10, and TC-12

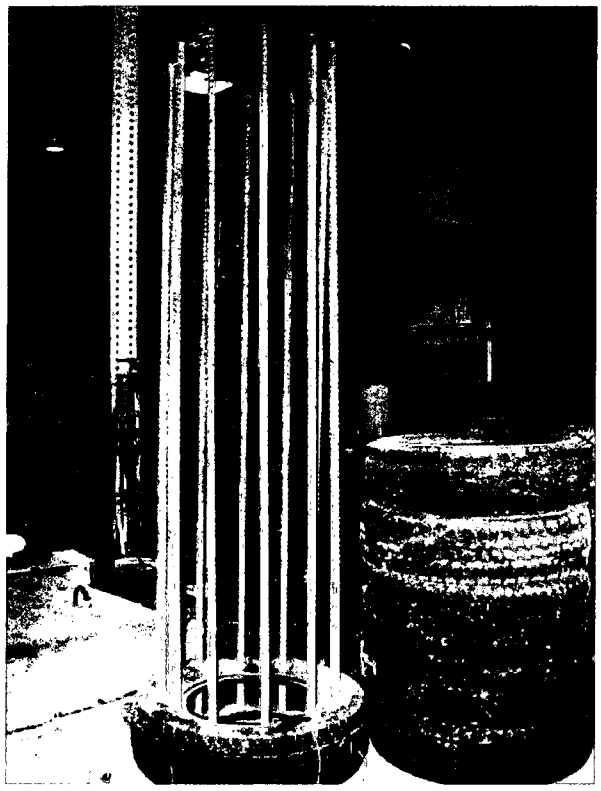

(a) TC-7

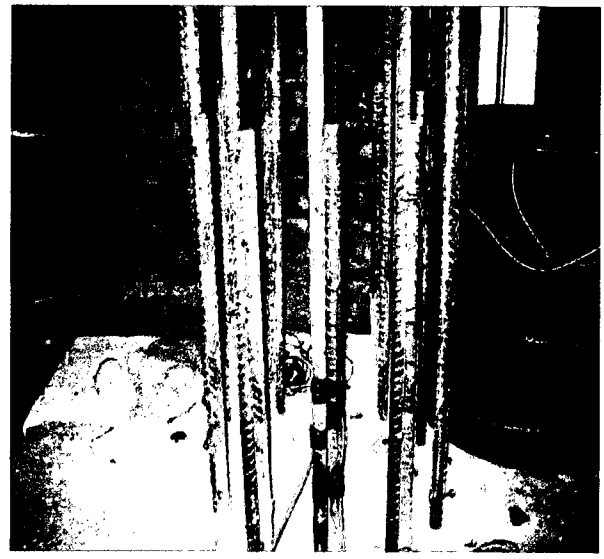

(b) TC-8

(c) TC-11

Figure 3.4: Construction of Column Cages for TC-7, TC-8, and TC-11

TC-9

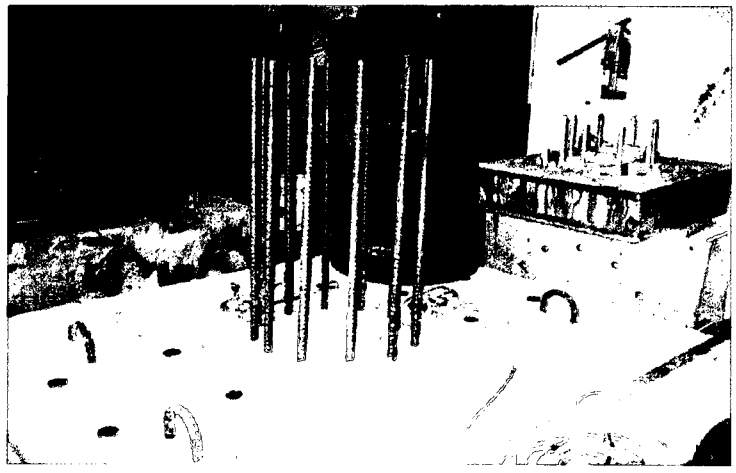

TC-10

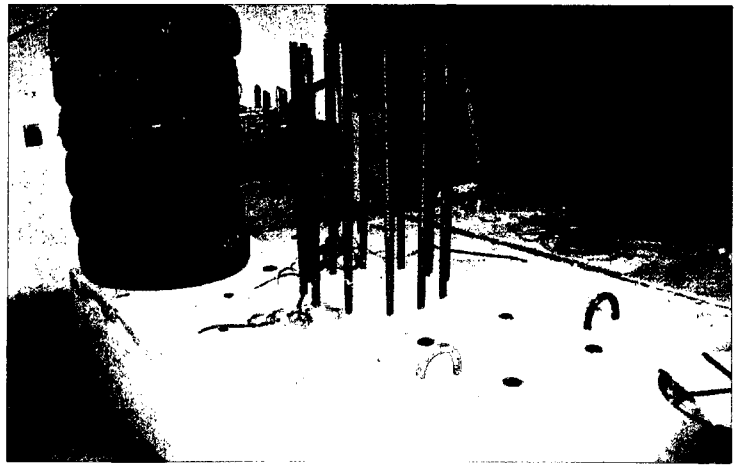

TC-12

Figure 3.5: Construction of Column Cages for TC-9, TC-10, and TC-12

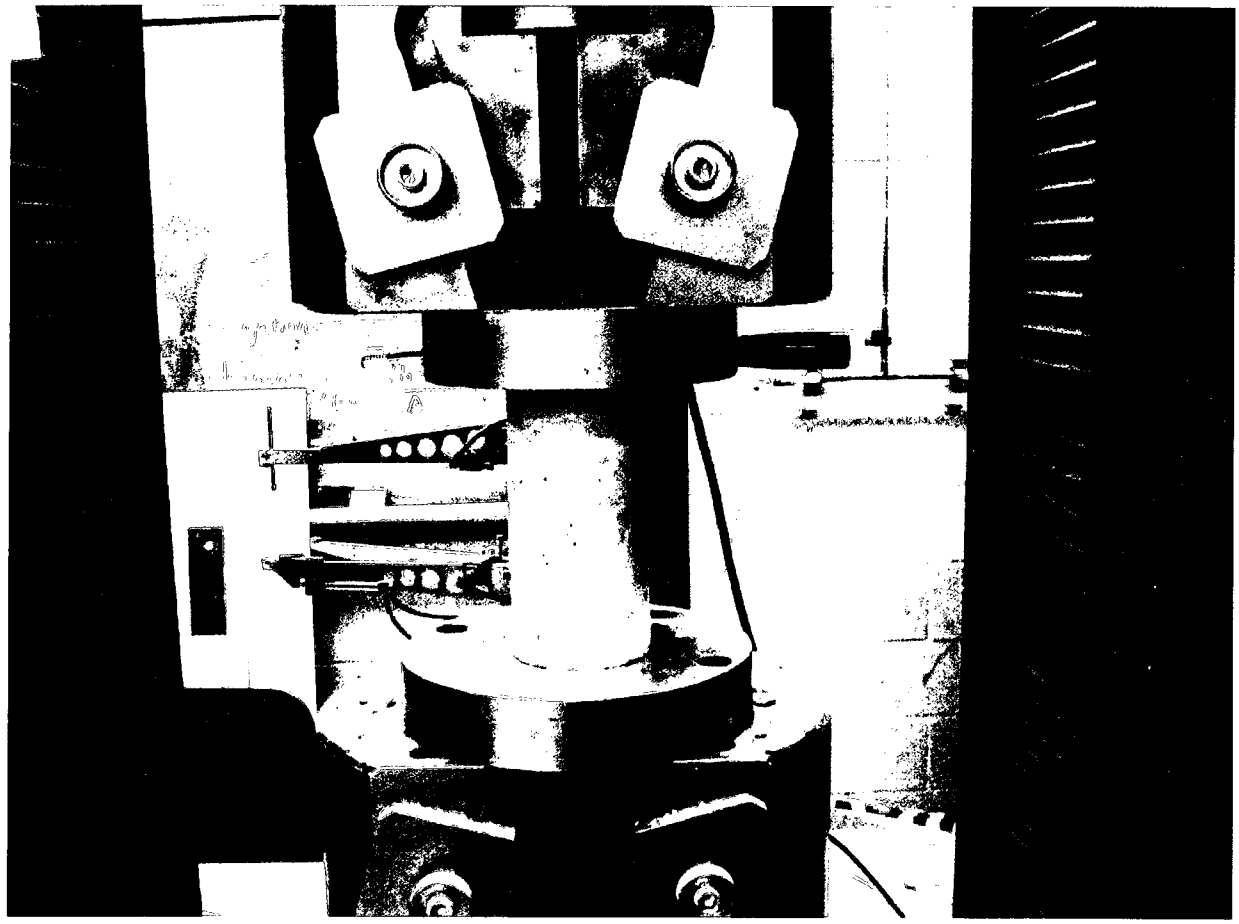

(a) Testing of Cylinder on a Galdabini Universal Testing Machine

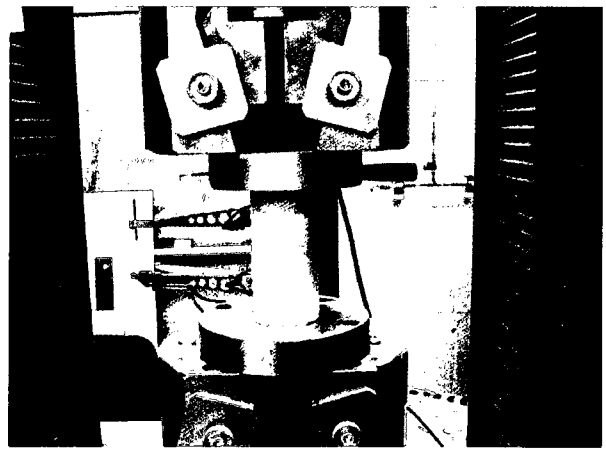

(b) Cylinder before Testing

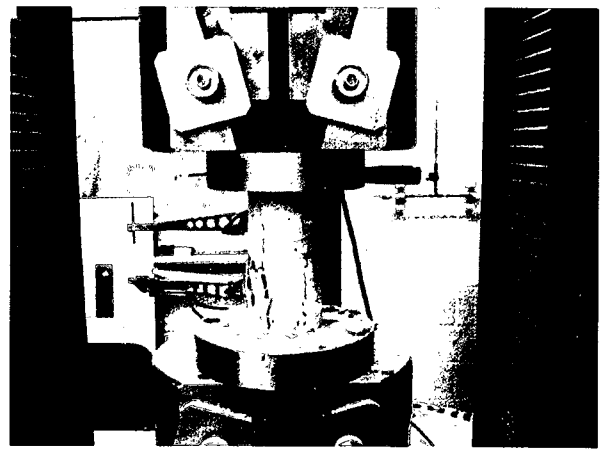

(c) Cylinder after Testing

Figure 3.6: Instrumentation and Testing of Standard Concrete Cylinders

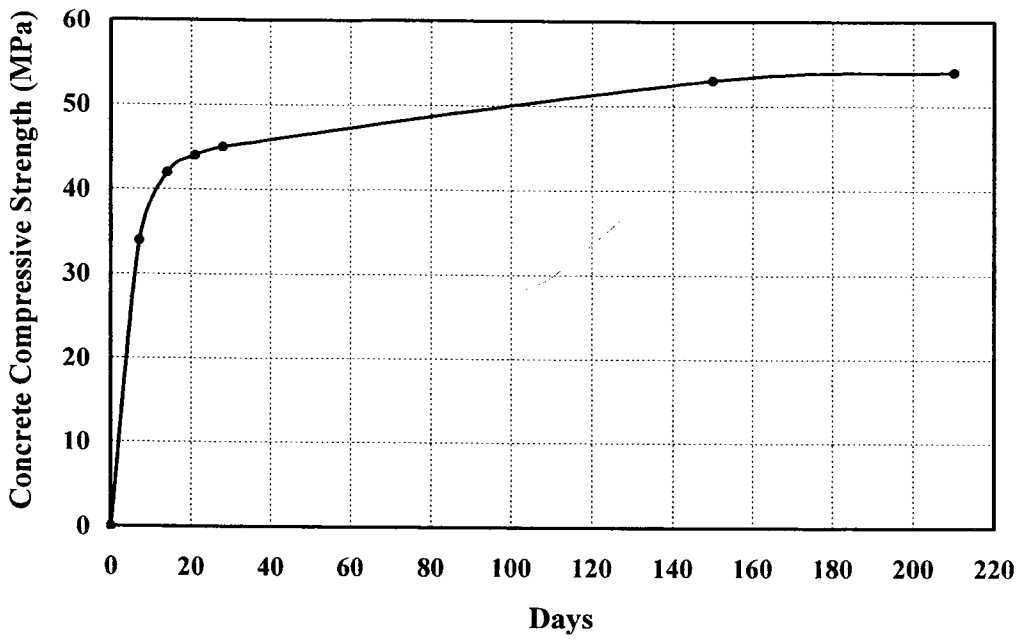

Figure 3.7: Development of Concrete Strength with Time

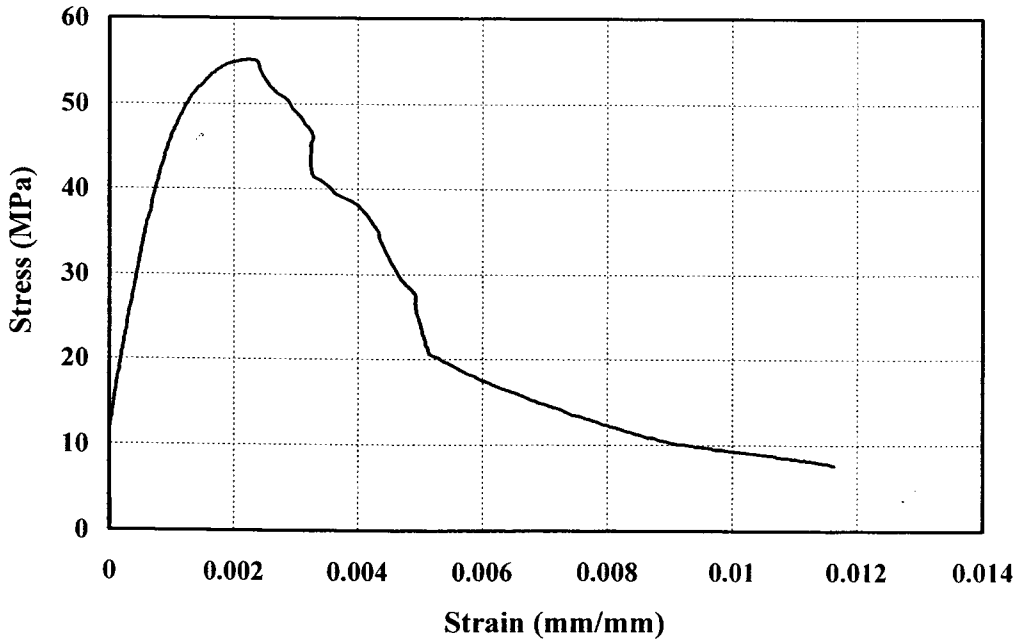

Figure 3.8: Stress-Strain Relationship for Column Concrete

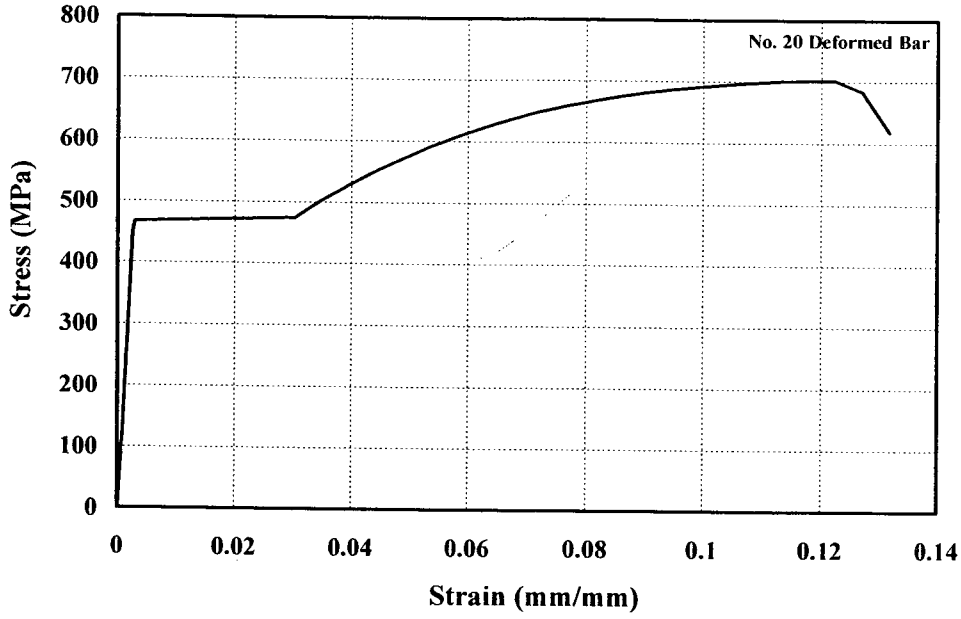

(a) No. 20 Longitudinal Reinforcement used in Columns TC-9, TC-10, and TC-12

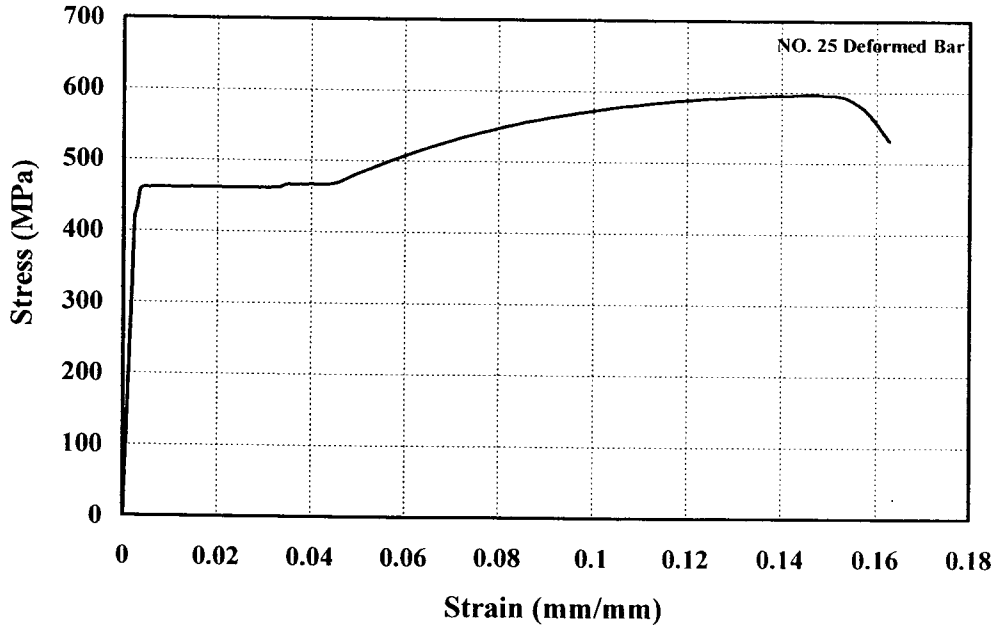

(b) No. 25 Longitudinal Reinforcement used in Columns TC-7, TC-8, and TC-11

Figure 3.9: Stress-Strain Relationships of Deformed Longitudinal Reinforcement

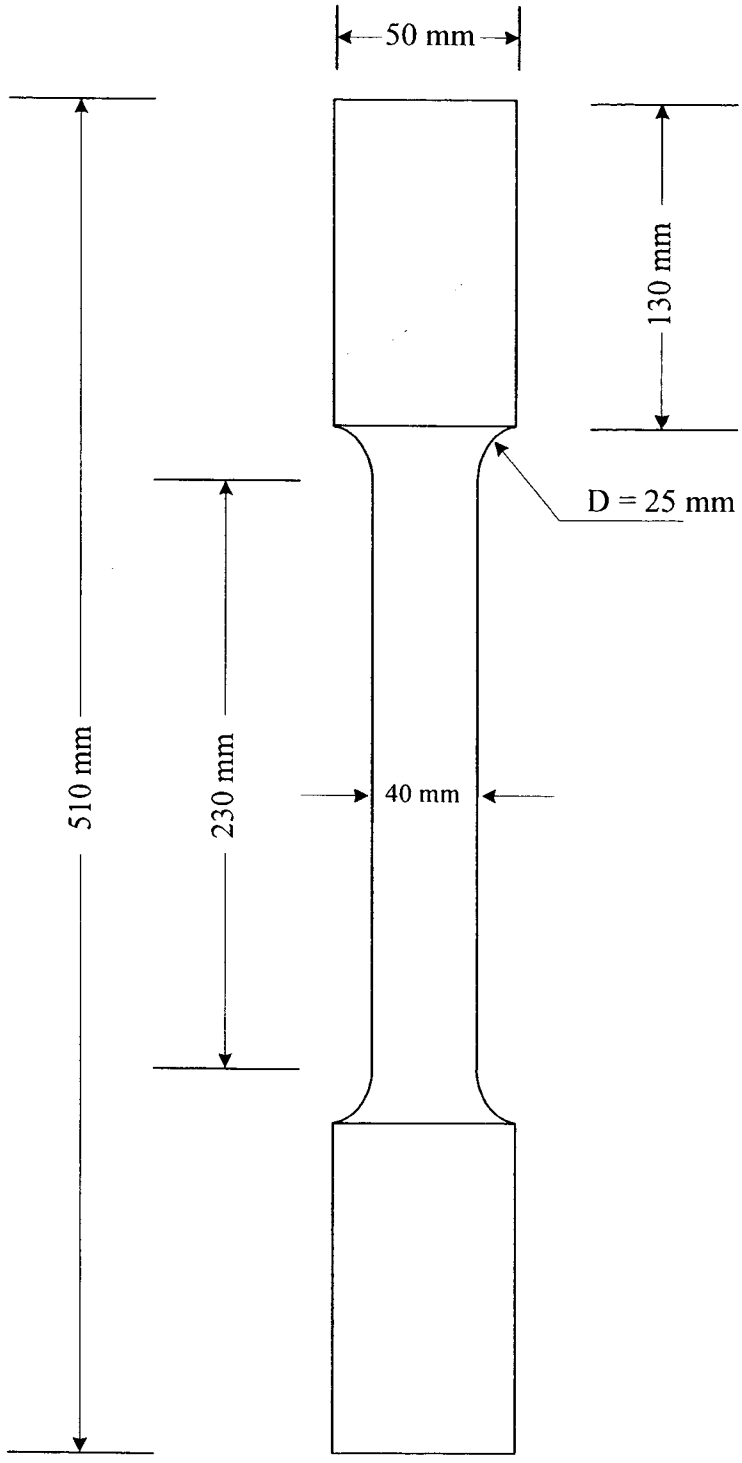

Figure 3.10: Geometry of a Typical Tire Coupon

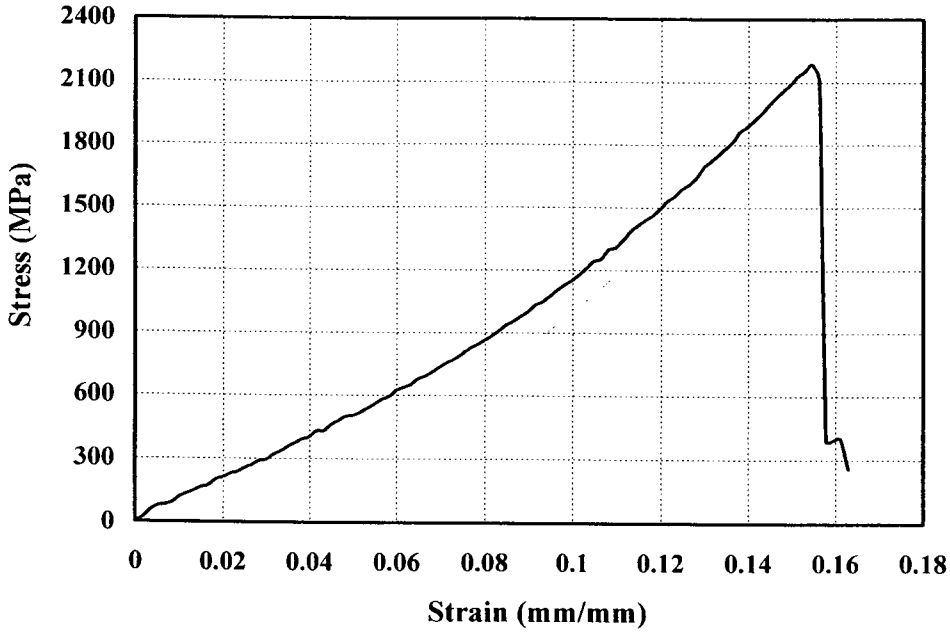

a) Stress-Strain Relationships for Good Year Tire (TC-7)

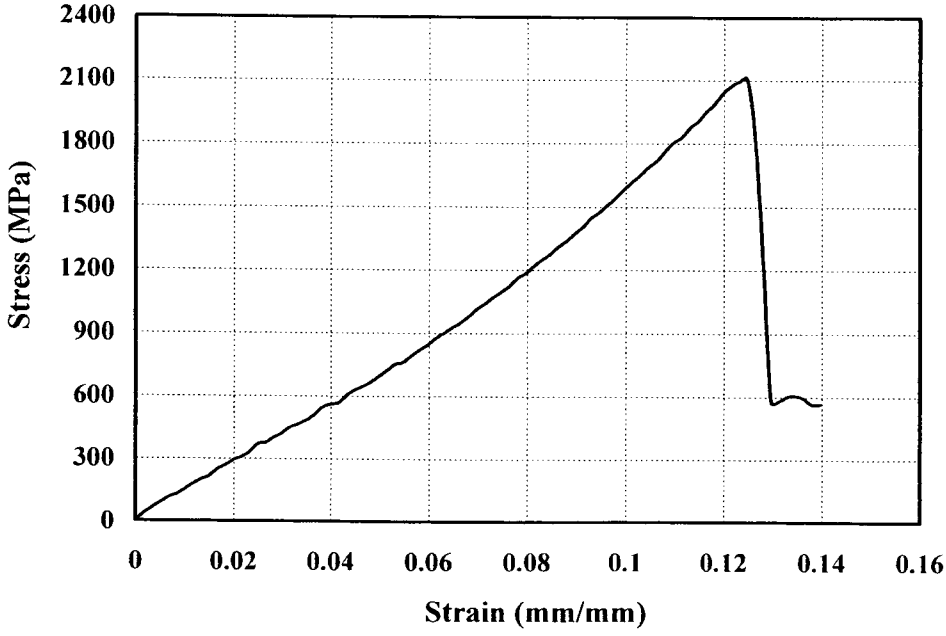

b) Stress-Strain Relationships for Michelin Tire (TC-8)

Figure 3.11: Stress-Strain Relationships of Different Brand Names of Tires Established Through Coupon Tests

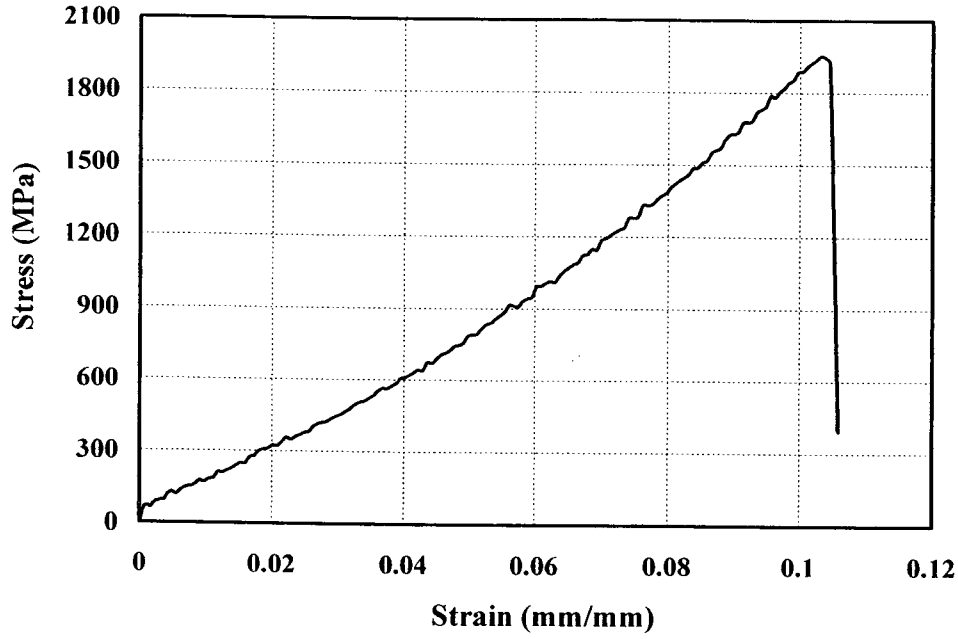

c) Stress-Strain Relationships for Firestone Tire (TC-9)

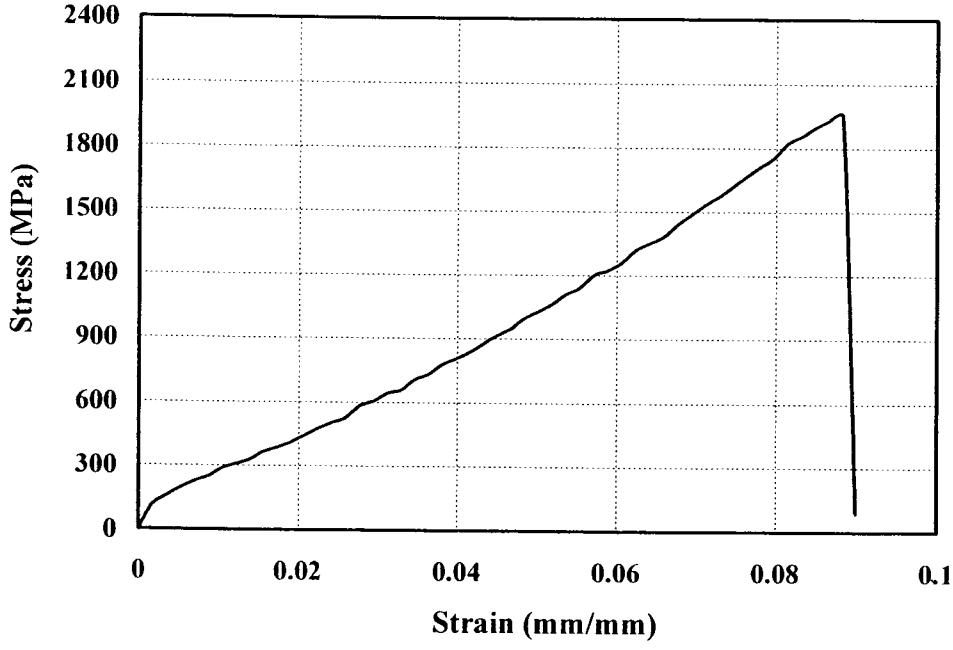

d) Stress-Strain Relationships for Yokohama Tire (TC-12)

Figure 3.11 (Cont'd): Stress-Strain Relationships for Different Brand Names of Tires Established Through Coupon Tests

(a) Overall View of Tire Coupons

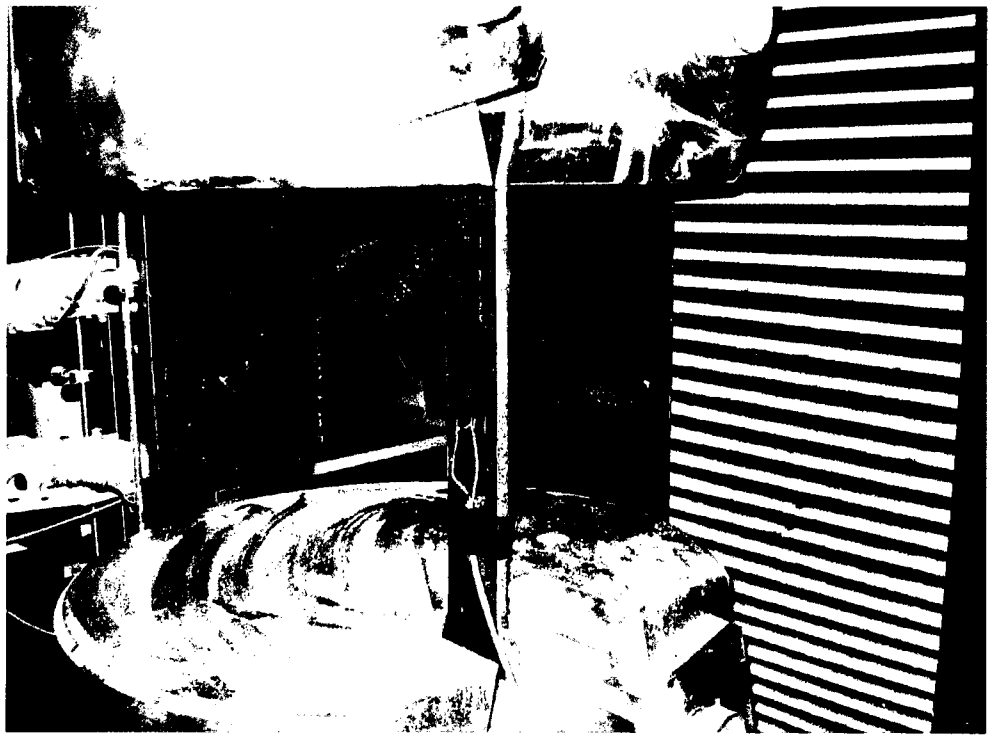

(b) A Tire Coupon Test by a Galdabini Universal Testing Machine

Figure 3.12: General View and Test Setup of a Standard Tire Coupon

Figure 3.13: Typical Tire Coupons during Tension Tests

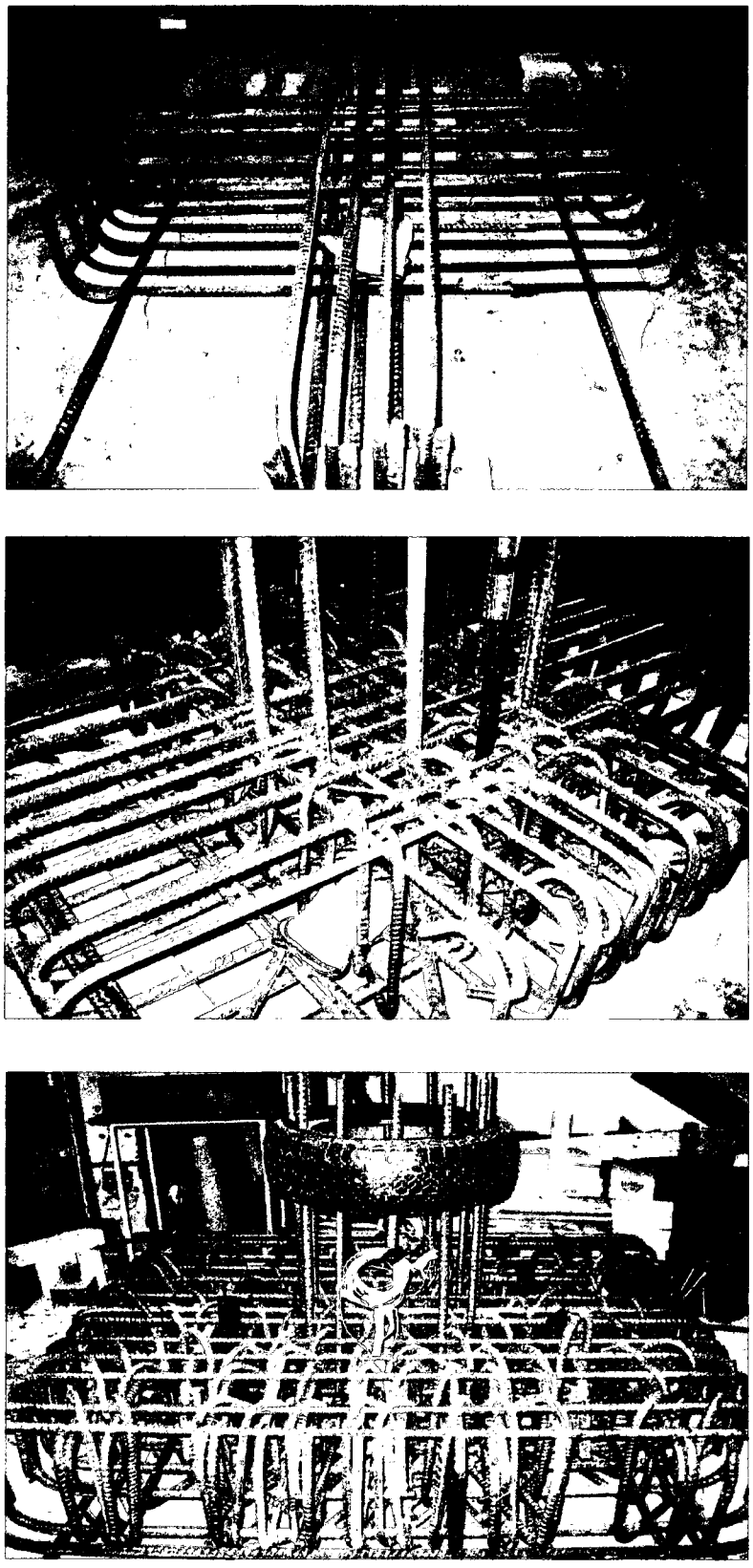

Figure 3.14: Assembly of a Typical Footing Reinforcement Cage

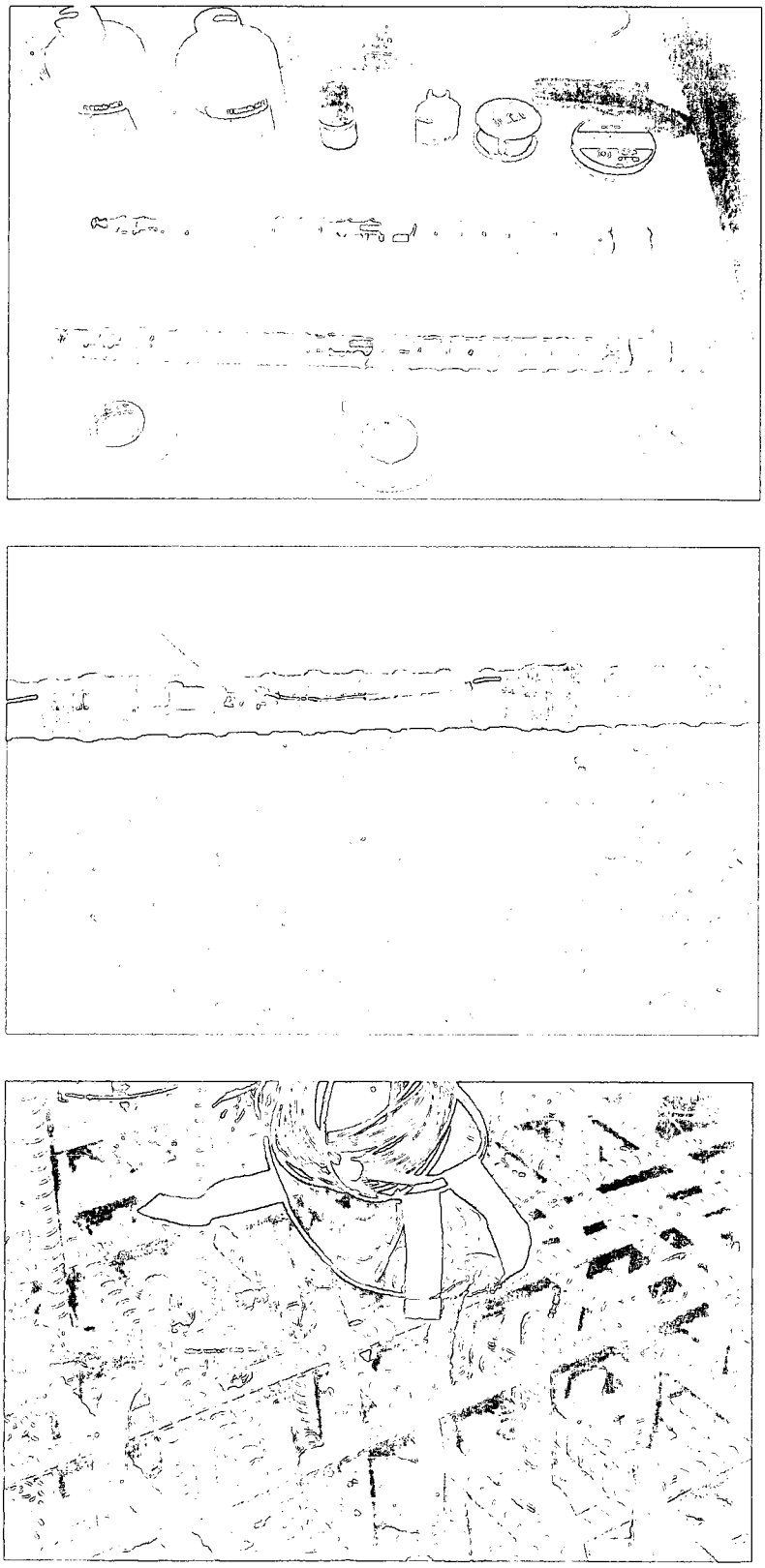

Figure 3.15: Strain Gauges and Wiring on Completed Reinforcement Cages

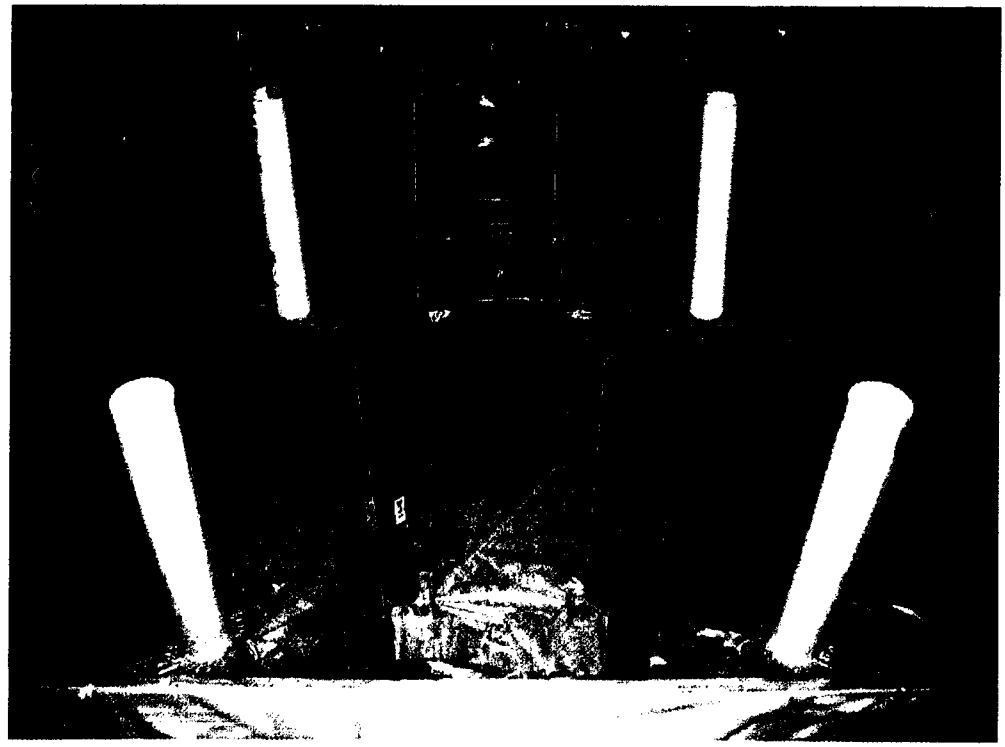

(a) Formwork Prior to Placement of Reinforcement Cage

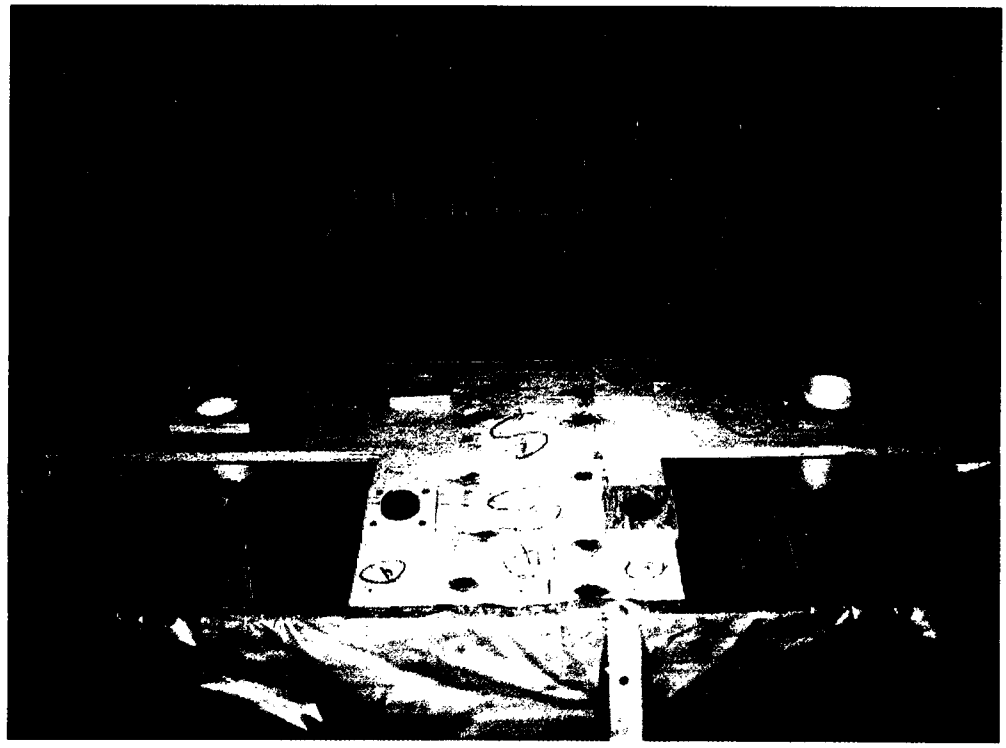

(b) Reinforcement Cage inside Formwork

Figure 3.16: Placement of Reinforcement Cages in Formwork

(a) Footings Shortly Before Casting

(b) Footings at Completion

Figure 3.17: Casting of Concrete Footings

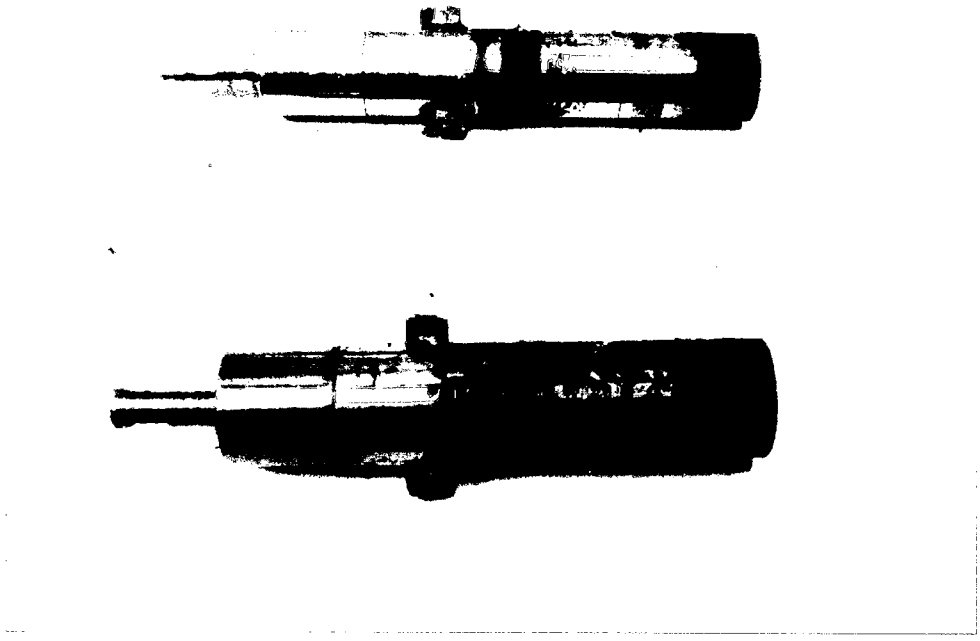

(a) Top View of Cutter Tubes (20 mm and 25 mm)

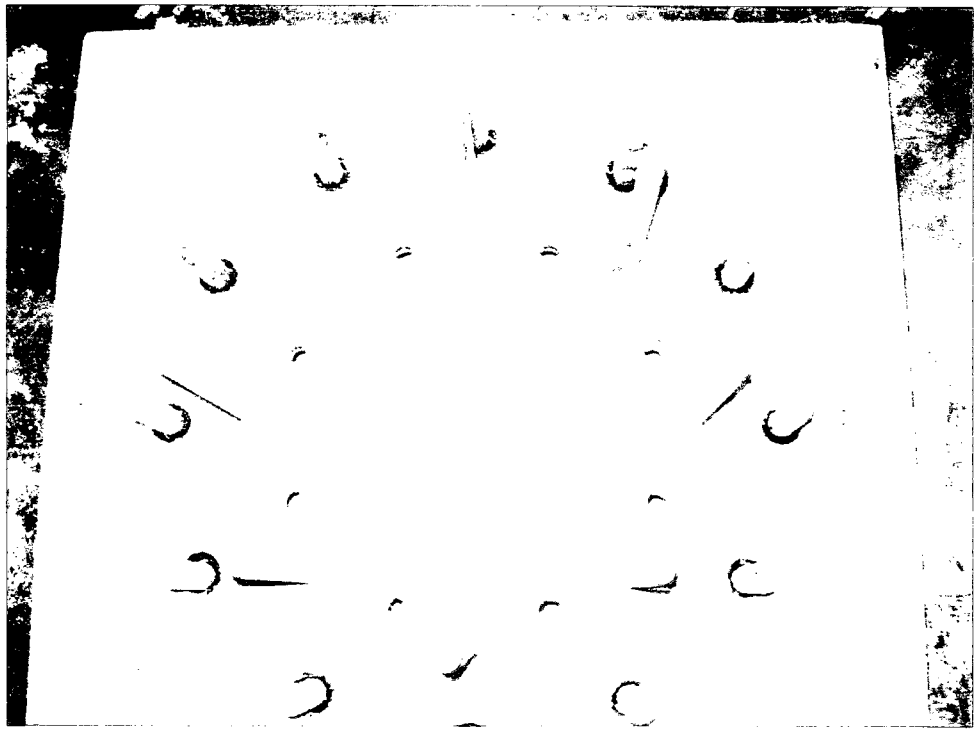

(b) Top View of Tire Template used for Columns TC-7, TC-8, and TC-11

Figure 3.18: General Views of Tire Templates and Cutter Tubes

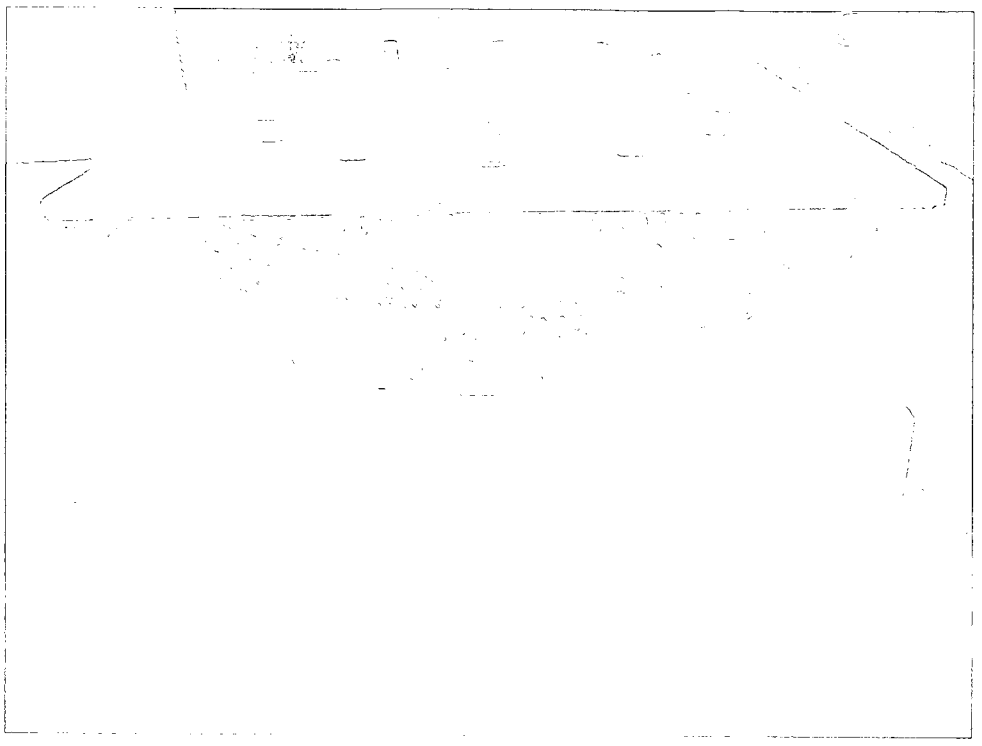

(a) Front View of Tire inside the Template (15" or 16" Tires)

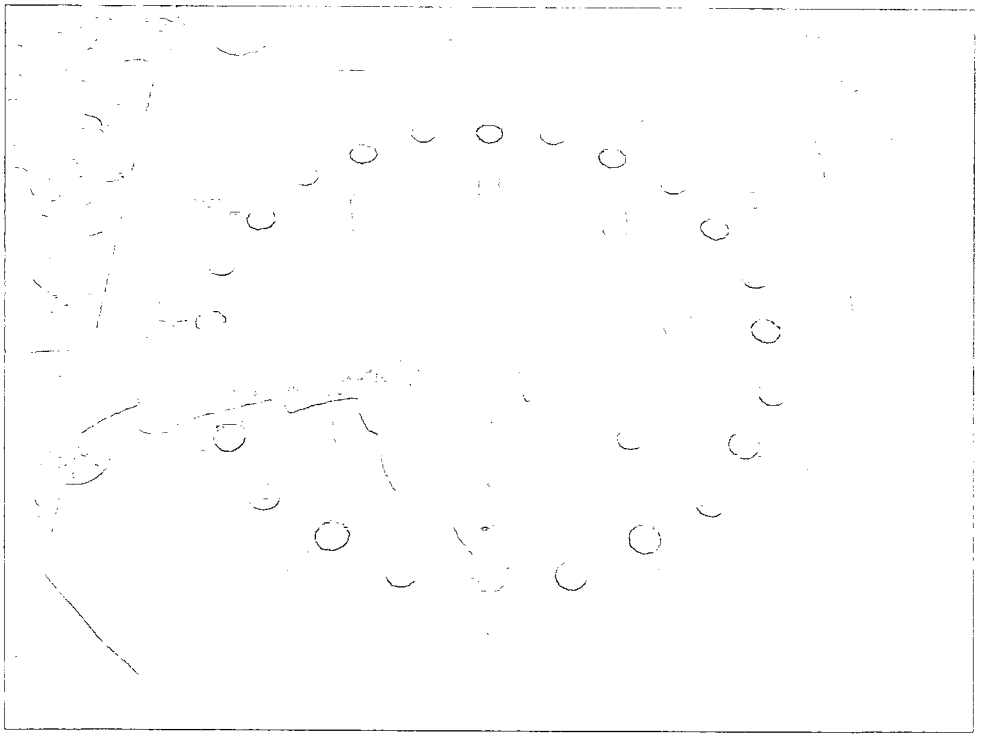

(b) Drilling of Holes in a Tire (13" and 14" Tires)

Figure 3.19: Tire Hole Fabrication

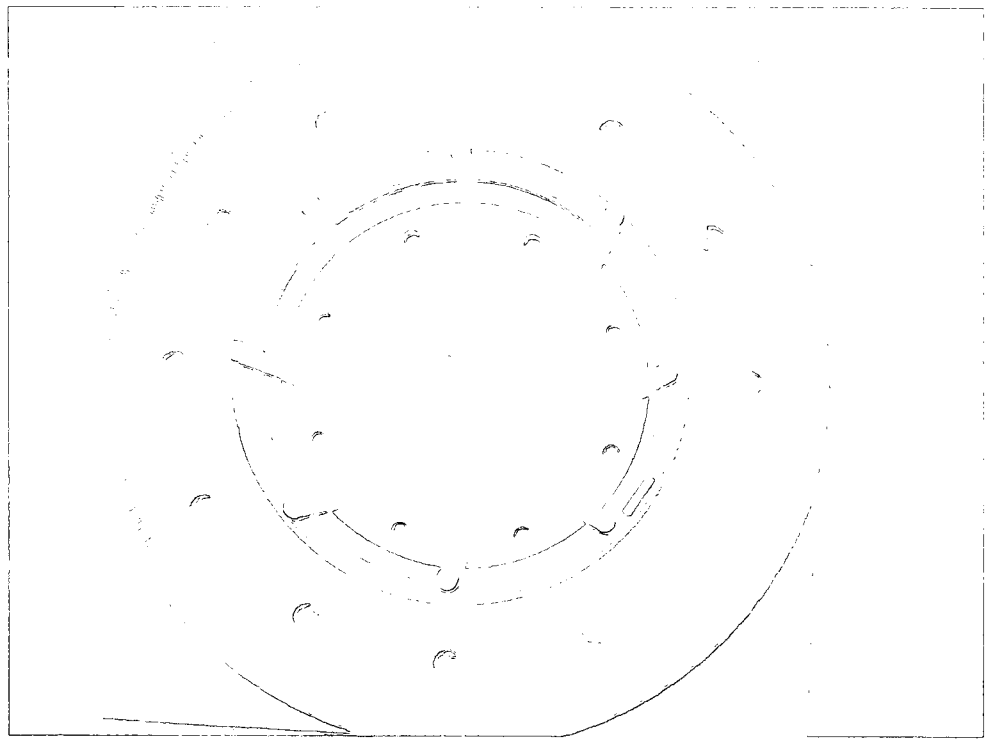

(c) Top View of Tire inside the Template (15" or 16" Tires)

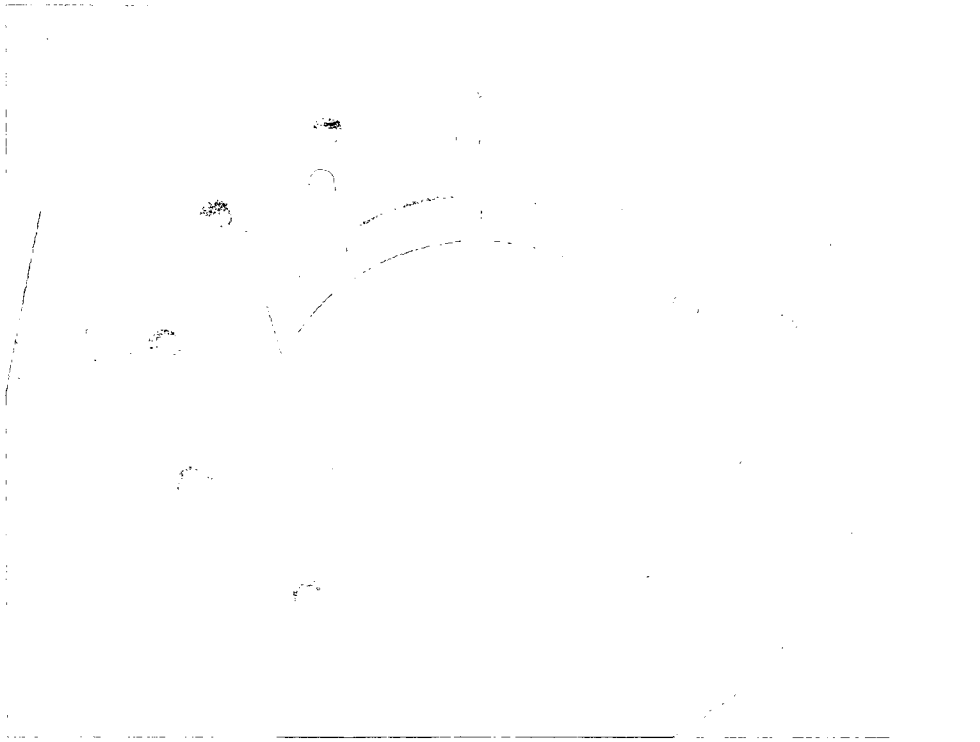

(d) Top View of Tire inside the Template (13" or 14" Tires)

Figure 3.19 (Cont'd): Tire Hole Fabrication

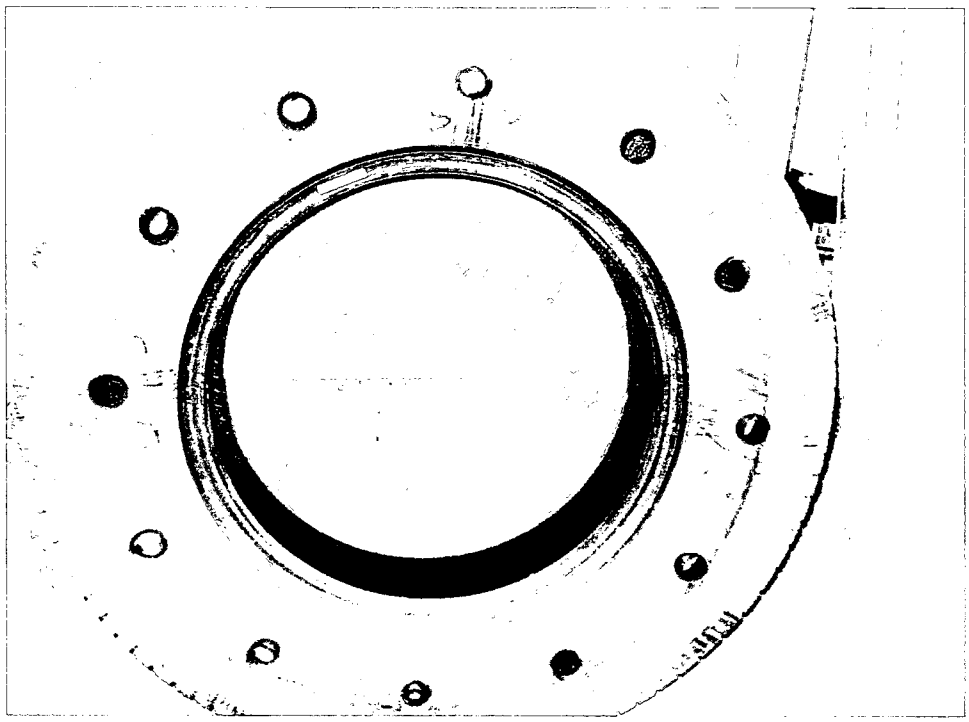

(e) Front View of a Tire after Drilling of the Holes (16" Tire)

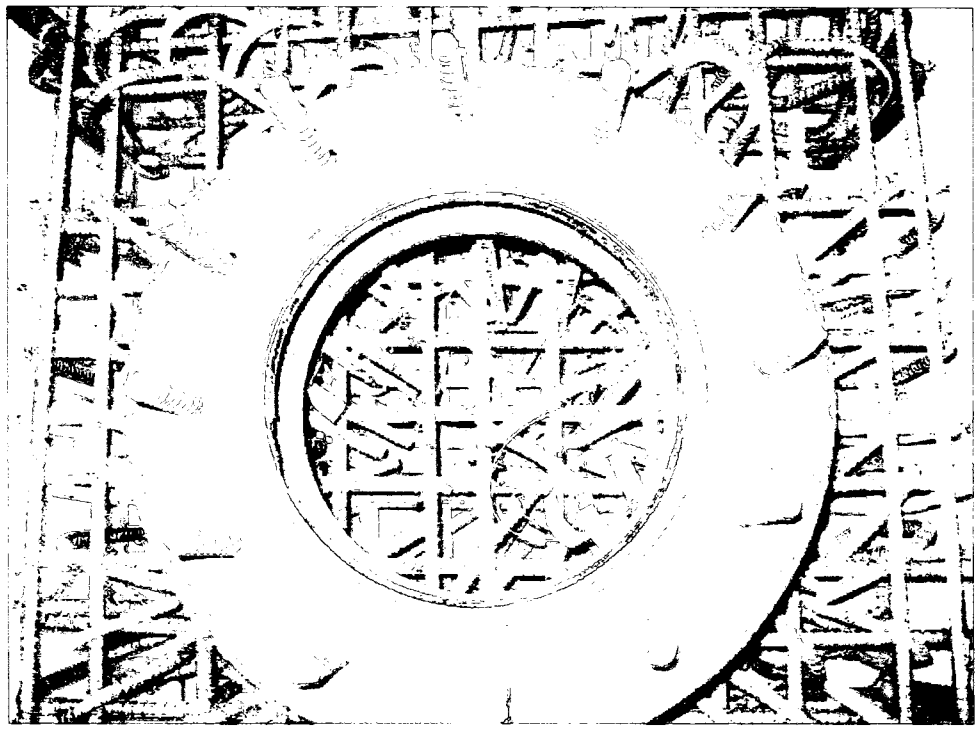

(f) Insertion of Re-Bars through Pre-Drilled Holes (13" Tire)

Figure 3.19 (Cont'd): Tire Hole Fabrication

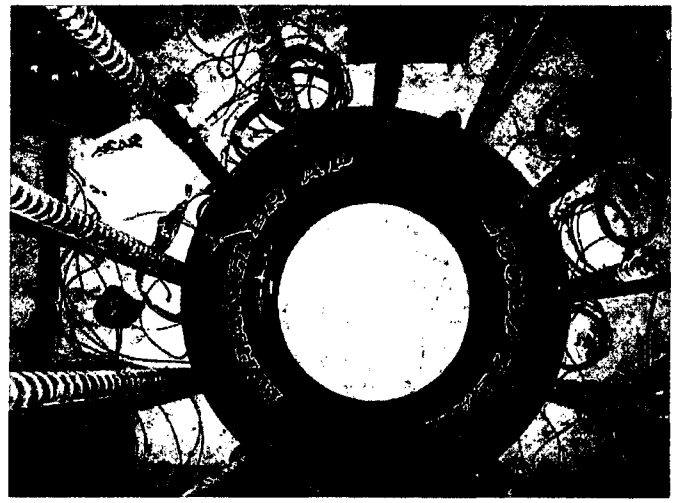

(a) Placement of the First Tire in TC-7

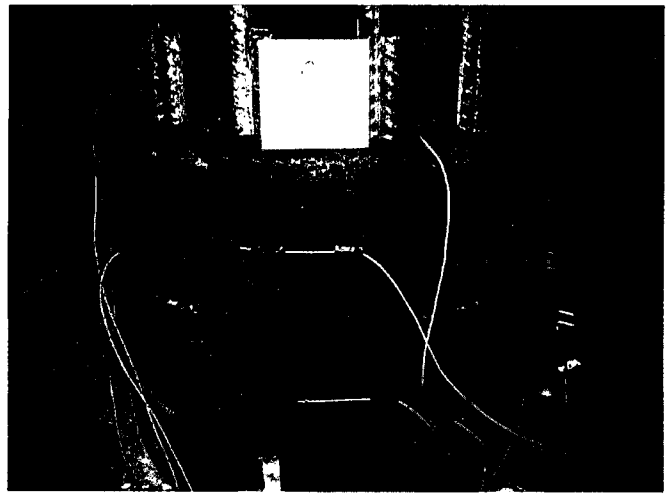

(b) Front View of Tire Insertion in TC-8

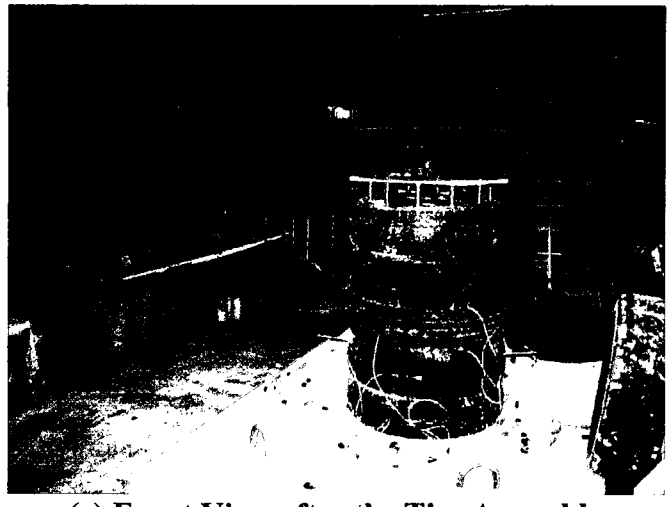

(c) Front View after the Tire Assembly

Figure 3.20: Tire Assembly for Columns TC-7 through TC-12

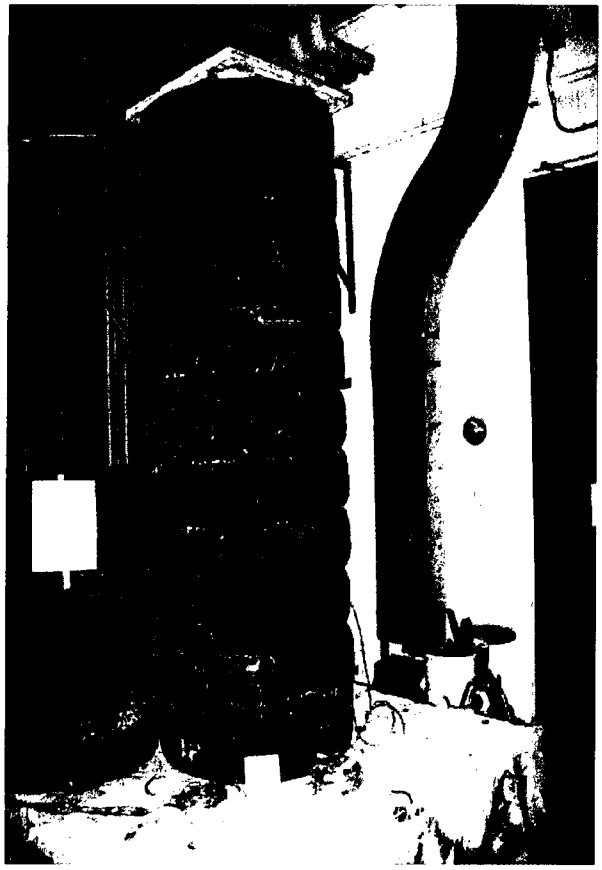

(a) Side View of TC-7

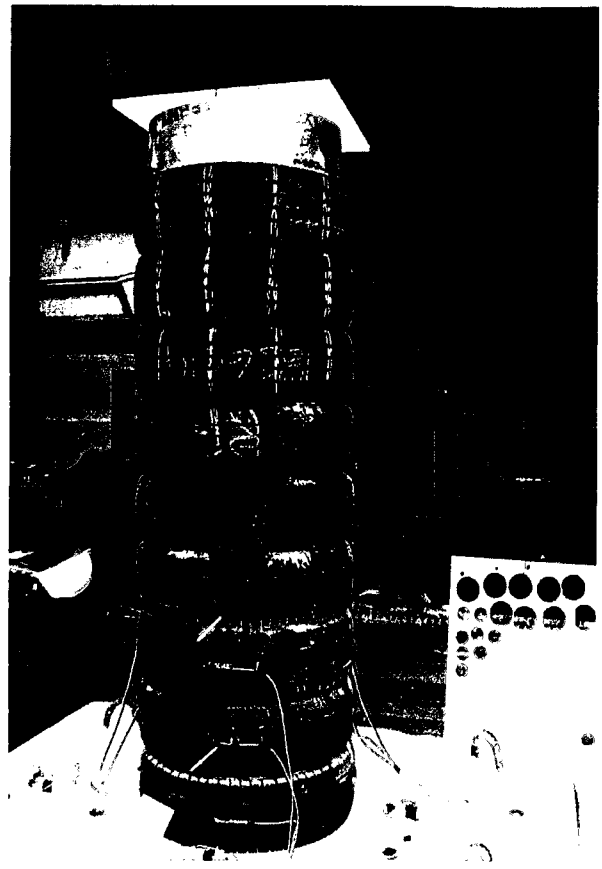

(b) Front View of TC-9

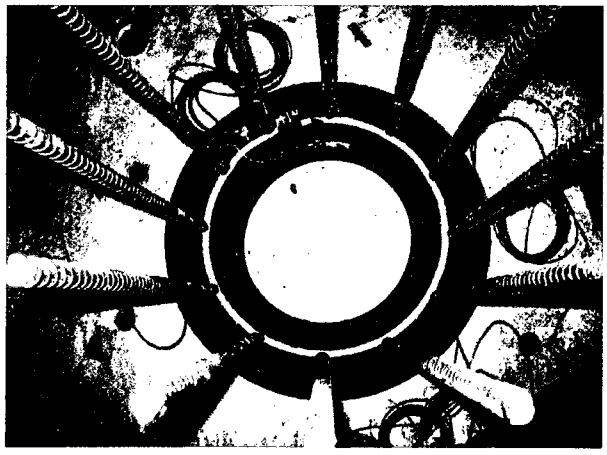

(c) Top View of TC-10

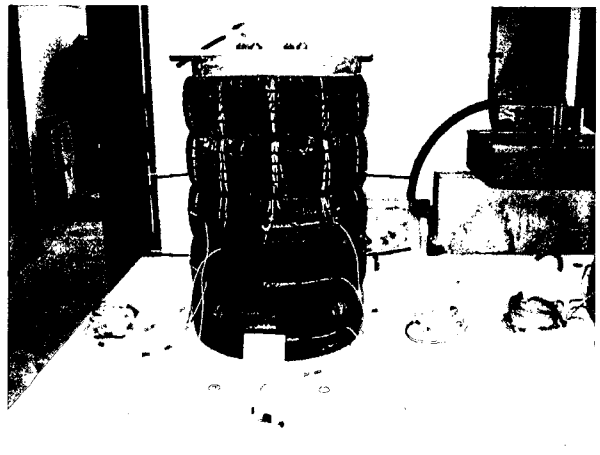

(d) Front View of TC-12

Figure 3.20 (Cont'd): Tire Assembly for Columns TC-7 through TC-12

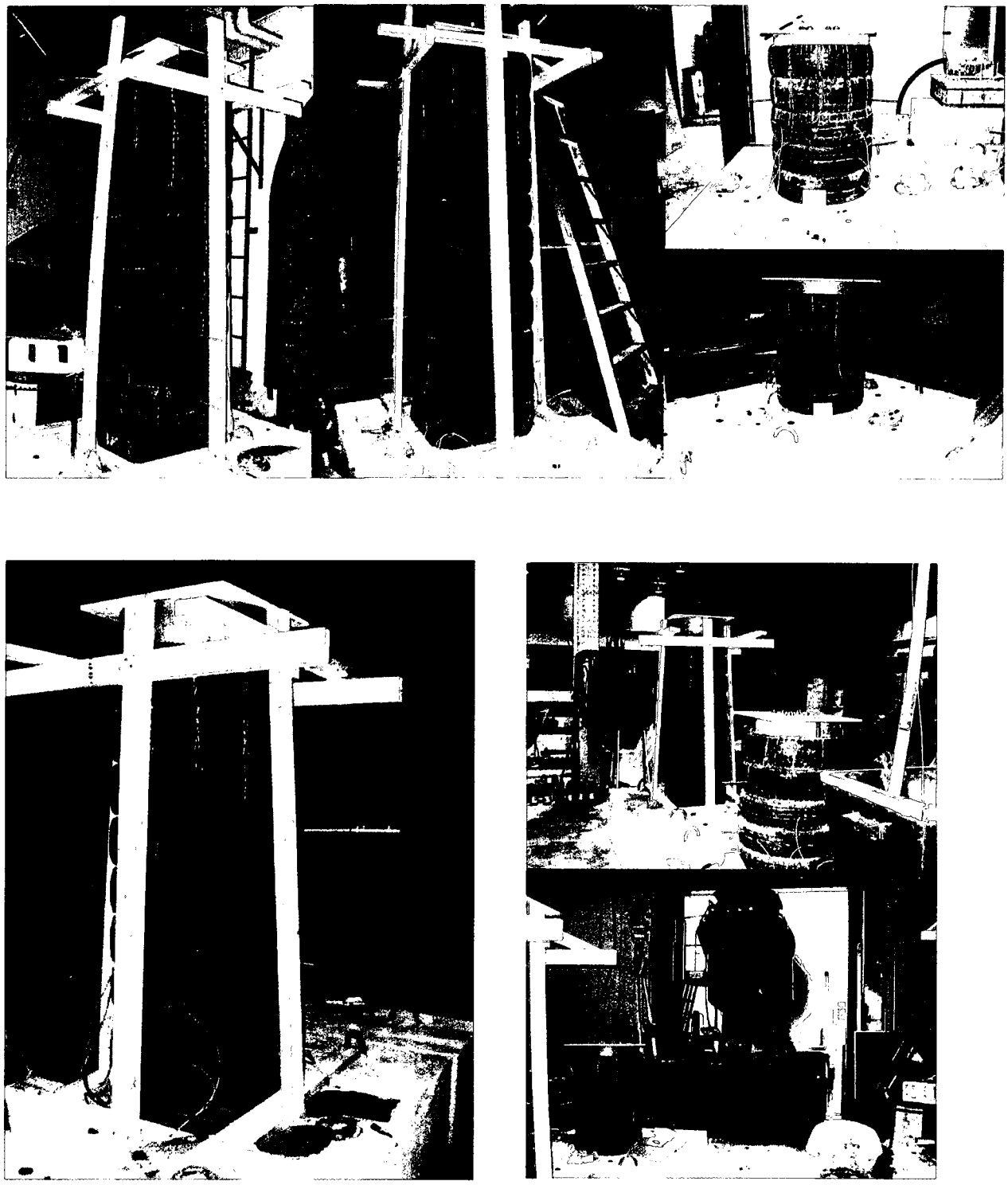

a) Shortly Before Casting

Figure 3.21: Casting of Column Specimens

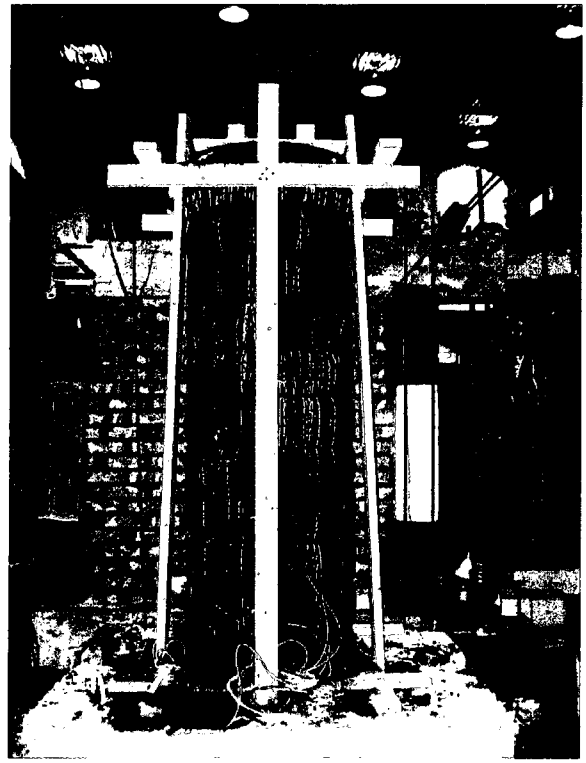

b) At completion

Figure 3.21 (Cont'd): Casting of Column Specimens

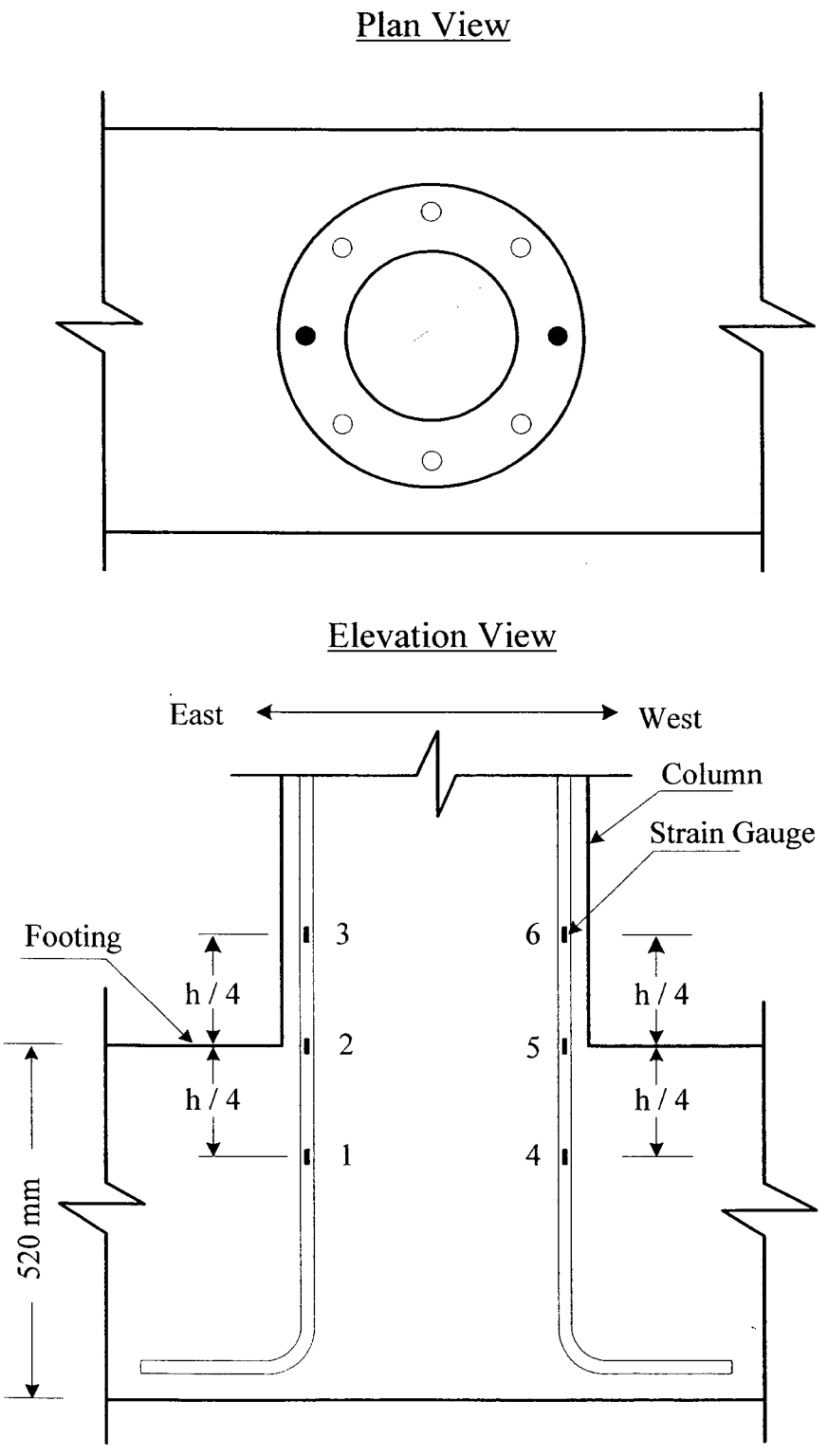

Figure 3.22: Location of Strain Gauges on Longitudinal Reinforcement for Regular Specimens (TC-7, TC-10, TC-11, and TC-12)

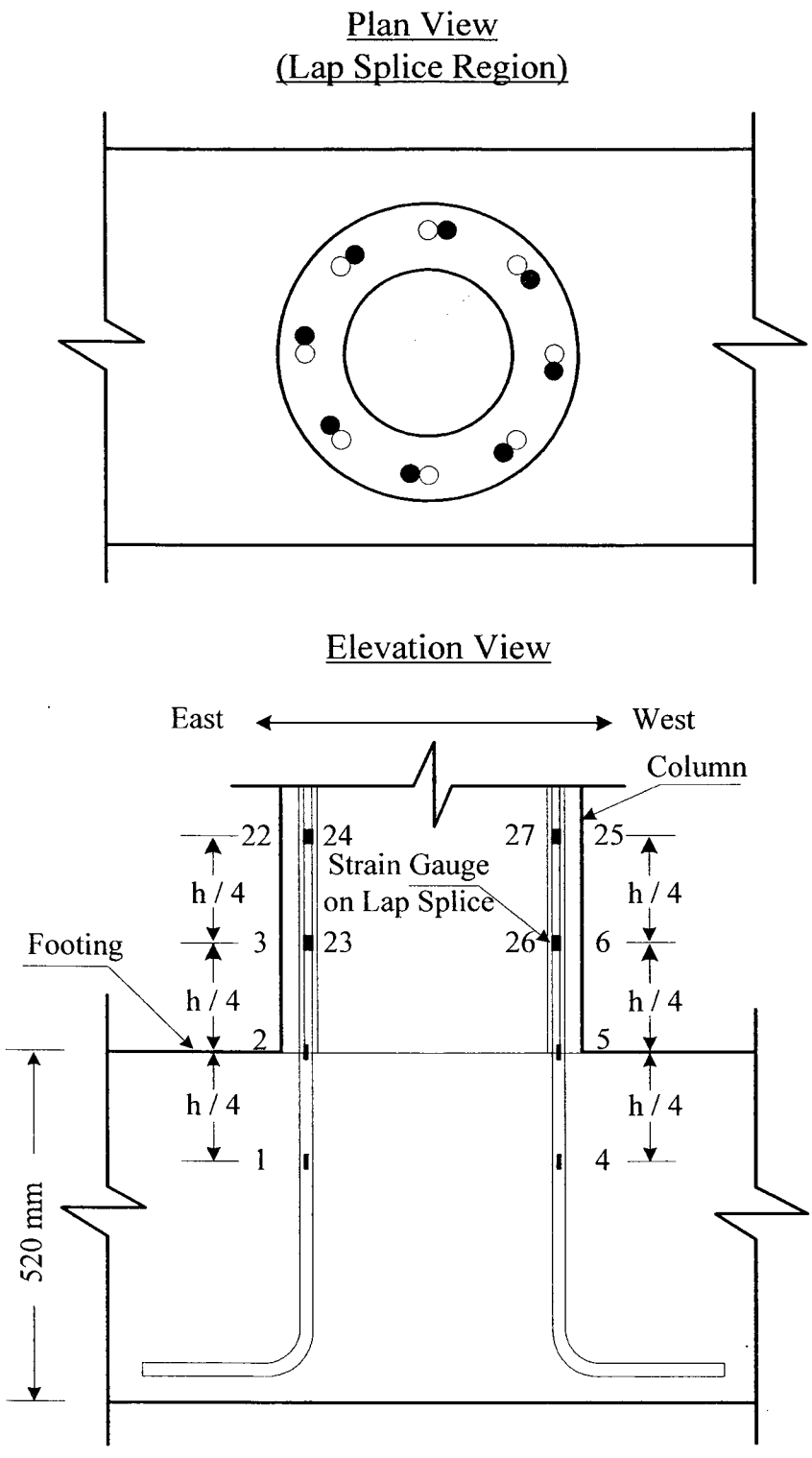

Figure 3.23: Location of Strain Gauges on Longitudinal Reinforcement for Lap Spliced Specimens (TC-8 and TC-9)

Gauges	Locations
7,8,9	First tire from the bottom on the east and west
10,11	First tire from the bottom on the south and north
12,13,14	Second tire from the bottom on the east and west
15,16	Second tire from the bottom on the south and north
17,18,19	Third tire from the bottom on the east and west
20,21	Third tire from the bottom on the south and north

Note that gauges 1 to 6 and 22 to 27 are for longitudinal reinforcement

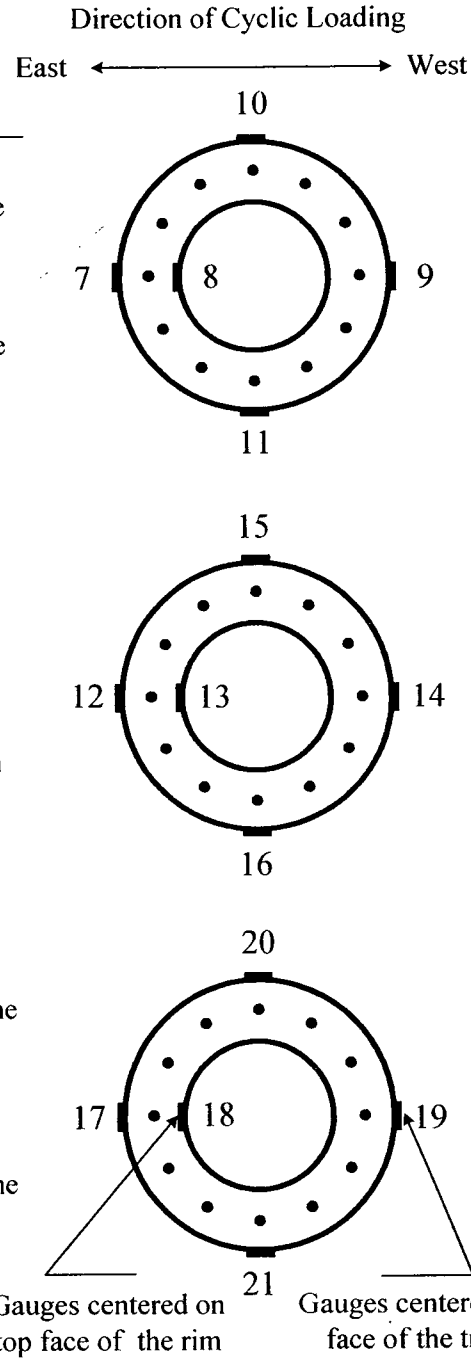

Figure 3.24: Location of Strain Gauges on Tires for all Specimens

(a) Top View for Strain Gauges on the Rim

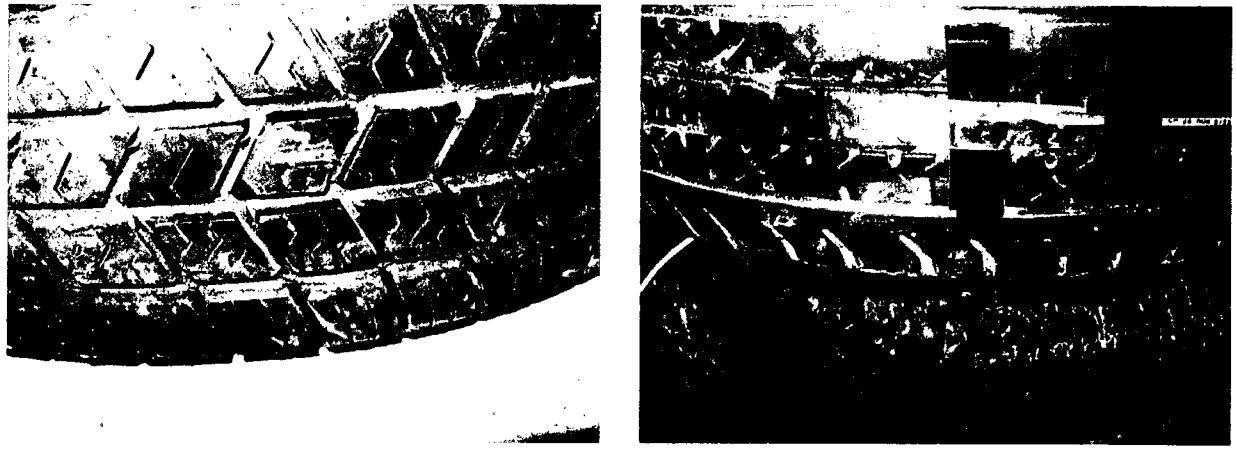

(b) Front View for Strain Gauges on the Tread

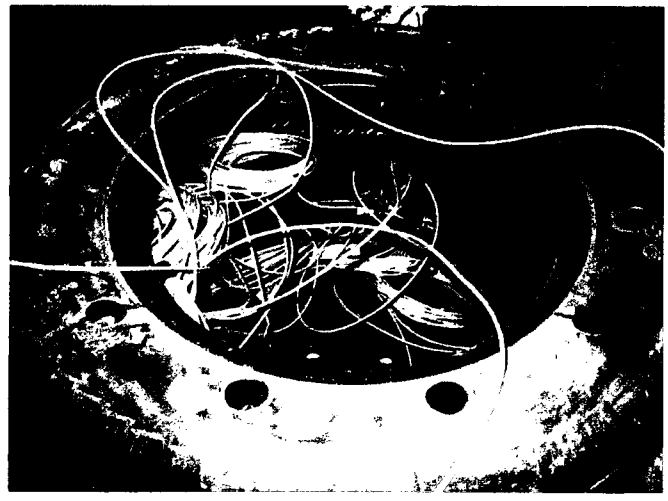

(c) Tire after Strain Gauges Installation

Figure 3.25: Locations of Strain Gauges on Tires for all Specimens

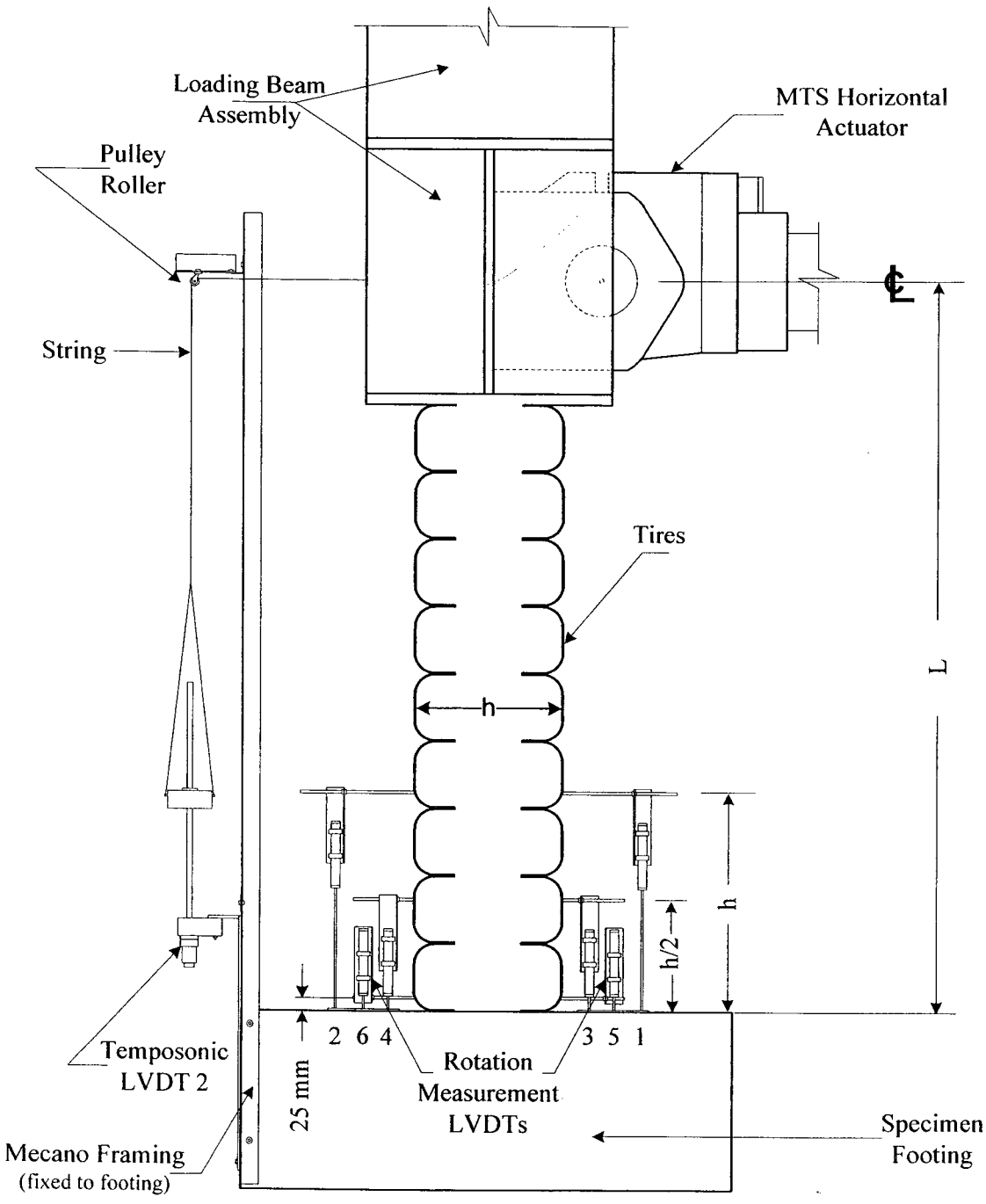

h = Depth of column cross-section (700 or 550 mm)

L = Height of the Specimen (2500, 2000, 1500, and 1200mm)

Figure 3.26: Instrumentation for Displacement Measurements for all Specimens

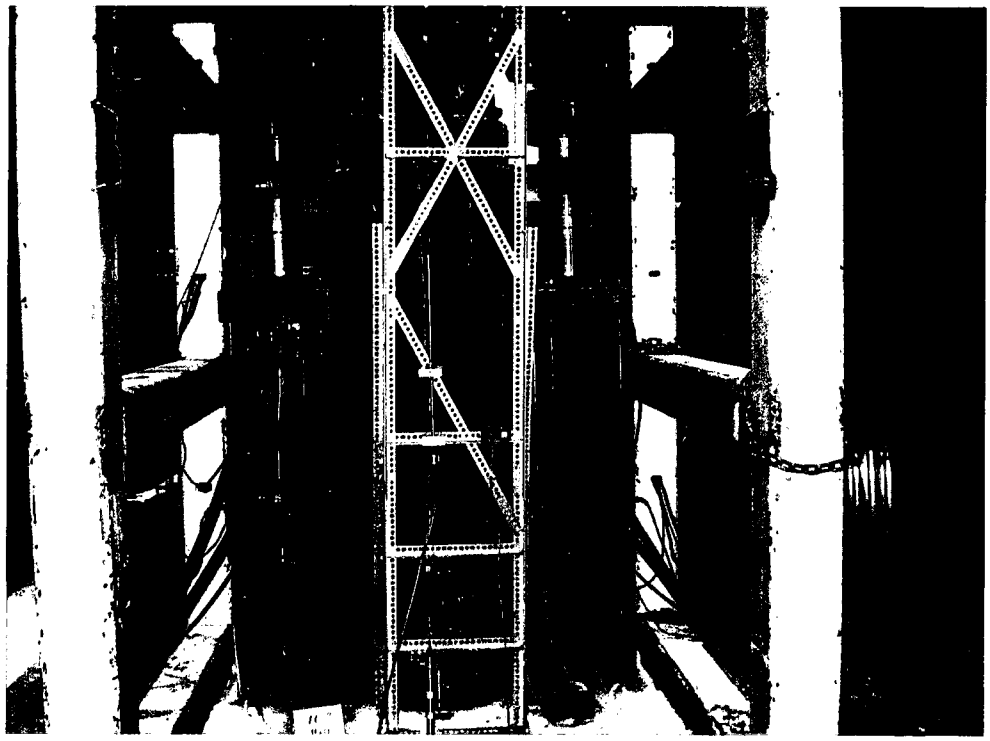

(a) West View

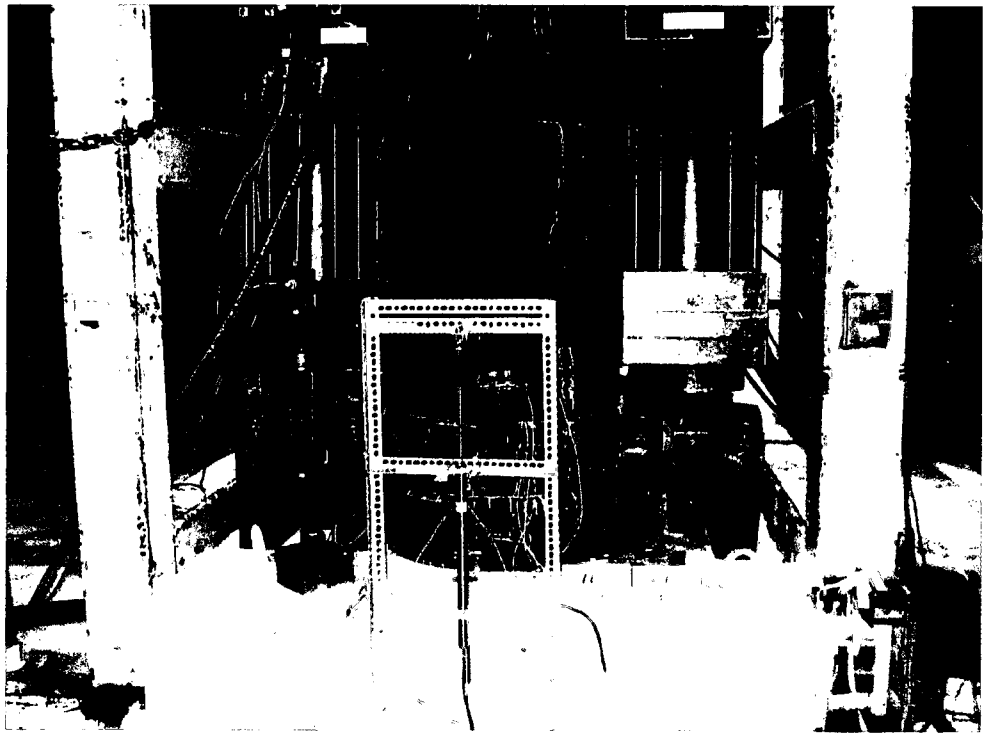

(b) East View

Figure 3.27: Instrumentation

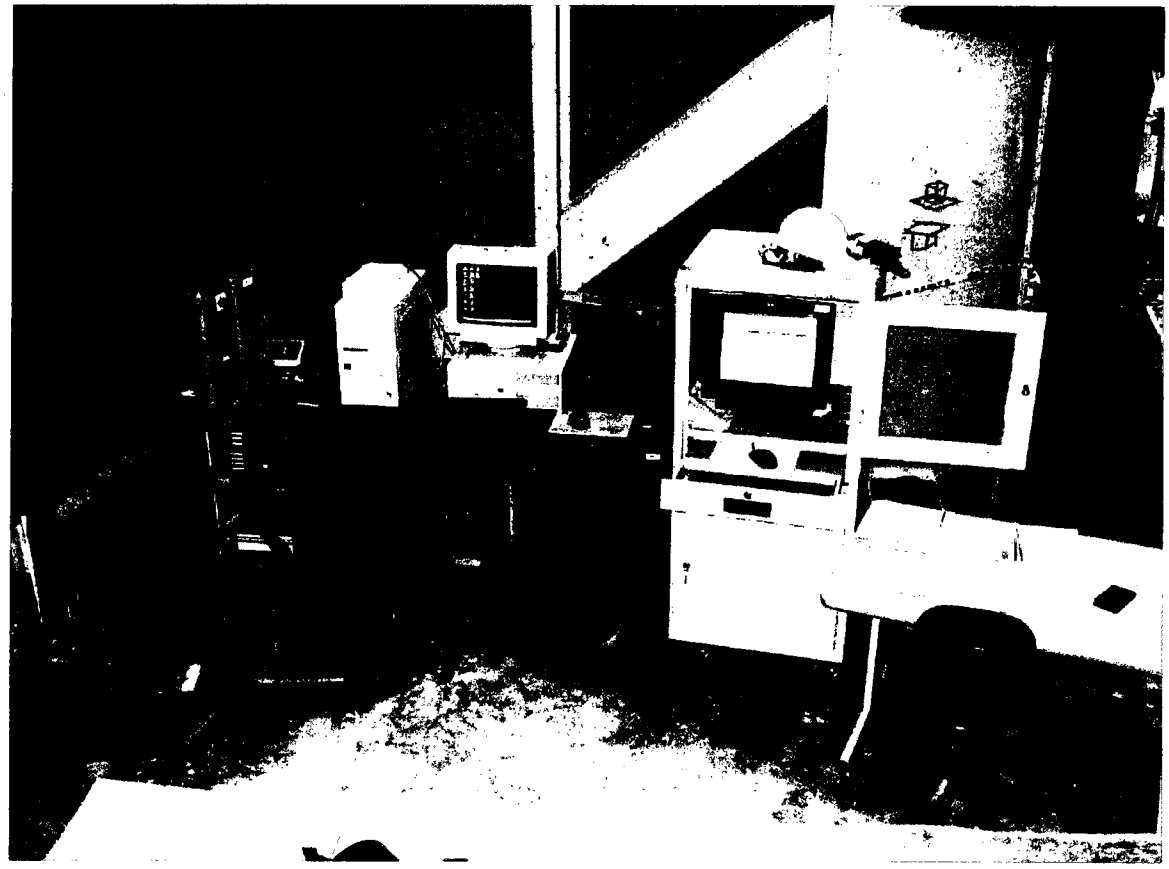

(a) Data Acquisition System and MTS Controller

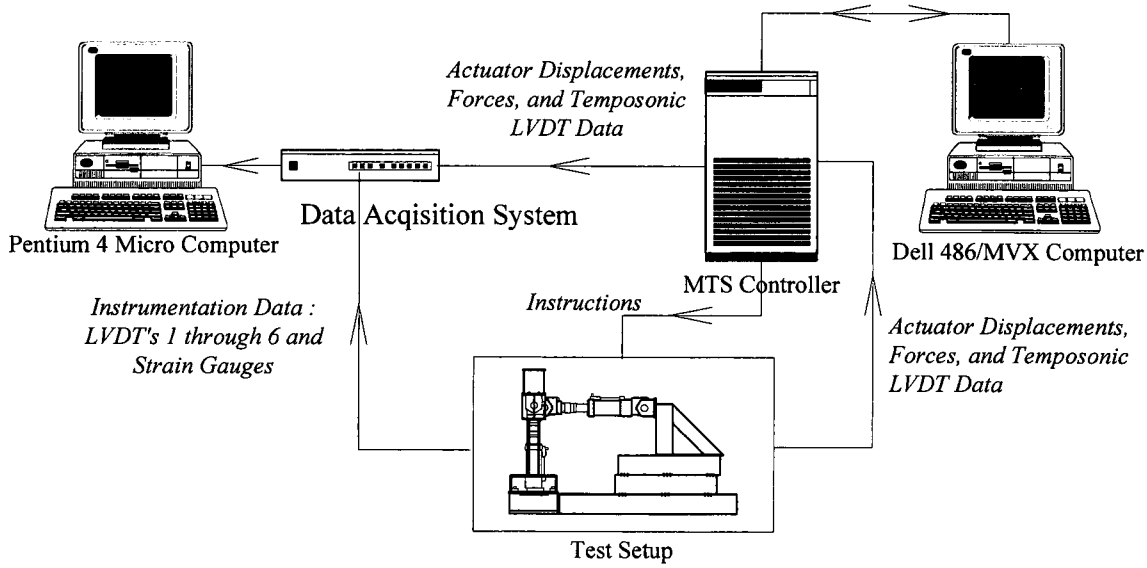

(b) Schematic Network Diagram

Figure 3.28: Data Acquisition System, MTS Controller, and Network Diagram

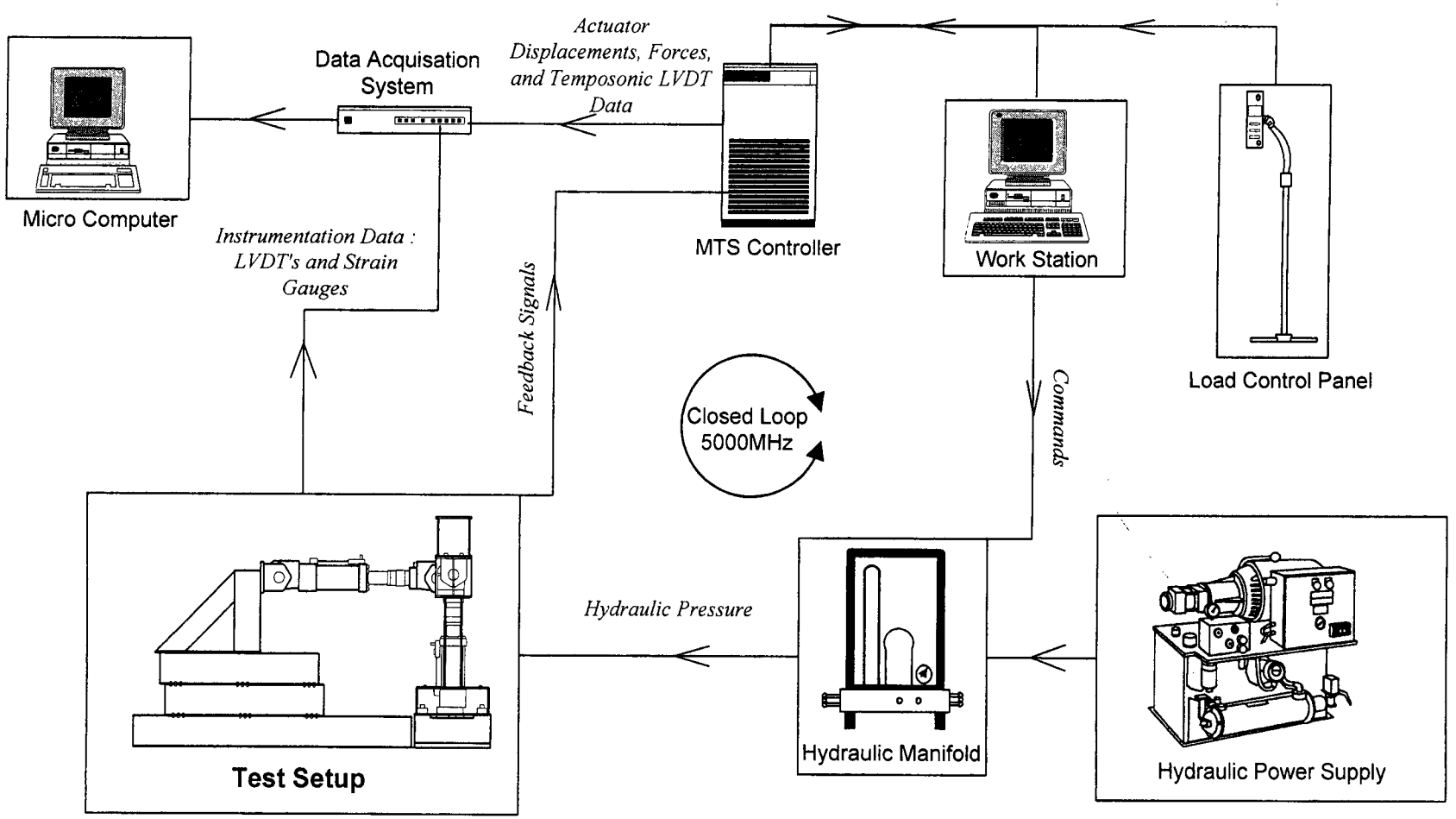

Figure 3.28 (Cont'd): Data Acquisition System, MTS Controller, and the Network Diagram

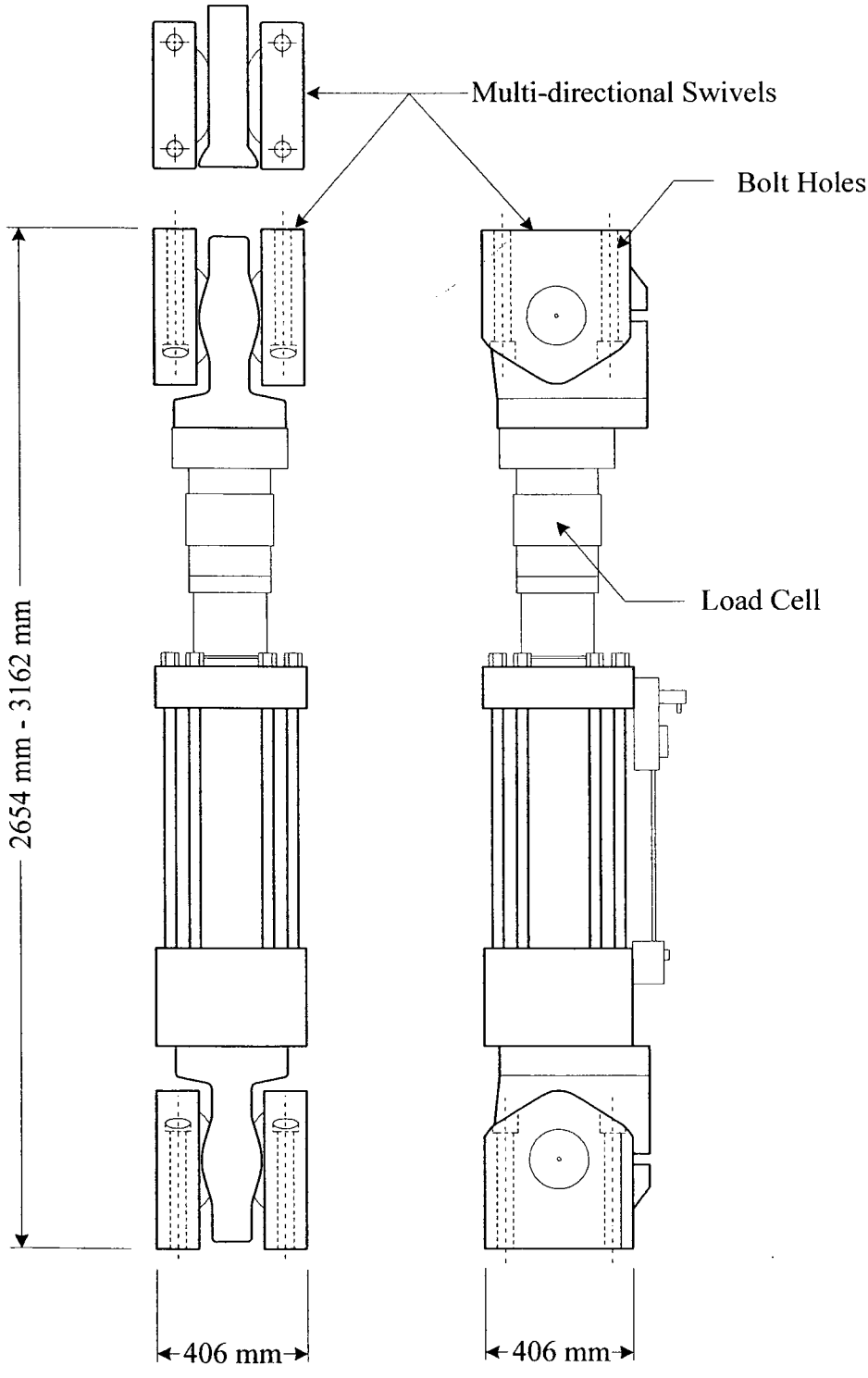

Figure 3.29: Details of the MTS Actuators

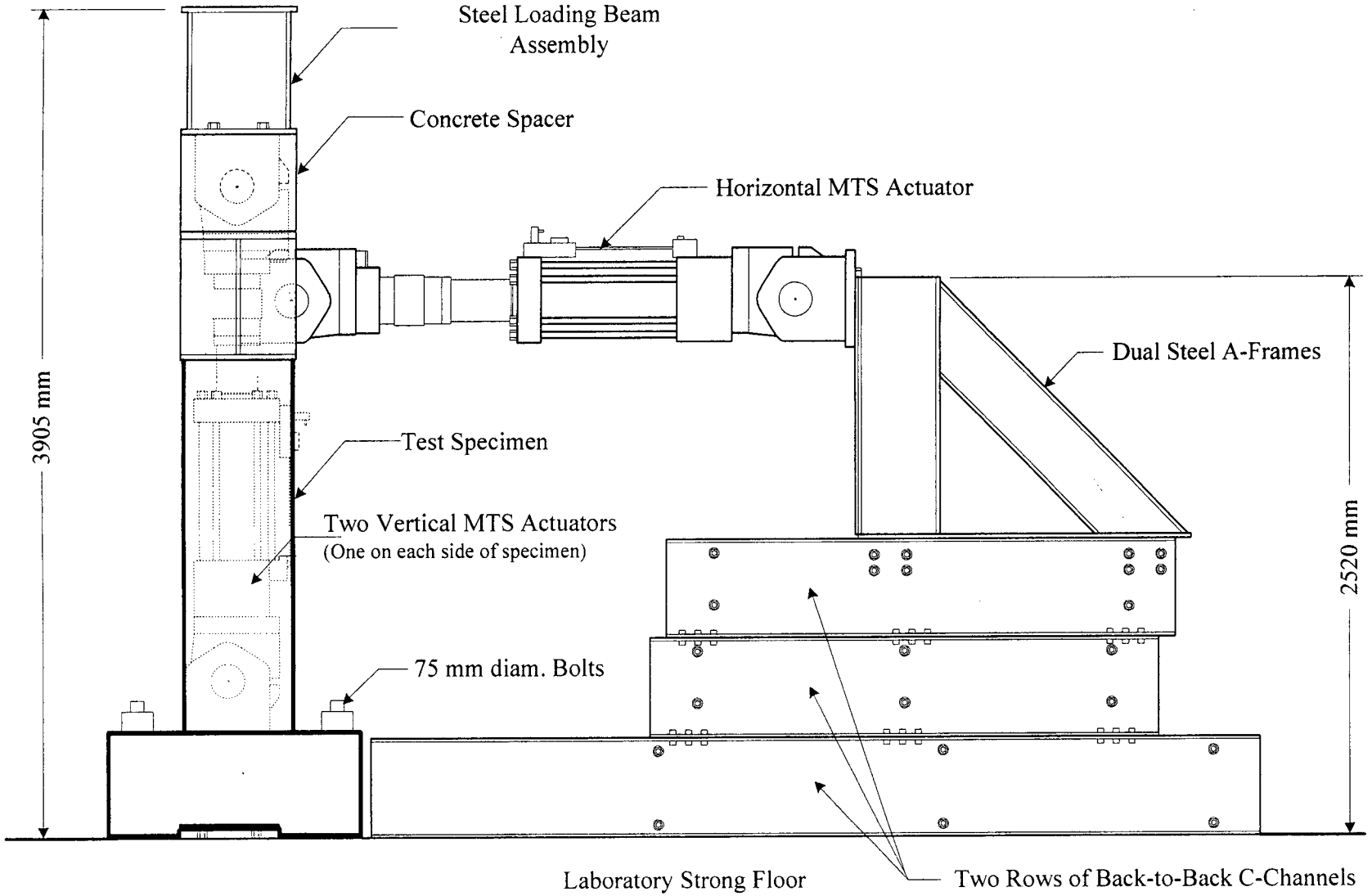

Figure 3. 30: Side Elevation of the Test Setup

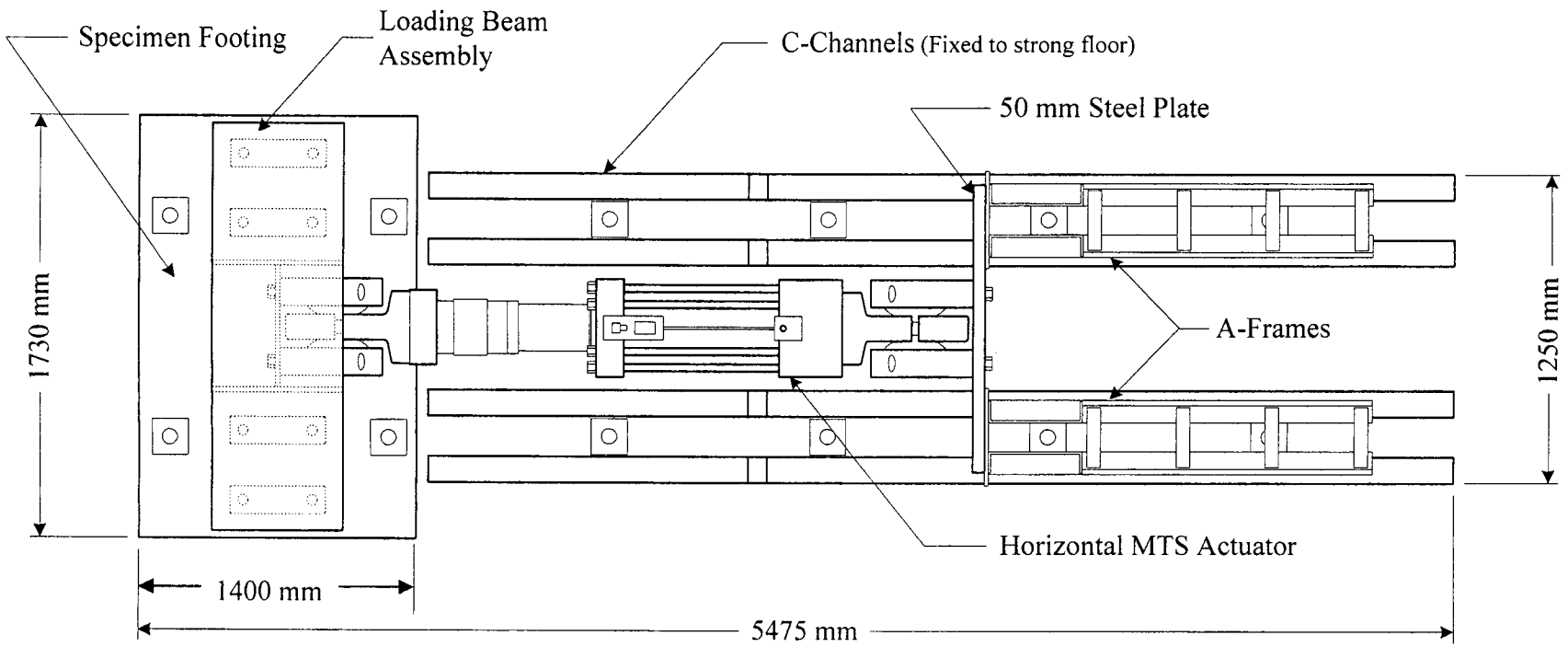

Figure 3.31: Plan View of Test Setup

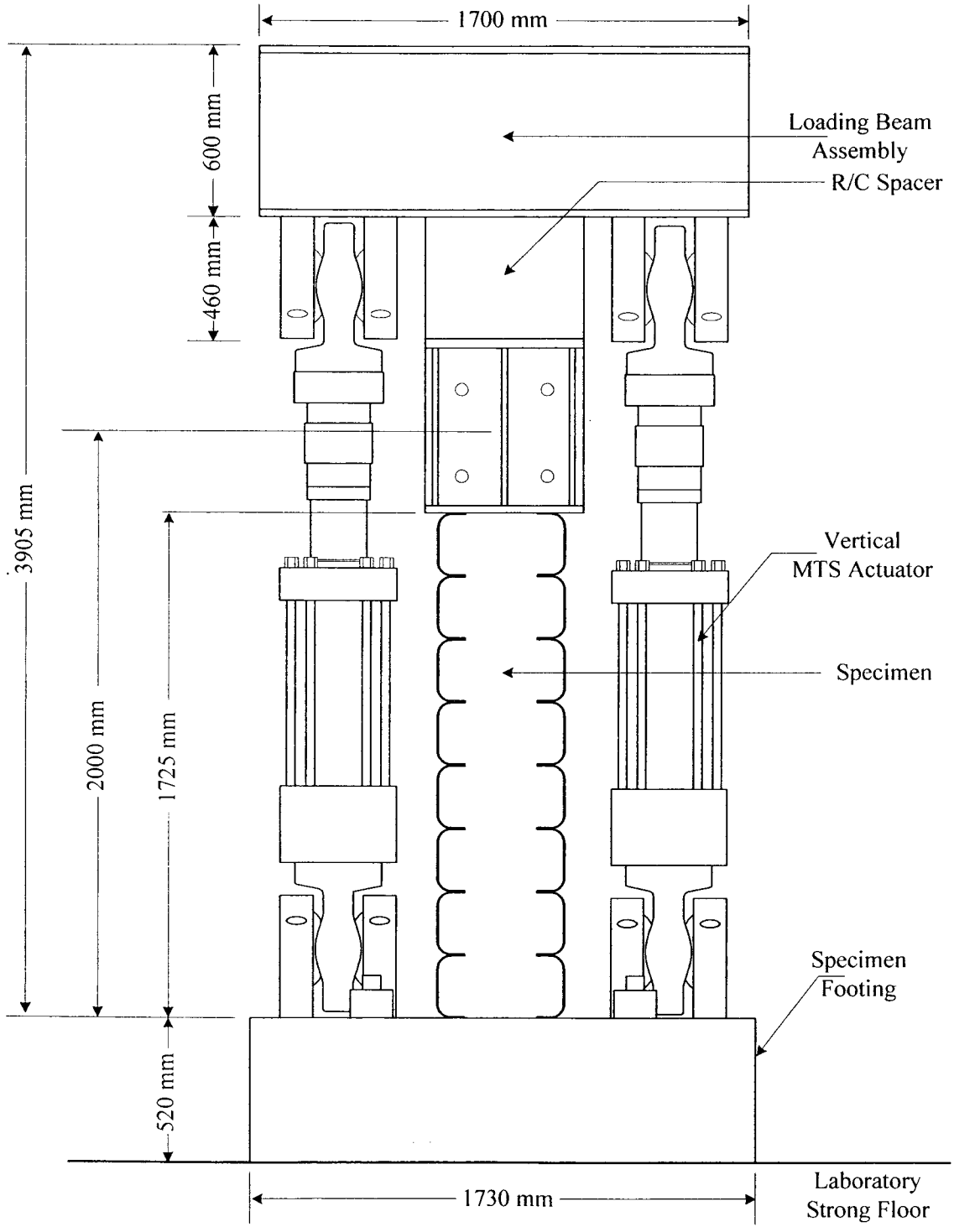

Figure 3.32: Front Elevation of the Test Setup

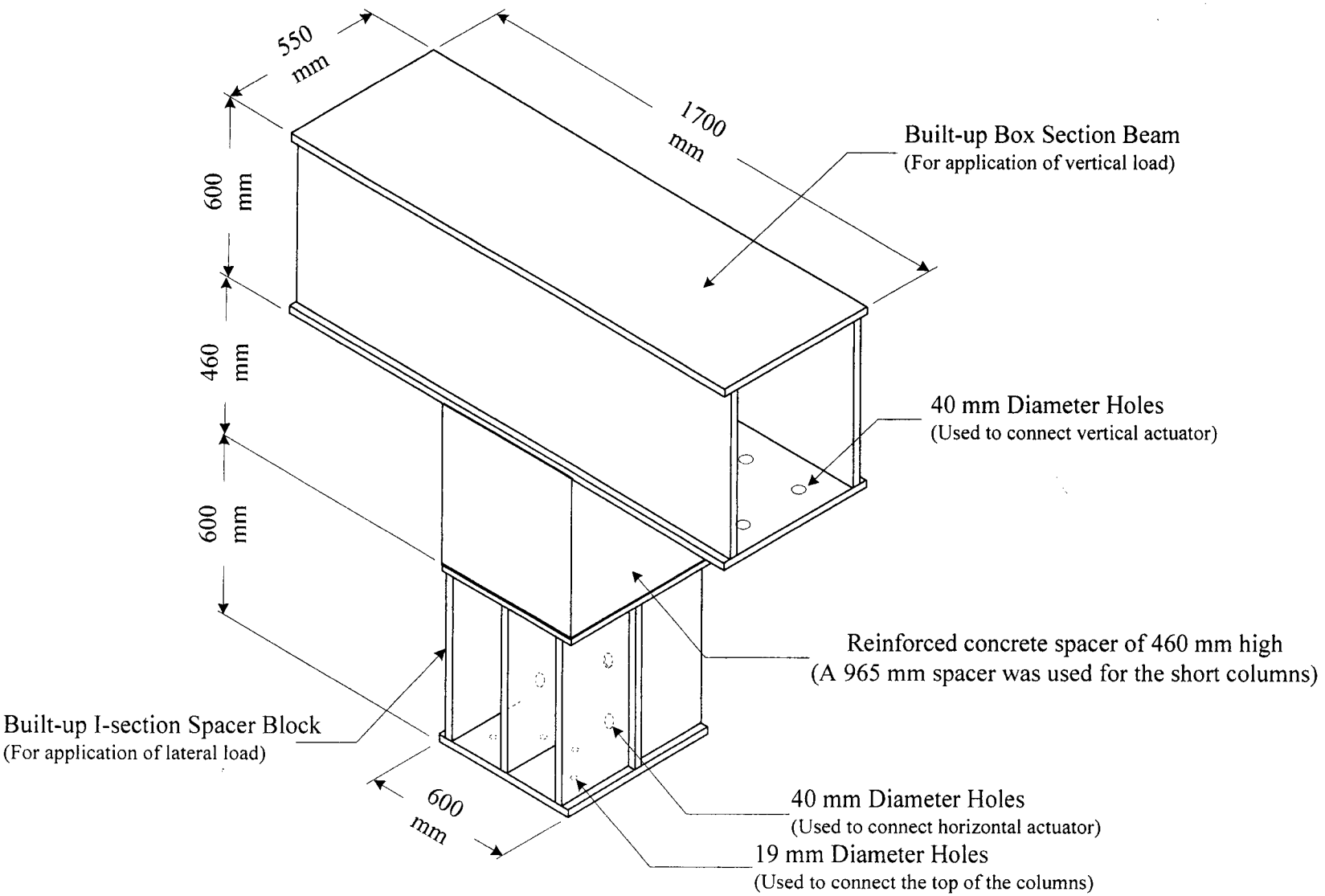

Figure 3.33: Details of Loading Beam Assembly

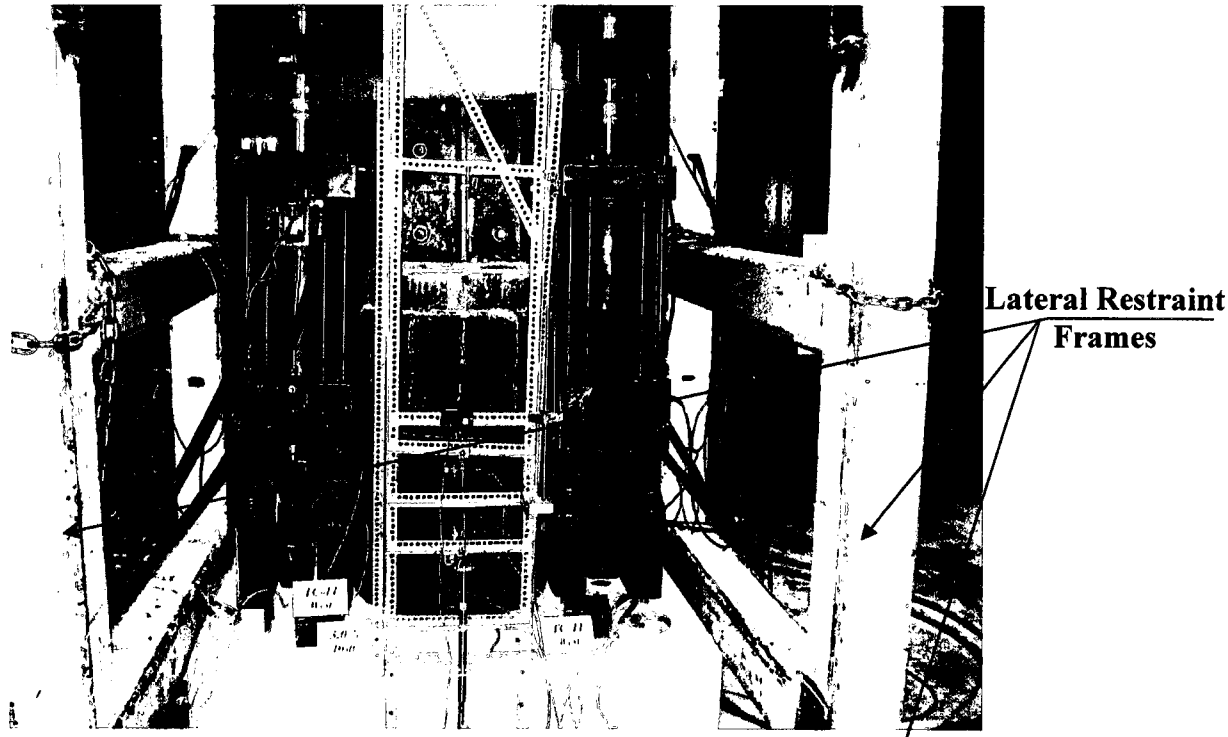

(a) Front View

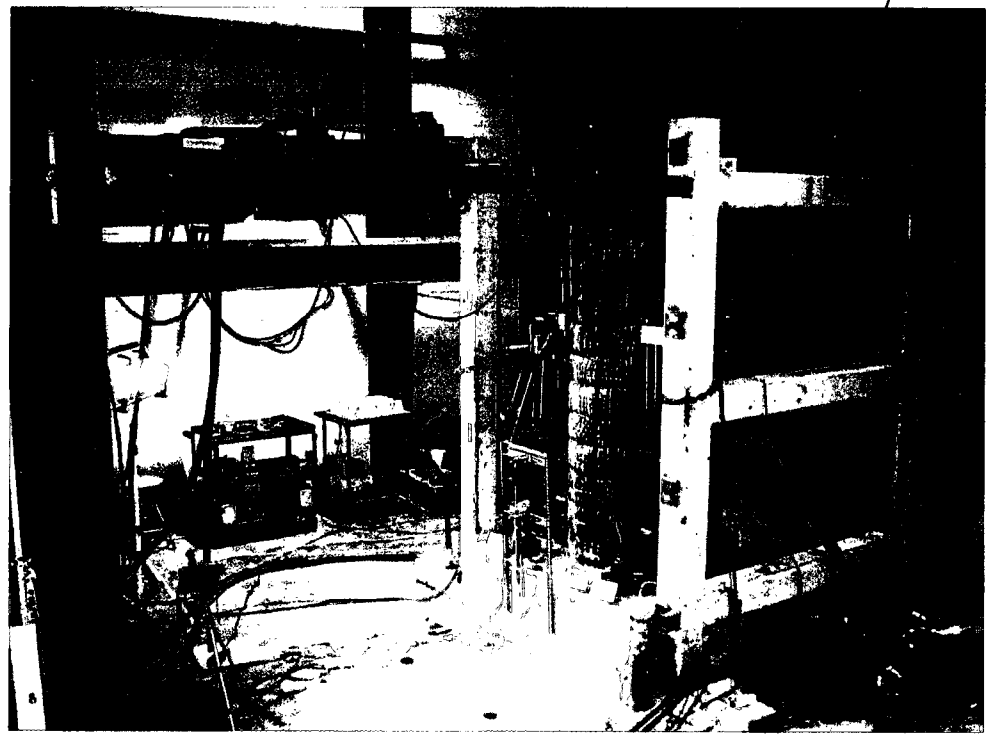

(b) Side View

Figure 3.34: General Views of Lateral Restraint Frames

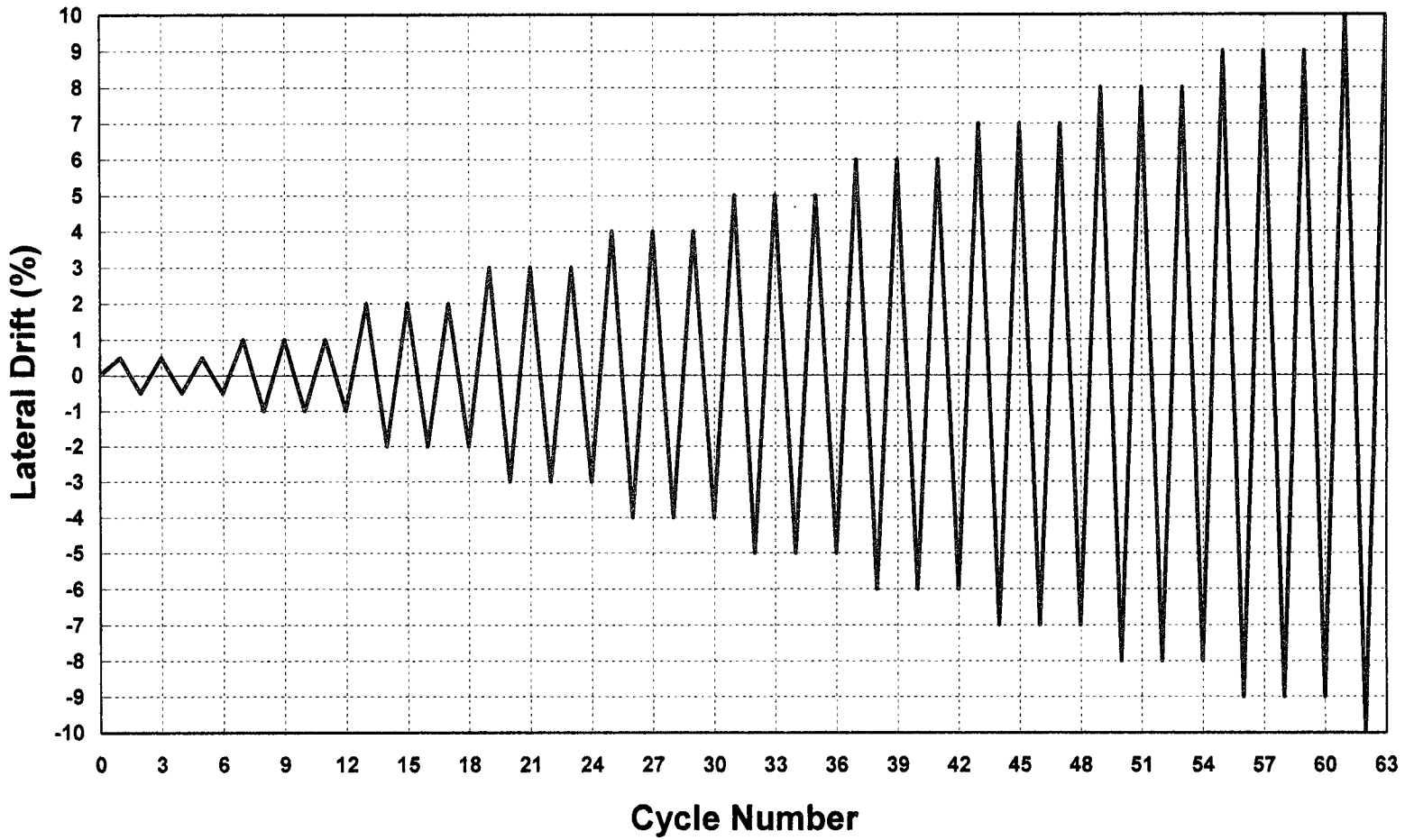

Figure 3.35: Loading Program

CHAPTER 4

Experimental Results and Evaluation of Data

4.1 General

Observed behaviour and test data for each column are presented and discussed in this chapter. The observations include overall specimen behaviour, rupturing of tires, crushing of concrete, and buckling of longitudinal reinforcement. The observed behaviour, as well as strain, displacement and force measurements were recorded during the tests. Photographs were taken at the end of each drift level, as well as at different stages of loading when significant changes occurred in behaviour. The hysteretic behaviour is presented in terms of force-displacement and moment-displacement relationships. Strains in longitudinal reinforcement and tires are presented and discussed. Hysteretic moment-total rotation, moment-anchorage slip rotation, and moment- flexural rotation relationships are also presented and discussed. Some of the data could not be recorded either due to damaged strain gauges or exceeding the stroke limits of LVDT's.

4.2 Observed Behaviour of Test Columns

All columns initially behaved in a similar manner. Unlike conventional reinforced concrete columns, the damage in tire covered columns was not visible until the rupturing of tires has taken place and the concrete crushed and/or spalled at large inelastic deformations, often accompanied by bar buckling. Horizontal (lateral) force resisted by columns was used to plot force-displacement hysteretic relationships. Moments used to plot hysteretic relationships were computed as the lateral force times the shear span plus the vertical component of axial force times the horizontal displacement Δ, ($P-\Delta$ effect). The force-displacement relationships reflect degradation in lateral force resistance caused by $P-\Delta$ effects, whereas

the hysteretic relationships for moments show only the strength decay caused by column damage.

Three sets of rotation readings were obtained from each column by means of six LVDTs. The first set consisted of rotations due to combined flexure and anchorage slip within distance "h" from the column-footing interface (h is the cross-sectional diameter of column, equal to either 700 mm or 550 mm). This was referred to as total rotation of the assumed hinging region relative to the footing. The second set also gave total rotations, but this time within h/2 from the column-footing interface. The latter was intended to reflect the rigid-body rotation of column base, caused by the extension of longitudinal column reinforcement within the footing, and was recorded at approximately 25 mm above the column-footing interface. All rotation readings were discontinued to be recorded shortly before the end of testing to safeguard the instrumentation against possible damage. Flexural rotations of the hinging region were obtained by subtracting those caused by anchorage slip.

The columns were loaded until the lateral load resistance dropped by at least 20%, i.e., down to 80% or less of the peak resistance. The amount of damage on each column varied depending on the level of axial force and the degree of confinement provided by steel reinforcement in tires. A discussion of column behaviour is provided below for each specimen.

4.2.1 Performance of Column TC-7

Column TC-7, with a high aspect ratio and continuous longitudinal reinforcement, was designed to perform predominantly in the flexure mode. The longitudinal reinforcement consisted of twelve No. 25 (25.2 mm diameter) deformed bars. There was no conventional transverse reinforcement in this column. The height (shear span) of the column was 2500 mm from the point of inflection to the point of application of the force. The column was tested under a constant compressive force of 1900 kN, which represented 10% of its concentric capacity. The actual test started with the application of full axial load, followed by lateral load reversals in the displacement control mode.

During the first three cycles at 0.5% lateral drift with 12.5 mm lateral displacement, no damage was observed and the maximum lateral load recorded was 177 kN. There was no yielding in the reinforcement.

When the load increased to 1% drift ratio, the strain readings on the longitudinal reinforcement indicated yielding during the third cycle of this deformation level. The strains in the extreme longitudinal bar on the east side reached 0.24% at 175 mm (h/4) below the column footing interface, and reached 0.25% at column footing interface on the west side. The strain reading at 175 mm above the footing indicated 0.21% on the west side. At 175 mm below the footing surface no yielding was recorded until after the third cycle of 2% drift. At the end of the 2% drift, strain gauges No. 1 & 5 on the longitudinal reinforcement were damaged and stopped reading. The strains in the rim of the third tire from the base reached developed 0.32%, 0.33% and 0.48% during the first, second and third cycles at 3% drift ratio, respectively. The strains on the tread of the second tire reached 0.21% during the second cycle of 3% drift level. The strains on the tread of the first tire, and the rim of the second tires reached 0.33% and 0.41%, respectively on the east side, at the end of the third cycle of 4% drift ratio.

At the beginning of 5% drift, Gauge Nos. 5 and 6 were damaged. The strains in longitudinal reinforcement, at 175 mm below the footing, reached 0.47% and 0.55% at the end of 5% drift cycles. The maximum lateral load at 5% drift was 403 kN. No damage to column was visible until the end of 5% drift cycles, as evidenced by Figure 4.1. The column survived 5% drift cycles without any visibly severe damage, but most of the strain gauges were damaged.

At the beginning of 6% drift, high strains were recorded on the treads of the first tire on the west side and the second tire on the east side. Subsequently, the first and second tires from the bottom started to separate from each other on the east side. There was an increase in the volume due to the internal cracking and resulting expansion of concrete inside the tire. The strains in the rims were increased to 0.48% at this load stage. There was a slight drop in lateral load resistance at the end of the second cycle of 6% drift. Loud sound was heard as

the longitudinal reinforcement ruptured on the west side. Subsequently, the second tire ruptured on the East side, as evidenced in Figure 4.1 (c).

There was a significant drop in load resistance at 7% drift ratio. This was attributed to the rupturing of longitudinal reinforcement in tension and the rupturing of the second tire from the bottom. The buckling of longitudinal reinforcement was observed at this stage of loading, as shown in Figure 4.1 (f).

This column was able to develop 6.5% lateral drift prior to sustaining 20% decay in strength. At the end of the second cycle of 7% drift, the lateral load dropped suddenly to 50% of peak resistance, and the test was stopped due to a safety concern. There was extensive damage observed on the east side of the second tire, which was accompanied by the buckling of longitudinal bars as seen in Figure 4.1 (f). The duration of the test for this column was about two and a half hours. Figure 4.1 shows the behaviour of column TC-7 during selected stages of testing. All pictures were taken at the last cycle of each drift level.

The hysteretic force-displacement and moment-displacement relationships are illustrated in Figure 4.2 and Figure 4.3. These relationships indicate that the column developed ductile behaviour and showed stable hysteresis loops. The behaviour was typical of flexure-dominant response, with well-rounded hysteresis loops up to 6% drift ratio. The decay in load resistance dropped by about 50% at the end of the second cycle of 7% lateral drift due to the rupturing of the second tire and the buckling of compression reinforcement. Hysteretic moment-total rotation, moment-anchorage slip rotation, and moment-flexural rotation relationships are shown in Figure 4.4, Figure 4.5, and Figure 4.6, respectively. Figure 4.4 and Figure 4.6 include total and flexural rotations at h and h/2 distances above the footing (h = 700 mm). The rotations caused by flexure are equal to the difference between the total rotations and rotations caused by anchorage slip.

Strain gauges 2, 11, 15, 16, 20, and 21 were damaged since the beginning of the test. Strain gauge data recorded from other gauges are included in Figure A.1 and Figure A.2 in Appendix A. It should be noted that some of the strain gauges were damaged during 5% to

6% drift cycles, before the end of test. Therefore, the data shown do not provide strains beyond this deformation level. The stain data also indicated that most of the stains in the bars and in the tires reached their yield capacity, except for some gauges in the rims of tires.

4.2.2 Performance of Column TC-8

Column TC-8 was identical to TC-7, except for the spliced longitudinal reinforcement. The longitudinal bars were spliced at the bottom of the column with a splice length of 30 times the bar diameter. This splice length was somewhat less than that recommended by the Standard (CSA A23.4 2004) for column design, because it was intended to investigate if the presence of tires as confinement reinforcement would allow the use of a shorter splice length. The column was subjected to the same level of axial load as that for TC-7 which corresponded to 10% of its concentric capacity. The lateral deformation history remained the same.

The column capacity was different than that of the companion column (TC-7). The maximum lateral load recorded at 0.5% drift ratio was 201 kN. There was no yielding in the reinforcement at the end of 0.5% drift ratio, except the strain gauge No. 23 in the starter bar on the east side developed high strains. The load resistance increased to 302 kN at the beginning of 1% drift cycles. Strain Gauge Nos. 11, 15, 20, and 27 were damaged during the preparation of column, prior to the test.

A slight reduction in lateral force resistance (9%) was recorded relative to TC-7 during 2% drift cycles. Strain Gauge Nos. 24, 25, and 26 on the longitudinal bars were damaged and stopped functioning at this stage of testing. This was attributed to the slippage of reinforcement at the end of the second cycle at 2% drift. This was followed by some degradation of strength at the end of 3% drift cycles. At this stage, the treads in the second tire developed high strains, reaching 0.26% due to the lateral expansion of concrete within the hinging region. The longitudinal reinforcement at 175 mm above the column-footing interface yielded, developing 0.33% strain.

An opening between the first and the second tire on the west side was observed due to damage to concrete during the third cycle at 4% drift and the first cycle at 5% drift ratio. This is shown in Figure 4.7 (c). All the strain gauges on the starter and longitudinal bars within the splice region were damaged (Gauges 6, 22, 23, 24, 25, 26, and 27). It was observed during the test that the internal transverse steel in treads and rims of tires were effective in providing clamping force to maintain bond between the spliced reinforcement and concrete until the steel strain in the treads and rims increased beyond 0.6% to 0.8%.

The opening between the first and the second tire became more visible at the end of 6% drift cycles, exposing the longitudinal reinforcement. These tires developed tread strains of 0.39% during 6% drift cycles. This was attributed to the tendency of longitudinal reinforcement to buckle, which was prevented by tire confinement. The opening between the two tires penetrated towards the east side during 7% drift cycles, as can be seen in Figure 4.7 (d).

The column survived 8% lateral drift without a significant drop in load resistance. At the end of 8% drift cycles the temposonic was out of range of its stroke limit. At the first cycle of 9% drift, the second tire from the bottom ruptured on the west side, as shown in Figure 4.7 (e). When the column was pushed further to start the second cycle, the tread part of the tire stretched more, followed by the rupturing of steel within the treads on the west side of the second tire. The test was discontinued at the end of the second cycle at 9% drift ratio. Figure 4.7 shows the behaviour of Column TC-8 during selected stages of testing. The duration of the test for this column was approximately four hours.

The hysteretic lateral force-lateral displacement and moment-lateral displacement relationships obtained during testing are shown in Figure 4.8 and Figure 4.9. These relationships indicate that the column showed stable hysteresis loops up to 3% lateral drift. However, it maintained its strength, with some decay, well into the 8% drift range. The hysteresis loops indicated the slippage of longitudinal reinforcement, as evidenced by pinching of the loops, while maintaining significant load resistance. The area under the force-deformation relationship, and hence the energy dissipation was reduced significantly. Figure 4.10, Figure 4.11, and Figure 4.12 show hysteretic moment-total rotation, moment-

anchorage slip rotation, and moment-flexural rotation relationships for Column TC-8, respectively. Figure 4.11 indicates that, approximately $1/3^{rd}$ of the total rotation, measured as anchorage slip, could be attributed to the slippage of spliced reinforcement, leaving $2/3^{rd}$ to flexure.

Figure A.3 and Figure A.4 in Appendix A illustrate the strain gauge data for longitudinal and starter bars, as well as treads and rims of tires. Most of the gauges were damaged between 5% and 6% drift cycles. Hence, the strain readings could not be recorded beyond this deformation level.

4.2.3 Performance of Column TC-9

Column TC-9 was a flexure dominant column with spliced longitudinal reinforcement, but had smaller cross-section than TC-8, confined by smaller size tires. The longitudinal reinforcement size was also smaller, consisting of twelve No. 20 (19.5 mm diameter) deformed bars. There was no conventional transverse reinforcement, other than the tires serving as transverse reinforcement. The column height (shear span) was 2000 mm, measured to the point of application of the horizontal force. This longitudinal bars were spliced with a splice length of 30 times the bar diameter. The column was tested under a constant compressive force of 1950 kN, which represented 16% of its concentric capacity. The actual test started with the application of full axial load, followed by lateral load reversals applied in displacement control mode. The Strain Gauges 14, 19, 20, 25, and 27 were damaged during construction, prior to testing.

The capacity of this column was smaller than those of the previous two tests, because of the reduced column size. The maximum lateral load recorded at 0.5% drift was 156 kN. This load resistance increased to 205 kN at the end of 1% drift cycles. Yielding of the starter bars on extreme east and west sides were observed at the end of the second and third cycles of 1% lateral drift ratio. The strains recorded were within the yield plateau, approximately equal to 0.35%. The strain in the extreme tension starter bar, at column-footing interface, on the east side, reached 0.77% at the end of the 1% drift cycles. Also, at 135 mm and 270mm

above the column-footing interface, the strains in longitudinal reinforcement and the starter bars at the east and west, reached 0.21% during the last cycle of 2% drift. Subsequently, all the strain gauges within the hinging region went off scale due to the slippage of spliced reinforcement. The strains recorded in tire treads reached 0.33% at the end of the 2% drift cycles.

There was no strength degradation observed during the first two cycles of 3% drift, though an increased strain of 0.32% was observed in the first two tires from the base. At the end of 3% drift cycles, all the strain gauges on longitudinal reinforcement developed a minimum of tension and compression yielding.

A small gap formed between the first and the second tires during 4% drift cycles. During the second and third cycles of 6% drift, the first tire from the bottom showed signs of expansion, and the space between the tires became wider. The rubber in treads stretched more, generating a gradual sound of stretching and rupturing of steel embedded in the tread rubber.

Slight strength decay was observed at the beginning of 7% drift cycle. The column capacity dropped by 13%, suddenly. The first tire ruptured on the west side, as illustrated in Figure 4.13 (d). The horizontal displacement LVDTs stopped functioning beyond this level as they reached their stroke limit. Gradual spalling of concrete occurred near the middle of the ruptured first tire on the west side, when the second cycle of 7% drift was applied. The longitudinal reinforcement buckled within the same region and the load dropped sharply to 134 kN. The test was then terminated due safety concerns. Figure 4.13 shows the behaviour of Column TC-9 at selected stages of testing. The duration of the test for this column was three hour and fifteen minutes.

The hysteretic relationships for lateral force-lateral displacement and moment-lateral displacement are shown in Figure 4.14 and Figure 4.15. These relationships show similar features as those discussed for Column TC-8, indicating initially stable response up to 3% drift ratio, followed by some slippage of spliced reinforcement. However, the column maintained its lateral load resistance with very little strength decay. The column capacity

dropped by 24% during the third cycles of 7% drift cycles when the first tire ruptured and the longitudinal bars buckled.

Figure 4. 16, Figure 4.17, and Figure 4.18 show hysteretic moment-total rotation, moment-anchorage slip rotation, and moment-flexural rotation relationships, respectively. Figure 4.17 indicates that approximately $1/3^{rd}$ of the total rotation could be attributed to the slippage of spliced reinforcement, measured as anchorage slip component of total rotation, and $2/3^{rd}$ caused by flexure. Figure A.5 and Figure A.6 illustrate the strain gauge data for longitudinal reinforcement and starter bars, as well as the treads and rims of tires, respectively.

4.2.4 Performance of Column TC-10

Column TC-10 was a shear critical circular column, with reduced shear span of 1200 mm. The longitudinal reinforcement in this column was identical to that of the pervious column (TC-9). It consisted of twelve No. 20 (19.5 mm diameter) deformed steel bars. There was no conventional transverse reinforcement. This column was tested under the same axial load of 1950 kN as that applied to TC-9, which corresponds to 16% of its concentric capacity. The actual test started with the application of full axial load followed by lateral load reversals applied in the displacement control mode.

The lateral load capacity of the column was higher than the flexure dominant companion Column TC-9. The maximum lateral load recorded at 0.5% drift was 309 kN. The load resistance increased up to 339 kN at the begging of 1% drift cycles. Tensile strains in the longitudinal reinforcement reached 0.8% at the column-footing interface, at the end of the lateral drift cycles at 1%. Yielding of reinforcement was also observed at 135 mm below and above the footing at the end of 1% and 2% drift cycles, respectively with strains reaching up to 0.26%. Gauge 5 at column footing interface maintained high strain readings, and reached 1.23% strain at the end of 2% lateral drift.

At the beginning of 3% lateral drift cycles, strain gauges 2 and 5 on longitudinal reinforcement and 8, 12, 17, 20, and 21 on tires recorded strains well above the yield strain,

developing 0.8% and 0.84% on the longitudinal reinforcement and 0.39%, 0.45%, 0.25%, 0.33%, and 0.45% on the tires, respectively. No visual cracks were noticed in or between the tires. There was no spalling observed. Loud sound was heard at the end of the second cycle of 3% drift ratio when one of the longitudinal reinforcement on the west side ruptured. When the column was pushed towards the last cycle of 3% drift, the second tire ruptured on the west side. At the end of the third cycle of 3% drift, the third tire also ruptured completely on the north-east side. The strain gauges on tires developed higher strains at this stage of loading, showing between 0.24% and 0.49% strains. A 24% reduction in lateral load resistance was recorded when the column was pulled towards the last cycle of 3% lateral drift in the east direction. Similar reduction in load resistance was not observed when it was loaded towards west, because there was no rupture in tires on this side.

All of the strain gauges on the longitudinal reinforcement were damaged at the beginning of 4% drift cycles. The spalling of concrete extended gradually towards the west side, in the second tire. During the same stage of loading, the third tire suffered concrete spalling on the north side, which was accompanied by 33% strength decay. The second tire opened up more on the west side, followed by sudden buckling of longitudinal bars on east and west sides, leading to the failure of the column, as shown in Figure 4.19 (a). The specimen became unstable and the test was discontinued at this drift level due to safety concerns. Figure 4.19 shows some views of Column TC-10 during selected stages of testing.

The hysteretic relationships for lateral force-lateral displacement and moment-lateral displacement relationships are shown in Figure 4.20 and Figure 4.21. They indicate that the column was able to sustain its lateral load capacity during 2% drift cycles and showed gradual strength degradation during 3% drift cycles. At this load stage the strength decay was 33% as the concrete crushed at the second and third tire locations.

Figure 4.22, Figure 4.23, and Figure 4.24 show hysteretic moment-total rotation, moment-anchorage slip rotation, and moment-flexural rotation relationships, respectively. Figure 4.23 indicates that, at the end of testing, approximately $1/4^{th}$ of the total rotation was due to anchorage slip, and the remaining $3/4^{th}$ was due to flexure. The strain gauge data are plotted

in Figure A.7 and Figure A.8, showing strains until the gauges were damaged near the end of the test.

4.2.5 Performance of Column TC-11

Column TC-11 was a shear dominant column with reduced shear span and hence was companion to TC-10, except for the column size. It was reinforced with twelve No. 25 (25.2 mm diameter) deformed steel bars. The height of the column was 1500 mm, measured to the point of inflection. There was no conventional transverse reinforcement in the column in the form of ties. The column was tested under a constant compressive force of 1900 kN, which represented 10% of its concentric capacity.

The test started with the application of full axial load, followed by lateral load reversals, which were applied in the displacement control mode. No damage was observed during the three cycles at 0.5% drift. At the end of 1% drift, there was yielding in the longitudinal reinforcement, at the column-footing interface, the strains reaching 0.38% and 0.34% on the east and west sides, respectively.

The maximum lateral load resistance of 506 kN was attained at the beginning of 2% lateral drift. The first tire developed 0.25% strain in the tread, on the west side. Strain measurements on the longitudinal reinforcement indicated increased values, developing 1.4% and 1.1% on the east and west sides of column-footing interface (Gauge 2 and 5), at the end of 2% drift cycles. At the end of 3% drift cycles, the strains in the rims of the first, second, and third tires reached 0.39%, 0.34%, and 0.49%, respectively which indicated increased expansion of concrete in these tires. During 4% lateral drift, most strain gauges showed strains up to and exceeding 0.5%, but there was no visible damage observed up to the end of 5% lateral drift cycles. A small opening or separation of tires was observed during 6% drift cycles, between the first and second tires from the bottom, though no visible rupture was observed. At the beginning of 7% drift, stretching noise of tires was heard. During subsequent deformation cycles, the second tire on the east side ruptured during the last cycle at 7% drift as shown in Figure 4.25 (d).

The column sustained 8% drift cycles without significant strength decay. The failure was initiated by rupturing of the steel in the second tire, on the east side, which eventually led to the complete rupturing of this tire, exposing concrete. During the second and third cycles at 8% drift, the stretching and rupturing noise of the steel in treads of the second tire was noticeable, exposing cracked concrete as shown in Figure 4.25 (e). The gauges on the treads and rims of the second and third tire broke loose due to high pressures exerted by longitudinal bars. Also, some of the LVDTs went out of range, and were removed at this stage.

During the first cycle at 9% drift, there was no decay in lateral force resistance. The column failed during the third cycle at 9% drift due the fracture of the second tire, exposing crushed concrete, followed by the buckling of longitudinal reinforcement. A small rupture was also observed in the third tire, on the west side, as shown in Figure 4.25 (j). Testing was then terminated as the column was found to be unsafe to continue loading. Figure 4.25 shows selected views of Column TC-11 during testing. The duration of the test for this column was four hours and thirty minutes.

The hysteretic relationships of the lateral force-lateral displacement and moment-lateral displacement relationships are shown in Figure 4.26 and Figure 4.27. These relationships indicate that the column was able to sustain lateral loads up to the first cycle of 9% drift without significant strength decay. The column showed stable hysteresis loops up to the beginning of 9% lateral drift before the capacity dropped by 21% during the third cycle of 9% drift. The enhanced behaviour relative to Column TC-10 was attributed to improved stability of longitudinal reinforcement provided by the rims of this different type and size tire. The lateral load capacity of the column was higher than that recorded for the companion column TC-10, due to its increased size.

Figure 4.28, Figure 4.29, and Figure 4.30 show the hysteretic moment-total rotation, moment-anchorage slip rotation, and moment-flexural rotation relationships, respectively. Figure 4.29 indicates that approximately $1/10^{th}$ of the total rotation was caused by anchorage

slip, leaving the remaining 9/10th to flexure which means that there was little extension of longitudinal bars in the footing. Figure A.9 and Figure A.10 in Appendix A illustrate the strain gauge data. These readings are mostly limited to deformations of the third cycle at 6% drift, after which the gauges were damaged due to excessive deformations and/or crushing of concrete in the hinging region.

4.2.6 Performance of Column TC-12

Column TC-12 was companion to TC-10, with identical geometric and material properties. However, different brand name of tires was used in this column. The loading scheme was exactly the same as before, including the level of axial load (1950 kN) which corresponded to 16% of its concentric capacity. The actual test started with the application of full axial load followed by lateral load reversals applied in the displacement control mode, as before.

The observed behaviour at early stages of loading was very similar to that of TC-10. However, the load resistance was different in this column. During the three cycles at 0.5% drift, no damage was observed and the maximum lateral load recorded was 235 kN. At the end of 1% drift cycle, the strains in extreme longitudinal bar reached 0.62%, 0.75%, and 0.56% at the column-footing interface on the east and west sides, and at 135 mm above the footing (Gauge 2, 5, and 6), respectively.

The strain gauge at the column-footing interface on the west side was damaged at the second cycle of 2% drift. The strains continued to increase with imposed drift until the strain in Gauge 2 reached 1.1% at the end of 2% drift, while the strain in the tread of the first tire reached 0.35%. Strain measurements at the end of 3% cycles on the second and third tires indicated increased values, developing 0.50%, 0.39%, and 0.49% strains on the east and west sides (Gauge 7, 10, and 18) respectively. Strains in the rim of the first tire reached 0.38% and the strain gauges in the first, second and third tire recorded values of up to 0.5% at the end of 4% drift cycles. Some of the strain gauges on longitudinal reinforcement recorded increased strains during 5% drift cycles, reaching up to 1.5%. The second and third tires started to separate on the east side, and there was a small opening in between the tires on the

east side. There was no visible damage in the column until the end of 5% drift cycles. The opening between the tires became more noticeable when the column was loaded to 6% drift, as indicated in Figure 4.31 (d). Most of the strain gauges broke loose during the last cycle of 6% drift. There was little strength decay until the third cycle of 6% drift. As the third cycle was applied, the noise of rupturing longitudinal reinforcement could be heard one after the other and there was degradation in strength as observed in the hysteresis loop. Further stretching noise of tires was heard at the beginning of 7% drift, possibly de-bonding from the treaded rubber in the tires. The strain readings on the rim and treads of the second and third tires showed increased strains. The steel in the treads of the second tire ruptured on the west side, resulting in a drop of about 6% in load resistance. The progression of damage continued until the second cycle of 7% drift, at which stage the column resistance dropped suddenly by 38%. The subsequent cycle led to more rupturing of the second tire on the west and buckling of longitudinal reinforcement, crushing of core concrete and rupturing of the third tire on the north side, as shown in Figure 4.31 (e) and (f). Testing was discontinued at this stage due to the significant loss in strength. The duration of test for this column was four hours. Figure 4.31 shows performance of Column TC-12 during selected stages of testing.

The hysteretic relationship of the lateral force-lateral displacement and moment-lateral displacement relationships obtained experimentally are shown in Figure 4.32 and Figure 4.33. These relationships indicate that the column was able to sustain the imposed load up to 6% drift. There was no significant strength decay up to the first cycle of 7% drift, but the column developed degradation of strength during the second cycle of 7% drift. The improvement in behaviour relative to Column TC-10 was attributed to the number of cords in the treads of the tire, which was a different brand than those used in TC-10. The tires in TC-12 provided better shear resistance and improved confinement to the core concrete.

Figure 4.34, Figure 4.35, and Figure 4.36 show the hysteretic moment-total rotation, moment-anchorage slip rotation, and moment-flexural rotation relationships, respectively, for Column TC-12. Figure 4.35 indicates that approximately $1/10^{th}$ of the total rotations was caused by anchorage slip, and the remaining $9/10^{th}$ was caused by flexure. These rotations are the same as those measured in TC-11. Figure A.11 and Figure A.12 illustrate the strain

gauge data recorded. These readings reflect the strains measured until the gauges were damaged at approximately 7% drift, though some were damaged prior to testing, during construction.

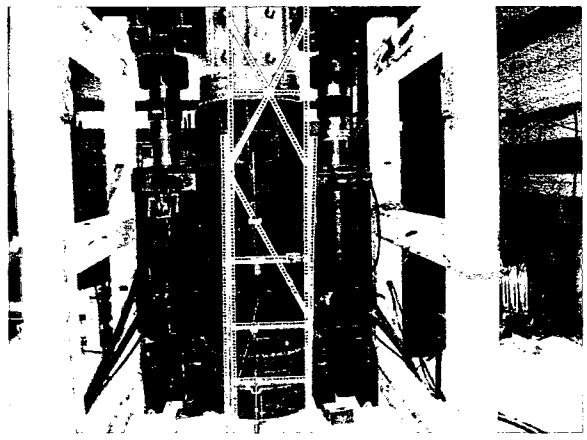

(a) At 2% Drift

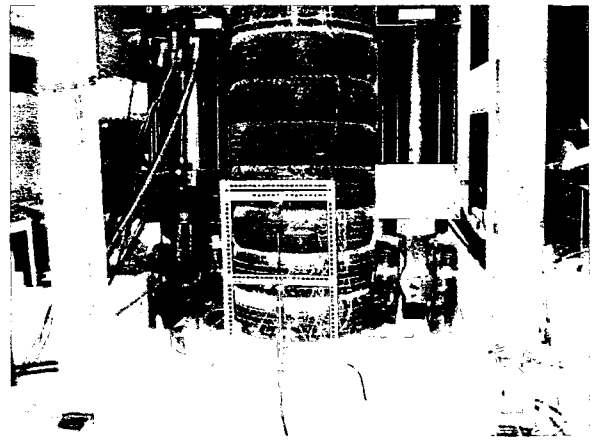

(b) At 5% Drift

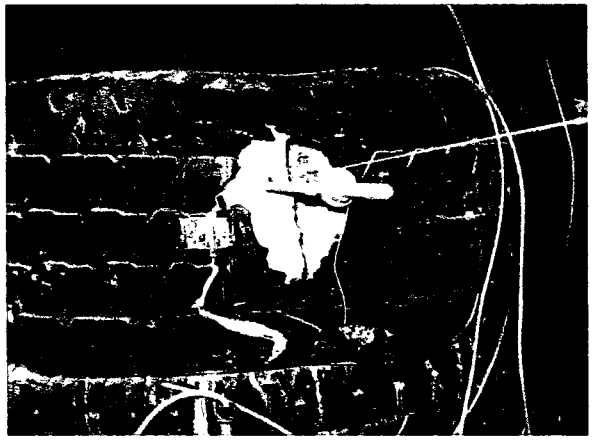

(c) At 6% Drift (End of 2nd Cycle)

(d) At 7% Drift, Close-up View

(e) At 7% Drift (End of 2nd Cycle)

(f) End of Test, Close-up View

Figure 4.1: Behaviour of Column TC-7 During Selected Stages of Testing

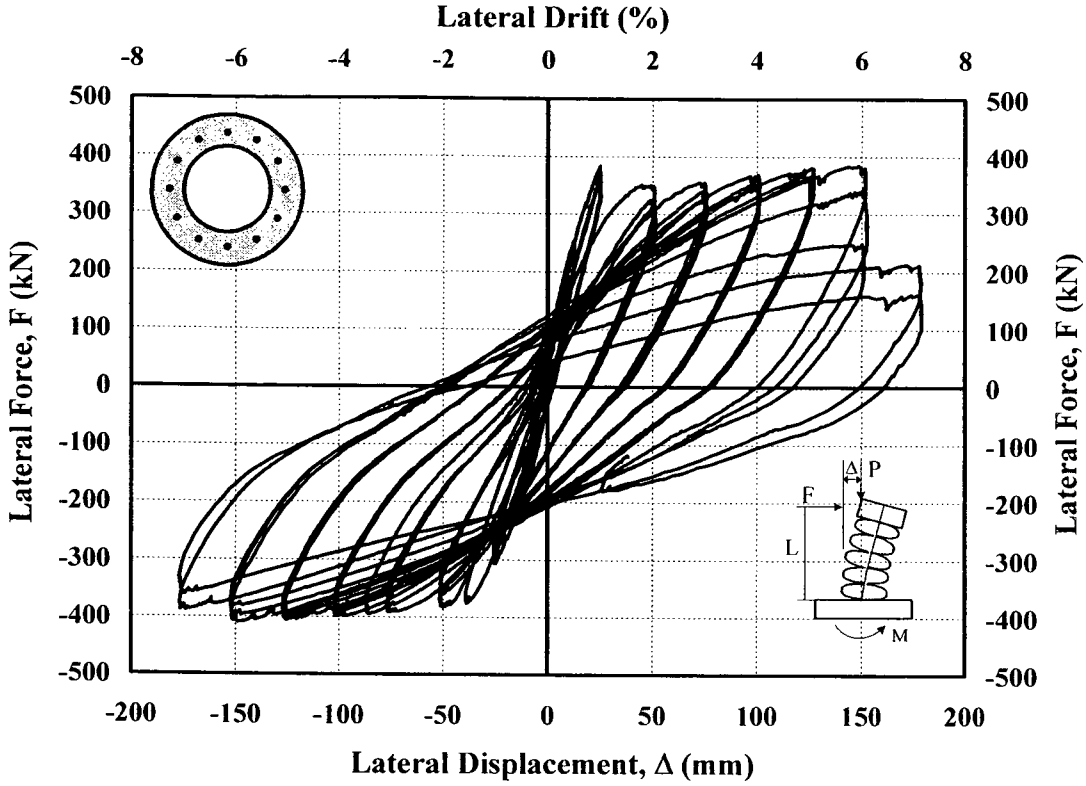

Figure 4.2: Hysteretic Force-Displacement Relationship for Column TC-7

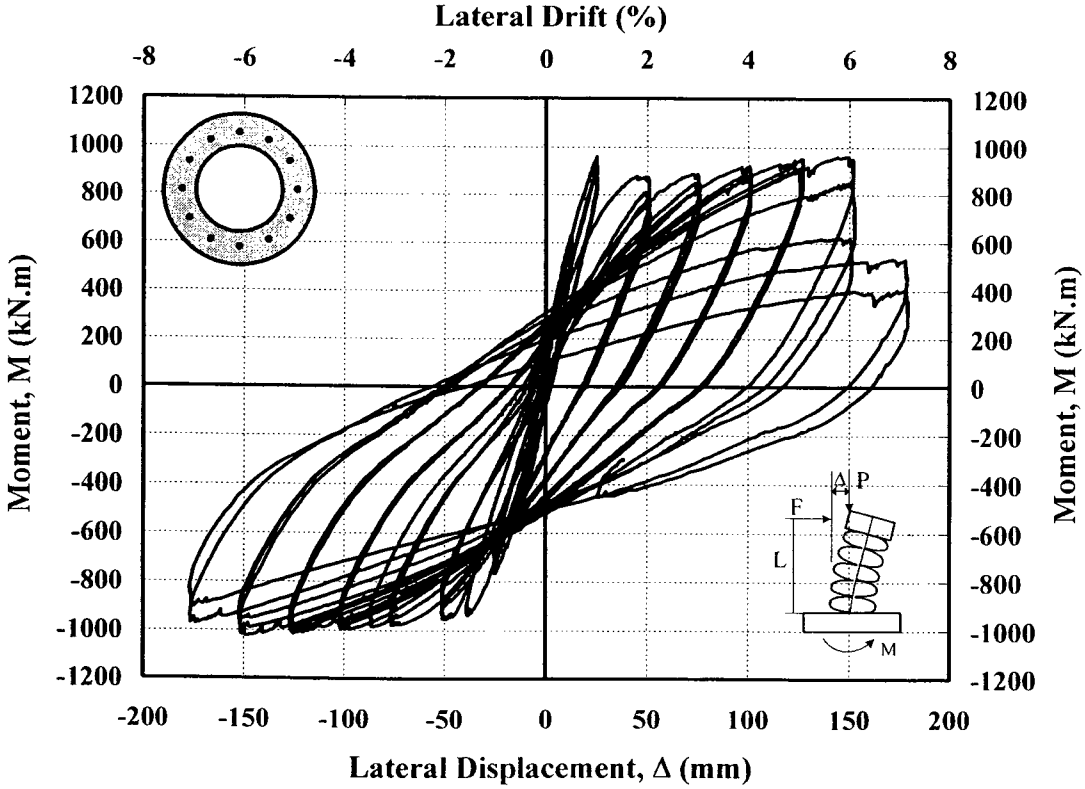

Figure 4.3: Hysteretic Moment-Displacement Relationship for Column TC-7

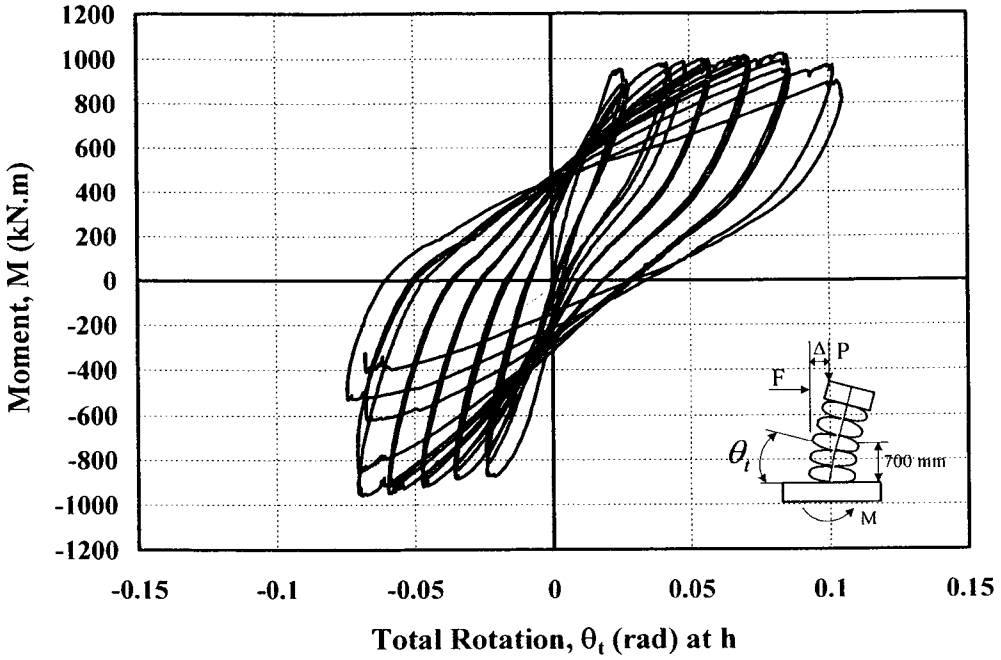

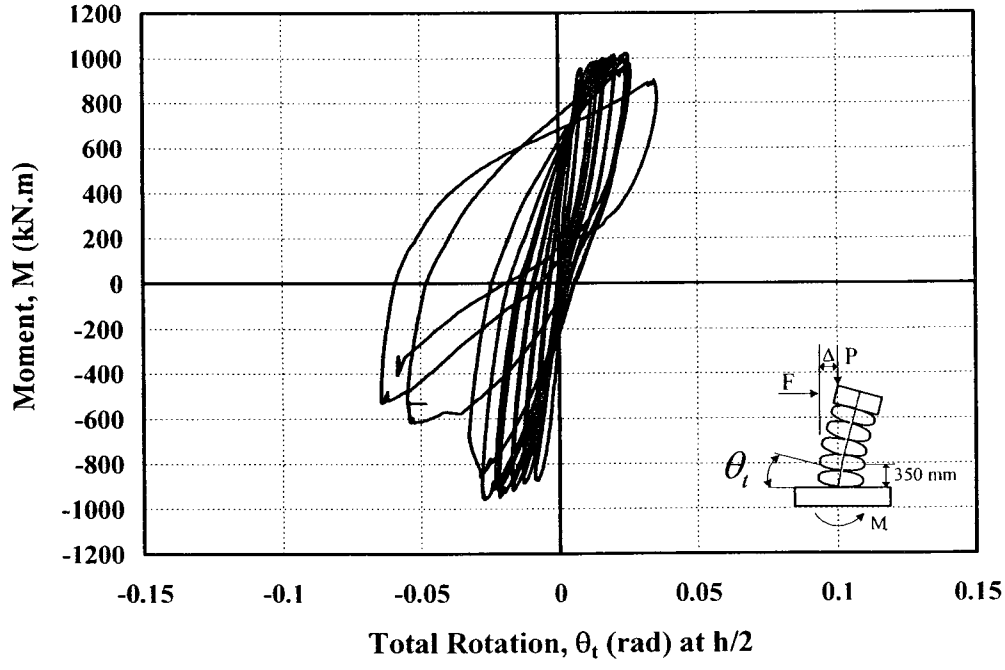

Figure 4.4: Moment-Total Rotation Relationship for Column TC-7

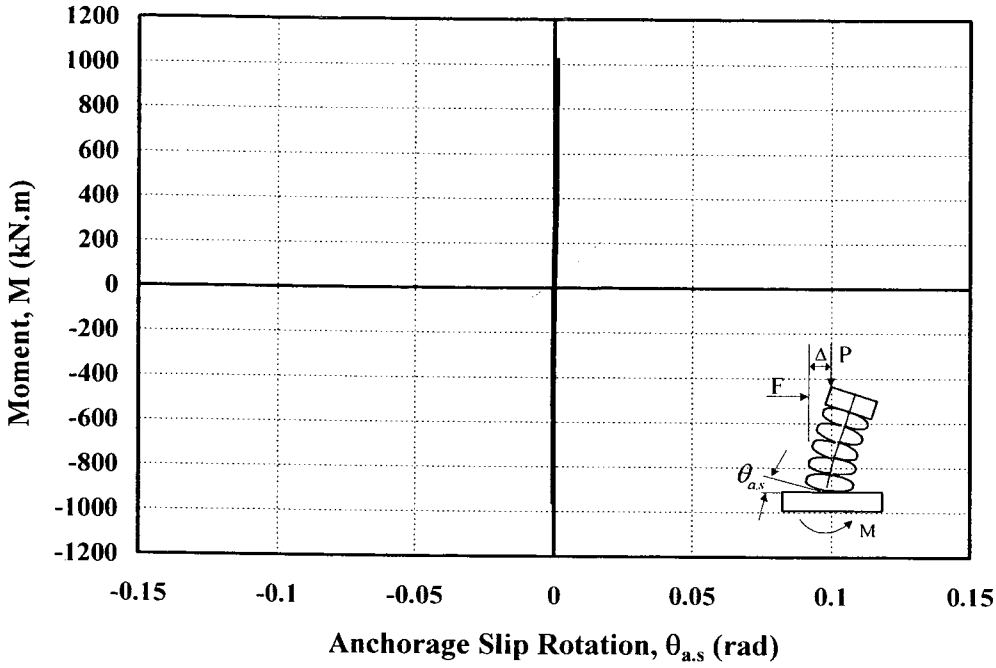

Figure 4.5: Moment-Anchorage Slip Rotation Relationship for Column TC-7

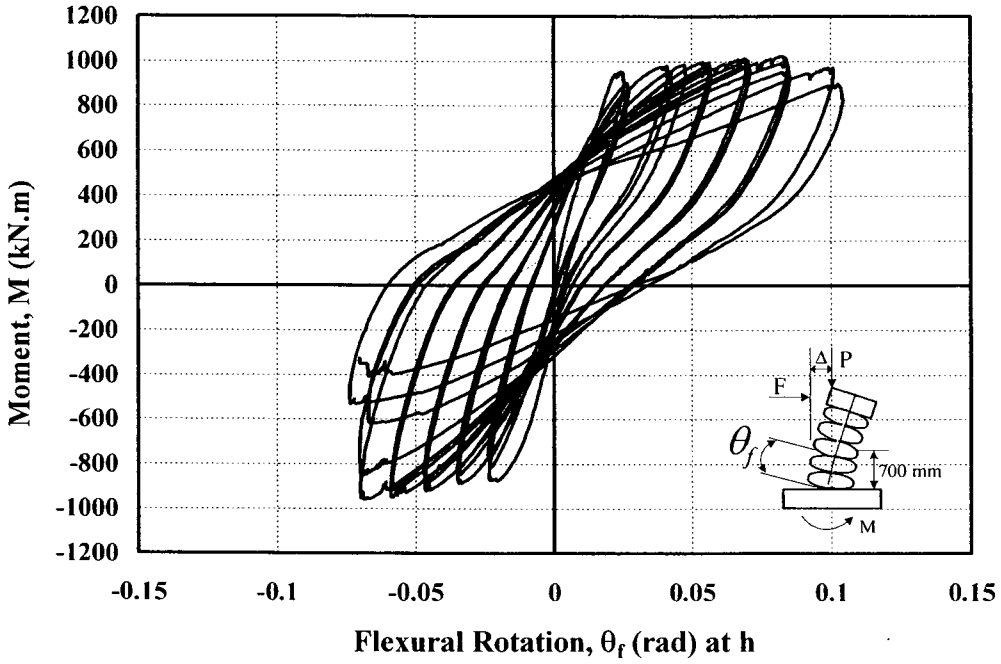

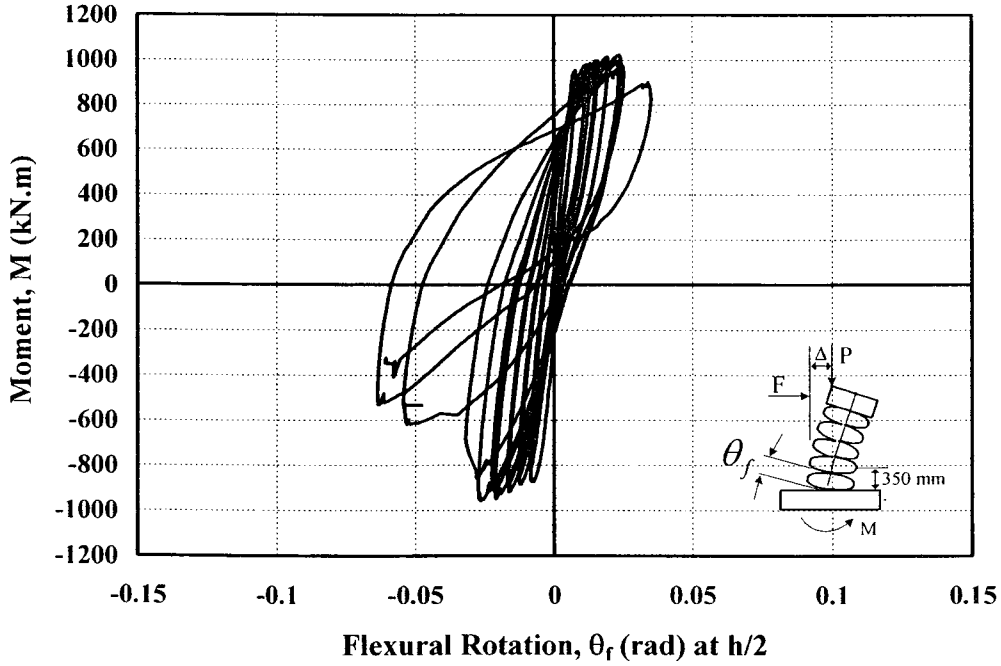

Figure 4.6: Moment-Flexural Rotation Relationship for Column TC-7

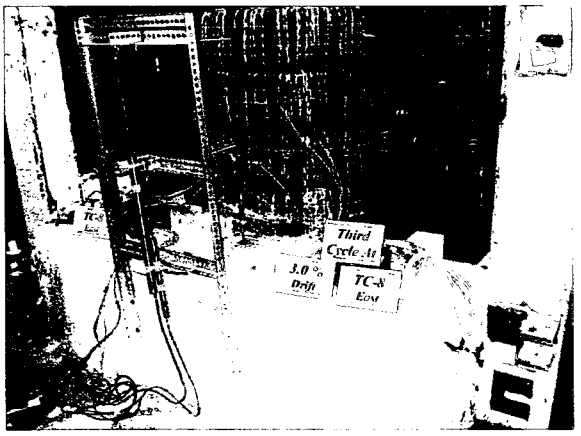

(a) At 3.0% Drift

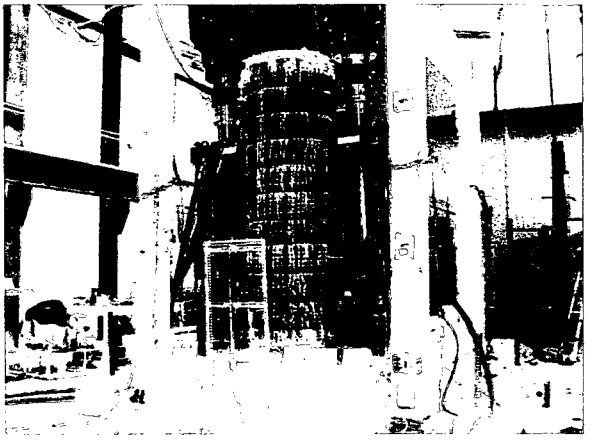

(b) At 6.0% Drift

(c) Opening between Tires at 5.0 % Drift

(d) Opening between Tires at 7.0 % Drift

(e) Rupture in 2nd Tire at 9.0% Drift

(f) End of Test, Close up view

Figure 4.7: Behaviour of Column TC-8 During Selected Stages of Testing

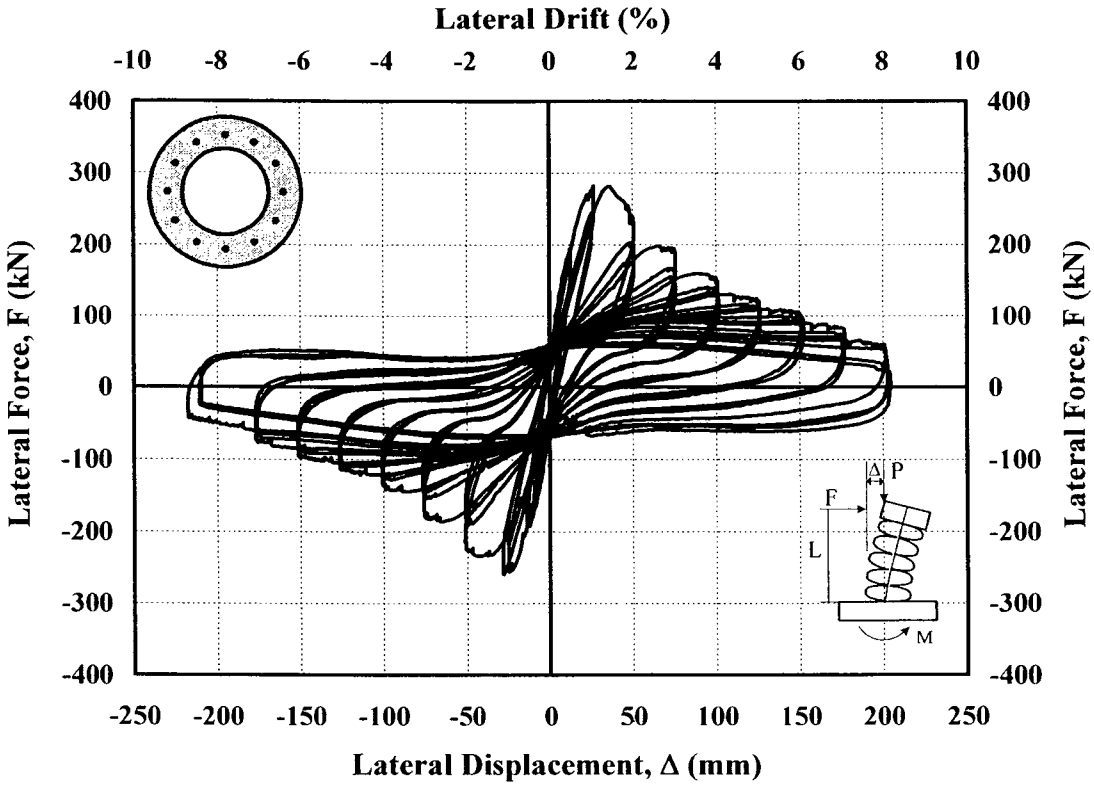

Figure 4.8: Hysteretic Force-Displacement Relationship for Column TC-8

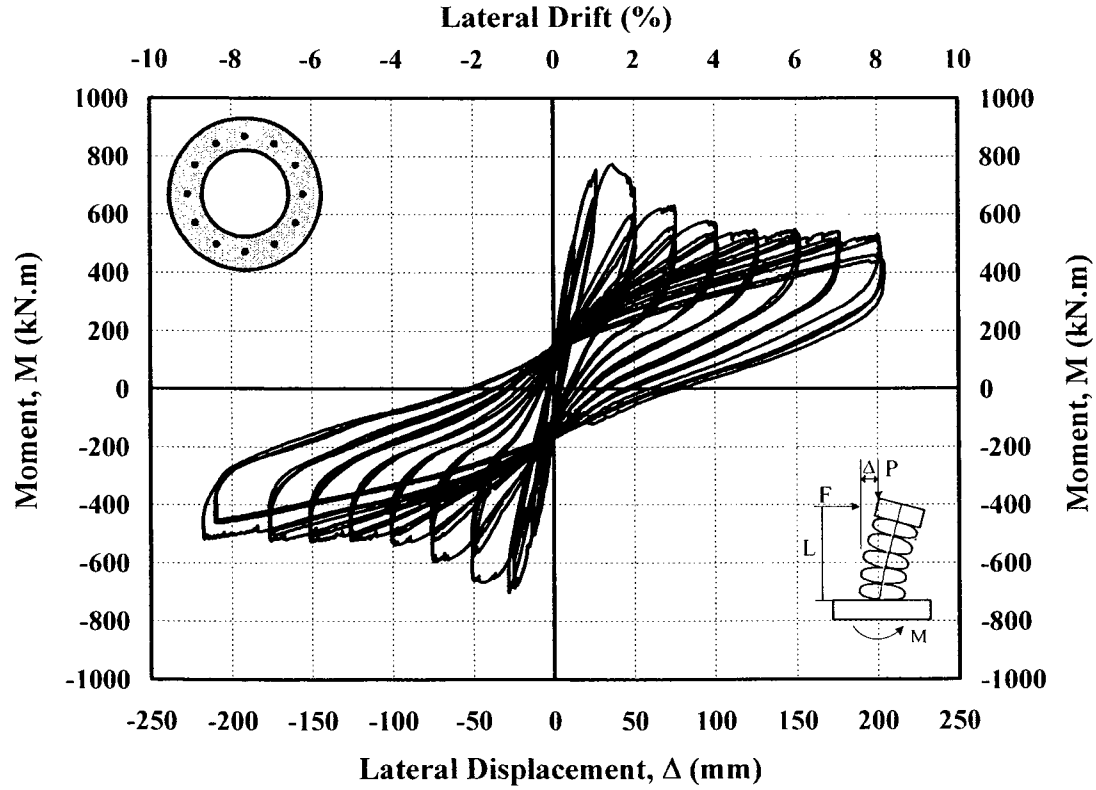

Figure 4.9: Hysteretic Moment-Displacement Relationship for Column TC-8

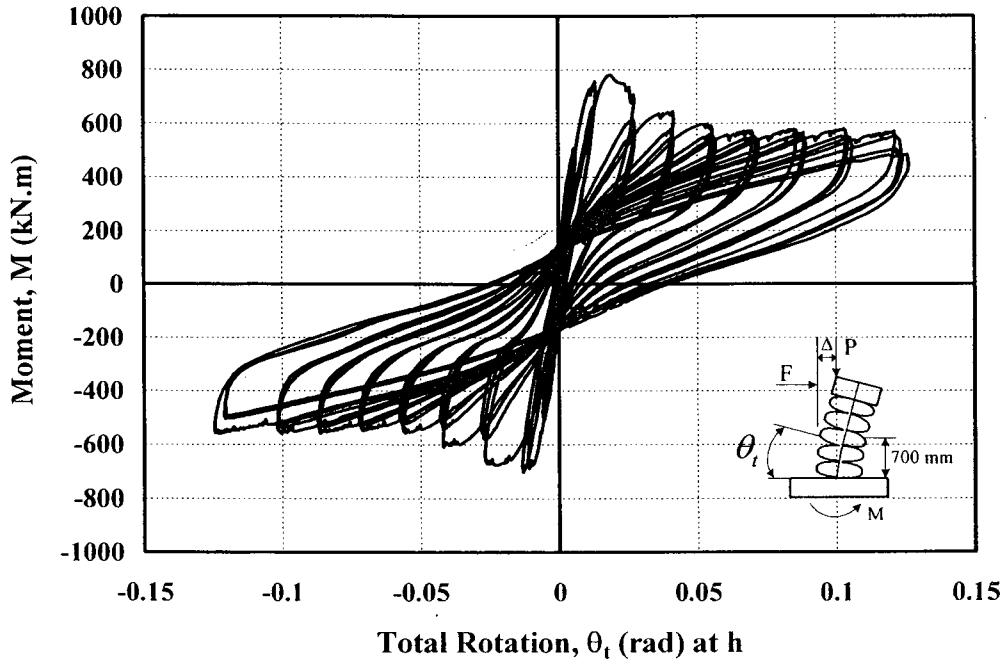

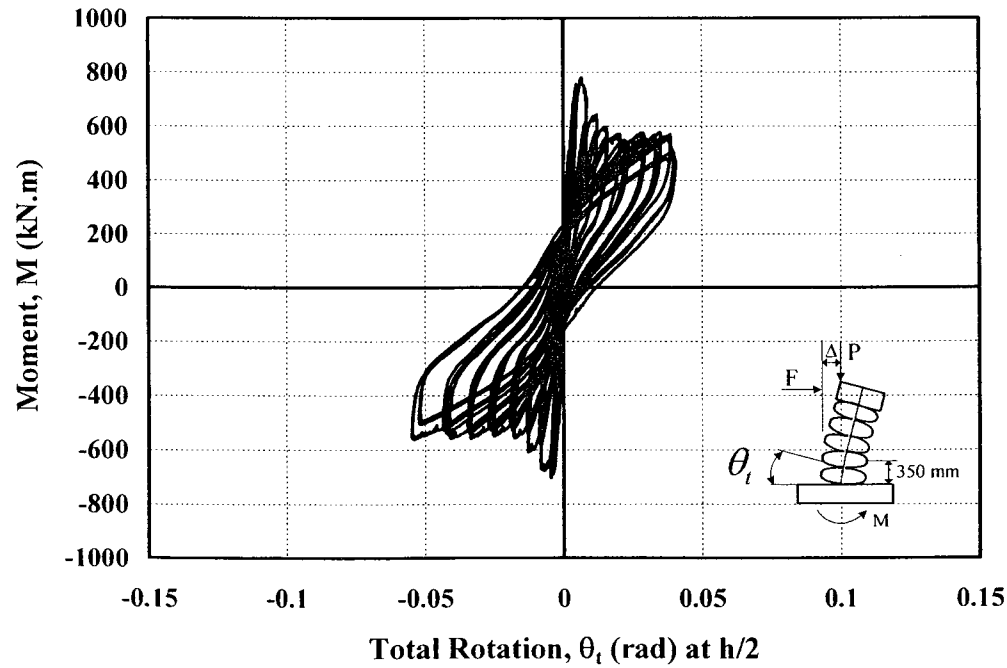

Figure 4.10: Moment-Total Rotation Relationship for Column TC-8

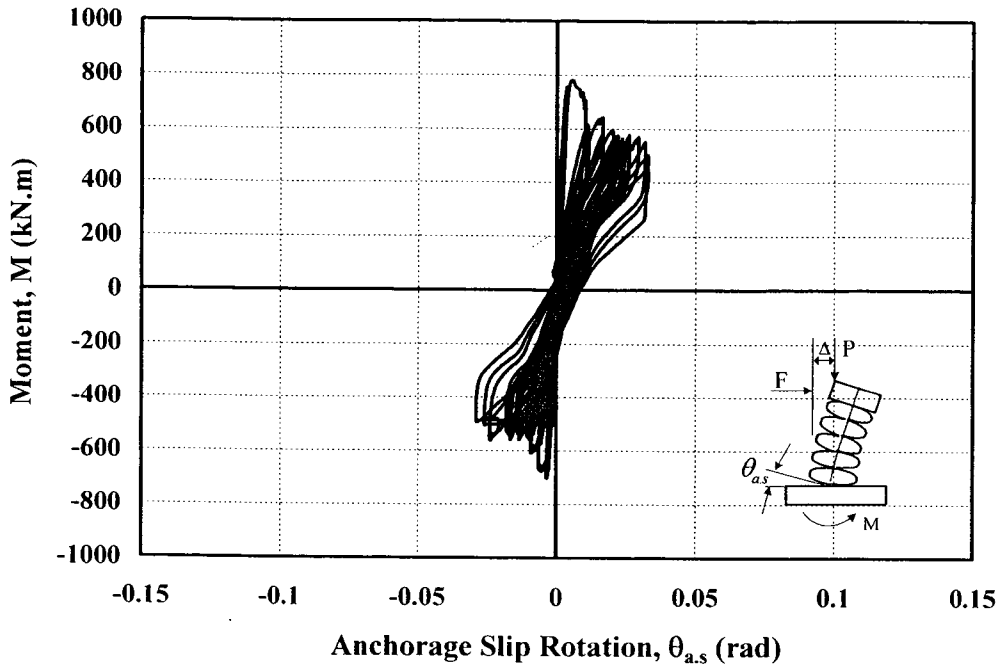

Figure 4.11: Moment-Anchorage Slip Rotation Relationship for Column TC-8

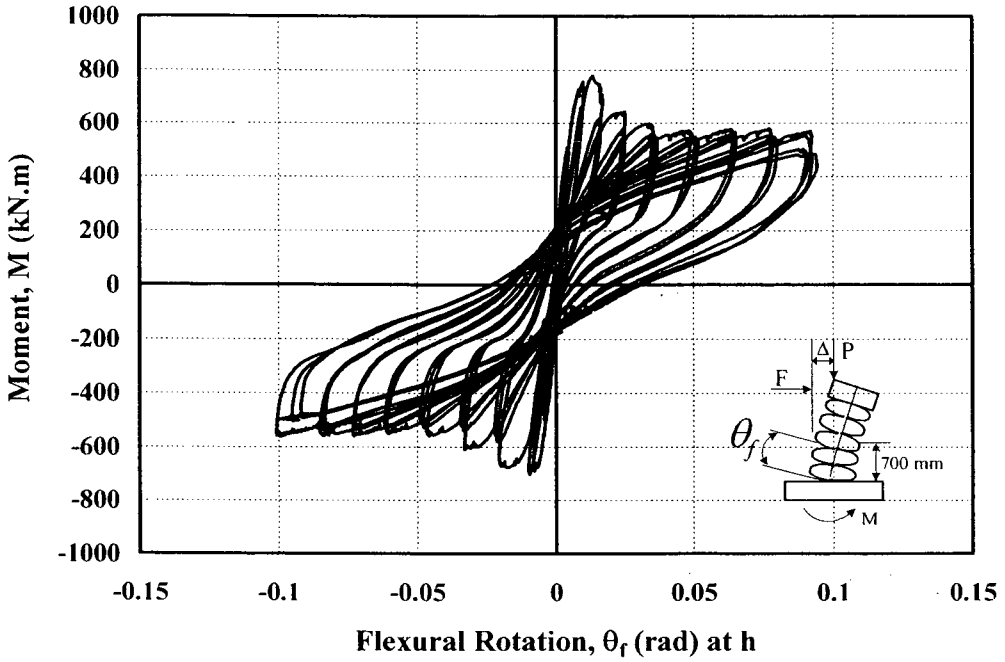

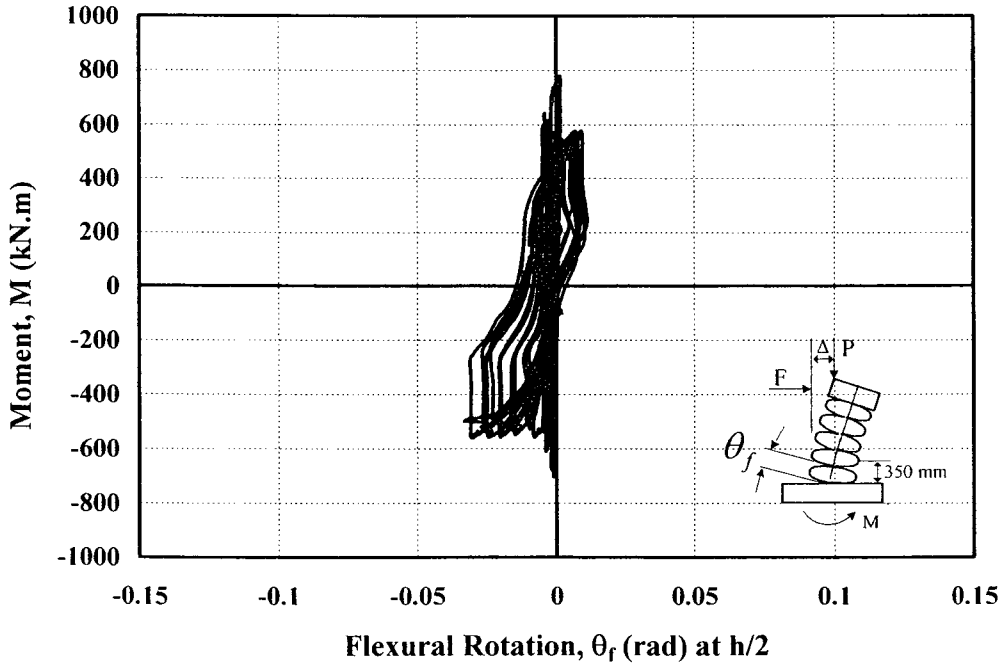

Figure 4.12: Moment-Flexural Rotation Relationship for Column TC-8

(a) At 2.0 % Drift

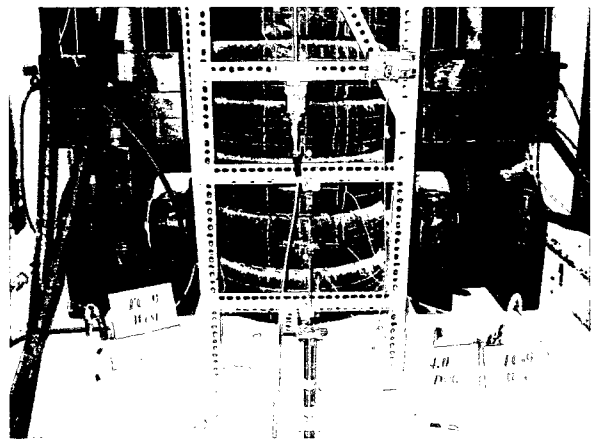

(b) At 4.0% Drift

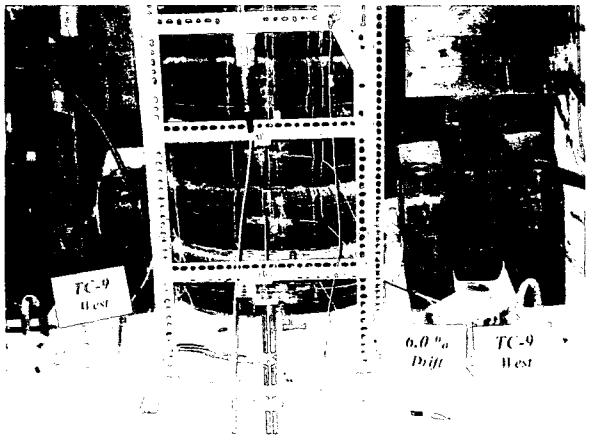

(C) At 6.0% Drift

(d) Rupture of the First Tire

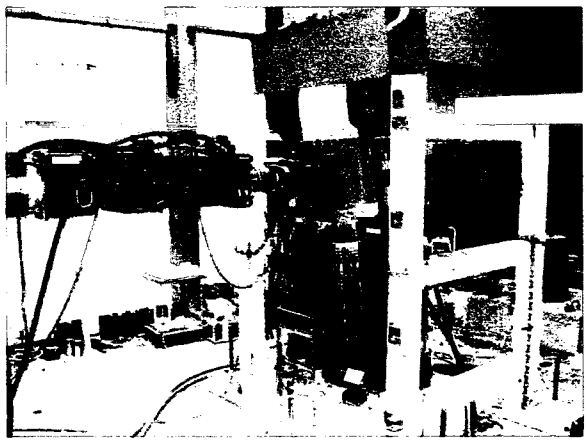

(e) At 7.0% Drift

(f) Buckling of Bars (West Side)

Figure 4.13: Behaviour of Column TC-9 During Selected Stages of Testing

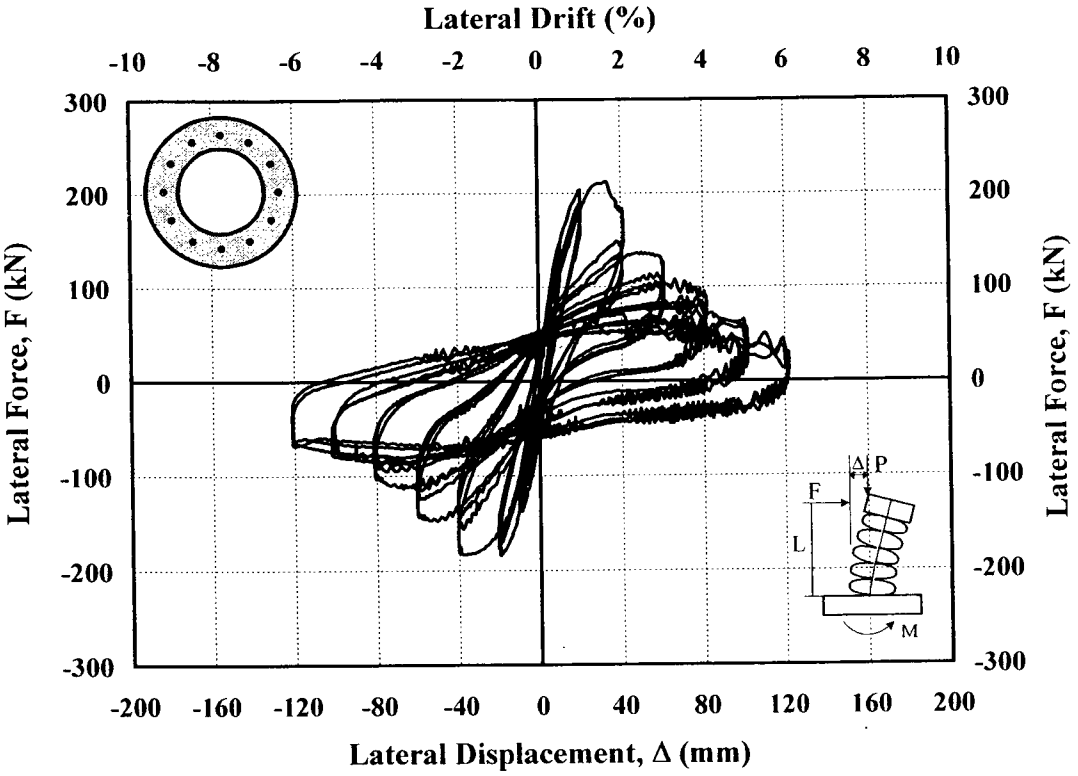

Figure 4.14: Hysteretic Force-Displacement Relationship for Column TC-9

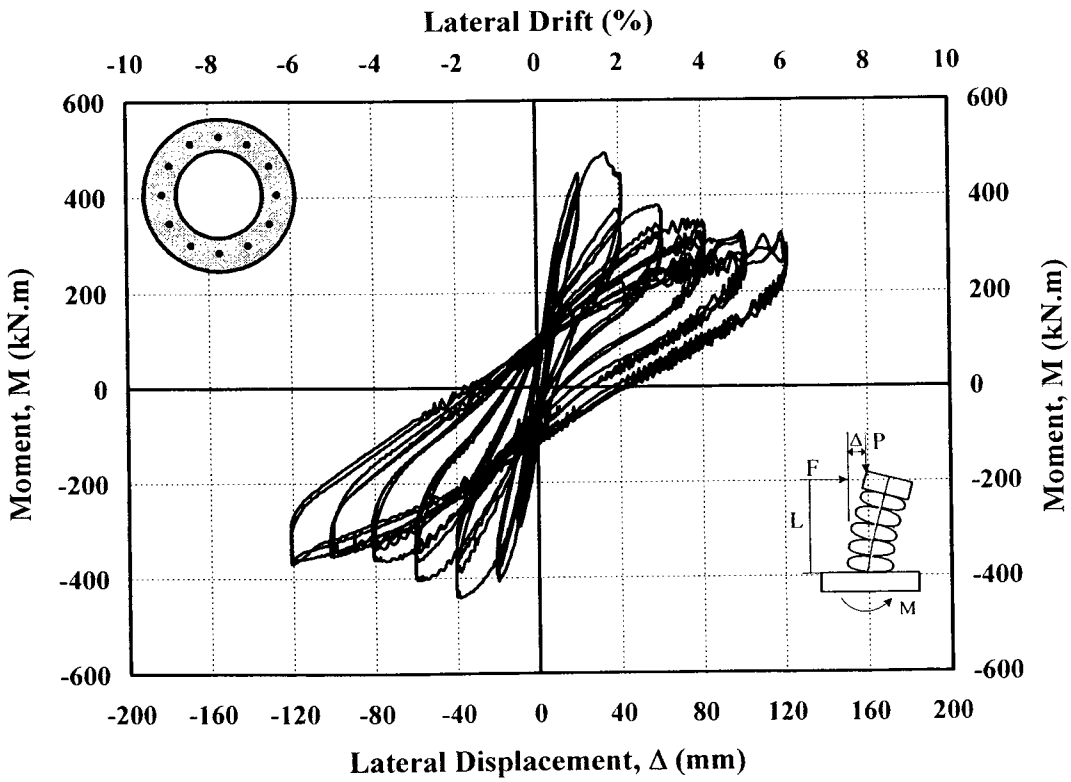

Figure 4.15: Hysteretic Moment-Displacement Relationship for Column TC-9

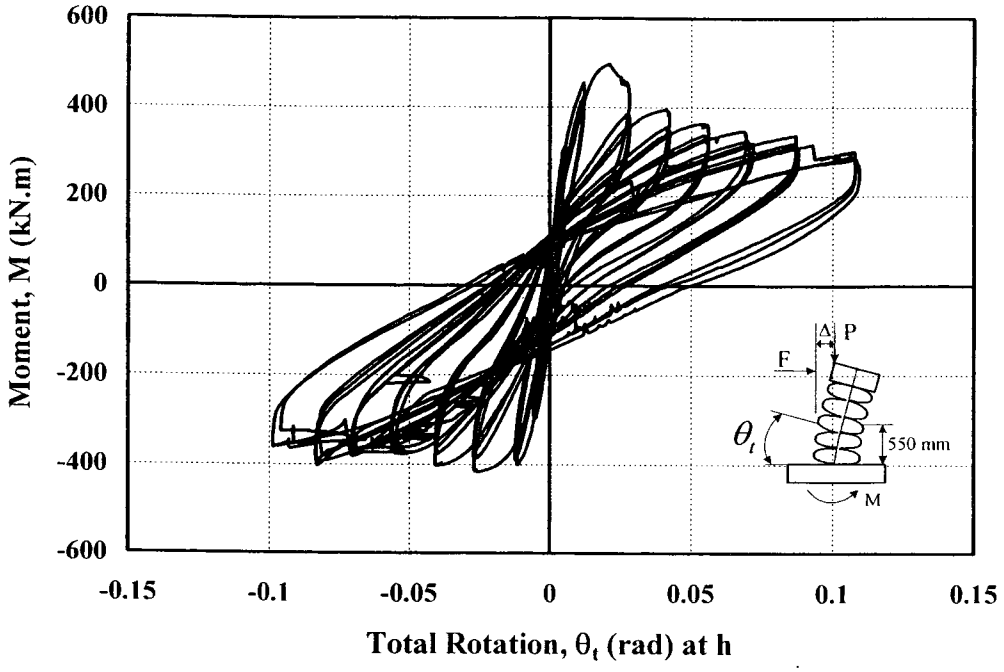

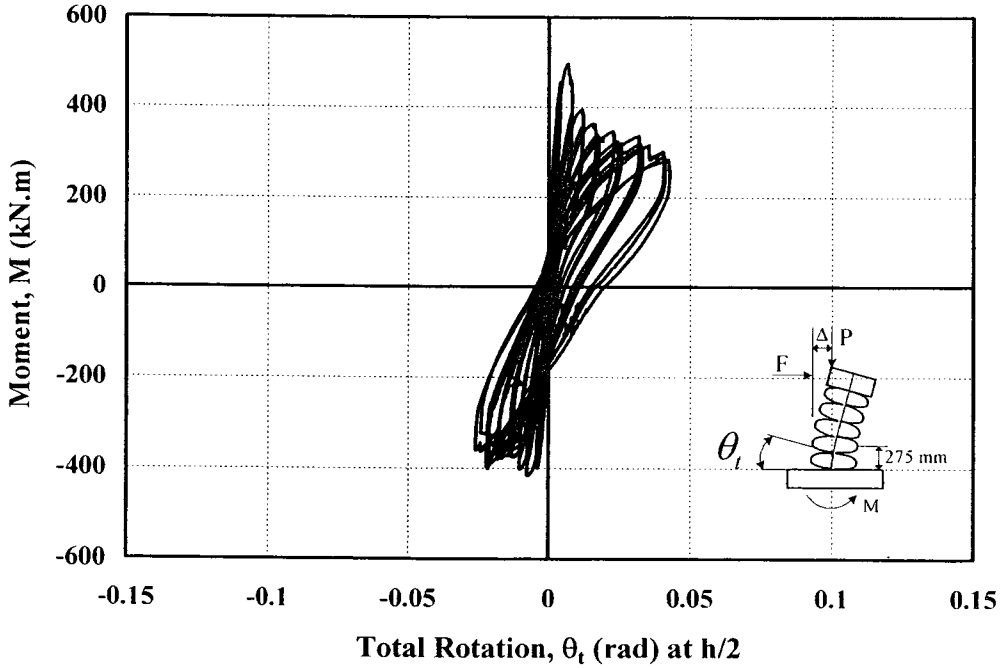

Figure 4. 16: Moment-Total Rotation Relationship for Column TC-9

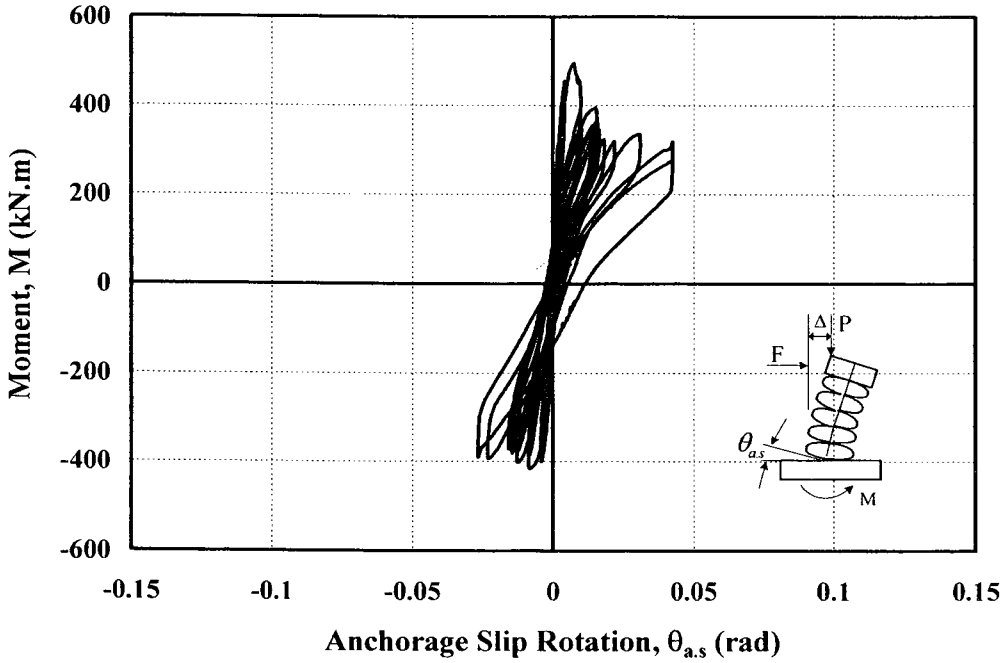

Figure 4.17: Moment-Anchorage Slip Rotation Relationship for Column TC-9

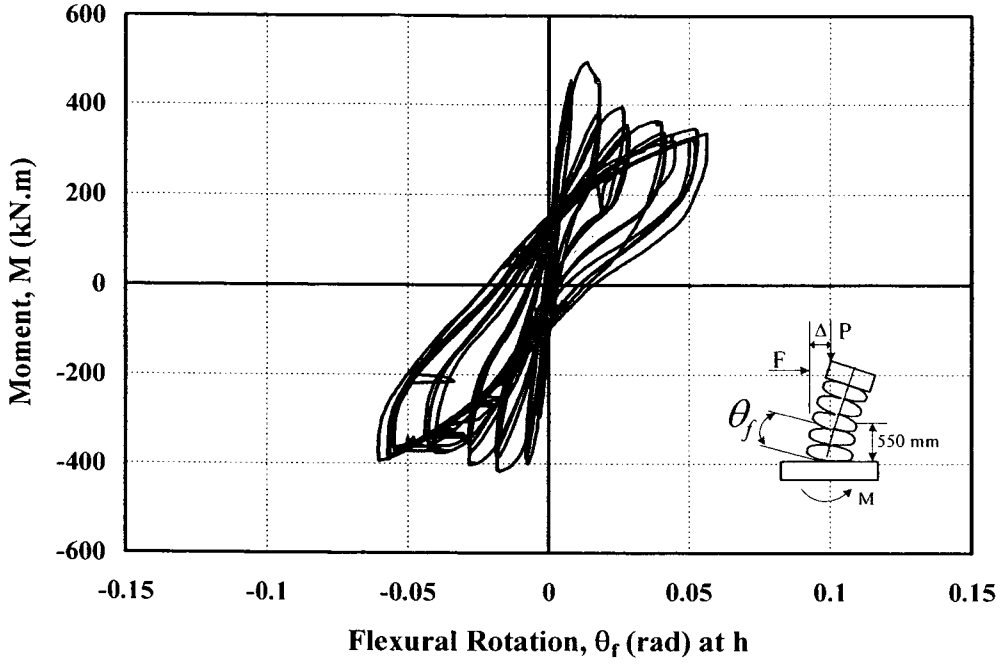

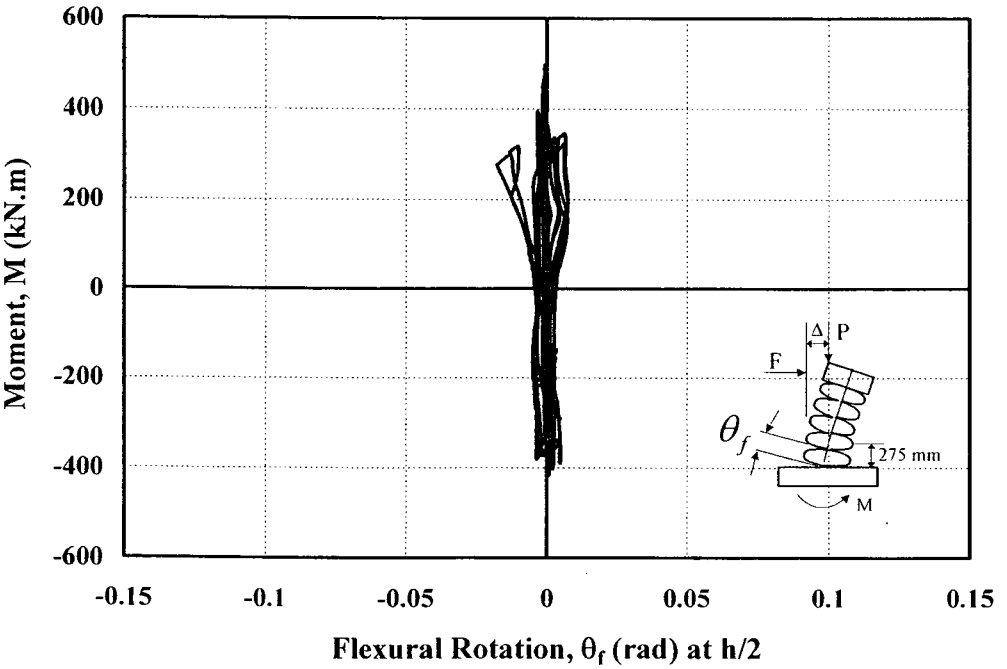

Figure 4.18: Moment-Flexural Rotation Relationship for Column TC-9

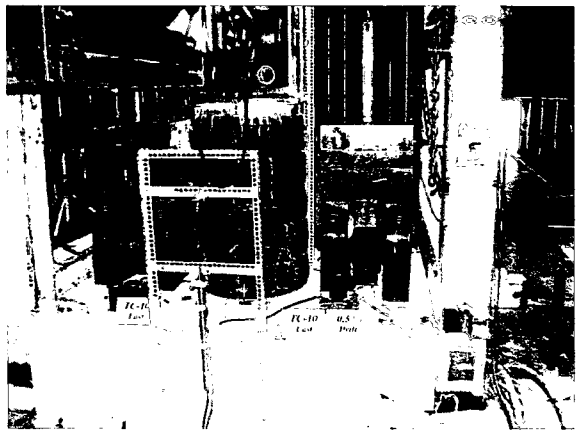

(a) At 0.5% Drift

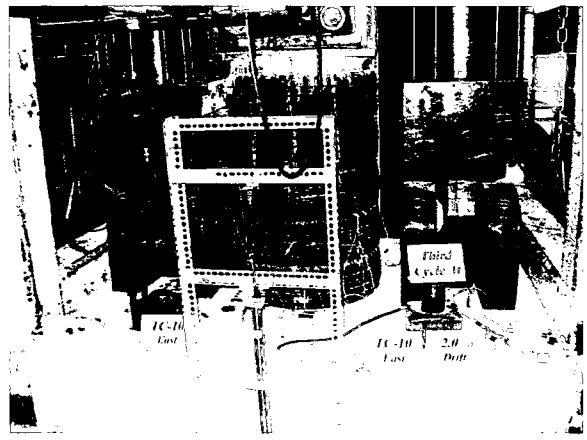

(b) At 2.0% Drift

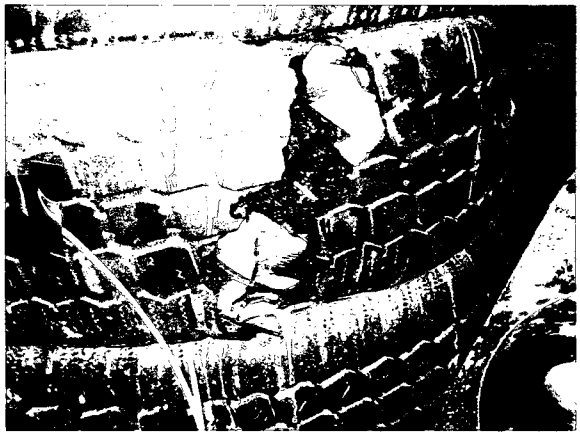

(C) At 3.0% Drift

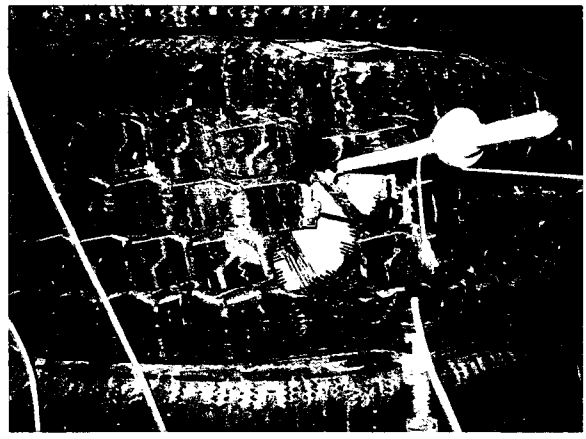

(d) At 3.0% Drift (West View)

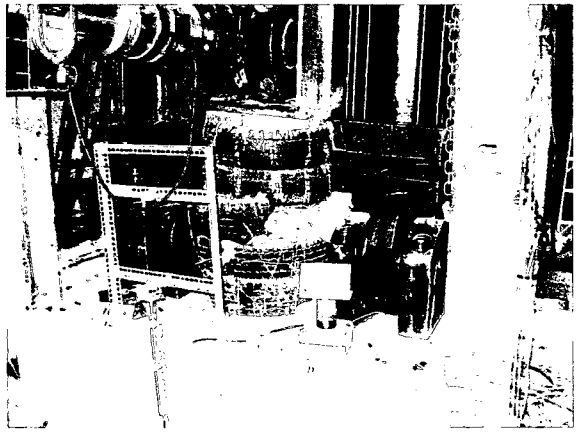

(e) At 4.0% Drift

(f) End of Test (Buckling of Bars)

Figure 4.19: Behaviour of Column TC-10 During Selected Stages of Testing

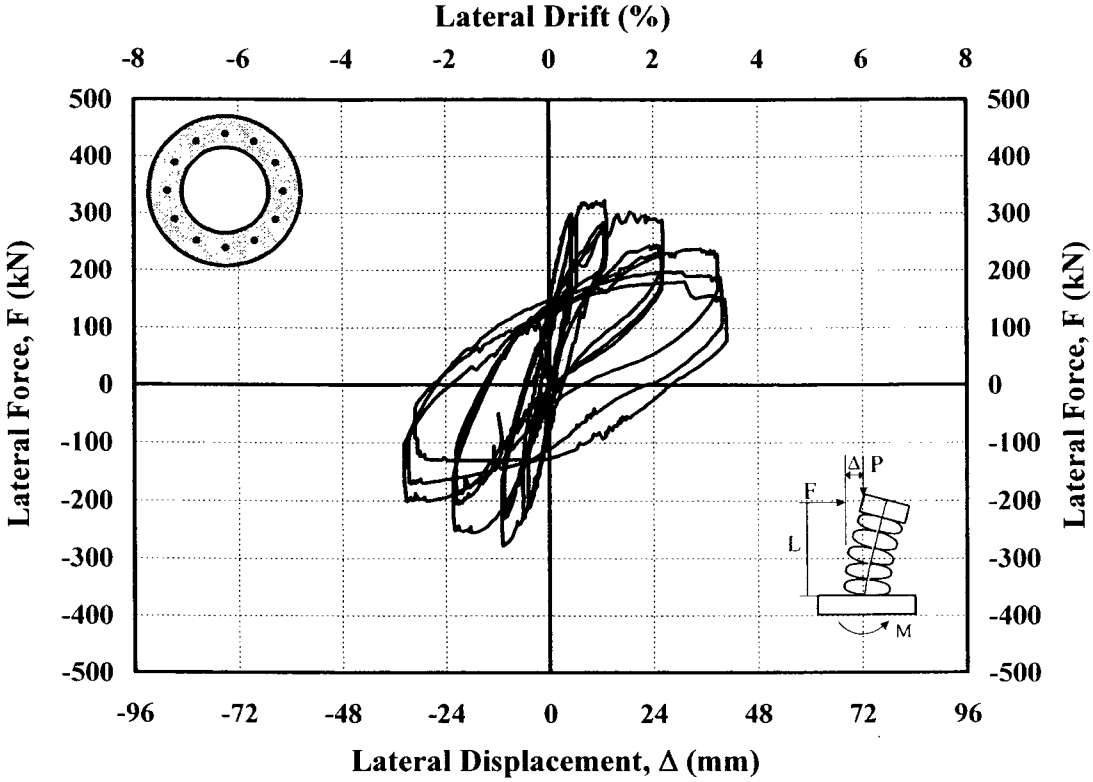

Figure 4.20: Hysteretic Force-Displacement Relationship for Column TC-10

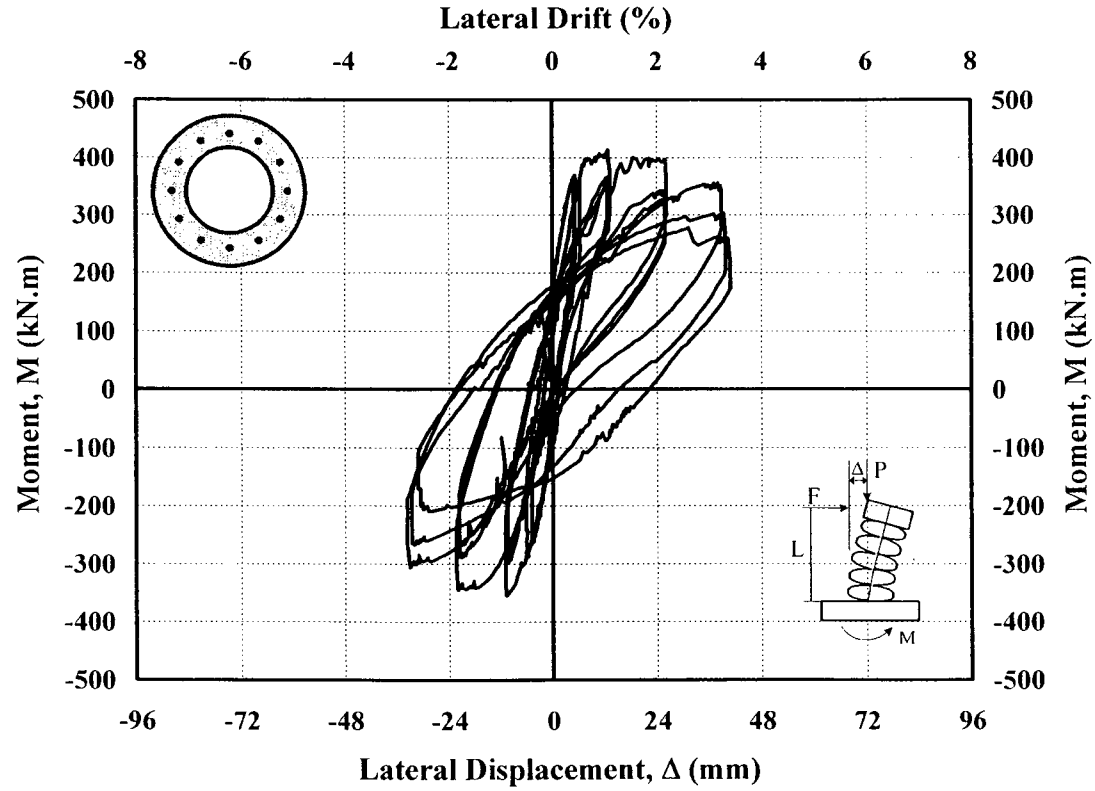

Figure 4.21: Hysteretic Moment-Displacement Relationship for Column TC-10

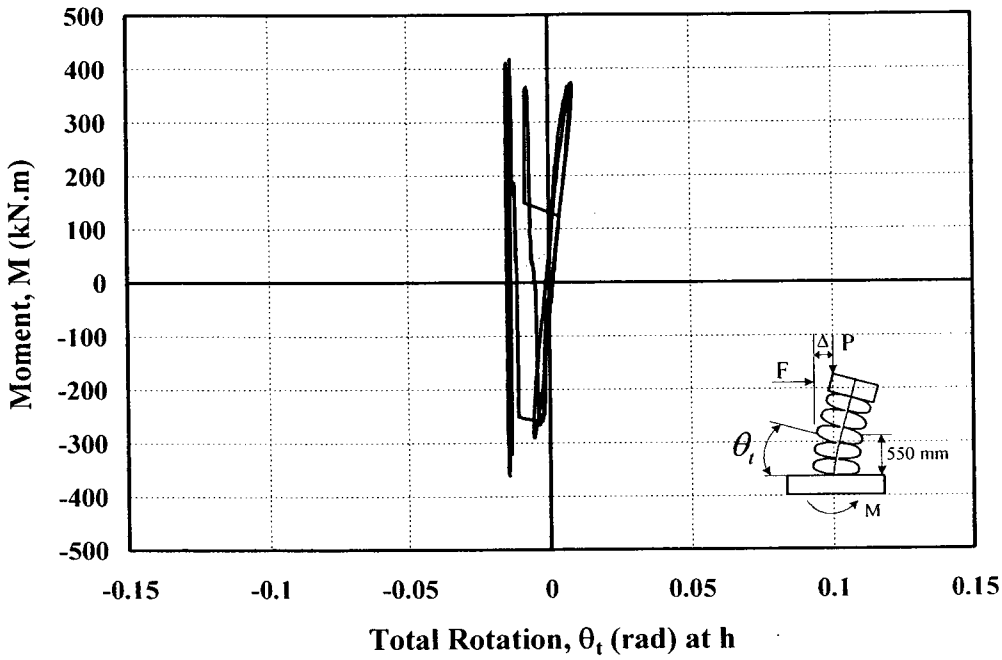

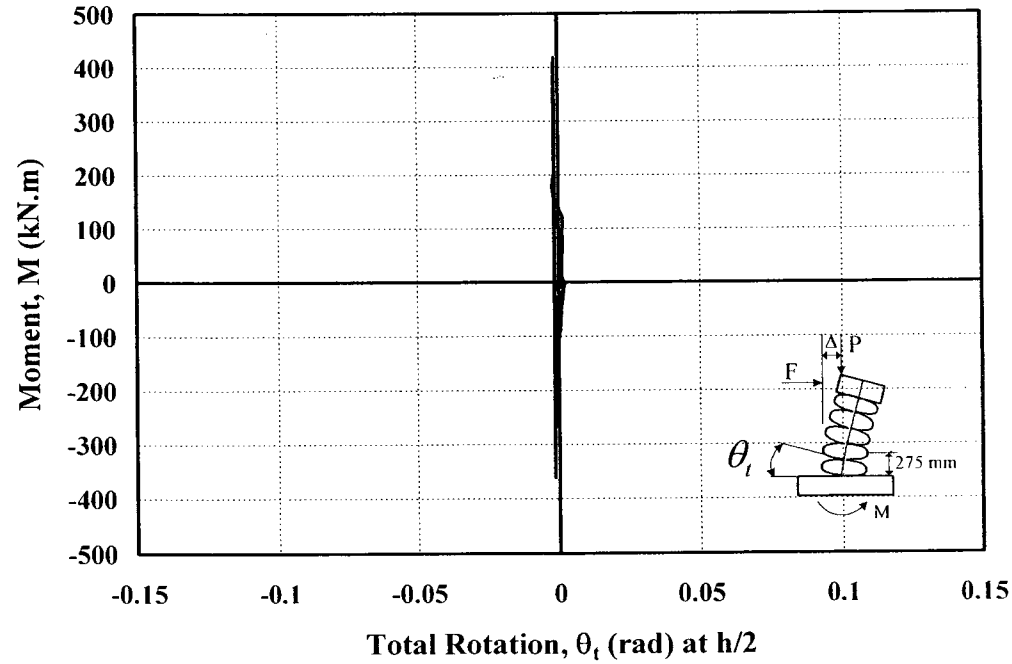

Figure 4.22: Moment-Total Rotation Relationship for Column TC-10

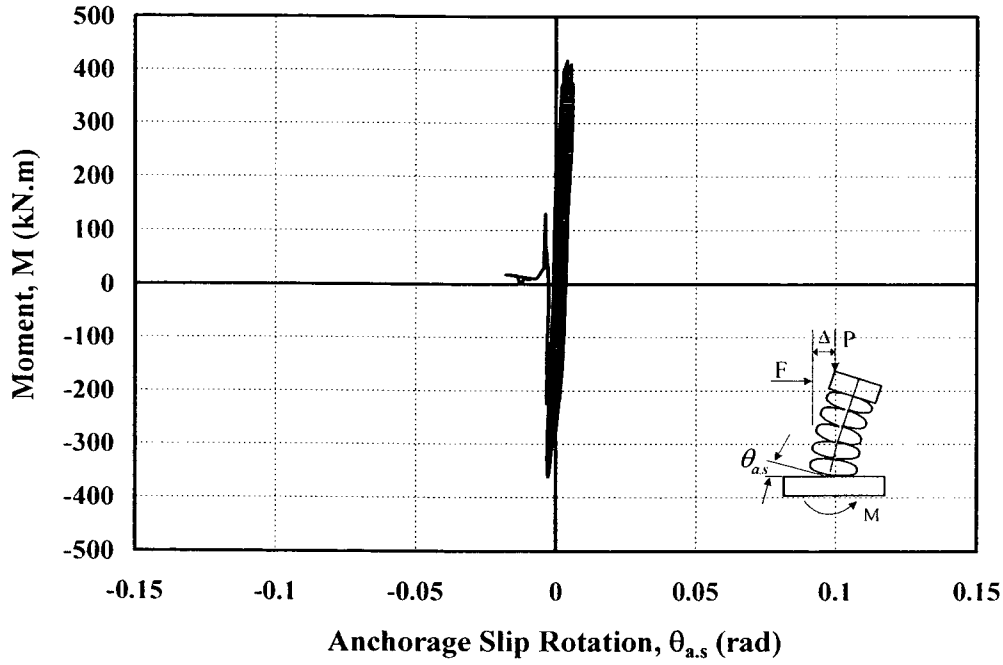

Figure 4.23: Moment-Anchorage Slip Rotation Relationship for Column TC-10

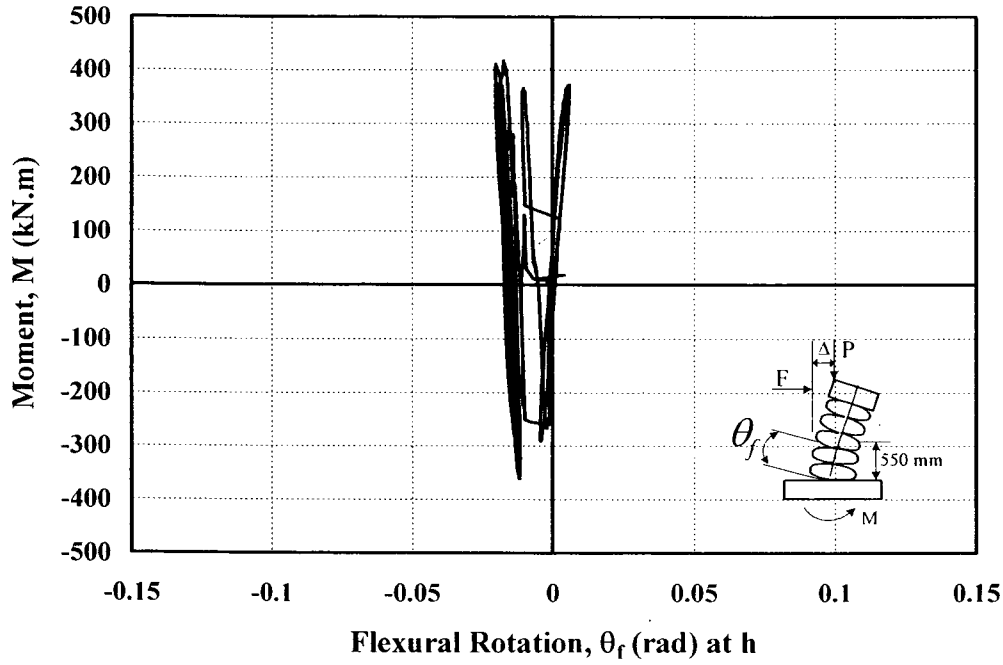

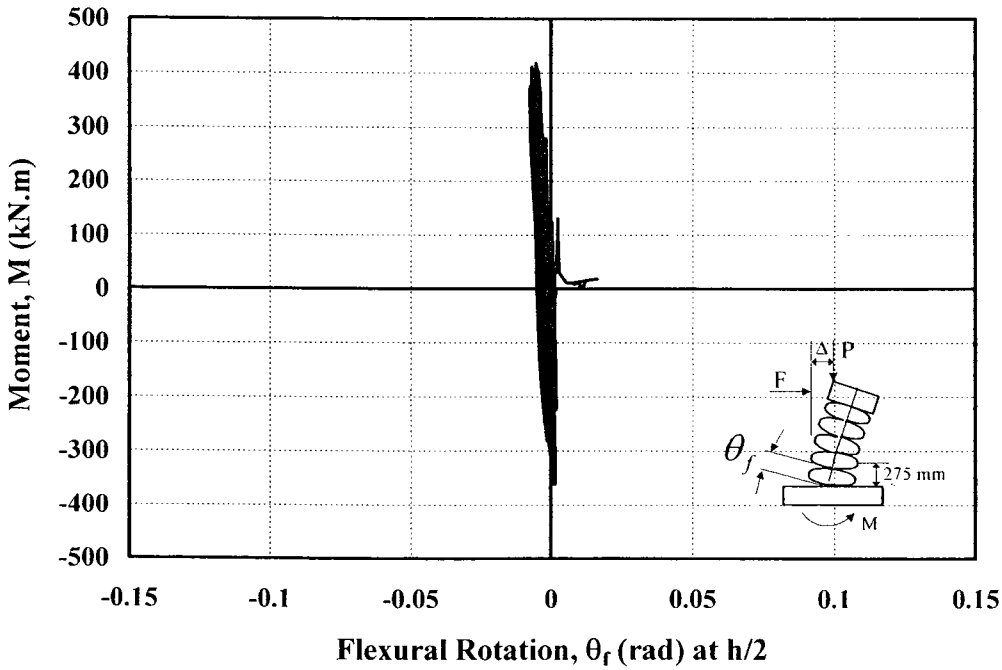

Figure 4.24: Moment-Flexural Rotation Relationship for Column TC-10

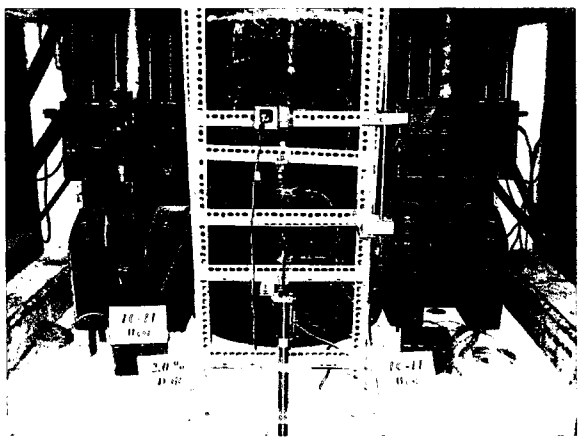

(a) At 2.0% Drift

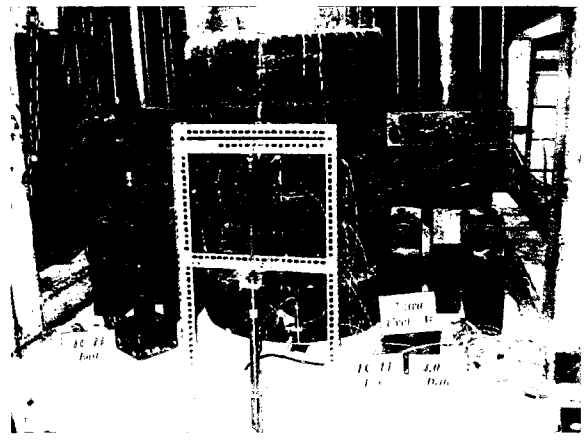

(b) At 4.0% Drift

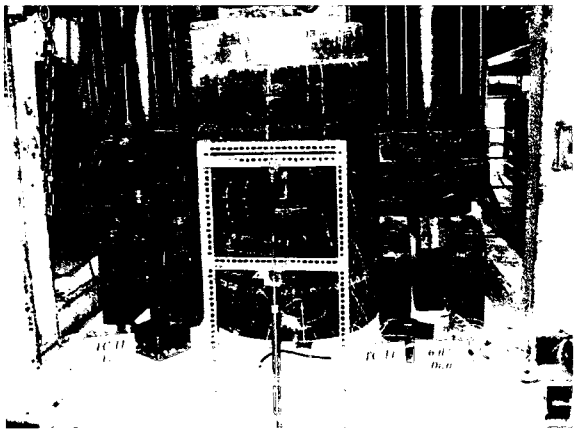

(c) At 6.0% Drift

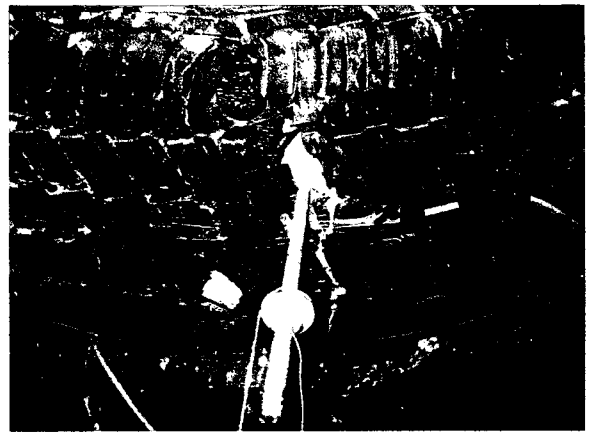

(d) At 7.0% Drift (East View)

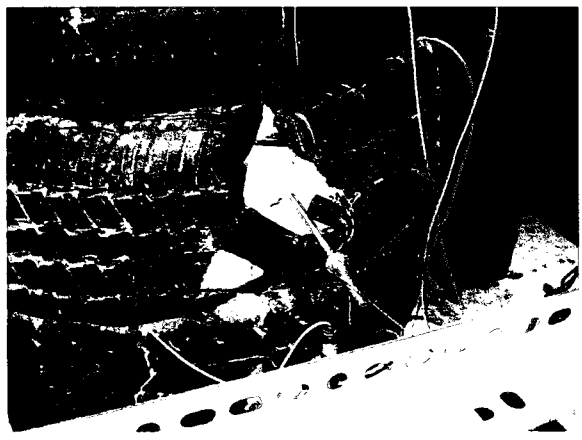

(e) At 8.0% Drift

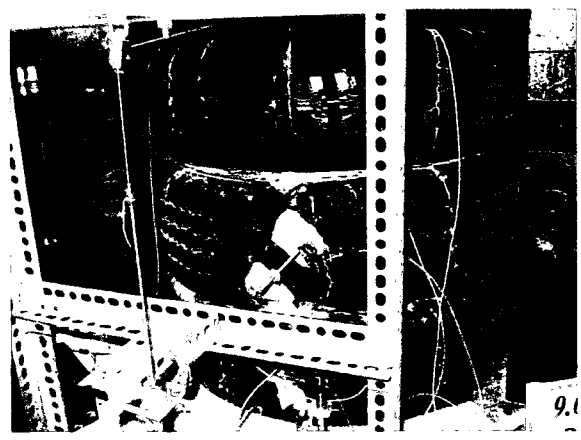

(f) At 9.0% Drift

Figure 4.25: Behaviour of Column TC-11 During Selected Stages of Testing

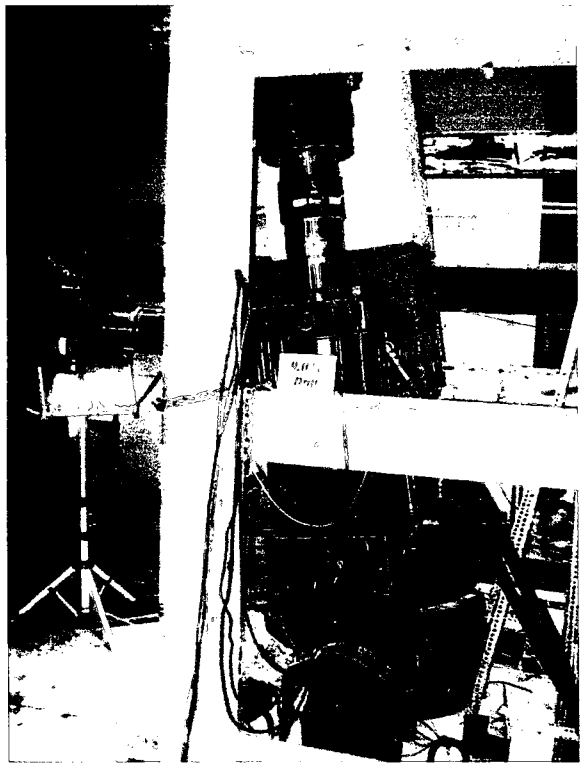

(g) At 9.0% Drift

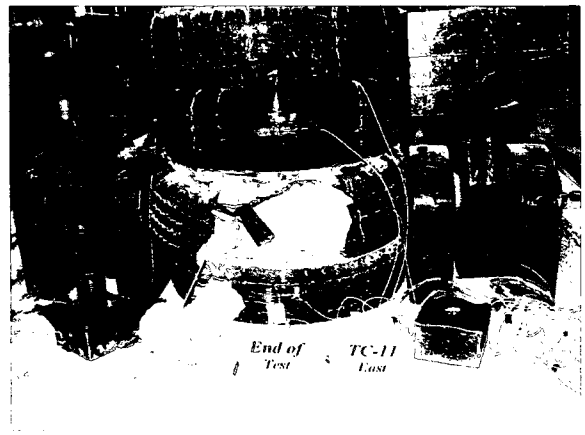

(h) End of Test

(i) Buckling of Re-bar (East View)

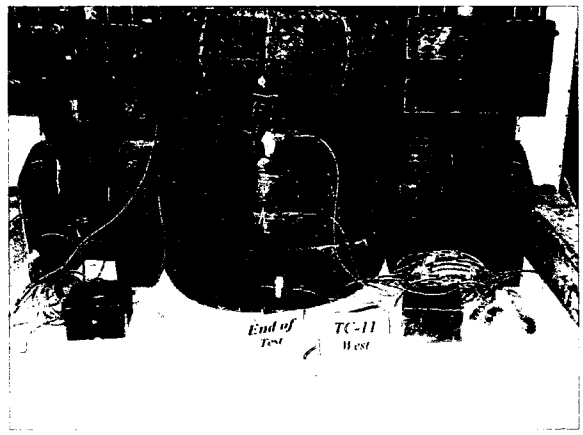

(j) End of Test (West View)

Figure 4.25 (Cont'd): Behaviour of Column TC-11 During Selected Stages of Testing

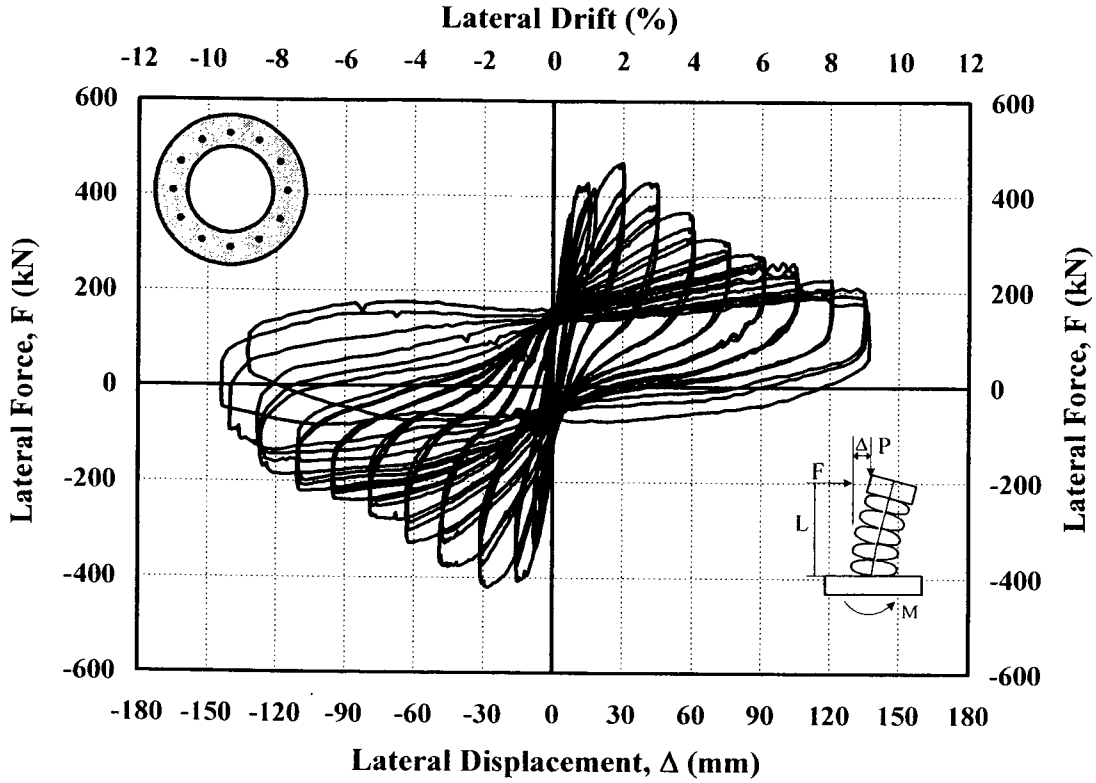

Figure 4.26: Hysteretic Force-Displacement Relationship for Column TC-11

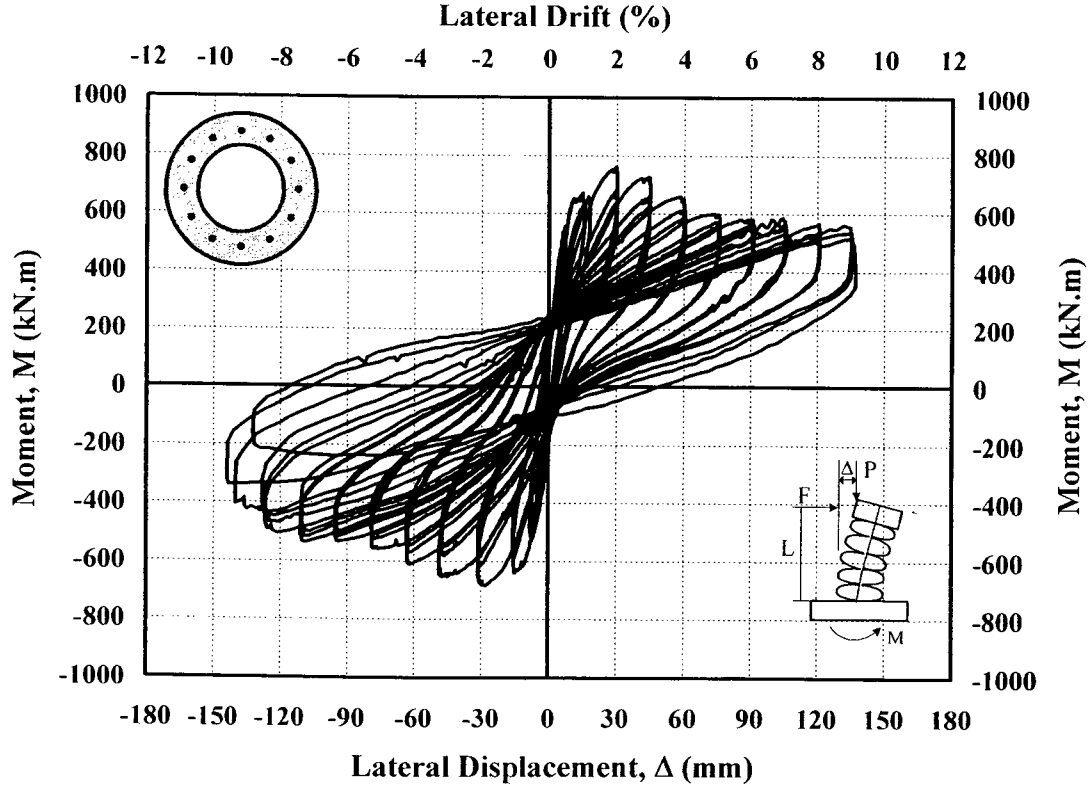

Figure 4.27: Hysteretic Moment-Displacement Relationship for Column TC-11

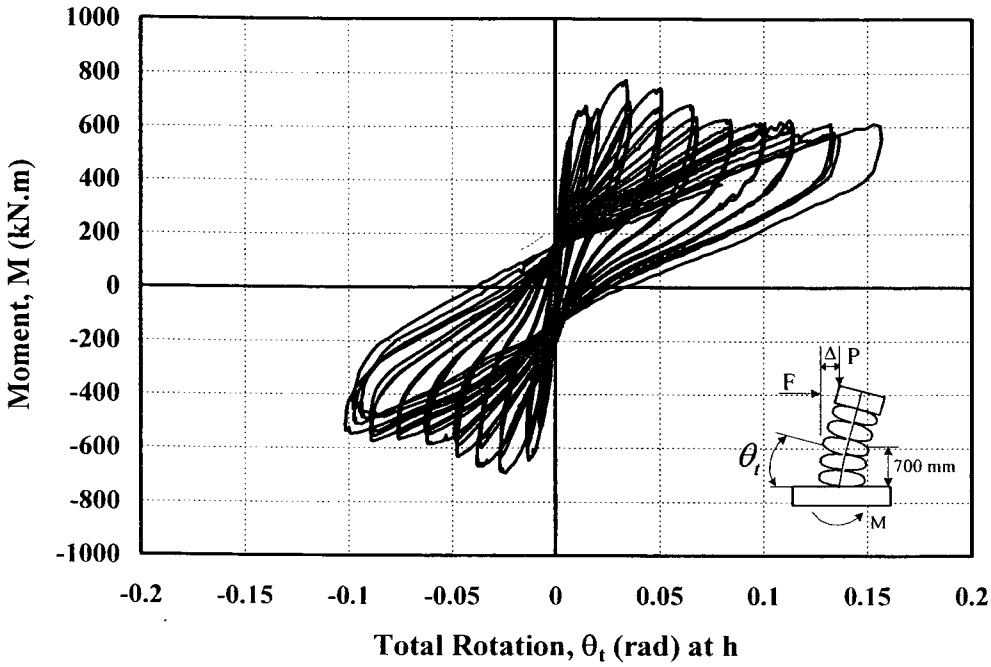

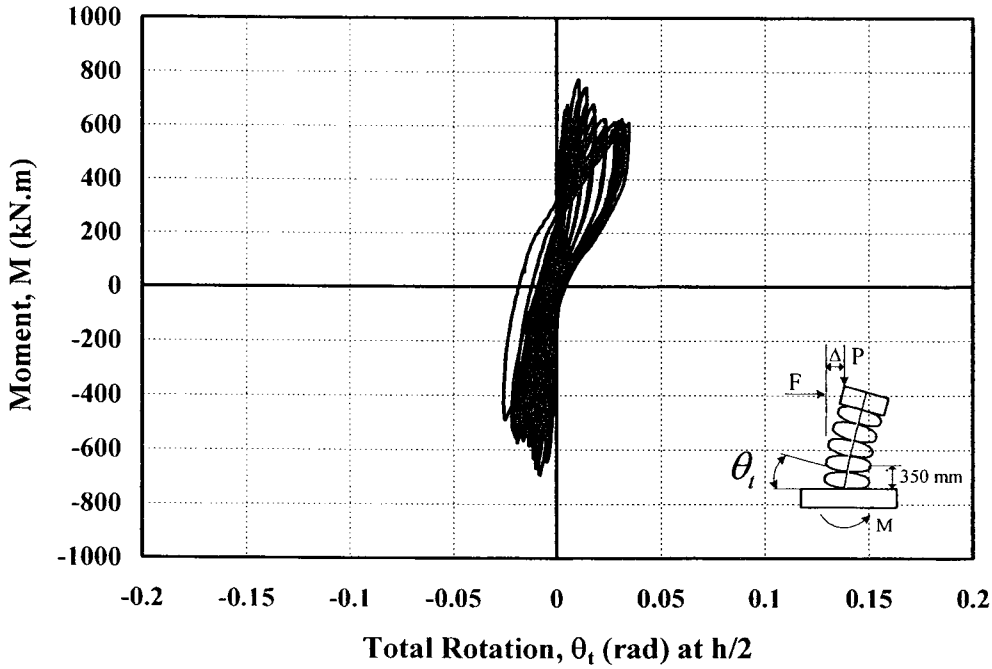

Figure 4.28: Moment-Total Rotation Relationship for Column TC-11

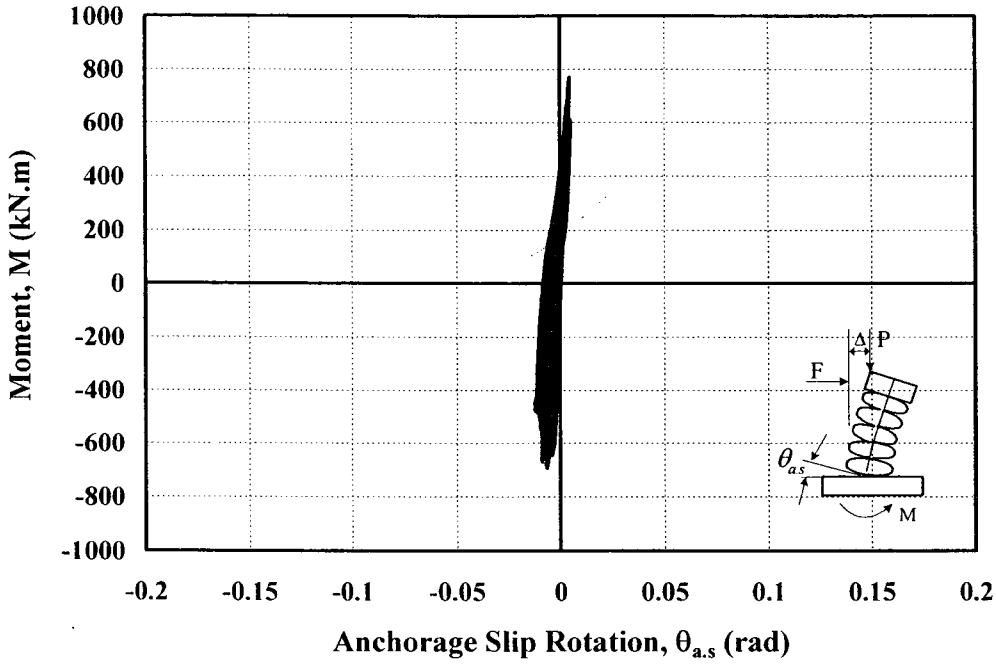

Figure 4.29: Moment-Anchorage Slip Rotation Relationship for Column TC-11

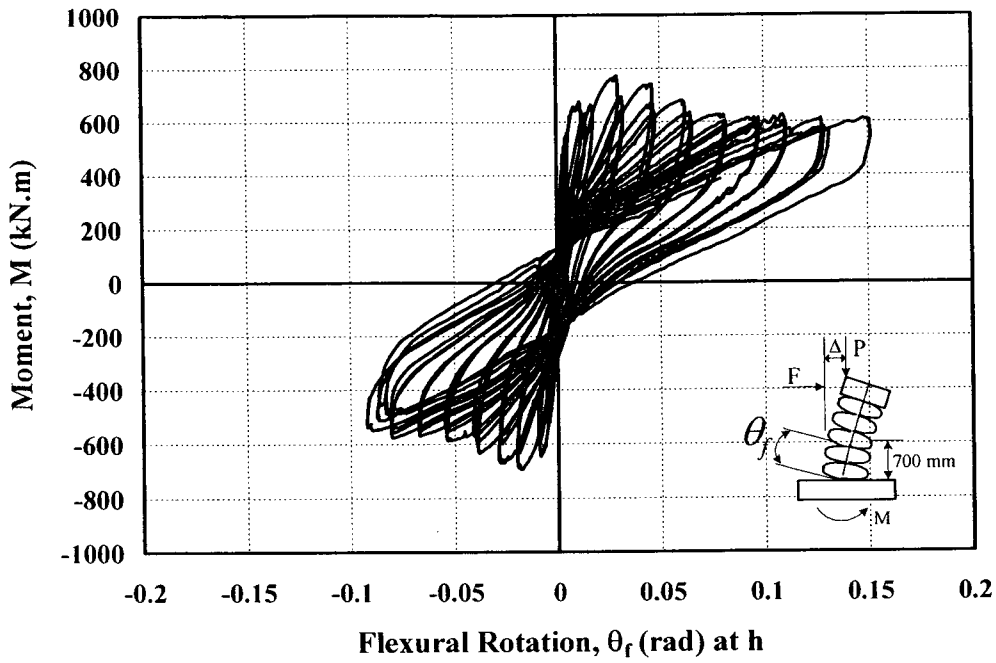

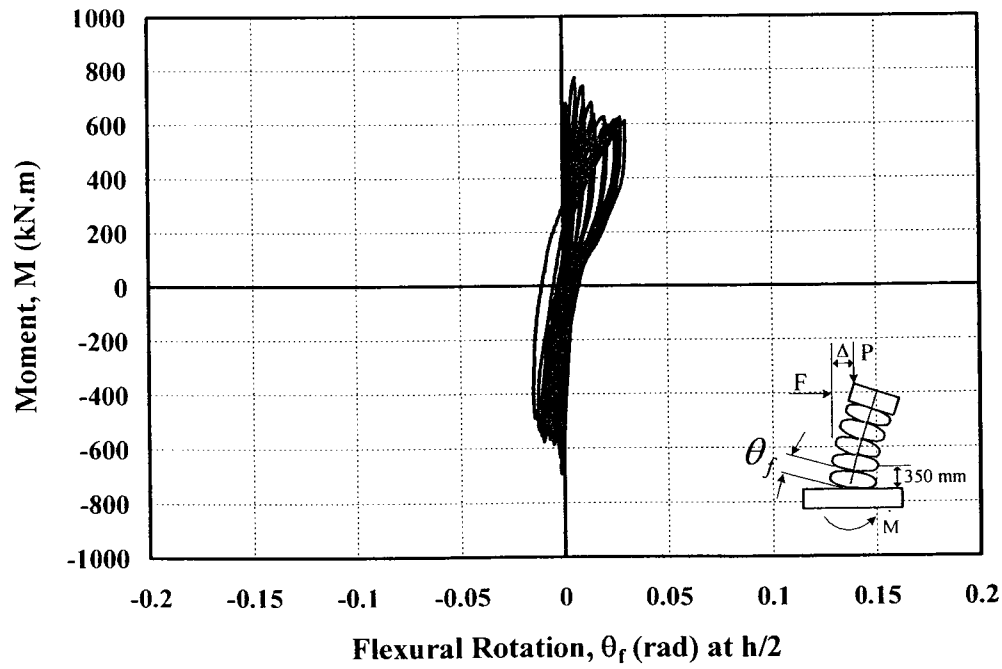

Figure 4.30: Moment-Flexural Rotation Relationship for Column TC-11

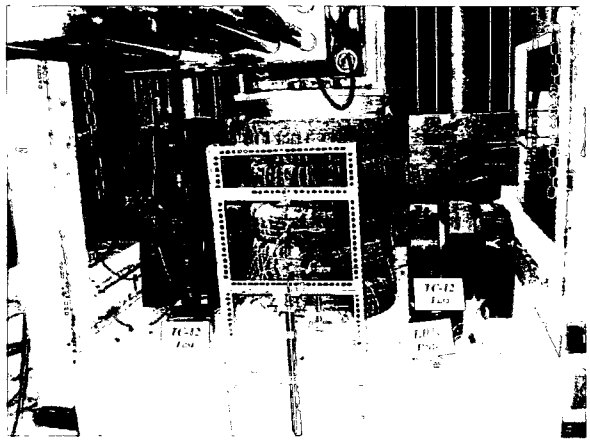

(a) At 1.0%Drift

(b) At 3.0% Drift

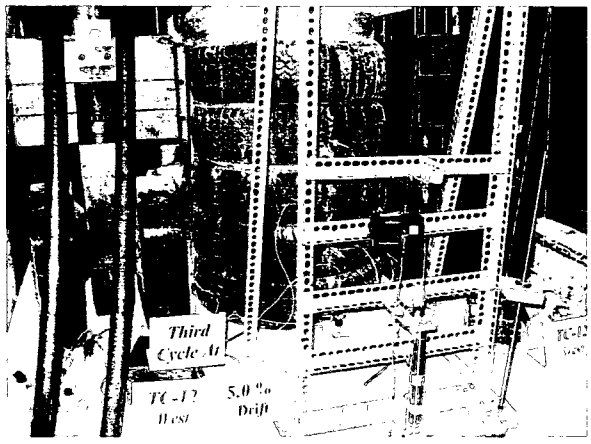

(c) At 5.0% Drift

(d) At 6.0% Drift

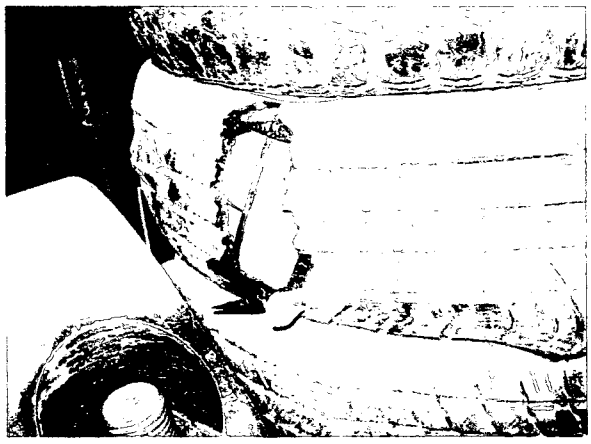

(e) At 7.0% Drift (North View)

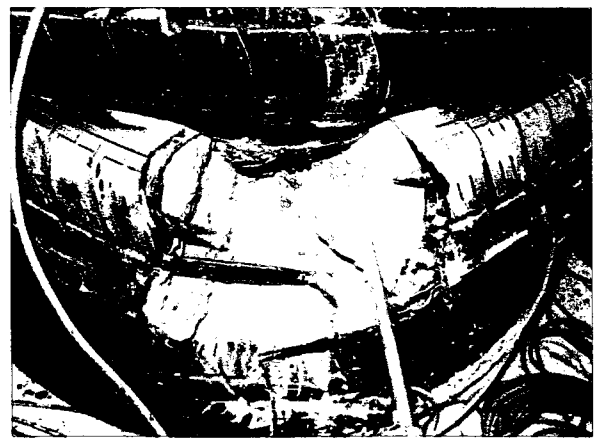

(f) End of Test

Figure 4.31: Behaviour of Column TC-12 During Selected Stages of Testing

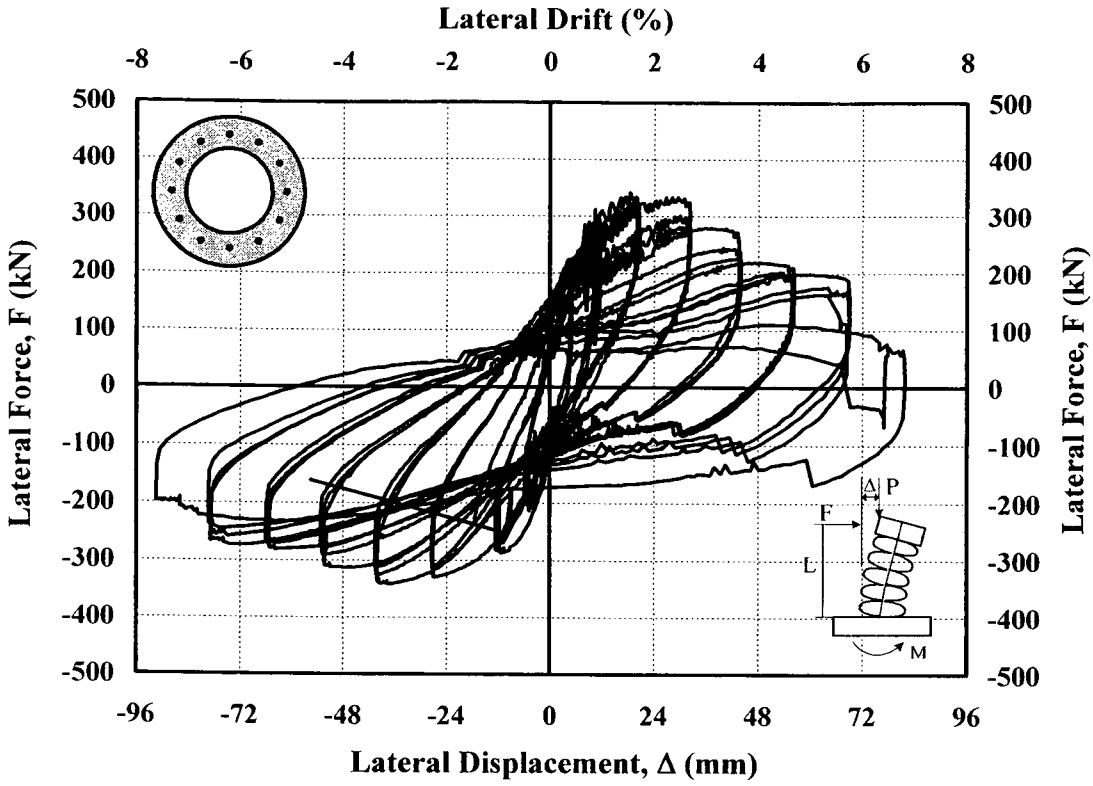

Figure 4.32: Hysteretic Force-Displacement Relationship for Column TC-12

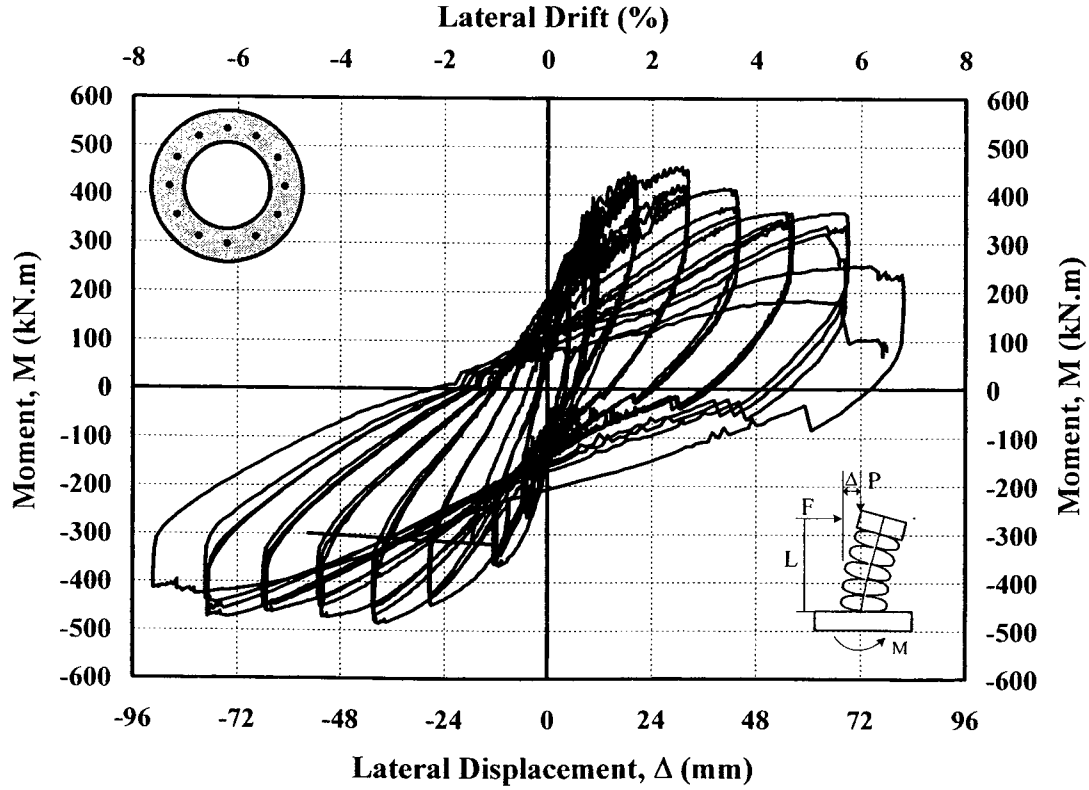

Figure 4.33: Hysteretic Moment-Displacement Relationship for Column TC-12

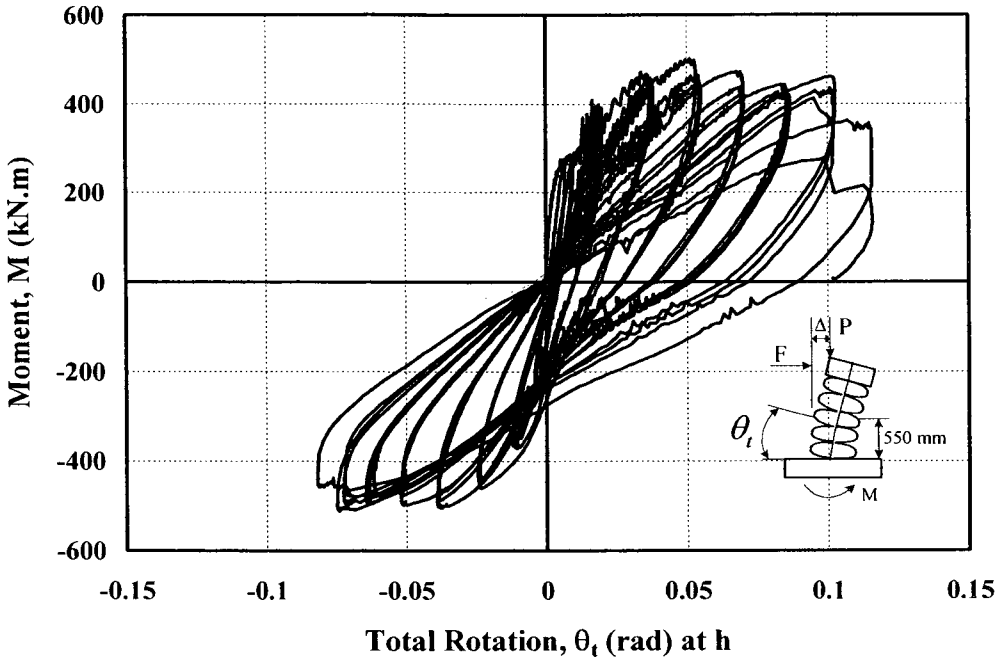

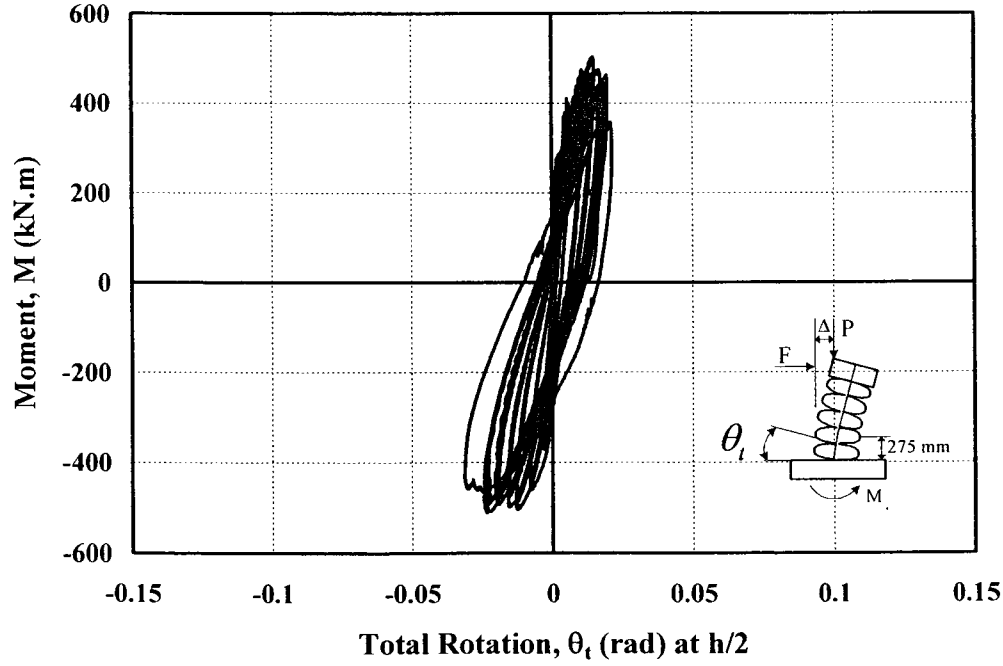

Figure 4.34: Moment-Total Rotation Relationship for Column TC-12

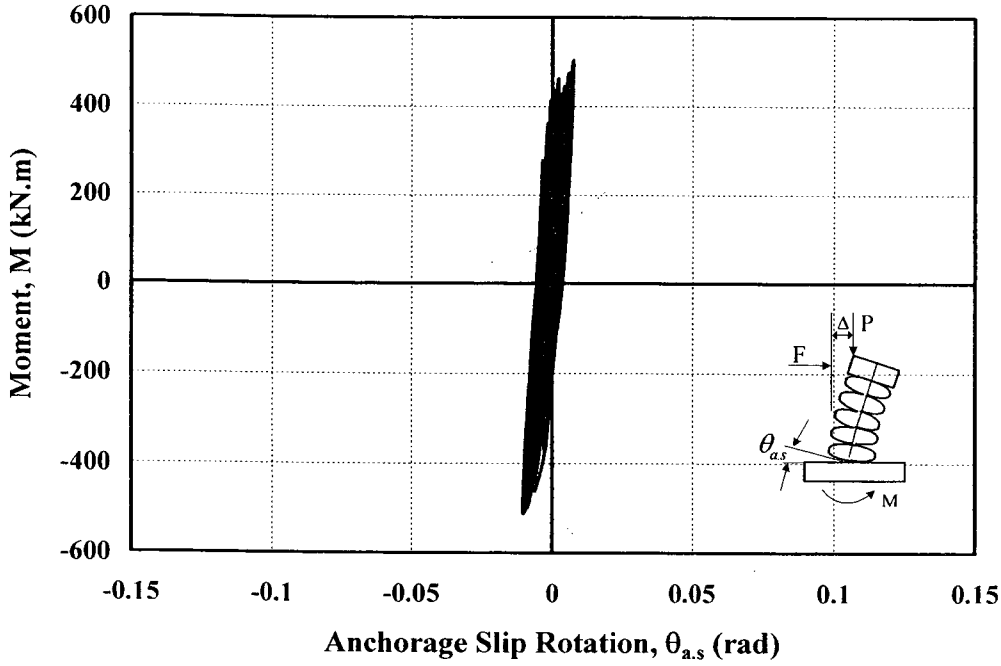

Figure 4.35: Moment-Anchorage Slip Rotation Relationship for Column TC-12

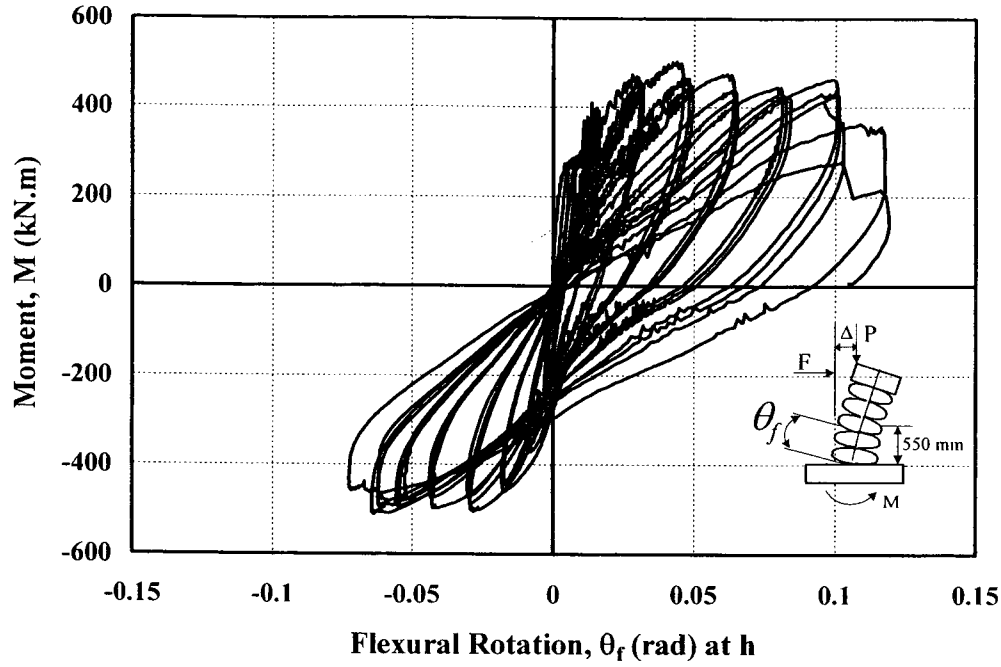

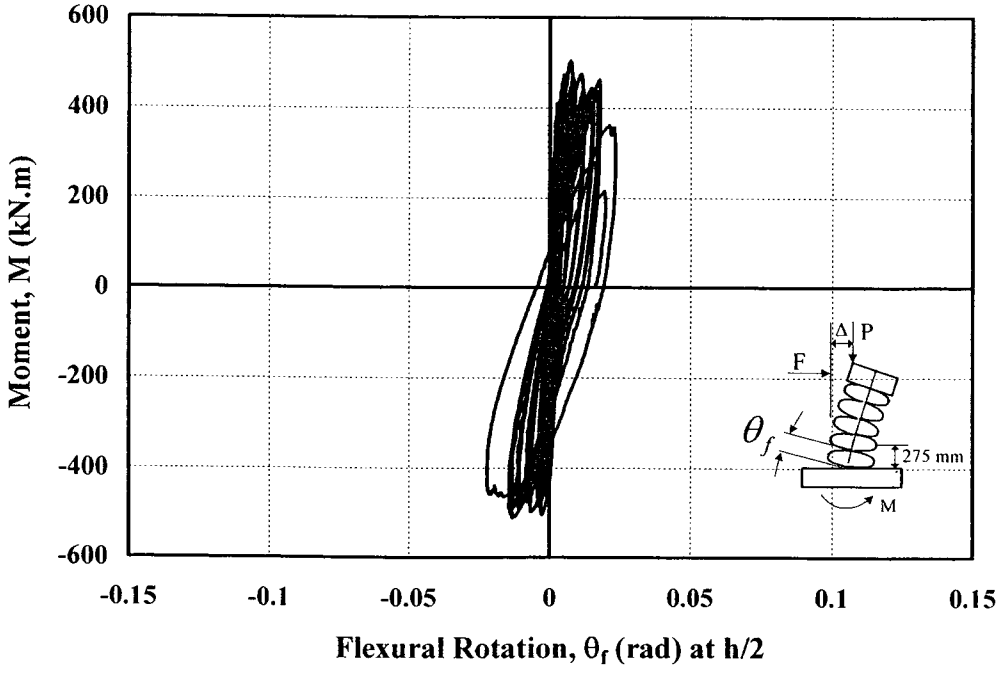

Figure 4.36: Moment-Flexural Rotation Relationship for Column TC-12

CHAPTER 5

Analytical Research

5.1 General

The experimental results obtained from both the previous test program (Phase I) conducted by the author as part of his M.A.Sc. studies at the University of Ottawa and the current test program (Phase II) were used to verify the applicability of current analytical techniques for the computation of column performance. This necessitated the development of a constitutive model for rubber-concrete composite behaviour. The applicability of an existing concrete confinement model was verified and the model was adapted to columns confined by steel belted tires. With the appropriate material models, column performance in flexure and shear were assessed using plane section analyses for flexure and truss analogy for diagonal tension. The analytical research also included the development of a design procedure for reinforced concrete bridge columns cast in steel-belted tires.

The analytical research consisted of four stages;

i. Development of an analytical model for stress-strain relationship of concrete with rubber layers to model the exterior perimeter region of column sections.
ii. Modification of an existing concrete confinement model to incorporate the effects of steel-belted radial tires as confinement reinforcement.
iii. The verification of existing flexural analysis techniques while incorporating the above models and generating force-deformation envelopes for experimentally recorded moment-lateral drift hysteretic relationships.
iv. Verification of shear force capacities.

5.2 *Analytical Model for Stress-Strain Relationship of Concrete-Rubber Composite Material*

The reinforced concrete columns transversely reinforced with tires contain layers of tire rubber around the column perimeter because of the presence of tire sidewalls. This is the same region that is subjected to compressive stresses under bending. Hence its behaviour is of utmost importance in predicting column strength and deformability. Performance of concrete with layers of rubber, under compression has not been investigated before. No analytical model is available to describe the stress-strain characteristics of this region. Therefore, a series of concrete cylinders were prepared with layers of tire sidewalls placed inside the cylinders to simulate and test compression regions of columns. These cylinders were intended to generate test data on the topic. A total of 55 cylinders were prepared and tested after 28 days of curing. Of this number, 45 cylinders were 100 mm in diameter and 200 mm in height. The remaining 10 cylinders had 150 mm diameter and 300 mm height. A concrete cylinder testing machine with a 2225 kN capacity was used for this purpose. The cylinders contained different layers of tire sidewalls in concrete, resulting different volumetric ratios of rubber in concrete. Figure 5.1 shows the size and shape of rubber pieces used in cylinders. Five different arrangements of tire rubber were used to investigate the significance of rubber in concrete as shown in Table 5.1. These included; i) three hollow circular rubber rings of either 30 mm width at 100 mm spacing placed in 150 mm cylinders or of 20 mm width at 50 mm spacing placed in 100 mm cylinders as shown in Figure 5.1(a); ii) double layers of 20 mm wide hollow circular rings at 50 mm spacing placed in 100 mm cylinders, iii) three solid tire rubber pieces having a full solid circular section of the same diameter as the 100 mm cylinder, as shown in Figure 5.1(b), iv) three solid circular pieces on top of each other, placed in the middle of 100 mm cylinders as seen in Figure 5.1(c), v) three rubber pieces with half solid circular sections, placed at every 50 mm spacing in 100 mm cylinders. In addition, 15 standard pure-concrete cylinders were tested to establish concrete strength. Figure 5.2 illustrates different arrangements of tire rubber used in cylinders during their preparations.

The cylinder tests indicate reduced modulus of elasticity and compressive strength. Accordingly, the peak strength was attained at about 35% to 40% of $f_c^{'}$ where $f_c^{'}$ indicates column concrete strength. The concrete strength was reduced from 40 MPa to 14 MPa (65% reduction) for columns tested in Phase II. The cylinder test results, shown in Figure 5.3 (a) are for concrete with the same volumetric ratio of rubber as that in Phase II columns. Similarly, the strength was reduced from 48 MPa to 19 MPa (60% reduction) in concrete having the same volumetric ratio of rubber as that in Phase I columns. The cylinder test results for this case are shown in Figure 5.3 (b). Similar reductions in concrete strength due to the presence of rubber were also reported by Eldin and Senouci (1993) who mixed concrete with chopped tire rubber.

The analysis of cylinder test data from the concrete-rubber composite material exhibited not only lower compressive strengths but also lower elastic moduli as compared with those of pure concrete. On the positive side, however, these cylinders demonstrated increased ductility. This is shown in Figure 5.3. The reduction in compressive strength of concrete due to the presence of rubber depended on the volumetric ratio of rubber in concrete. Table 5.2 shows average values of compressive strength for concrete with various volumetric ratios of rubber in cylinders. The relationship between the strength ($f_{cr}^{'}$) and volumetric ratio of rubber is depicted in Figure 5.4. The relationship indicates nonlinear behaviour. This relationship can be idealized as a polynomial with second order parabola defined by the following expression.

$$f_{cr}^{'} = f_c^{'}(53\rho_r^2 - 13\rho_r + 1) \qquad (5.1)$$

Where, $\rho_r \leq 0.13$

ρ_r is equal to the ratio of the volume of rubber to volume of concrete.

Next, the shape of the stress-strain relationship was investigated. The cylinder stress-strain relationships were normalized with respect to the peak stress and the corresponding strain,

and re-plotted in Figure 5.5. The results show that the ascending branch of the stress strain relationship can be modeled by a second order parabola. The expression suggested earlier by Hognestad (1951) for pure concrete, as modified for peak strength of concrete-rubber composite, produced good correlation with test data. The figure further indicates that the strain corresponding to the peak stress can be taken the same as that for pure concrete. For normal strength concrete this value may be taken as 0.002. The peak strength as defined in Eq. (5.1) and the corresponding strain can then be used along with Hognestad's parabola to define the ascending branch of the model.

The descending branch of the stress-strain relationship can be idealized by a linear line segment passing through the strain of 0.0038 at 85% of the peak strength beyond the peak. This implies that the descending branching follows the same behaviour as that suggested by Hognestad for pure concrete. The proposed model for concrete-rubber composite is illustrated in Figure 5.6.

The proposed model and its effect on column concentric capacity, $P_{o,r}$ was calculated for each test column. The reduction in concrete strength, due to the presence of rubber, resulted in reduced column concentric capacity which translated into increased percentages of column axial load applied during the tests. The summary of column axial forces is given in Table 5.3.

5.3 *Analytical Model for Concrete Confined by Steel-Belted Radial Tires*

One of the primary functions of steel-belted tires in columns is to improve the confinement of concrete and enhance inelastic deformability. Concrete inside the tires is confined by the steel embedded in tires. However, the level of confinement is different in different regions of concrete. The exterior-most perimeter portion of column concrete, between the treaded portion and the rim, is confined only by the high-strength steel wires in the treads. The inside core, enclosed by tire rims, is confined by both the steel in the treads as well as the steel in the rims. Lateral confinement pressures generated by tires are illustrated in Figure 5.7. Their effects have to be considered in defining the stress-strain characteristics of confined concrete

inside the column. This requires analytical modeling of confined concrete. Of the concrete confinement models proposed earlier, the model developed by Saatcioglu and Razvi (2002) is the only model that allows the superposition of the effects of different types and arrangements of confinement reinforcement in the same column. Therefore, this model was adopted in the current research program, but modified to incorporate the effects of high-grade steel used in tires, with appropriate levels of effective steel stress, as the high-grade steel wires in tires did not reach their yield strengths. With this modification, the applicability of the model was verified by comparing analytical and experimental force-displacement relationships, as presented in Section 5.4. The confinement model is summarized in the following paragraphs.

The original model developed by Saatcioglu and Razvi (1992) is based on the concept of equivalent uniform confinement pressure. It involves the computation of equivalent uniform confinement pressure with due considerations given to the type, amount, arrangement, spacing and grade of transverse reinforcement. In the current research program the columns had circular cross-sections with maximum efficiency due to the ability to develop hoop tension. They also consisted of two regions of concrete with two types of transverse steel, i.e., wires in treads and in rims, making the choice of the model adopted especially attractive.

The model consists of a parabolic ascending branch, followed by a linear descending segment as shown in Figure 5.8. If the effect of confinement is negligible (i.e, K = 0) the model becomes identical to that proposed by Hognestad (1951) for unconfined concrete. The following equations define the stress-strain relationship for ascending and descending branches in Eqs. (5.2) and (5.3), respectively.

$$f_c = f'_{cc}\left[2\left(\frac{\varepsilon_c}{\varepsilon_1}\right)-\left(\frac{\varepsilon_c}{\varepsilon_1}\right)^2\right]^{\frac{1}{1+2K}} \tag{5.2}$$

$$f_c = f'_{co}-(\varepsilon_c-\varepsilon_{01})\left(\frac{0.15f'_{co}}{\varepsilon_{85}-\varepsilon_{01}}\right) \tag{5.3}$$

Where, $f_c^{'}$, ε_c, $f_{co}^{'}$, and ε_{o1} are concrete stress and strain; and the unconfined concrete strength and corresponding strain in member respectively. ε_{85} is the strain at 85% of maximum stress. $f_{cc}^{'}$ is the confined concrete strength which is computed using equivalent uniform confinement pressure ($f_{\ell e}$). The equivalent uniform confinement pressure in circular columns with closely spaced circular reinforcement is the same as the average lateral pressure (f_ℓ). The average pressure can be computed as total force in transverse reinforcement divided by the concrete core area over which it acts. In columns confined by tires, the lateral pressure is different in two different regions of the column. The exterior-most portion of column concrete, enclosed by the treaded portion is confined only by the steel in the treads and the lateral pressure should be calculated as $f_{\ell t}$. The inside core, enclosed by tire rims is confined by both the steel in the treads as well as the steel in the rims. The lateral pressure for this region is calculated as $f_\ell = f_{\ell t} + f_{\ell r}$, where, $f_{\ell t}$ is equal to the lateral pressure in the treaded portion of the tire and $f_{\ell r}$ is equal to the lateral pressure in the rims. The lateral confinement pressures can be computed from Eqs. (5.4) through (5.6).

$$f_{\ell t} = \frac{2A_{st}f_{st}}{sD_t} \tag{5.4}$$

$$f_{\ell r} = \left(\frac{2A_{sr}f_{sr}}{sD_r}\right) \times 2 \tag{5.5}$$

$$f_{\ell e} = f_\ell = f_{\ell t} + f_{\ell r} \tag{5.6}$$

The transverse yield strength f_{sr} and f_{st} in above expressions refers to the maximum stress that can be developed in rim and tread confinement reinforcement, respectively as full confinement mechanism is developed. This value is equal to the yield strength of steel in ordinary grade 400 MPa reinforcement. In high-strength steel embedded in tire rubber, the maximum stress that can be developed may be limited to a stress level that is below the yield strength. This stress level was found in earlier research to be dependant on the efficiency of confinement arrangement and the level of axial compression on columns (Saatcioglu and Razvi, 2002, Saatcioglu et al 2008). As the confinement efficiency increases, as in the case of closely spaced circular reinforcement, the effectiveness of high-grade transverse reinforcement increases. Similarly, as the level of axial compression increases, the

compression zone in columns increases, resulting in larger lateral expansion of concrete and higher mobilization of stresses in transverse reinforcement. In the tire reinforced bridge columns tested in the current investigation, the level of axial compression was limited to 10% to 16% of column concentric capacity. This level of axial compression may be considered to be low. However, the confinement efficiency of closely spaced circular wire reinforcement embedded in rubber covering the entire column surface is very high. Experimental data is needed to assess the level of steel stress in tires that is appropriate for use in the model. Therefore, the strain gauge data obtained in the experimental phase of the investigation was scrutinized to assess the appropriate level of steel stress at approximately the onset of strength decay. In this range of high inelastic deformations, it was experimentally observed that the strain values varied between 0.003 and 0.008 depending on the location and the performance of strain gauges. Having examined a large number of strain data, including those obtained from the rim steel, it was concluded that most columns developed a strain value of approximately 0.004 before they experienced strength decay under reversed cyclic loading. Therefore, the stress corresponding to this level of strain is suggested for use in the confinement model developed by Saatcioglu and Razvi. This translates into $f_{st} = f_{sr} = 0.004E_s$.

The peak stress (strength) for confined concrete $f_{cc}^{'}$ is expressed in the model in terms of unconfined concrete strength $f_{co}^{'}$, and equivalent uniform confinement pressure $f_{\ell e}$. The confined concrete strength can be computed as the sum of unconfined concrete strength in the column and the incremental effect of equivalent uniform lateral pressure as computed above. This is illustrated below.

$$f_{cc}^{'} = f_{co}^{'} + k_1 f_{\ell e} \tag{5.7}$$

Where, $f_{cc}^{'}$ is the strength of confined concrete. When the above equation is applied to the confinement of concrete within the perimeter of tire-confined columns, then the confined and unconfined strength values apply to those of the perimeter region, including the strength reduction effect of the rubber side wall. When it is used for the core concrete enclosed by the rim, then the strength values refer to pure concrete in the core and the confinement pressure is the superposition of lateral pressured due to the steel in treads, and the steel in the rims.

Coefficient k_1 in Eq. (5.7) reflects the effectiveness of lateral pressure on increasing concrete strength. It was observed experimentally that the rate of increase in concrete strength due to lateral pressure decreases with the magnitude of pressure (Saatcioglu and Razvi 1982). Coefficient k_1 varies with lateral pressure $f_{\ell e}$ as indicated in Eq. (5.8). The strength enhancement factor used in Eq. (5.2) can then be defined as given in Eq. (5.9).

$$k_1 = 6.7(f_{le})^{-0.17} \tag{5.8}$$

$$K = \frac{k_1 f_{\ell e}}{f'_{co}} \tag{5.9}$$

The strain corresponding to the peak stress of confined concrete, expressed below, is also a function of the ratio "K" which is specified in Eq. (5.9).

$$\varepsilon_1 = \varepsilon_{01}(1+5K) \tag{5.10}$$

Where ε_{01} is the strain corresponding to the peak stress of unconfined concrete, and should be determined under the same rate of loading as for confined concrete. In the absence of test data it may be taken as 0.002.

The slope of the descending branch of the stress-strain model, defining the ductility of confined concrete, is expressed as a function of the level of concrete confinement. This is done by specifying the post-peak strain ε_{85} at 15% strength loss beyond the peak, and assuming a linear idealization. Eq. (5.11) defines ε_{85} as a function of the amount of transverse confinement reinforcement.

$$\varepsilon_{85} = 260\rho\varepsilon_1 + \varepsilon_{085} \tag{5.11}$$

A value of 0.0038 may be used for ε_{085} which represents the strain at 85% strength level beyond the peak stress of unconfined concrete. The amount of transverse reinforcement is expressed in terms of reinforcement ratio ρ, which gives the area ratio of transverse steel. The following expressions can be used to establish the reinforcement ratio for transverse steel in tires for the tread and rim steel ρ_{st} and ρ_{sr}, respectively.

$$\rho_{st} = \frac{2A_{st}}{S(D_t)} \tag{5.12}$$

$$\rho_{sr} = \frac{4A_{sr}}{S(D_r)} \tag{5.13}$$

$$\rho = \rho_{st} + \rho_{sr} \tag{5.14}$$

D_t and A_{st} are the diameter and the area of steel in the tread. D_r and A_{sr} are the diameter and the area of steel in the rims.

5.4 *Flexural Analysis of Tire-Confined R/C Columns*

The performance of column specimens tested in the experimental phase was investigated analytically. Because tire reinforced concrete columns had not been researched earlier, analytical techniques specifically intended for such columns do not exist. Therefore, the applicability of available analytical methods for conventional columns had to be verified first. This involved the implementation of plane section analysis for flexure, combined with member analysis based on well accepted principles of mechanics. The sectional analysis required new material constitutive models. The models developed and described earlier in the chapter were adopted to compute column flexural strengths, as well as moment-curvature relationships. The latter was subsequently employed to generate member response.

Moment capacity under combined flexure and axial force was computed and compared with experimental results for all columns. Current methods of analysis commonly used for conventional reinforced concrete columns were used to assess their applicability to columns confined with steel-belted tires. Flexural capacities of test columns were computed by plane-section analysis of critical sections with due considerations given to the stress-strain relationships of materials. The stress-strain relationship used for longitudinal reinforcement was obtained from coupon tests conducted in the Structures Laboratory. The concrete properties were obtained from cylinder tests and implemented in the analysis through the material models described earlier. The presence of rubber layers within the perimeter region of columns resulting from the presence of tire side walls was accounted for. The confining effects of tires were incorporated by using the Saatcioglu and Razvi confinement model with appropriate stress values for the steel embedded in tires. The flexural capacity was computed by using RC-Section computer program, which was developed for plane-section analysis

based on given material stress-strain models. The geometric characteristics of column cross-sections were specified based on the actual measurements taken from test specimens. Figure 5.9 illustrates the sectional characteristics of tire reinforced columns. As can be seen in the figure, the columns had narrower sections between the tires because of the shape of tires. This was considered in sectional analysis and the concrete between the treaded portions at the outermost portion of columns and the side walls was deducted from the section size. Hence the cross-sectional dimension was taken as 458 mm for TC-1, TC-2, TC-9, TC-10, and TC-12, and 620 mm for TC-7, TC-8, and TC-11 as traced by the exterior edge of tire side-walls. The longitudinal reinforcement was placed in their appropriate places within the section.

Nominal moment capacity of the critical column section at the base was computed three times for each column; i) using the material models discussed in Sections 5.2 and 5.3, with due consideration given to the presence of rubber in the exterior portion of columns and the effects of concrete confinement, ii) using a stress-strain relationship for unconfined concrete, without the effects of confinement and the presence of rubber side walls, and iii) using the rectangular stress block specified in ACI 318-08 building code. The results are tabulated in Table 5.4. They are also compared with experimentally recorded moment capacities in the same table. Columns TC-1, TC-2 and TC-7 were flexure dominant columns with continuous longitudinal reinforcement. Hence, plane-section analysis for flexure was expected to provide sufficiently close results to those recorded experimentally. The rectangular stress block and the second order parabola in the form of Hognestad's model did not incorporate the presence of rubber side walls in the concrete compression zone. On the other hand, the confining effect of tires was also neglected. These two effects tended to offset their effects on strength and produced somewhat close results to the test values. However, the computed values for smaller columns (TC-1 and TC-2) showed lower values than the test data, whereas the value for the larger column (TC-7) was higher than that obtained experimentally. It appeared that these two analyses would be dependant on column and tire sizes, axial load, as well as the content of rubber side walls. The third analysis, which reflected both the effects of embedded rubber and concrete confinement, produced reasonably good and consistent agreement with test data. Therefore, this approach is recommended for use in design.

The capacity calculations were carried out for all columns including those that had spliced reinforcement and those with short shear spans under high shear stresses. In all cases, however, the critical section developed yielding. Although these columns experienced strength degradation with increased inelasticity, as discussed later in the section, they all developed their flexural capacities. The comparison of computed and experimental capacities shows similar trends as those for Columns TC-1; TC-2; and TC-7. These comparisons also indicate that the use of appropriate concrete properties, with strength reduction due to the presence of rubber side walls and the strength increase due to concrete confinement produce better correlations with experimental data.

The sectional analysis also produced moment-curvature relationship. Once the sectional response was established in the form of moment-curvature relationship, flexural deformations were then computed over the length of the columns by constructing the distribution of curvatures over the column height. Integration of curvatures provided column rotations, and the moments of the area under the curvature distribution provided lateral displacements and lateral drift ratios.

The above approach provides a straight forward computational methodology within the ascending branch of the moment-curvature relationship. Beyond the peak load, the members continue experiencing plastic deformations as stresses redistribute towards the point of inflection. As inelastic deformations increase, the strength begins deteriorating and the plastic hinge continue propagating. The prediction of plastic hinge length and the distribution of curvatures within this region is a challenging task which is debated among researchers. It is a common practice to assume a plastic hinge length (ℓ_p) with constant curvatures, for the computation of plastic deformations in high deformation range. It was reported in the literature that the hinging length in columns can vary between $h/2$ and h depending on a number of parameters (Park and Paulay 1975) where, h is the column cross-sectional dimension in the direction of loading. In view of the experimental observations of the current research project it was found appropriate to use $h/2$ as the plastic hinge length for tire-confined columns under relatively low levels of axial compression. The moment resistance beyond yielding was computed to be approximately constant. For the purpose of

computing inelastic displacements, incrementally increasing curvature values were taken from the moment-curvature relationship. The displacements were then computed following the procedure outlined above and illustrated in Figure 5.10. This resulted in a moment-displacement relationship under monotonically increasing lateral loads, as typically obtained from push-over analysis. The sectional analysis, however, neglected the bending and buckling of compression reinforcement typically observed at high levels of inelastic deformations. Therefore, the strength decay associated with compression bar buckling was not reflected in sectional and member analyses. The analytically computed moment-displacement relationships are compared with experimentally recorded hysteretic relationship in Figure 5.11 through Figure 5.13.

The correlations between the analytically computed envelop curves and envelops of experimentally recorded hysteretic relationships are very good. The first three columns compared are flexural dominant columns (TC-1, TC-2, and TC-7) with long shear spans and continuous longitudinal bars. The comparisons show excellent agreements up to the onset of strength decay, which was not modeled in analytical computations. This comparison clearly indicates that the conventional flexural analysis techniques commonly used for ordinary steel reinforced concrete columns can be used for tire confined columns of the geometry and arrangement considered in the current investigation, provided that the appropriate material models are incorporated. The test data under reversed cyclic loading showed faster decay at later stages of loading as compared to the analytical envelops that were intended for monotonic loading. This is to be expected because of the degrading effects of cyclic loading, as well as the compression buckling of longitudinal reinforcement, neither of which is accounted for in the analysis.

The next pair of columns compared consists of splice deficient columns (TC-8 and TC-9). Column TC-8 was identical to TC-7, except for the spliced longitudinal reinforcement. Similarly, Column TC-9 was identical to TC-1 and TC-2, except for the spliced reinforcement. The level of axial compression on these columns varied between 11% and 21% of concentric capacity. The longitudinal bars in TC-8 and TC-9 were spliced at the bottom of the column with a splice length of 30 times the bar diameter. These columns

started developing slippage of longitudinal bars within the splice region shortly after developing the first cycle at yield displacement. Consequently, the column resistance dropped in subsequent cycles, showing a wide discrepancy relative to the computed envelop-curves which neglected any potential slippage of spliced reinforcement. This is illustrated in Figure 5.13. The comparison also indicates that the flexural strength prior to the bar slippage could be computed with reasonable accuracy. This observation is in conformity with the strain gauge data, which indicated yielding of longitudinal bars in the critical section when column capacity is developed.

The comparisons of computed flexural response and measured experimental hysteretic response were extended to include columns with short shear spans. Figure 5.14 and Figure 5.15 show the comparisons. These columns had shear capacities closer to shear forces associated with flexural yielding. This was especially true for Columns TC-10 and TC-12 where the yielding of longitudinal reinforcement occurred; signifying the development of flexural capacity, but the effects of shear distress became evident shortly thereafter. Column TC – 10 developed visible rupturing of tires along a diagonal tension failure plane. The columns with relatively short shear spans under high shear force reversals (TC-10, TC-11, and TC-12) exhibited faster degradation under cyclic loading, causing the discrepancy of results between the computed envelops and recorded hysteresis loops.

5.5 Shear Analysis of Columns with Steel-Belted Tires as Transverse Reinforcement

Two different shear-span-to-depth ratios of columns were considered in the current investigation to study two different levels of shear stress reversals. Three of the columns had relatively short shear spans to investigate the performance of columns under high shear force reversals. These columns either had a 550 mm cross-section with a shear span of 1200 mm or a 700 mm diameter section with 1500 mm shear span, with a shear-span-to-depth ratio of 2.2. The difference in cross-sectional size would reflect the differences in concrete shear resistance. Also, different sizes and different types of columns have different amounts and strength of steel wires in tires, with different levels of tire contribution to shear. The

experimental data provided invaluable information on the contribution of steel-belted radial tries to shear resistance to validate the applicability of the simplified approach of CSA Standard A23.3-2004, which was developed for conventional steel reinforced concrete elements.

The shear resistance specified in CSA A23.3-2004 is based on the computation of concrete and transverse reinforcement contributions to diagonal tension caused by shear. This is shown below.

$$V_r = V_c + V_s \tag{5.15}$$

$$V_c = \phi_c \lambda \beta \sqrt{f_c'} b_w d_v \tag{5.16}$$

$$V_s = \frac{\phi_s A_v f_y d_v \cot\theta}{s} \tag{5.17}$$

Where, β = 0.18 and θ = 35° as per CSA A23.3-2004. The materials resistance factors ϕ_c, ϕ_s, and the mass density factor λ for nominal shear capacity and normal density concrete should be taken as 1.0. The above expressions are intended to provide conservative estimates of shear capacity and they do not include axial load as a parameter. They may be adapted to columns transversely reinforced with steel-belted tires. However, it is important to recognize that tires often have very high strength steel wires which do not yield under the influence of shear induced diagonal tension until a significant diagonal crack develops. At this stage, cracked concrete looses aggregate interlock and ability to transfer shear across the crack. This implies that concrete shear resistance diminishes very quickly as crack widths increase. It was observed experimentally that cracked concrete can maintain its shear resistance at least up to the stress level that corresponds to 0.004 transverse strain and this limit has been adopted by CSA Standard S806-02 (CSA S806 2002) in defining the effectiveness of high-strength FRP transverse reinforcement when full resistance of concrete to shear, V_c, is relied upon. This value was found to conform to the current test results. With this strength limit on tire steel, the above expressions were used to compute the shear capacity of columns that are transversely reinforced with steel-belted tires. These expressions are repeated below as adapted to tire reinforcement.

$$V_n = V_c + V_{str} \tag{5.18}$$

$$V_c = 0.18\sqrt{f_c'}b_w d_v \tag{5.19}$$

$$V_{str} = \frac{A_{vtr} f_{str} d_v \cot\theta}{s} \tag{5.20}$$

Where,

V_{str} = shear stress resistance provided by steel-belted tires.

f_{str} = stress in steel embedded in tire prior to the loss of aggregate interlock mechanism in concrete. May be taken as $0.004E_s \leq f_{ytr}$

A_{vtr} = total area of transverse reinforcement embedded in tire

d_v = effective shear depth, taken as the greater of $0.9d$ or $0.72h$

s = the width of the treaded portion of tire

E_s = modulus of elasticity of steel (200,000 MPa)

f_{ytr} = yield strength of steel in tire

Shear force capacities of test columns, based on the above expressions, are shown on experimental force-displacement hysteretic relationships in Figure 5.16 and Figure 5.17. Computed shear capacities are higher than the shear force associated with flexural yielding. Therefore the columns did develop flexural yielding. However, as concrete shear resistance started degrading under cyclic loading, Columns TC-10 and TC-12 started developing strength decay. This was more evident in Column TC-10 where the drop in concrete shear resistance could not be offset by the relatively lower grade wires in the tires. This column failed through diagonal tension which resulted in the rupturing of tires along the inclined shear plane. The contribution of concrete and tire steel to shear resistance are tabulated in Table 5.5 for all the columns tested. It may be concluded from the limited number of columns tested that the CSA A23.3 shear expressions for simplified approach may be used to compute the shear capacity of columns with steel-belted tires as transverse shear reinforcement.

5.6 *Proposed Design Procedure for Columns with Steel-Belted Tires as Transverse Reinforcement*

Reinforced concrete columns can be designed using steel-belted tires as stay-in-place formwork and transverse reinforcement. The tires are placed on top of each other and secured in place by puncturing holes and passing longitudinal re-bars through these holes. The resulting assembly provides a rigid and strong formwork for concrete while securing the longitudinal column reinforcement in place. Once the concrete is placed and cured, the columns develop flexural and shear resistances to gravity and lateral loads. Once cast, tires provide confinement to compression concrete, improving flexural strength and deformability. They also provide shear strength, controlling diagonal tension cracks caused by shear.

The following design procedure, adopted from the design of conventional steel reinforced concrete columns, may be used in design. The procedure provides design recommendations for flexure and shear. The design can be performed by incorporating the appropriate load factors specified in the National Building Code of Canada (NBCC 2005) and the material resistance factors (ϕ factors) specified in CSA A23.3 (2004) for concrete and steel.

5.6.1 *Design for Flexure*

Flexural design capacity of columns under bending and axial load can be established through sectional analysis. The sectional analysis can be conducted by following the same steps as those used for ordinary column sectional analysis for conventional steel reinforced concrete columns. Plane sections before bending are assumed to remain plane after bending with strains along the depth of the section related linearly. An important difference between an ordinary steel reinforced concrete and tire reinforced concrete columns is the presence of rubber side walls in the concrete compression zone, which tend to reduce concrete strength. Furthermore, the tapered shape of tires along their perimeter edges and the resulting reduction in sectional area should also be accounted for. A typical column section, the variation of strains under strain gradient and the corresponding stress and force diagrams are

illustrated in Figure 5.9. It is important to consider two distinctly different zones of compression concrete in sectional analysis; i) the central core, which is made up of pure concrete confined by the rim steel, as well as the tread steel, and ii) the perimeter region with rubber side walls resulting in approximately 40% to 60% reduction in concrete strength, confined by the tread steel. The properties of concrete in these two distinctly different zones can be obtained from the stress strain models presented earlier in this chapter.

Another unique aspect of columns cast in tires is the constraints placed on geometry. Because the tires are available only in certain sizes, with certain characteristics of wires embedded in the rubber, the design may be performed in the form of verification of column capacity for a specific size of column as dictated by the selected tire size. Although there is some flexibility in the selection of longitudinal reinforcement and hence the percentage of main column reinforcement for flexure, the same can not be said for transverse reinforcement, whether used for confinement or shear.

5.6.2 Check for Column Confinement

The tires used as transverse reinforcement provides confinement to compression concrete, which improves column inelastic deformability. Because the designer can not change the amount of steel in tires to achieve certain confinement and corresponding column deformability, it is suggested that the column deformability be checked for the specific size and type of tires used in design. This may be done by employing the displacement-based design expression developed by Saatcioglu et al (2008) for FRP stay-in-place formwork. There is a direct correspondence between the FRP tubes and the tire assembly used in the current investigation as a tube for transverse reinforcement. However, it is important to incorporate the appropriate material properties in adopting this expression. The following is the expression suggested by Saatcioglu et al (2008) for the FRP tubes:

$$\rho_F = 4.2\frac{f_c'}{f_F}\frac{1}{\sqrt{k_c}}\frac{P_e}{\phi P_o}\delta \qquad (5.21)$$

Where, ρ_F is the area ratio of FRP reinforcement, f_F is the maximum stress that can be developed in FRP tube prior to significant strength decay, k_c is the confinement efficiency parameter and is taken as 1.0 for circular tubes and P_e / P_o is the ratio of maximum axial compression that can be developed in a column during an earthquake to column concentric capacity. The inelastic deformability of column is expressed in terms of drift ratio capacity δ. The ϕ factor in the expression is a capacity reduction factor to allow for a margin of safety, and may be taken as 0.9.

Eq. (5.21) can be re-written for tire confined columns. In this case the confined concrete has two regions; the perimeter region where tire side walls are within the compression zone and the core concrete enclosed by the rims. Depending on the level of axial compression on the column and the location of the neutral axis, either one or both regions fall within the compression zone. However, under strain gradient, the highly compressed exterior most portion of compression concrete is affected by confinement the most. Hence, it may be appropriate to ignore the confinement effect of the rims for most columns where the core concrete confined by the rims is often located close to the neutral axis. This is appropriate for columns under low levels of axial compression and may produce conservative drift predictions for columns under high axial compression. Therefore, the confinement steel ratio may be taken as that for the tread steel (ρ_{st}) and the concrete strength may be taken as that for the concrete-rubber composite material ($f_{cr}^{'}$) around the perimeter of column. When solved for drift ratio δ to check for available drift capacity, Eq. (5.21) becomes;

$$\delta = \rho_{st} \frac{f_{st}}{4.2 f_{cr}^{'}} \frac{\phi P_o}{P_e} \tag{5.22}$$

The above expression can be used to compute drift capacity δ. It was verified against flexure dominant columns tested (TC-1; TC-2; and TC-7). The vertical lines, shown on the hysteretic relationships shown in Figure 5.11 and Figure 5.12, indicate good correlations of computed drift capacities with test data. This computed drift capacity can then be compared with the drift demand associated with the performance level expected from the column

during an earthquake. Fully ductile columns are usually designed for 4% drift to ensure collapse prevention after a strong earthquake. Moderately ductile columns may be required to develop 2% drift for life safety.

5.6.3 Shear Design Check

Steel-belted tires can be used as shear reinforcement. This was verified earlier through experimental and analytical research. This type of transverse reinforcement provides enhancement to diagonal tension resistance of columns. It also enhances diagonal compression capacity of columns through the confinement of compression struts, but this aspect of shear resistance mechanism was not quantified because of the relatively low percentage of steel contained in the tires, which would make the columns critical in diagonal tension. Shear design should be performed such that the column shear capacity should be sufficiently high to prevent premature shear failure prior to flexural yielding.

Once a column is designed for flexure for a selected tire size, then the shear capacity should be checked to ensure adequate shear strength. This can be done by using Eqs. (5.18) through (5.20). If the computed capacity of shear is not high enough to allow the yielding of longitudinal reinforcement in flexure, then the column design should be revised.

Table 5.1: Summary of Experimental Design for Concrete Cylinders with Tires

Tire Group	No. of Rubber Piece	Diameter of the Rubber Piece (mm)	Replicates
3 Hollow Circular Rubber Rings (3HCRR)	3	150 & 100	7+8
6 Hollow Circular Rubber Rings (6HCRR)	6	100	5
3 Solid Ring (3SR)	3	100	5
6 Solid Ring (6SR)	6	100	5
3 Half Solid Rubber Ring (3HSRR)	3	100	5
6 Half Solid Rubber Ring (6HSRR)	6	100	5
Pure Concrete Cylinders (PC)	-	150 & 100	5+10

Table 5.2: Variation of Compressive Strength with Percentage Volume of Rubber

Tire Group	No. of Rubber Pieces	Volumetric Ratio of Rubber	Compressive Strength (MPa)
Pure Concrete Cylinders (PC)	0	0	38.32
Half Solid Rubber Ring (HSRR)	3	5.25	20.70
Hollow Circular Rubber Rings (HCRR)	3	6.72	15.82
Solid Ring (SR)	3	10.5	3.35
Hollow Circular Rubber Rings (HCRR)	6	13.44	10
Solid Ring (SR)	6	21	2.5

Table 5. 3: Column Axial Load Relative to Concentric Capacity

Label	Axial Load				
	P (kN)	P_o (kN)	P / P_o	$P_{o,r}$ (kN)	P / P_{or} (kN)
TC-7	1900	19789	10%	12921	15%
TC-8	1900	19789	10%	12495	15%
TC-9	1950	12180	16%	8477	23%
TC-10	1950	12180	16%	8477	23%
TC-11	1900	19789	10%	12921	15%
TC-12	1950	12180	16%	8477	23%

Table 5.4: Comparisons of Analytical and Experimental Moment Capacities

Column Specimen	Computed Moment, M_n (kN.m)			Experimental Moment, M_n (kN.m)
	Based on ACI 318 Rectangular Block	Based on Hognestad's Model	Based on Confined Concrete Model	
TC-1	362	371	367	377
TC-2	395	419	418	424
TC-7	962	1000	891	932
TC-8	874	908	806	660
TC-9	461	493	504	400
TC-10	461	493	422	382
TC-11	868	899	797	658
TC-12	461	493	532	462

Table 5.5: Comparisons of Shear Force Capacities between CSA A23.3-2004 and Experimental Values

Column	f_{str} (MPa)	V_c (kN) CSA	V_{str} (kN) CSA	$V_n = V_c + V_{str}$ (kN)	V_{exp} (kN)	$\frac{Theory}{Exper.}$
TC-10	800	235	157	392	296	1.3
TC-11	800	419	265	672	460	1.4
TC-12	800	235	252	487	335	1.4

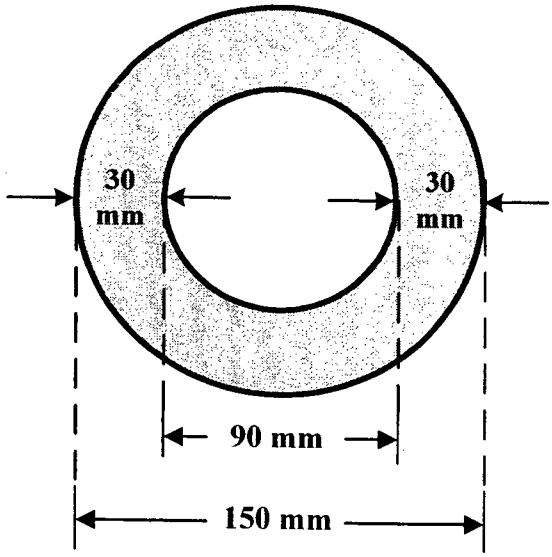

Rubber Ring for 100 mm Cylinder

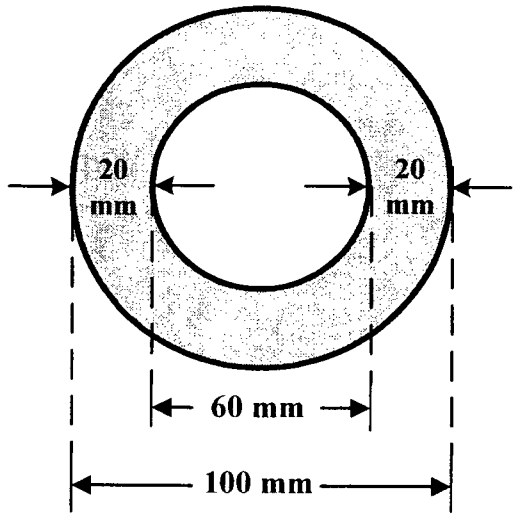

Rubber Ring for 150 mm Cylinder

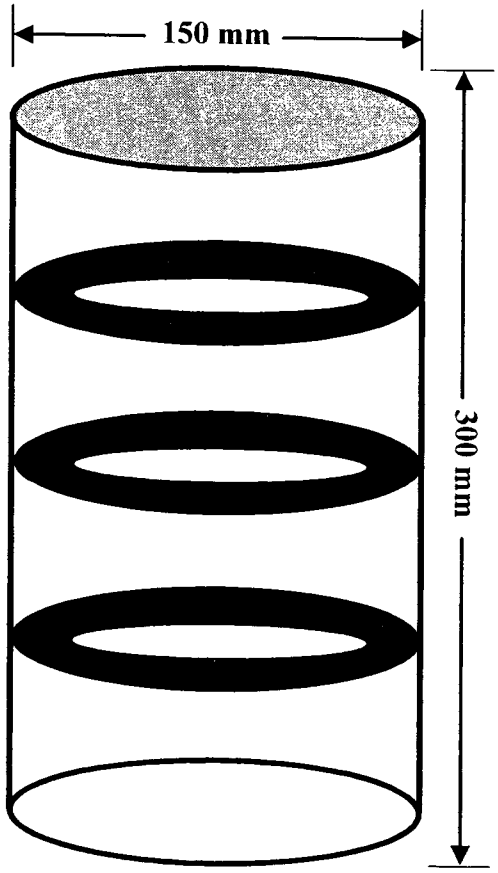

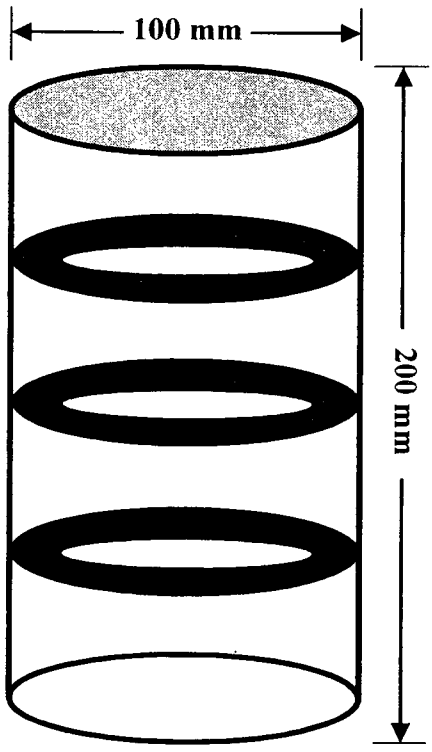

(a) Three Hollow Circular Rubber Rings

Figure 5.1: Tire Rubber Arrangements in Cylinders

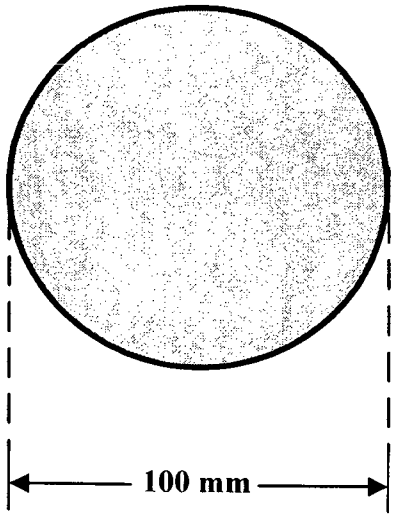

Solid Rubber Piece for
100 mm Cylinder

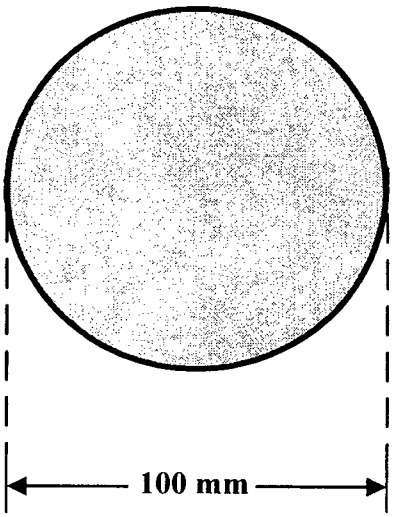

Solid Rubber Piece for
100 mm Cylinder

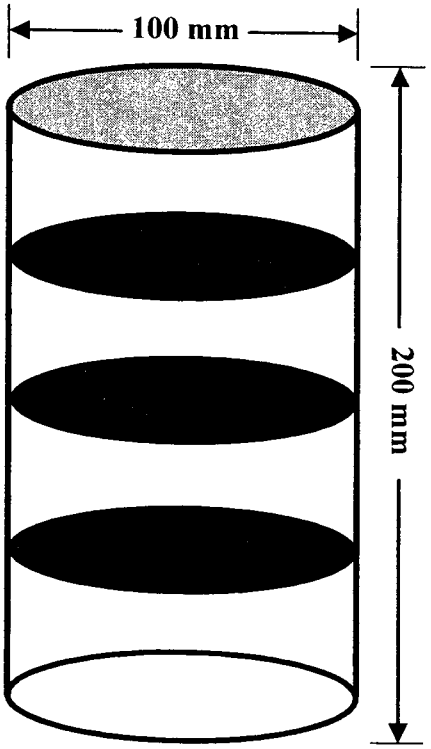

(b) Three Solid Rubber pieces

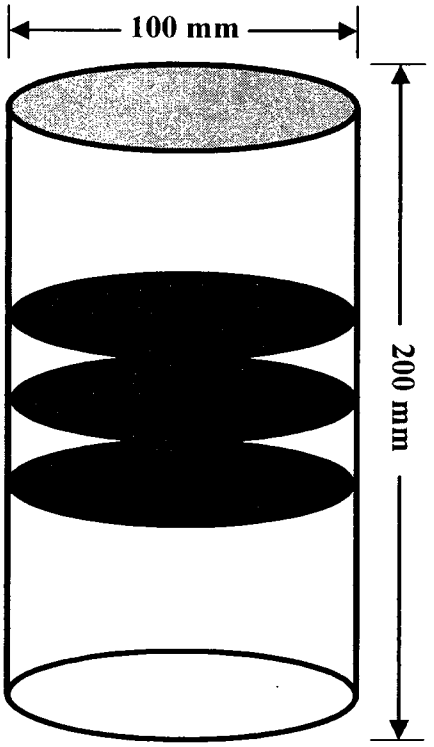

(c) Three Solid Rubber pieces in the Middle

Figure 5.1 (Cont'd): Tire Rubber Arrangements in Cylinders

(a) Concrete Tire Cylinders Shortly before Casting

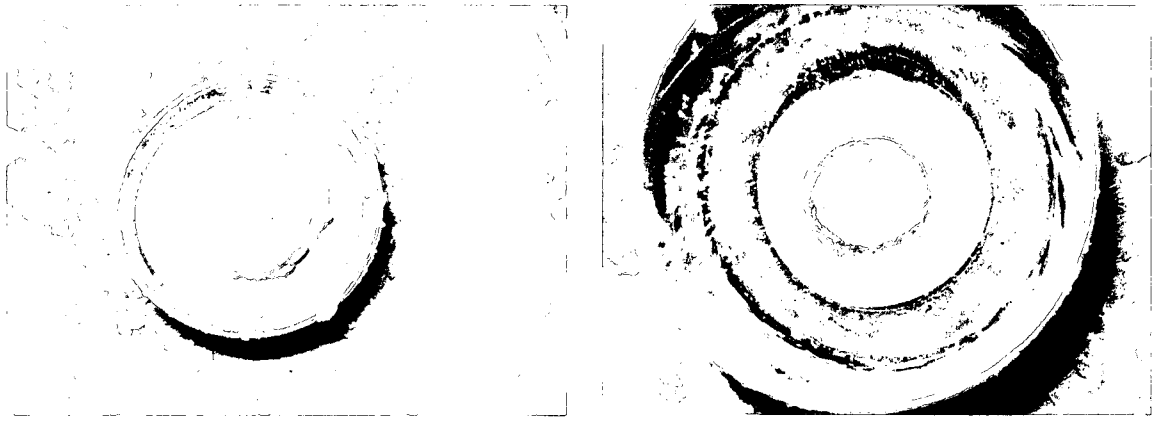

(b) Concrete Tire Cylinders during Casting

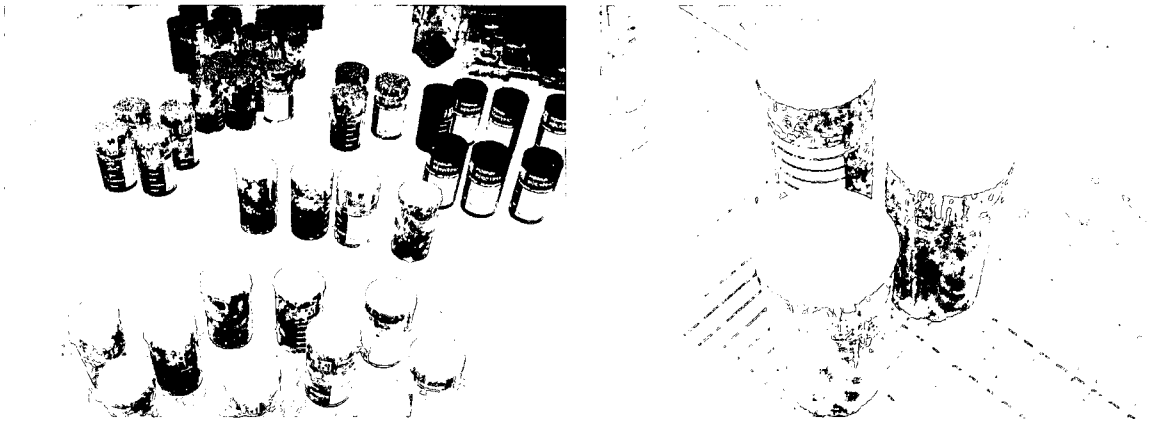

(c) At Completion

Figure 5.2: Tire Arrangements and Casting of Cylinders

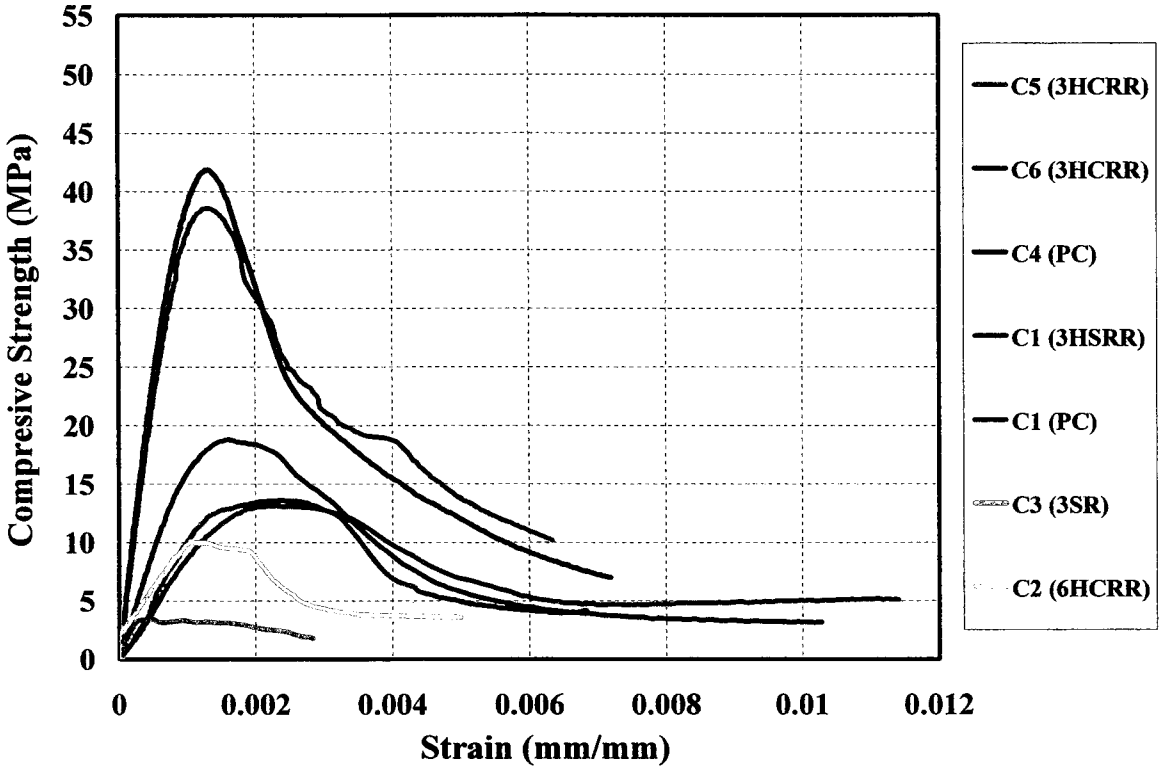

(a) Stress-Strain Relationships for Concrete Cylinders with Rubber (Phase II)

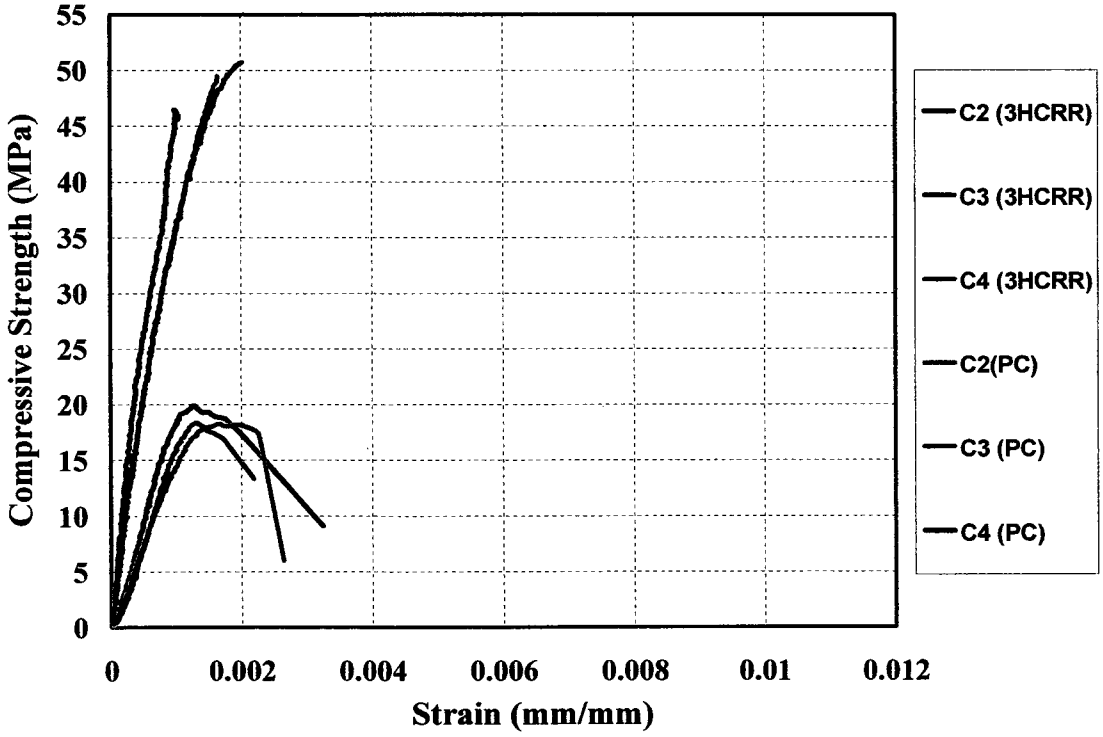

(b) Stress-Strain relationships for Concrete Cylinders with Rubber (Phase I)

Figure 5.3: Stress-Strain Relationships for Concrete Cylinders with Rubber

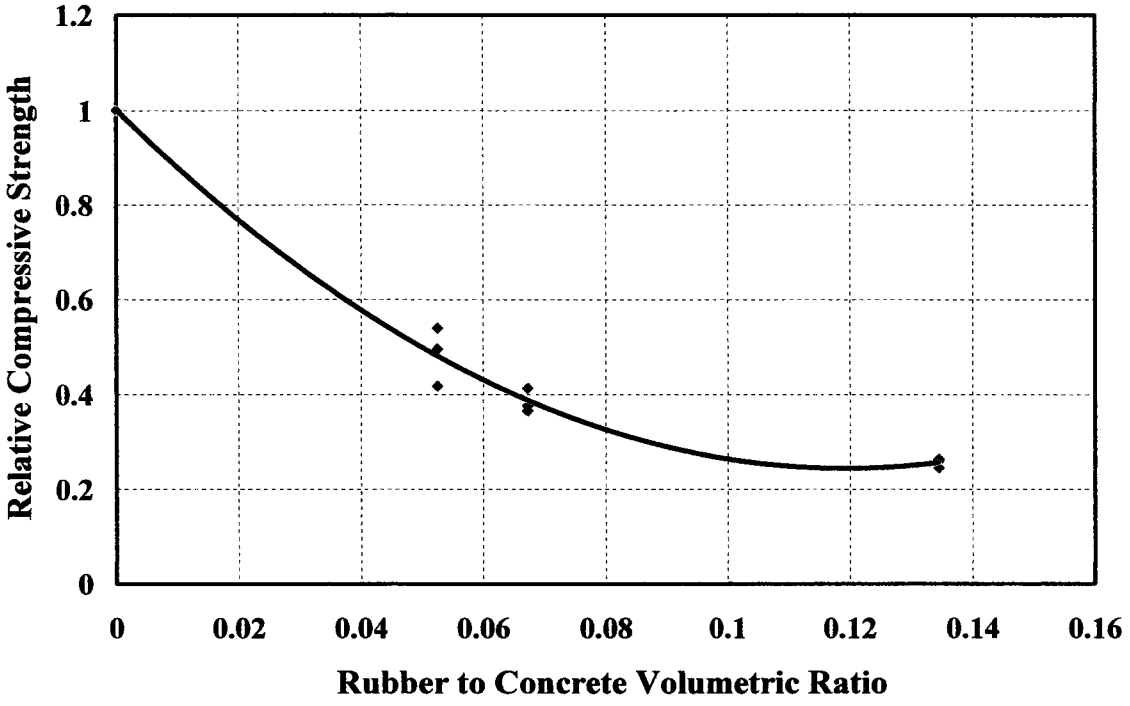

Figure 5.4: Cylinder Compressive Strength versus Volumetric Ratio of Rubber

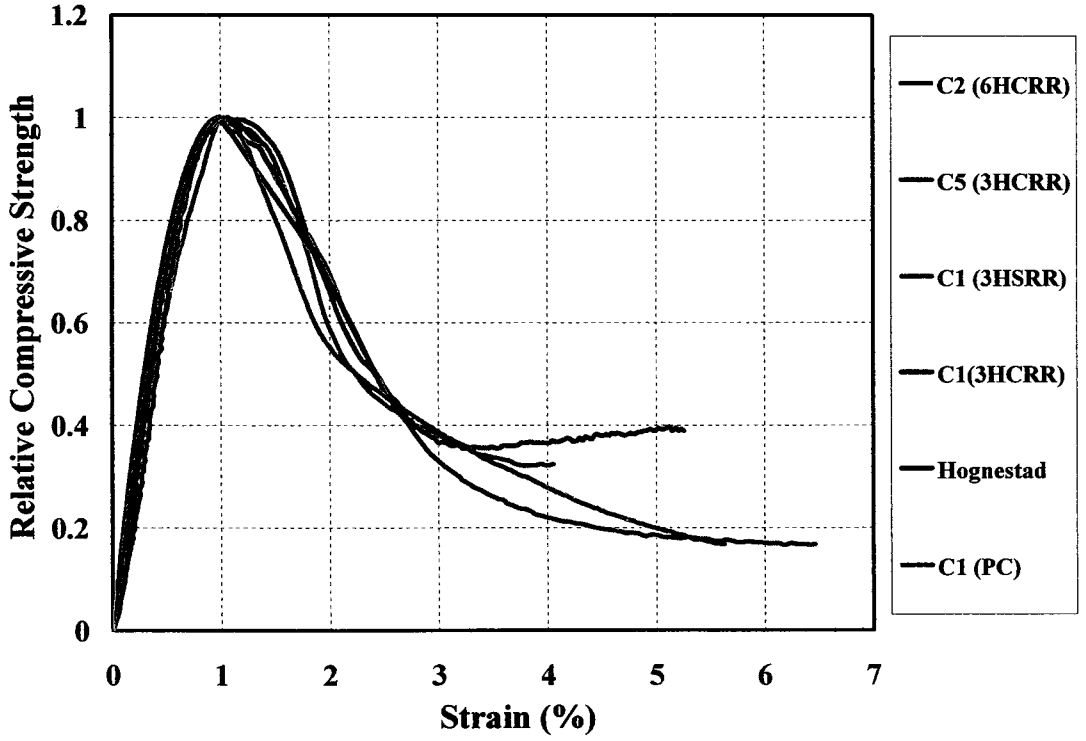

Figure 5.5: Normalizing Stress-Strain Relationships of Concrete Cylinders with Different Tire Arrangements

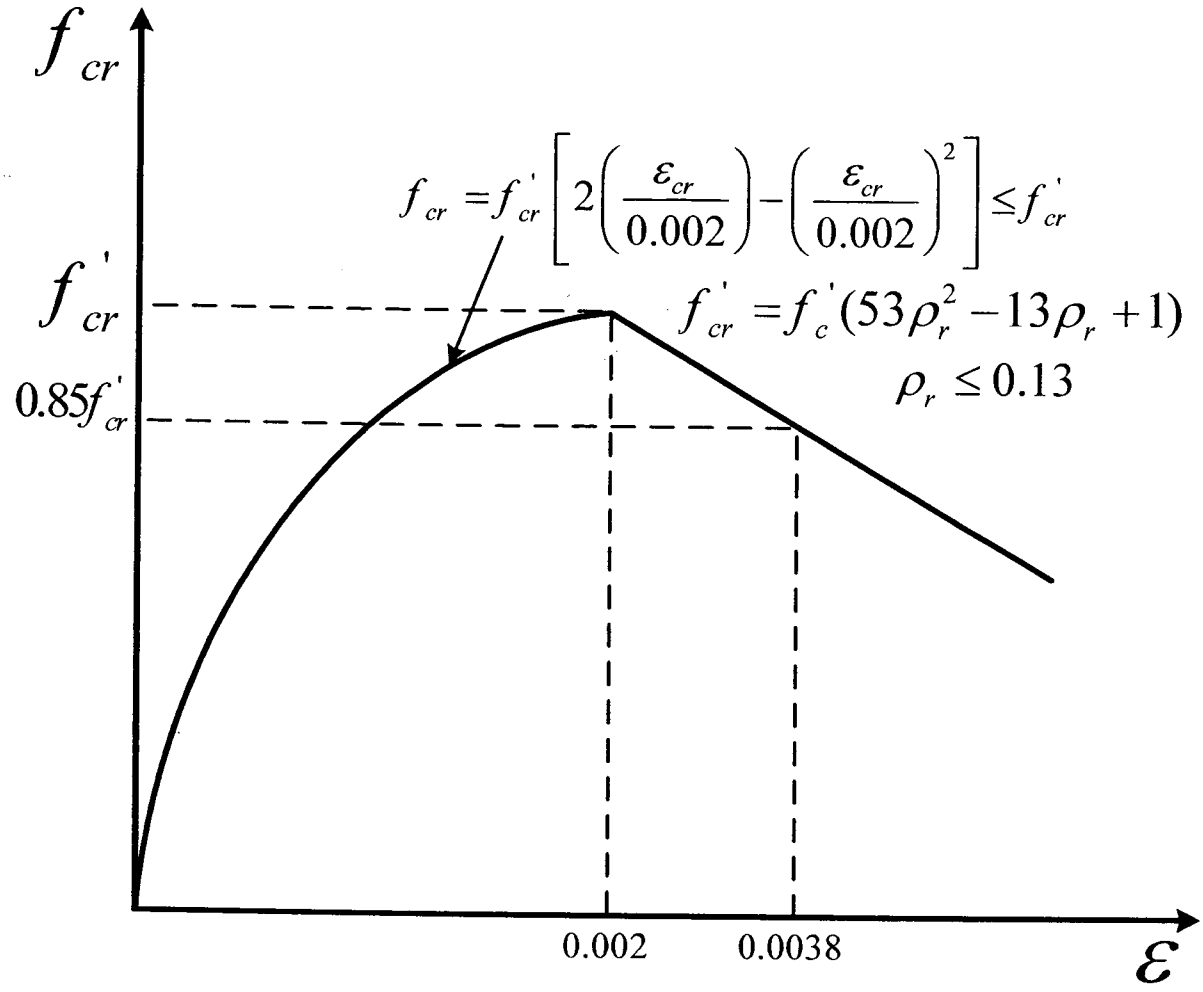

Figure 5.6: Stress-Strain Model for Concrete with Rubber Layers

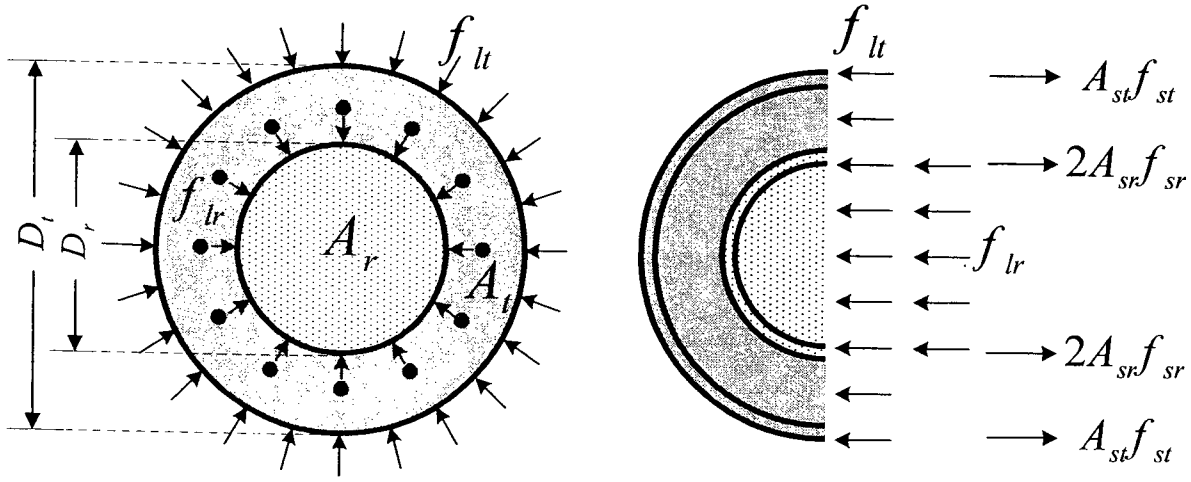

Figure 5.7: Lateral Pressure Distributions in Steel-Belted Tire Column

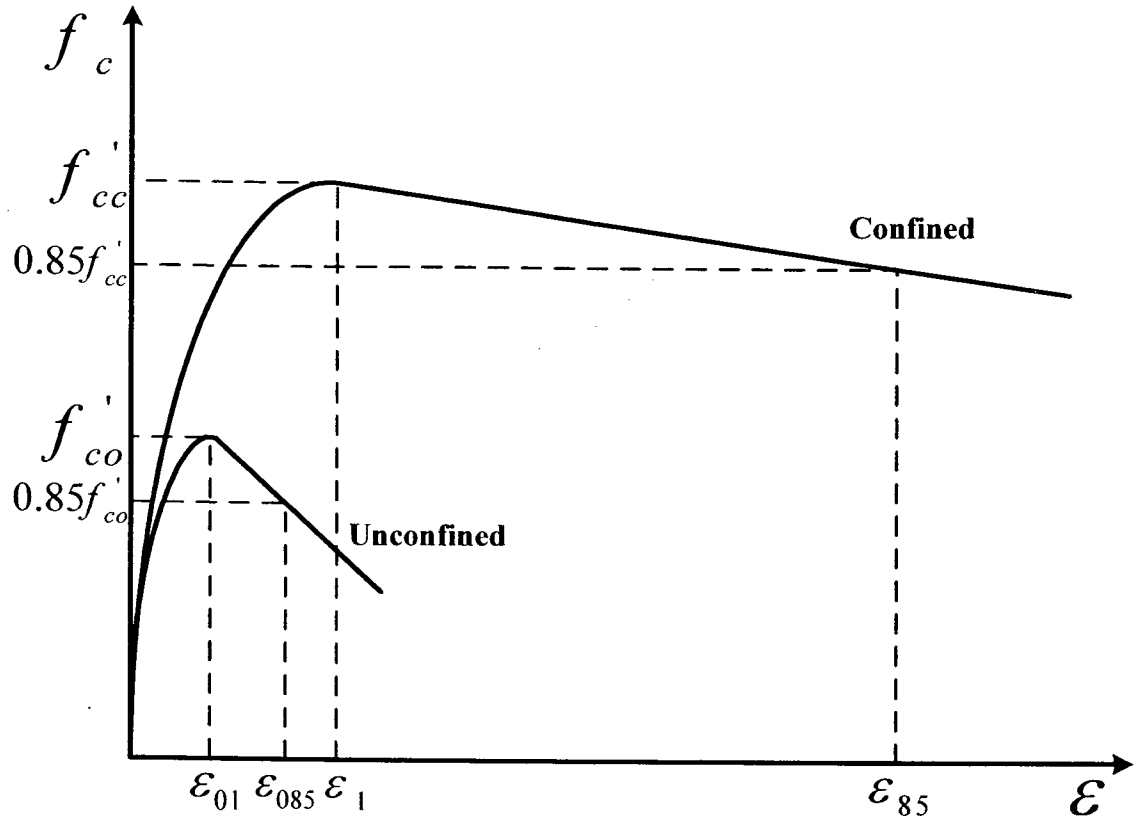

Figure 5.8: Stress-Strain Relationships for Unconfined and Confined Concrete (Saatcioglu and Razvi, 2002)

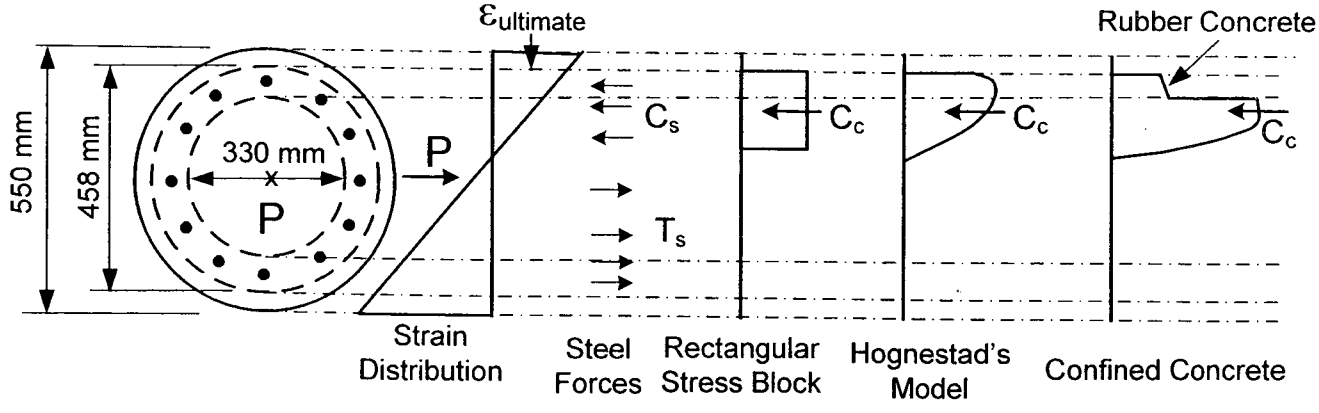

Figure 5.9: Sectional Analysis

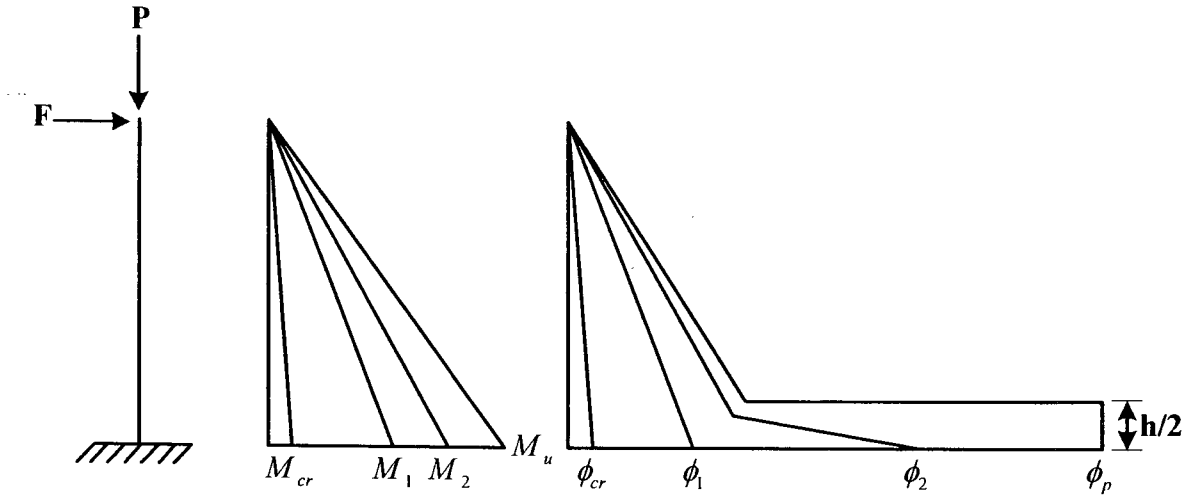

Figure 5.10: Progression of Plastic Hinging and Distribution of Curvatures at Each Control Point used to Compute Lateral Displacements

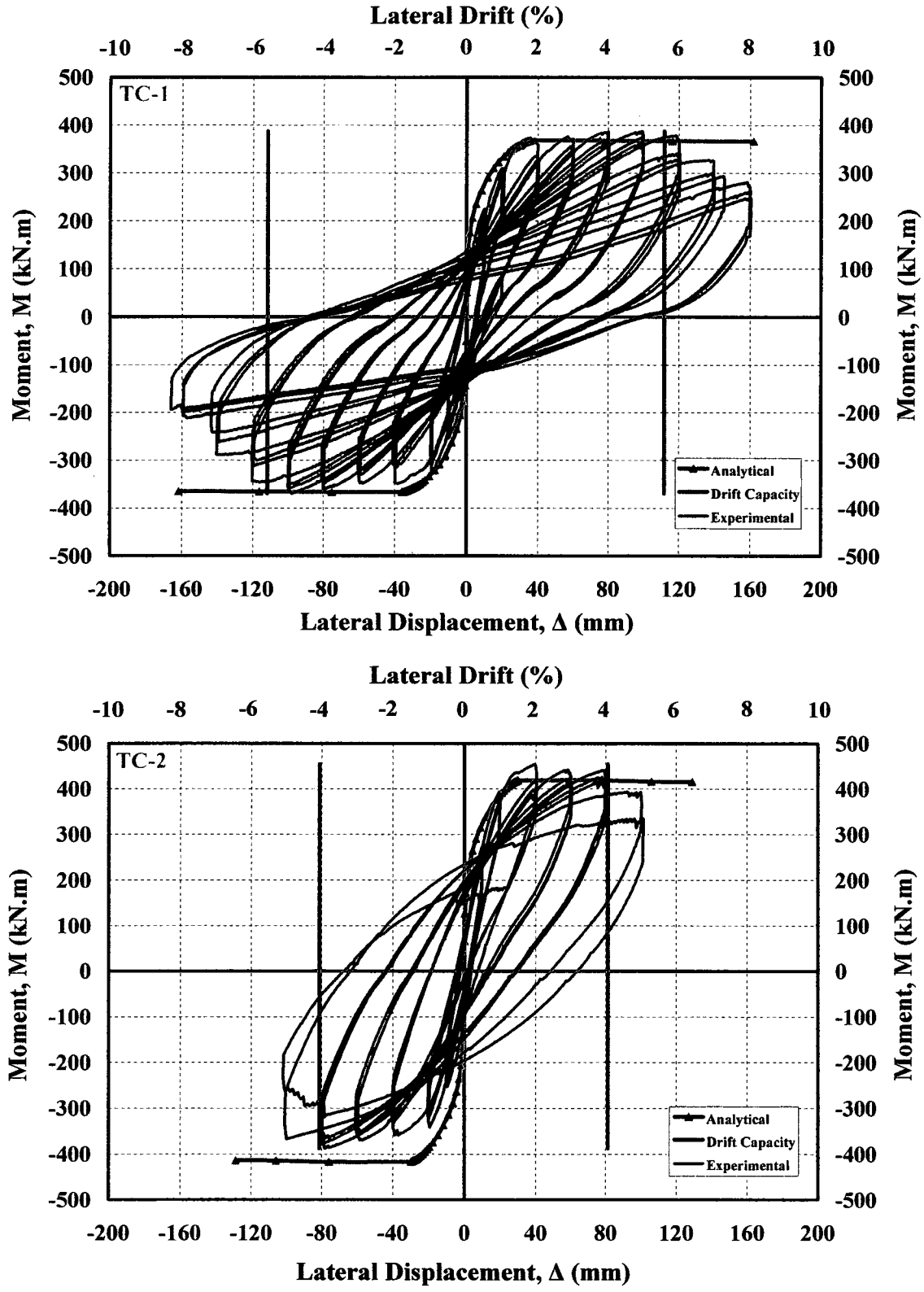

Figure 5.11: Comparisons of Analytical and Experimental Moment-Displacement Relationships for Columns TC-1 and TC-2

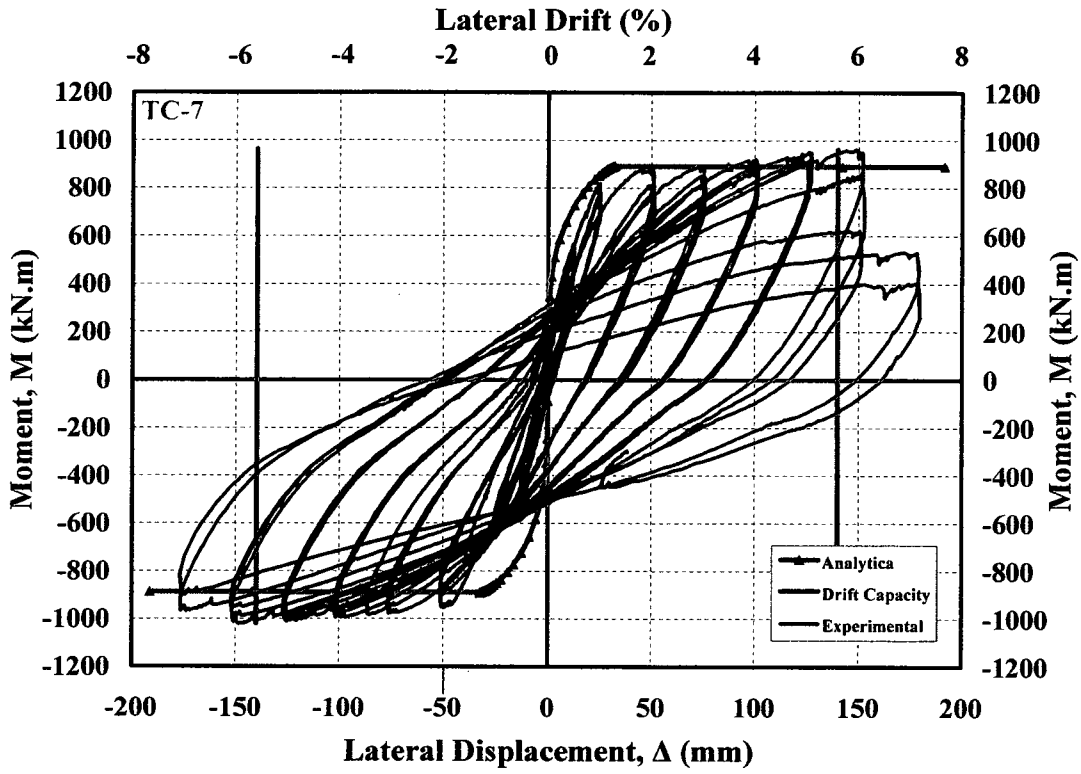

Figure 5.12: Comparisons of Analytical and Experimental Moment-Displacement Relationships for Column TC-7

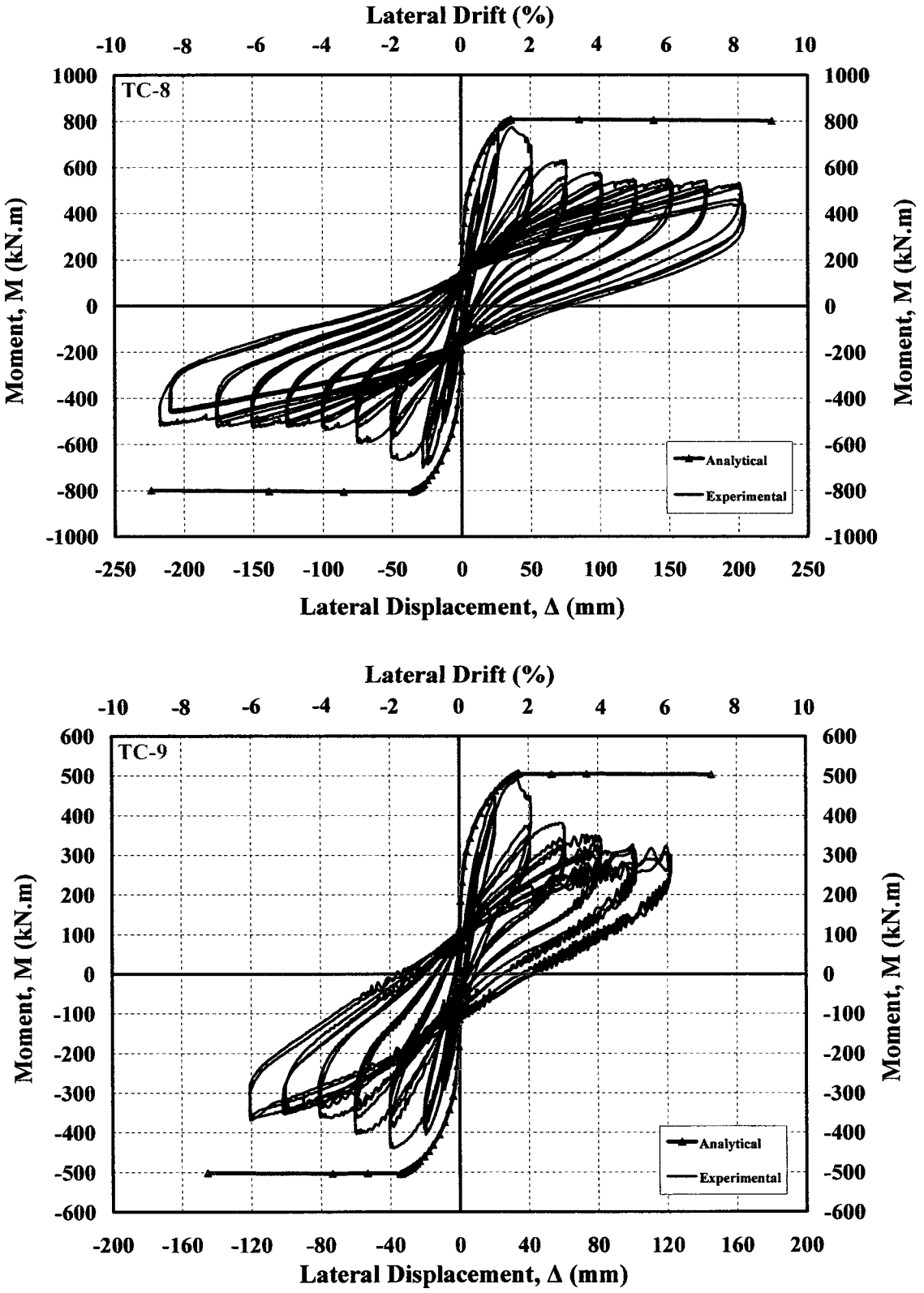

Figure 5.13: Comparisons of Analytical and Experimental Moment-Displacement Relationships for Columns TC-8 and TC-9

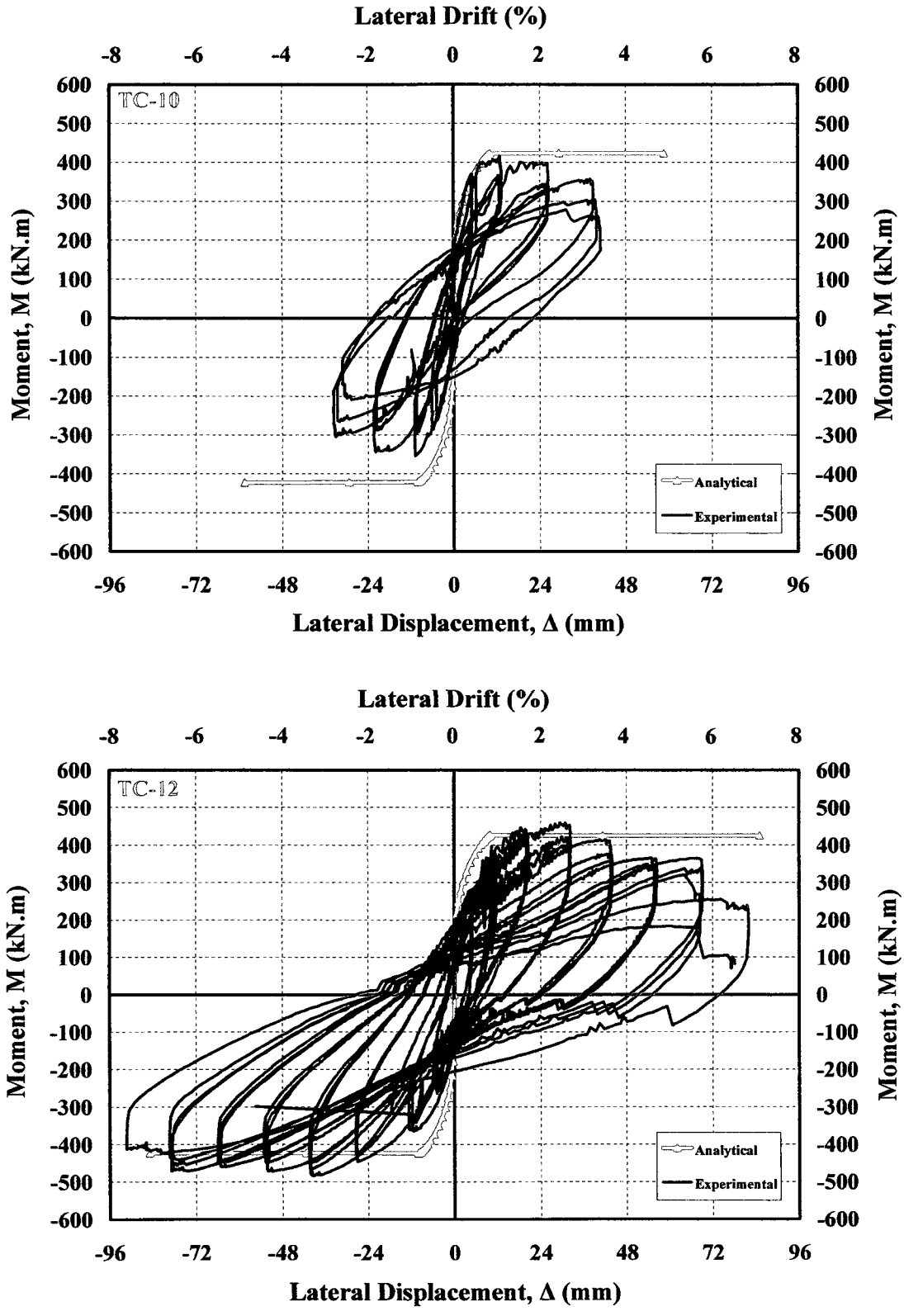

Figure 5.14: Comparisons of Analytical and Experimental Moment-Displacement Relationships for Column TC-10 and TC-12

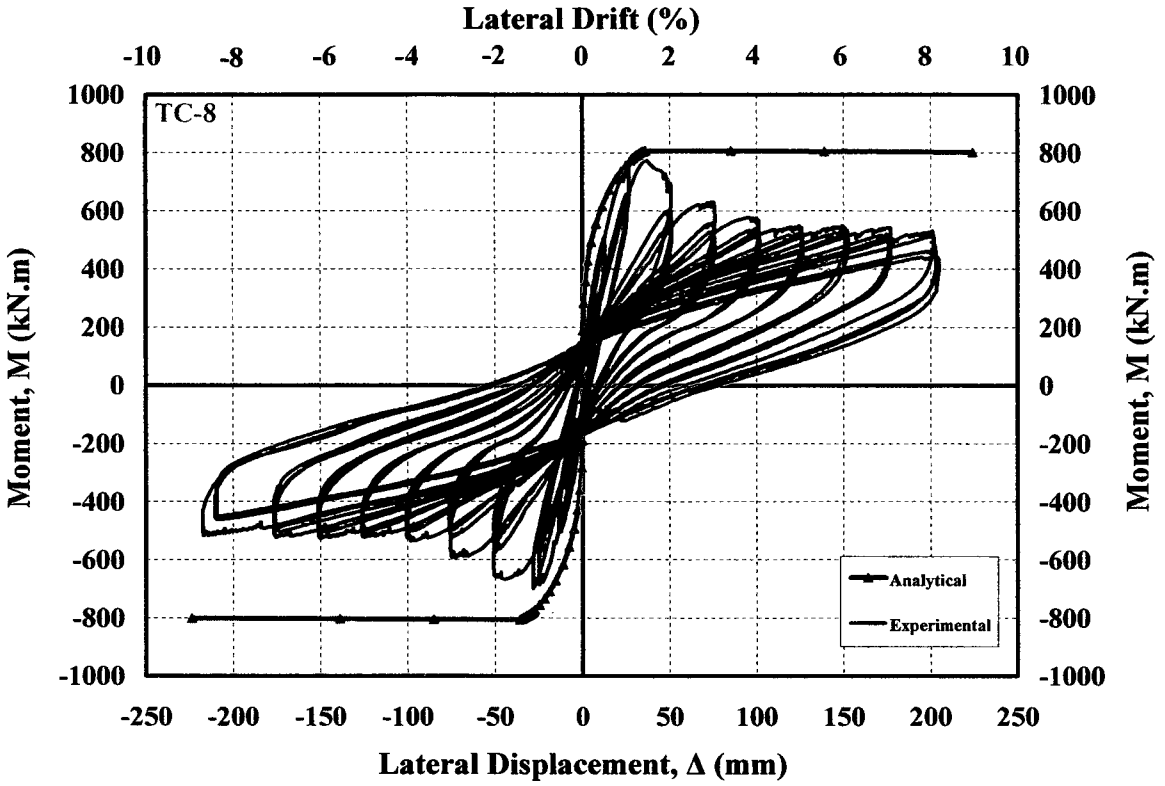

Figure 5.15: Comparisons of Analytical and Experimental Moment-Displacement Relationships for Columns TC-11

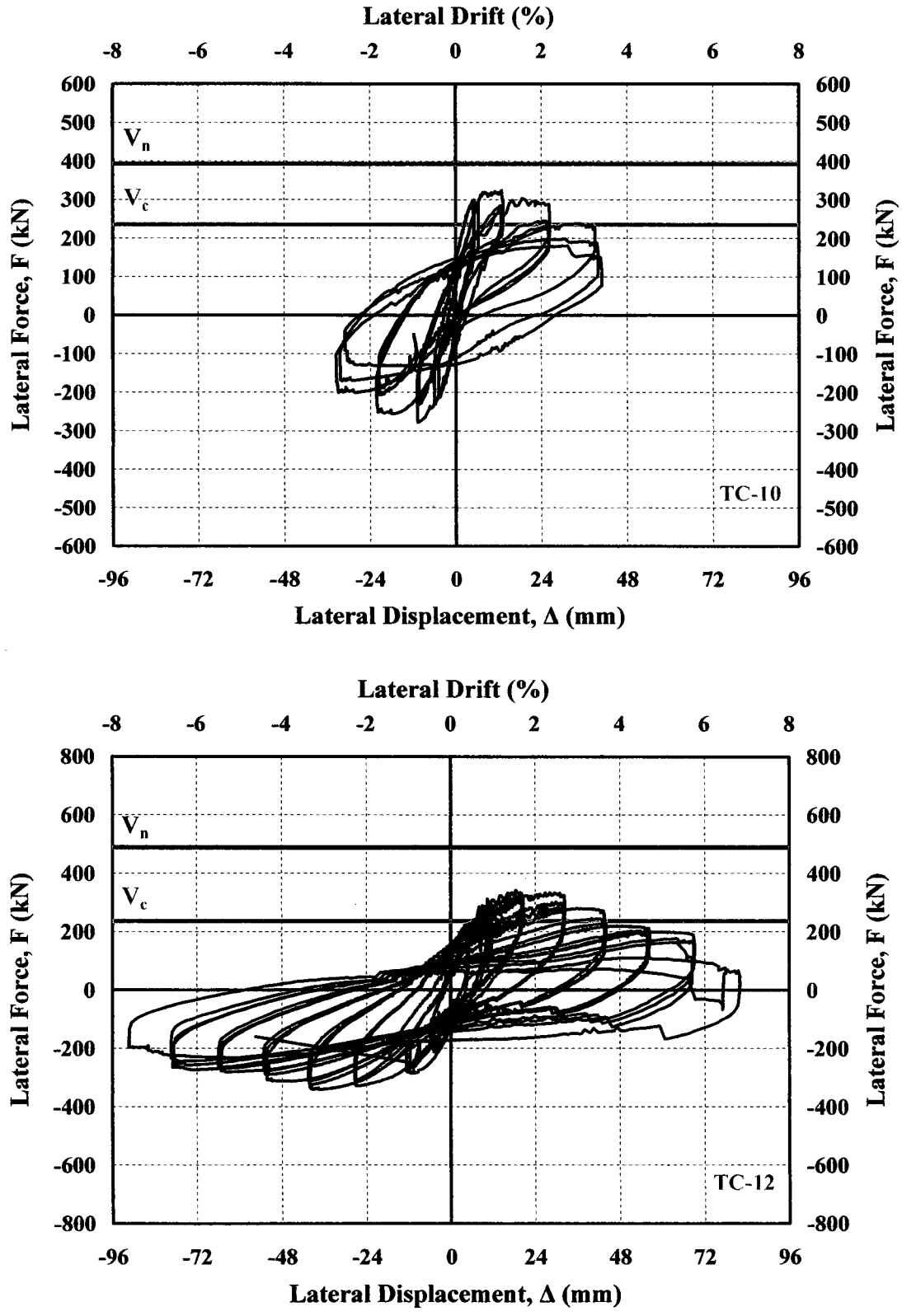

Figure 5.16: Comparison of Computed Shear Force Capacities and Experimental Force-Displacement Relationships for Columns TC-10 and TC-12

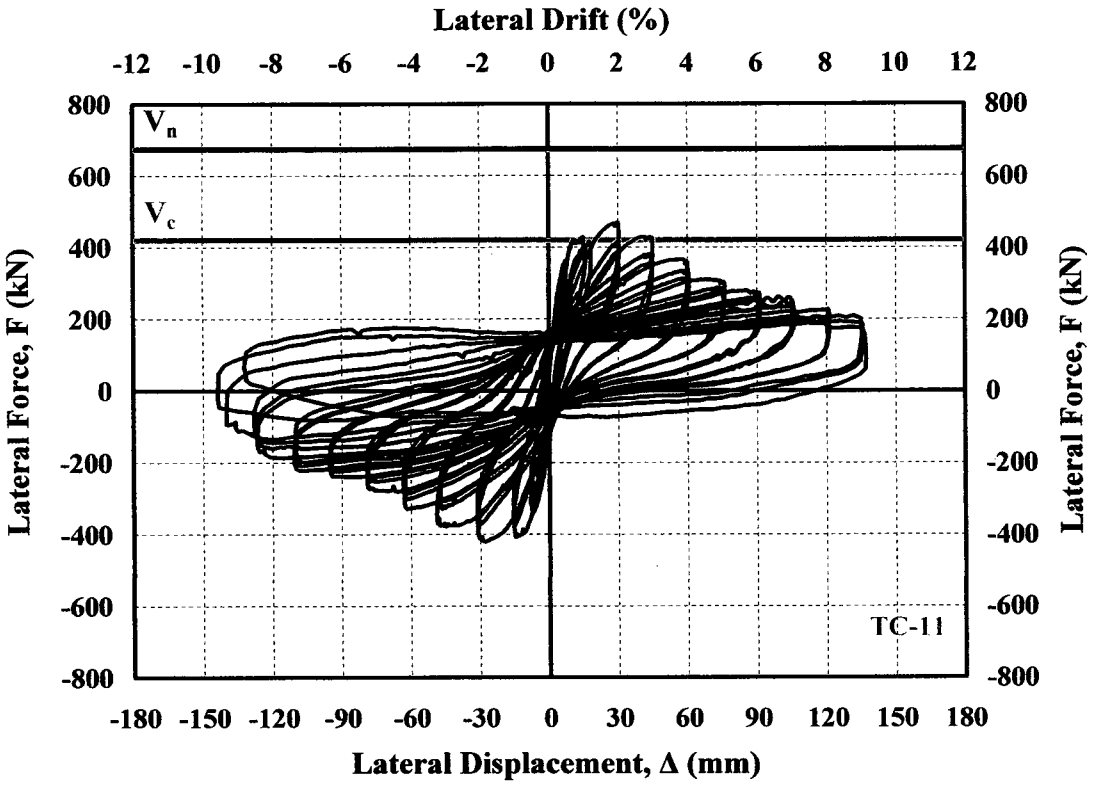

Figure 5.17: Comparison of Computed Shear Force Capacities and Experimental Force-Displacement Relationships for Column TC-11

CHAPTER 6

Summary and Conclusions

6.1 Summary

Many structural failures during past earthquakes have been attributed to poor column behaviour in the inelastic range. In order to prevent this poor behaviour, columns are designed to have adequate ductility, by suitably confined plastic hinge regions. This is usually done by providing transverse reinforcement of sufficient amount and proper arrangement, with close spacing. An alternative to conventional confinement reinforcement is to use steel-belted tires. However, this application of tires has not been researched in the past. Hence, there is no experimental data available on columns confined with tires, though confining columns with steel-belted tires may be a feasible alternative.

An extensive experimental and analytical research was conducted to investigate the applicability of steel-belted tires as transverse column reinforcement. A total of six full size circular columns were designed, constructed and tested under constant axial compression and incrementally increasing lateral deformation reversals. These columns were designed and built in full scale. They included flexure dominant columns with two different shear spans, covering a range of shear stress reversals. They also included spliced longitudinal reinforcement at the base. The test parameters consisted of cross-sectional dimension (tire sizes), splicing of longitudinal bars, level of axial load, and column height (shear span). Test results were presented in the form of hysteretic force-deformation relationships.

Analytical investigations included the development a stress-strain model for concrete with layers of tire rubber. This was necessary to conduct flexural analysis. It necessitated tests of a large number of concrete cylinders with different volumetric ratios of rubber in concrete.

The analytical research also included the verification and adaptation of an existing concrete confinement model to tire confined columns.

The material models were used to conduct sectional and member analyses. The results were compared with experimental data. A design procedure was formulated for reinforced concrete columns with steel-belted tires used as transverse reinforcement. The design method involved flexural and shear strength computations.

6.2 Conclusions

The following conclusions can be drawn based on the experimental and analytical research investigation presented in this thesis:

1. Columns confined with steel-belted tires can develop ductile behaviour under simulated seismic loading. The use of steel-belted tires as confinement reinforcement substantially increases deformability of the columns, developing lateral drift ratios ranging between 4% and 8% drift, depending on the level of axial compression.
2. Inelastic column deformabilities obtained in tire-reinforced columns are comparable to those obtained with conventional reinforcement. The column tests indicate that a bridge column confined by steel-belted radial tires under 10% of column concentric capacity can develop approximately 4% to 8% lateral drift without a significant loss of strength. The same column can sustain approximately 4% to 6% lateral drift when the axial compression is increased to 16%, indicating that column deformability decreases with increasing axial compression. The effect of axial compression is to increase flexural capacity while reducing column deformability. The increase in axial load from 10% P_o to 16% P_o resulted in approximately 2% reduction in drift capacity.

3. Tires provide effective confinement to the entire column section, unlike conventional steel reinforcement concrete columns that confined the core concrete only.
4. The strain data recorded during column tests indicate that the strength of steel-belted tire could be mobilized to a large extent, developing strains of 0.3% to 0.6% in most columns with a maximum value of 0.8%. The recommended strain value for use in design is 0.4%, which reflects a representative value for most columns.
5. The hysteretic force-deformation relationships for flexure dominant columns, with a shear-span-to-depth ratio of 3.6 indicate well rounded stable hysteresis loops, indicating high energy dissipation during seismic response.
6. Tire-confined columns with spliced longitudinal reinforcement, where the splice length is 30 times the bar diameter develop their flexural capacities but beyond the first cycle at 2% drift ratio, experience strength decay associated with the slippage of reinforcement. The tires do not provide sufficient clamping force to prevent splice slippage beyond 2% lateral drift ratio.
7. Columns with shear capacities higher than the shear force corresponding to flexural capacity perform well with stable hysteresis loops. Those with computed shear capacities of 85 to 98% of flexural capacity were able to develop flexural yielding but experienced strength decay thereafter. Columns subjected to high shear stress reversals show more pinched hysteresis loops.
8. The analytical model developed for the stress-strain relationship of concrete with internally placed rubber layers provides good agreement with experimental data when incorporated in moment-curvature analysis.
9. The confinement model proposed by Saatcioglu and Razvi can be applied to tire confined concrete columns with appropriate modifications introduced to stress limits for the wire steel in tire.
10. Flexural capacity of columns enchased in steel belted tires can be computed with good accuracy by plane section analysis. Such analysis should, however, incorporate appropriate concrete models reflecting the presence of tire side walls in concrete and the confinement effects of tire steel.

11. The hysteretic moment-displacement relationships obtained experimentally show good correlations with the moment-displacement envelope curves computed analytically. This implies that the analysis techniques intended for concrete columns reinforced with conventional steel reinforcement can be applied to tire-reinforced columns provided that appropriate material models are incorporated.
12. The basic concepts used for the design of conventional reinforced concrete columns can be employed in designing columns with steel-belted tires for flexure and shear, provided that appropriate material models are incorporated. Shear capacity of columns can be calculated using the general design method outlined in CSA A23.3-2004 with steel strain in tires limited to 0.4%.
13. Tire coupon tests show that the steel in tires exhibit almost linear behaviour, with ultimate tensile strain of approximately 0.8% to 1.1%. The tensile strength was approximately equal to 1600 MPa to 2200 MPa.
14. The experimental investigation indicates that steel-belted radial tires can be used as stay-in-place formwork, as well as transverse column reinforcement for shear and concrete confinement. The tires further have the advantage of protecting longitudinal steel against corrosion, while providing impact resistance and energy dissipation in the event of a vehicular collusion due to their high toughness (high plastic energy absorption) when used for bridges and parking structures.
15. Deformations due to anchorage slip can be significant if the axial load is low. The columns subjected to higher axial compression developed lower yield penetration into the footing.

6.3 Recommendations for Future Research

The following recommendations are made for future research:

1. The effect of steel cords inside the tire treads and rims varied from one brand name to the other as evidence in TC-10 and TC-12. This variation can be investigated through additional testing. Furthermore, different sizes of tires are available in the industry. More experimental and analytical research is needed on columns with different sizes and steel contents.

2. Further column tests are recommended to investigate the applicability of columns with tires as transverse reinforcement under higher axial loads, such as those used in buildings.
3. Additional analytical and experimental research is needed to address the modeling of spliced regions, with different splice lengths.
4. Additional column tests are recommended for shear-deficient and shear-dominant columns.
5. Tires are a combustible material. Although they are difficult to ignite, they can be fire hazard. To eliminate the possibility of potential fire damage, further research is required to explore the use of incombustible materials as fire retarders.

References

- Ahmed, I. and Lovell, C.W. (1993). "Rubber Soils as Lightweight Geomaterials." Transportation Research Record, No. 1422, Transportation Research Board, National Research Council, Washington, D.C., pp. 61-70.

- Ahmed, S. H., and Shah, S. P. (1982). "Stress-Strain Curves of Concrete Confined by Spiral Reinforcement." ACI Journal, Vol. 79, No. 6, pp. 484-490.

- ACI Committee 318, (2002). "Building Code Requirement for Reinforced Concrete (ACI 318-02) and Commentary (ACI 318R-02)." American Concrete Institute, Farmington Hills, Mich., 2002, 443 pp.

- ACI Committee 318, (2005). "Building Code Requirements for Reinforced Concrete (ACI 318-05) and Commentary (ACI 318R-05)." American Concrete Institute, Farmington Hills, MI, 430 pp.

- ACI Committee 318, (2008). "Building Code Requirements for Reinforced Concrete (ACI 318-08) and Commentary (ACI 318R-08)," American Concrete Institute, Farmington Hills, MI, 465 pp.

- Amirkhanian, S. N., (2003). "Establishment of an Asphalt-Rubber Technology Service (ARTS)." Proceedings of the Asphalt Rubber 2003 Conference, Brasilia, Brazil.

- Aydilek, A. H., Madden, E. T., and Demirkan, M. M. (2006), "Field Evaluation of a Leachate Collection System Constructed with Scrap Tires." Journal of Geotechnical and Geoenvironmental Engineering, Vol. 132, No. 8, ASCE, pp. 990-1000.

- Baingo, D., and Saatcioglu, M. (1995). "Performance of Circular High-Strength Concrete Columns under Lateral Load Reversal." Research Report, Department of Civil Engineering, University of Ottawa, Ottawa, Canada.

- Balmer, G. G. (1949). "Shearing Strength of Concrete under High Triaxial Stress-Computation of Mohr's Envelope as a Curve." Structural Research Lab. Report No. SP-23, U.S. Bureau of Reclamation, Denver, Co., 13 pp.

- Basset, R., and Uzumeri, S. M. (1986). "Effect of Confinement on the Behaviour of High-Strength Lightweight Concrete Columns." Canadian Journal of Civil Engineering 13(6): pp. 741-751.

- Benda, C. C. (1995). "Engineering Properties of Scrap Tires Used in Geotechnical Applications." Report No. 95-1, State of Vermont Agency of Transportation, Materials and Research Division, 30 pp.

- Bergado, D. T., and Youwai, S. (2002). "Triaxial Compression Test on Compacted Rubber Shredded Tire with and Without Silty Sand Mixture." In Proceeding of the International Workshop on Lightweight Geomaterial, Mar 26-27, 2002, Tokyo, Japan, pp. 69-76.

- Bernal, A. (1996). "Laboratory Study on the Use of Tire Shreds and Rubber Sand in Backfills and Reinforced Soil Applications." PhD Thesis, Purdue University.

- Bernal, A., Lovell, C.W., and Salgado, R. (1996). "Laboratory Study on the use of Tire Shreds and Rubber-Sand in Backfills and Reinforced Soil Applications." FHWA/IN/JHRP-96/12, Purdue University, West Lafayette, Indiana.

- Bresler, B., and Gilbert, P. H. (1961). "Tie Requirements for Reinforced Concrete Columns." Journal of ACI, Vol. 58, No. 5 pp. 555-570.

- Bugaldian, Adel. (1999). "Concrete Columns Confined with Scrap Tires." M.A.Sc. Thesis, Department of Civil Engineering, University of Ottawa, Ottawa, Canada, 174 pp.

- Bugaldian, Adel. (2005). "Concrete Columns Confined with Scrap Tires." Proceedings of the Second Student Conference on Earthquake Engineering and Engineering Seismology, Ottawa-Carleton Earthquake Engineering Research Centre (OCEERC), Ontario, Canada, 11 pp.

- Bugaldian, A., and Saatcioglu, M. (2008). "The Use of Steel –Belted Automobile Tires as Column Confinement Reinforcement." Proceedings of the 14th World Conference on Earthquake Engineering (14WCEE), Beijing, China, Oct. 12-17, 2008

- Bugaldian, A., and Saatcioglu, M. (2008). "Scrap Tires as Column Transverse Reinforcement." Proceedings of the 2nd Canadian Conference on Effective Design of Structures (CCEDS-2), Hamilton, Ontario, May 20-23, 2008.

- Burdette, Edwin G., and Hilsdorf, Hubert K. (1971). "Behaviour of Laterally Reinforced Concrete Columns." Proceeding, ASCE, Vol. 97, ST2, pp. 587-602.

- Canadian Standards Association (CSA) Committee A23.3 (2004). "Design of Concrete Structures (A23.3-04)." Mississauga, Ontario, 240 pp.

- Canadian Standards Association (CSA) Committee S806 (2002). "Design and Construction of Building Components with Fiber-Reinforced Polymers (S806-02)." Rexdale, Ontario, 177 pp.

- Chan, W. L. (1955). "The Ultimate Strength and Deformations of Plastic Hinges in Reinforced Concrete Frameworks." Magazine of Concrete Research, 7(21), pp. 121–132.

- Chen, W. F. (1982). "Plasticity in reinforced concrete, McGraw-Hill, New York.

- Choubane, B., Sholar, G. A., Musselman, J. A., and Page, G. C. (1999). "A Ten-year Performance Evaluation of Asphalt-Rubber Surface Mixes." Transportation Research Record No. 1681, Washington, DC.

- Chu, C. J. and Shakoor, A. (1997). "Use of Shredded Scrap Tires in Soil Stabilization: Proceedings, IAEG Conference on Engineering Geology and the Environment, Athens, Greece, pp. 1687-1693.

- Cosgrove, T. A. (1995). "Interface Strength Between Tire Chips and Geomembrane for Use as a Drainage Layer in a Landfill Cover." Proceedings of Geosynthetics'95, Industrial Fabrics Association, St. Paul, MN, Vol. 3, pp. 1157-1168.

- Dalton, D. C. and Hoban, K. M. (1982). "Tire Walls in Highway Construction." In: The Highway Engineer. Feb.1982. pp. 2-9.

- Dantas Neto, S. A., Farias, M. M., Pais, J. C., Pereira, P. A., and Picado Santos, L. (2003). "Behaviour of Asphalt Rubber Hot Mixes Obtained with High Crumb Rubber Contents." Proceedings of the Asphalt Rubber 2003 Conference, Brasilia, Brazil.

- Drescher, A. and Newcomb, D. E. (1994). "Development of Design Guidelines for Use of Shredded Tires as a Lightweight Fill in Road Subgrade and Retaining Walls." Report No. MN/RC-94/04, Department of Civil and Mineral Engineering, University of Minnesota, Minneapolis, MN, 118 pages plus appendices.

- Edil, T. B. (2002). "Mechanical Properties and Mass Behaviour of Shredded Tire Soil Mixtures." In Proceeding of the International Workshop on Lightweight Geomaterial, Tokyo, Japan, pp. 17-32.

- Edil, T. B. and Bosscher, P. J. (1992). "Development of Engineering Criteria for Shredded Waste Tires in Highway Applications." Research Study No. 89-3, Wisconsin Department of Transportation, Division of Highways, Bureau of Highway Engineering, C.O. Materials Applied Research, Madison, WI, 86 pp.

- Eldin, N. N., and Senouci, A. B. (1992). "Use of Scrap Tires in Road Construction." Journal of Construction Engineering and Management, Vol. 118, No. 3, pp. 561-576.

- Eldin, N. N., and Senouci, A. B., (1993). "Rubber-Tire Particles as Concrete Aggregate." Journal of Materials in Civil Engineering, ASCE, Vol. 5 No. 4, pp. 478-496.

- Elnabelsy, G., and Saatcioglu, M. (2004). "Seismic Retrofit of Circular and Square Bridge Columns with CFRP Jackets." Proceedings of the Fourth International Conference on Advanced Composite Materials in Bridges and Structures (ACMBS-4), Calgary, Alberta, Canada.

- Esch, D. C. (1982). "Construction and Benefits of Rubber Modified Asphalt Pavements." Transportation Research Record No. 860, TRB, National Research Council, Washington, DC.

- Fafitis, A., and Shah, S. P. (1985). "Predictions of Ultimate Behaviour of Confined Columns Subjected to Large Deformation." ACI Structural Journal, Vol. 82, No. 4, pp. 423-433.

- Fam, A., Flisak, B. and Rizkalla, S. (2003). "Experimental and Analytical Modeling of Concrete-Filled FRP Tubes Subjected to Combined Bending and Axial Loads." ACI Structural Engineering Journal, Vol. 100, No. 4, pp. 499-509.

- Fam, A. and Rizkalla, S. (2002). "Flexural Behaviour of Concrete-Filled Fiber Reinforced Polymer Circular Tubes." Journal of Composites for Construction, Vol. 6, No. 2, pp. 123-132.

- Fam, A., Schnerch, D. and Rizkalla, S. (2005). "Rectangular Filament-Wound GFRP Tubes Filled with Concrete under Flexural and Axial Loading: Experimental Investigation." Journal of Composites for Construction, Vol. 9, No. 1, pp. 25-33.

- Forsyth, R. A., and Egan, J. P. (1976) "Use of Waste Materials in Embankment Construction." Transportation Research Record, No. 593, pp. 3-8.

- Garga, V. K., and O'Shaughnessy, V. (2000a). "Tire-Reinforced Earthfill Part 1: Construction of a Test Fill, Performance and Retaining Wall Design." Canadian Geotechnical Journal 37, pp. 75-96.

- Geisler, E., Cody, W. K., and Niemi, M. (1989). "Tires for Subgrade Support." ASCE Paper No. 897550, Presentation. American Society of Agriculture Engineers, ASAE, St. Joseph, MI.

- Ghani, A. N. A., Ahmad, F., and Hamir, R. (2002). "Strength, Elasticity and Deformation Characteristics of Composite Geomaterial Containing Tire Shreds." In Proceeding of the 3rd Iranian International Conference on Geotechnical Engineering and Soil Mechanics. pp. 251-255. Tehran: Center for Scientific Documentation and Publications.

- Grira, M. and Saatcioglu, M. (1996). "Concrete Columns Confined with Welded Reinforcement Grids." Dept. of Civil Engineering, University of Ottawa, Ottawa, Canada, Report OCEERC p.89.

- Heimdahl, T. C. (1998). "Deformability of Shredded Tires." MSCE Thesis, University of Minnesota, St. Paul, Minn.

- Hognestad, E. (1951). "A study of Combined Bending and Axial Load in Reinforced Concrete Members." University of Illinois. Engineering Experiment Station, Bulletin Series No. 399, 128 pp.

- Holleran, G., and Van, K. J. (2000). "Asphalt Rubber Concrete Leads to Cost Effective Pavement Rehabilitation Reduced Thickness." Synopses for 1st International Conference World of Pavement, Sydney, Australia.

- Huang, B., Li, G., Pang, S. S., and Eggers, J. (2004). "Investigation into Waste Tire Rubber-Filled Concrete." Journal of Materials in Civil Engineering, Vol. 16, No. 3, pp. 187-194.

- Hudson, Fred M. (1966). "Reinforced Concrete Columns: Effects of Lateral Tie Spacing on Ultimate Strength." Symposium on Reinforced Concrete Columns, SP-13, American Concrete Institute, Detroit, pp. 235-244.

- Humphrey, D. N. (1999). "Civil Engineering Application of Tire Shreds." The Tire Industry Conference, Hilton Head, South Carolina.

- Humphrey, D. N., and Eaton, R. A. (1995). "Field Performance of Tire Chips as Subgrade Insulation for Rural Roads." Proceedings of the Sixth International Conference on Low-Volume Roads, Transportation Research Board, Washington, D.C., Vol. 2, pp. 77-86.

- Humphrey, D. N., and Sandford, T. C. (1993). "Tire Chips as Lightweight Subgrade Fill and Retaining Wall Backfill." Proceedings of the Symposium on Recovery and Effective Reuse of Discarded Materials and By-Products for Construction of Highway Facilities, Federal Highway Administration, Denver, Colorado, pp. 5-87 to 5-99.

- Humphrey, D. N., and Tweedie, J. J. (2002). "Tire Shreds as Lightweight Fill for Retaining Walls-Results of Full Scale Field Trials." Proceeding of the International Workshop on Lightweight Geomaterial, Tokyo, Japan, pp. 261- 268.

- Iacobucci, R. D., Sheikh, S. A., and Bayrak, O. (2002). "Retrofit of Square Concrete Columns with Carbon Fiber-Reinforced Polymer for Seismic Resistance." ACI Structural Journal, Vol. 100, No. 6, pp. 785-794.

- Itakura, Y., and Yagenji, A. (1992). "Compressive Test on High-Strength R/C Columns and their Analysis Based on Energy Concept." Pro. Of 10th World Conference on Earthquake Engineering, Madrid, pp. 2599-2602.

- Kent, D. C., and Park, R. (1971). "Flexural Members with Confined Concrete." Journal of Structural Division, ASCE, Vol. 97, pp. 1969-1990.

- Khalid, H. A., and Artamendi, I. (2004). "Mechanical Properties of Conventional and Modified Asphalt using Rubber from used Tires." Engineering Sustainability Jl., Proceedings of the Institution of Civil Engineers, Vol. 157, No.1 pp. 37-43.

- Kupfer, H., Hilesdorf, H. K., and Rusch H. (1969). "Behaviour of Concrete under Biaxial Stress." ACI Structure Journals, Vol. 66, No. 2, pp. 656-666.

- Légeron, F., and Paultre, P. (2000). "Behaviour of High-Strength Concrete Columns under Cyclic Flexure and Constant Axial Load." ACI Structural Journal, Vol. 97, No. 4, pp. 591-601.

- Légeron, F., and Paultre, P. (2003). "Uniaxial Confinement Model for Normal and High-Strength Concrete Columns." ASCE Structural Journal, Vol. 129, No. 2 pp. 241-252.

- Lee, K. M., Cheng, B. K. W., and Yip, C. L. Y. (2002). "Lightly Cemented Scrap Rubber Tire Chips as Lightweight Geo-Materials." Proceeding of the International Workshop on Lightweight Geomaterial, Mar 26-27, Tokyo, Japan.

- Lee, J., Salgado, R., Bernal, A., and Lovell, C. W. (1999). "Tire Shreds and Rubber Sand as Lightweight Backfill Material." Journal of Geotechnical and Geoenvironmental Engineering, ASCE, Vol. 125, No. 2 pp. 132-141.

- Lehman, D., Moehle, J., and Mahin, S., Calderone, A., and Henry, L. (2004). "Experimental Evaluation of the Seismic Performance of Reinforced Concrete Bridge Columns." Journal of Structural Engineering, Vol. 130, No. 6, pp. 869-879.

- Liu, L., Foster, S. J., and Attard, M. M. (2000). "Strength of Tied High-Strength Concrete Columns Loaded in Concentric Compression." ACI Structural Journal 97(1), pp. 149-156.

- Long, N. T. (1993). "Le pneusol: recherche–réalisations–perspectives." Thèse de Doctorat, Institut National des Science Appliquées de Lyon, Lyon, France.

- Malek, AB., K., and Stevenson, A. (1986). "The Effects of 42 Years Immersion in Sea Water on Natural Rubber." Journal of Material Sciences, No. 21, pp. 147-154.

- Malvar, L. J., and Simons, D. (1996). "Concrete Material Modeling in Explicit Computations." Proceedings, Workshop on Recent Advances in Computational Structural Dynamics and High Performance Computing, USAE Waterways Experiment Station, Vicksburg, MS, pp. 165-194.

- Malvar, L. J., Crawford, J. E., Wesevich, J. W., and Simons, D. (1997). "A Plasticity Concrete Material Model for DYNA3D." International Journal of Impact Engineering, Vol. 19, No. 9/10, pp. 847-873.

- Mander, J. B., Priestley, M. J. N., and Park, R. (1988). "Theoretical Stress-Strain Model for Confined Concrete." Journal of Structural Engineering, ASCE, Vol. 114, No. 8, pp. 1804-1826.

- Manion, W. P., and Humphery, D. N., (1992). "Use of Tire Chips as Lightweight and Conventional Embankment Fill, Phase I-Laboratory." Technical Paper 91-1, Technical Services Division, Maine Department of Transportation, Maine.

- Masad, E., Taha, R., Ho, C. and Papagiannakis, T. (1996). "Engineering Properties of Tire/Soil Mixtures as a Lightweight Fill Material." Geotechnical Testing Journal, ASTM, Vol. 19, No. 3, pp. 297-304.

- Mes, D. (1999). "Seismic Retrofitting of Concrete Bridge Columns by External Prestressing." M.A.Sc. Thesis, Department of Civil Engineering, University of Ottawa, Ottawa, Ontario, Canada, pp. 125.

- Mirmiran, A., Shahawy, M., El Khoury, C., and Naguib, W. (2000). "Large Beam-Column Tests on Concrete-Filled Composite Tubes." ACI Structural Journal, ACI, Vol. 97, No. 2, pp. 268-276.

- Mirmiran, A., Shahawy, M., Samaan, M., El Echary, H., Mastrapa, J. C., and Pico, O. (1998b). "Effect of Column Parameters on FRP-Confined Concrete." Journal of Composites for Construction, ASCE, Vol. 2, No. 4, pp. 175-185.

- Mirmiran, A., Shahawy, M., and Samaan, M. (1999). "Strength and Ductility of Hybrid FRP-Concrete Beam-Columns." Journal of Structural Engineering, ASCE, Vol. 125, No. 10, pp. 1085-1093.

- Mitchell, D., De Vall, R. H., Saatcioglu, M., Simpson, R., Tinawi, R., and Tremblay, R. (1995). "Damage to Concrete Structures due to the 1994 Northridge Earthquake." Canadian Journal of Civil Engineering, Vol. 22, No.2, pp. 361-377.

- Moo-Young, H., Sellasie, K., Zeroka, D., and Sabnis, G. (2003). "Physical and Chemical Properties of Recycled Tire Shreds for use in Construction." Journal of Environmental Engineering., Vol. 129, Issue 10, pp. 921–929.

- Mugumura, H., Watsnsbe, F., Iwashimizu, T., and Mitsueda, R. (1983). "Ductility Improvement of High Strength Concrete by Lateral Confinement." Transactions of the Japan Concrete Institute, Vol. 5, pp. 403-410.

- O'Shaughnessy, V., (1997). "Reinforcement of Earth Structures using Scrap Tires." Ph.D. Thesis, Dept. of Civil Engineering, University of Ottawa, Ottawa, Canada, 372 pp.

- O'Shaughnessy, V., and Garga, V. K. (2000). "Tire Reinforced Earthfill, Part 3: Environmental Assessment." Canadian Geotechnical Journal, 37(1), 97, pp. 117-131.

- Ozbakkaloglu, T., and Saatcioglu, M. (2006). "Seismic Behaviour of High-Strength Concrete Columns Confined by Fiber-Reinforced Polymer Tubes." Journal of Composite for Construction, Vol. 10, No. 6, pp. 538-549

- Ozbakkaloglu, T., and Saatcioglu, M. (2007). "Seismic Performance of Square High-Strength Concrete Columns in FRP Stay-in-Place Formwork." Journal of Structural Engineering, Vol. 133, No. 1, pp. 44-56.

- Ozcebe, G., Saatcioglu, M. (1987). "Confinement of Concrete Columns for Seismic Loading." ACI Structural Journal, Vol. 84, No.4, pp. 308 – 315.

- Ozcebe, G., Saatcioglu, M. (1989). "Hysteretic Shear Model for Reinforced Concrete Members." ASCE Journal of Structural Engineering, Vol. 115, No.1, pp. 132 - 148.

- Palit, S. K., Sudhakar Reddy K., and Pandey, B. B. (2004). "Laboratory Evaluation of Crumb Rubber Modified Asphalt Mixes." Journal of Materials in Civil Engineering, Vol. 16, No. 1, pp. 45-53.

- Park, R., and Paulay, T. (1975). "Reinforced Concrete Structures." John Wiley and Sons, New York, 769 pp.

- Patrick M. Strenk, Joseph Wartman, Dennis G. Grubb, Dana N. Humphrey, and Mark F. Natale (2007). "Variability and Scale-Dependency of Tire-Derived Aggregate." Journal of Materials in Civil Engineering, Vol. 19, No. 3, pp. 233-241.

- Paultre, P., and Légeron, F. (2008). "Confinement Reinforcement Design for Reinforced Concrete Columns." Journal of Structural Engineering, ASCE, Vol. 134, No. 5, pp. 738-749.

- Pessiki, S., Harries, K. A., Kestner, J. T., Sause R., and Ricles, J. M. (2001). "Axial Behaviour of Reinforced Concrete Columns Confined with FRP Jackets." Journal of Composites for Construction, ASCE, Vol. 5, No. 4, pp. 237-245.

- Pfister, James F. (1964). "Influence of Ties on the Behaviour of Reinforced Concrete Columns." ACI Journal, Proceedings Vol. 61, No. 5, pp. 521-536.

- Rangan, B. V., Saunders, P., and Seng, E. I. (1991). "Design of High-Strength Concrete Columns." Evaluation and Rehabilitation of Concrete Structures and Innovations in Design, ACI SP 128-52, pp. 851-862.

- Razvi, S. (1995). "Confinement of Normal and High-Strength Concrete Columns." Ph.D. Thesis, Department of Civil Engineering, University of Ottawa, Ottawa, Canada, 416 pp.

- Razvi, S., and Saatcioglu, M. (1989). "Confinement of Reinforced Concrete Columns with Welded Wire Fabric." ACI Structural Journal, Vol. 86, No. 5, pp. 615-623.

- Razvi, S. R., and Saatcioglu, M. (1996). "Tests of High-Strength Concrete Columns under Concentric Loading." Research Repot OCEERC 96-03, Ottawa Carleton Earthquake Engineering Research Center, Department of Civil Engineering, University of Ottawa, Ottawa, Canada, 147 pp.

- Richart, F. E., Brandtzaeg, A., and Brown, R. L. (1928). "A Study of the Failure of Concrete under Combined Compressive Stresses." Bulletin No. 185, Engineering Experimental Station, University of Illinois, Urbana, Ill., 104.

- Richart, F. E., Brandtzaeg, A., and Brown, R. L. (1929). "The Failure of Plain and Spirally Reinforced Concrete in Compression." Bulletin No. 190, Engineering Experimental Station, University of Illinois, Urbana, Ill., 74.

- Rochette, P., and Labossiere, P. (2000). "Axial Testing of Rectangular Column Models Confined with Composites." Journal of Composites for Construction, ASCE, Vol. 4, No. 3, pp. 129-136.

- Roy, H. E. H., and Sozen, M. A. (1964). "Ductility of Concrete." Proceedings of the International Symposium on Flexural Mechanics of Reinforced Concrete. ASCE-ACI., pp. 213-224.

- Rubber Manufacturers Association. (1997). "Design Guidelines to Minimize Internal Heating of Tire Shred Fills." Rubber Manufacturers Association Washington, D.C.

- Saadatmanesh, H., Ehsani, M. R., and Lin, J. (1996). "Seismic Strengthening of Circular Bridge Pier Models with Fiber Composites." ACI Structural Journal Vol. 96, No. 6, pp. 639-647.

- Saadatmanesh, H., Ehsani, M. R., and Lin, J. (1997). "Seismic Retrofitting of Rectangular Bridge Columns with Composite Straps." Earthquake Spectra Vol. 13, No. 2, pp. 281-304.

- Saatcioglu, M., and Baingo, D. (1999). "Circular High-Strength Concrete Columns under Simulated Seismic Loading." Journal of Structural Engineering, ASCE, Vol. 125, No. 3, pp. 272-280.

- Saatcioglu, M., and Bruneau, M. (1994). "Performance of Reinforced Concrete Structures during the 1992 Erzincan Earthquake." ACI Concrete International Journal, Vol. 16, No. 9, pp. 51-56.

- Saatcioglu, M., and Grira, M. (1999). "Confinement of Reinforced Concrete Columns with Welded Reinforcement Grids." ACI Structural Journal, Vol. 96, No. 1, pp. 29-39.

- Saatcioglu, M., Mitchell, D., Tinawi, R., Gardner, N. J., Gillies, A. G., Ghobarah, A., Anderson, D. L., and Lau, D. (2001). "The August 17, 1999 Kocaeli (Turkey) Earthquake - Damage to Structures." Canadian Journal of Civil Engineering, Vol. 28, No. 8, August 2001. Winner of the CSCE 2001 Casimir Gzowski Metal.

- Saatcioglu, M., and Razvi, S. R. (1992). "Strength and Ductility of Confined Concrete." Journal of Structural Engineering, ASCE, Vol. 118, No. 6, pp. 1590-1607.

- Saatcioglu, M., Razvi, S. R. (2002). "Displacement-Based Design of Reinforced Concrete Columns for Confinement." ACI Structural Journal, Vol. 99, No.1, pp. 3-11.

- Saatcioglu, M., Ozbakkaloglu, T. and Elnabelsy, G. (2008). "Seismic Behaviour and Design of Reinforced Concrete Columns Confined with FRP Stay-in-place

Formwork." ACI-SP, American Concrete Institute, Farmington Hills, Michigan, U.S.A., pp. 149-170.

- Saatcioglu, M., and Yalcin, C. (2003) "External Prestressing Concrete Columns for Improved Seismic Shear Resistance." ASCE Journal of Structural Engineering, Vol. 129, No.8, pp. 1057-1070.

- Sato, T., and Ibushi, K. (1988). "Effect of Confinement on Ductile Behaviour of Reinforced Concrete Short Columns." Transactions of the Japan Concrete Institute, Vol., 10, No. 5, pp. 337-344.

- Scott, B. D., Park, R., and Priestley, M. J. N. (1982). "Stress-Strain Behaviour of Concrete Confined by Overlapping Hoops at High and Low Strain Rates." ACI Journal, Vol. 79, No. 1, pp. 13-27.

- Seible, F., Burgueño, R., Abdallah, M. G., and Nuismer, R. (1996). "Development of Advanced Composite Carbon Shell Systems for Concrete Columns in Seismic Zones." Pro. Of 11th World Conference on Earthquake Engineering, Pergamon, Elsevier Science, Oxford, Paper No. 1375.

- Seible, F., Priestley, M. J .N., and Hegemier, G. A. and Innamorato, D. (1997). "Seismic Retrofit of RC Columns with Continuous Carbon Fiber Jackets." Journal of Composites for Construction, ASCE, Vol.1, No.2, pp. 52-62.

- Shao, Y., and Mirmiran, A. (2005). "Experimental Investigation of Cyclic Behaviour of Concrete-Filled Fiber Reinforced Polymer Tubes." Journal of Composites for Construction, ASCE, Vol.9, No.3, pp. 263-273.

- Sheikh, S. A., and Khoury S. S. (1993). "Confined Concrete Columns with Stubs." ACI Structural Journal, V. 90, No. 4, pp. 414-431.

- Sheikh, S. A., Shah, D. V., and Khoury, S. S. (1994). "Confinement of High-Strength Concrete Columns." ACI Structural Journal, Vol. 91, No. 1, pp. 100-111.

- Sheikh, S. A., and Uzumeri, S. M. (1980). "Strength and Ductility of Tied Concrete Columns." Journal of Structural Engineering, ASCE, Vol. 106, No. 5, pp. 1079-1102.

- Sheikh, S. A., and Yau, G. (2002). "Seismic Behaviour of Concrete Columns Confined with Steel and Fiber-Reinforced Polymers." ACI Structural Journal, Vol. 99, No. 1, pp. 72-80.

- Somes. Norman F. (1970). "Compression Tests on Hoop-Reinforced Concrete." Proceedings, ASCE, Vol. 96, ST7, pp. 1495-1509.

- Sousa, J. B., Pais J. C., Saim R., Way G. B., and Stubstad R. N. (2002). "Mechanistic-Empirical Overlay Design Method for Reflective Cracking." Transportation Research Record 1809, Transportation Research Board, National Research Council, Washington, D.C.

- Strenk, P. M., Wartman, J., Grubb, D. G., Humphrey, D. N., and Natale, M. F. (2007). "Variability and Scale Dependency of Tire Derived Aggregate." Journal of Materials in Civil Engineering, ASCE, Vol. 19, No. 3, pp. 233-241.

- Tan., T., and Nguyen,. N. (2005). "Flexural Behaviour of Confined High-Strength Concrete Columns." ACI Structural Journal, Vol. 102, No. 2, pp. 198-205.

- Tweedie, J. J., Humphrey, D. N., and Sandford, T. C. (1998). "Tire Shreds as Lightweight Retaining Wall Backfill: Active Conditions." ASCE J. Geotech. and Geoenv. Eng., Vol. 124, No.11, pp. 1061-1070.

- Vinod, K. Garga and Vince, O'Shaughnessy (2000). "Tire-Reinforced Earthfill. Part 1: Construction of a Test Fill, Performance, and Retaining Wall Design." Canadian Geotechnical Journal, Vol. 37, pp 75-96.

- Way, G. B. (2003). "The Rubber Pavements Association, Technical Advisory Board Leading the Way in Asphalt Rubber Research." Proceedings of the Asphalt Rubber 2003 Conference, Brasilia, Brazil.

- Williams, J. (1987). "Guidelines for Using Recycled Tire Carcasses in Highway Maintenance." Report No. FHWA/CA/TL-87/07, California Department of Transportation, Sacramento.

- WYMCC. (1977). "Reuse of Worn Tires in Civil Engineering Construction." Internal Report. West Yorkshire Metropolitan County Council.

- Xiao, Y., and Ma, R. (1997). "Seismic Retrofit of RC Circular Columns Using Prefabricated Composite Jacketing." Journal of Structural Engineering, ASCE, Vol. 123, No. 10, pp. 1357-1364.

- Xi, Y., Li, Y., Xie, Z. H., and Li, Z. J. (2003a). "High Toughness of Rubber-Modified Concrete (RMC)." Final Report CU/SR-XI 2003/002. Colorado Commission of Higher Education, 63 pp.

- Xiao, Y., and Yun, H. W. (2002). "Experimental Studies on Full-Scale High-Strength Concrete Columns." ACI Structural Journal 99(2), pp. 199-207.

- Yalcin, C. (1997). "Seismic Evaluation and Retrofit of Existing Reinforced Concrete Bridge Columns." PhD Dissertation, Dept. of Civil Engineering, University of Ottawa, Ottawa, Canada. 316 pp.

- Yang, S., Lohnes, R. A., and Kjartanson, B. H. (2002). "Mechanical Properties of Shredded Tires." Geotech. Test. J., Vol. 25, No. 1, pp. 44–52.

- Youwai, S., and Bergado, D. T. (2003). "Strength and Deformation Characteristics of Shredded Rubber Tire-sand Mixtures." Canadian Geotechnical Journal, Vol. 40, No. 1, pp. 254–264.

- Zhu, Z. (2004). "Joint Construction and Seismic Performance of Concrete-Filled Fiber Reinforced Polymer Tubes." PhD Thesis, North Carolina State Univ., Raleigh, N.C.

- Zornberg, J. G., Cabral, A. R., and Chardphoom, V. (2004). "Behaviour of Tire Shred-Sand Mixtures." Canadian Geotechnical Journal, Vol. 41, No. 1, pp. 227–241.

Appendix A

Experimentally Recorded Strain Data

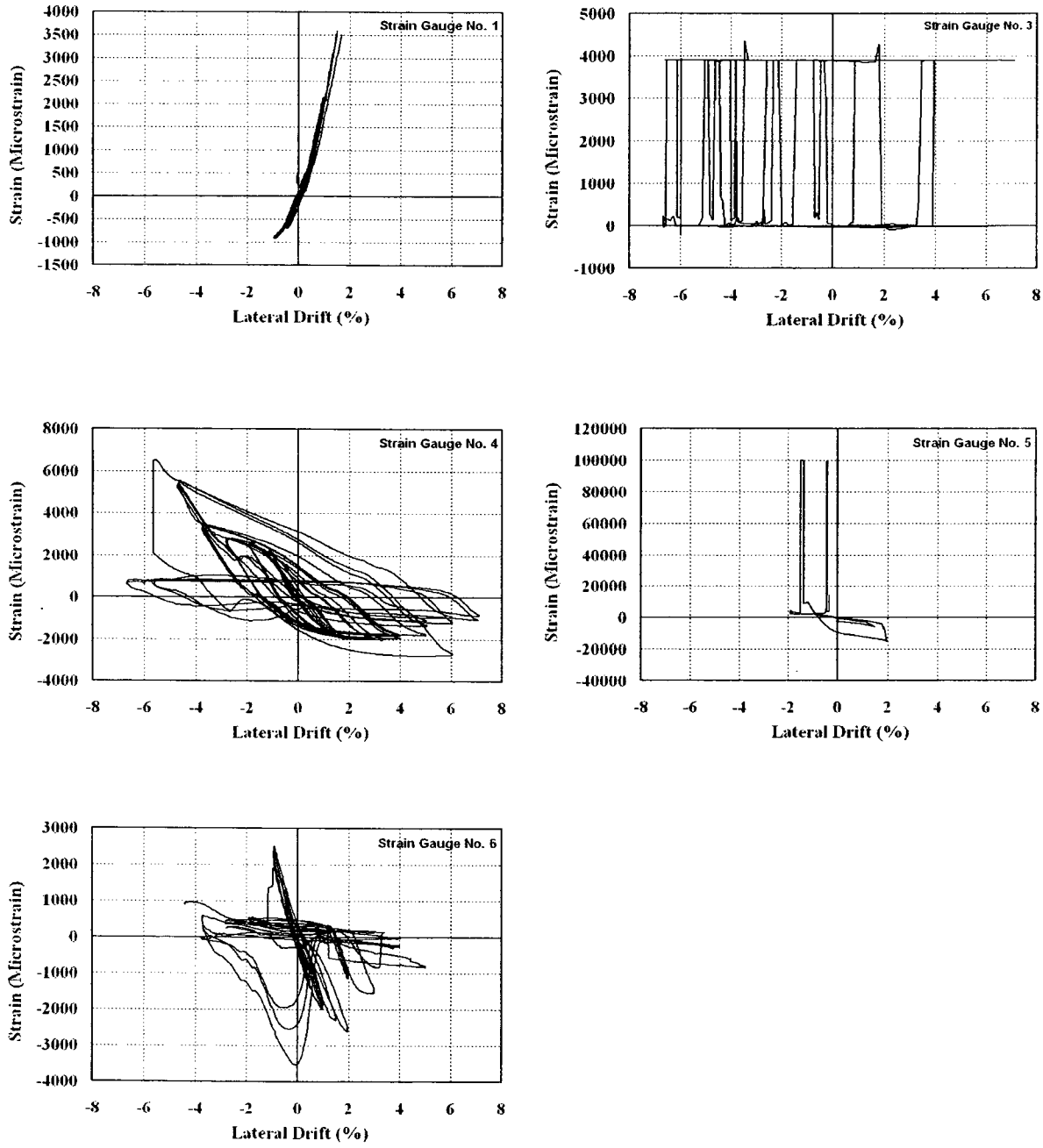

Figure A.1: Strain Gauge Data for Longitudinal Reinforcement in Column TC-7

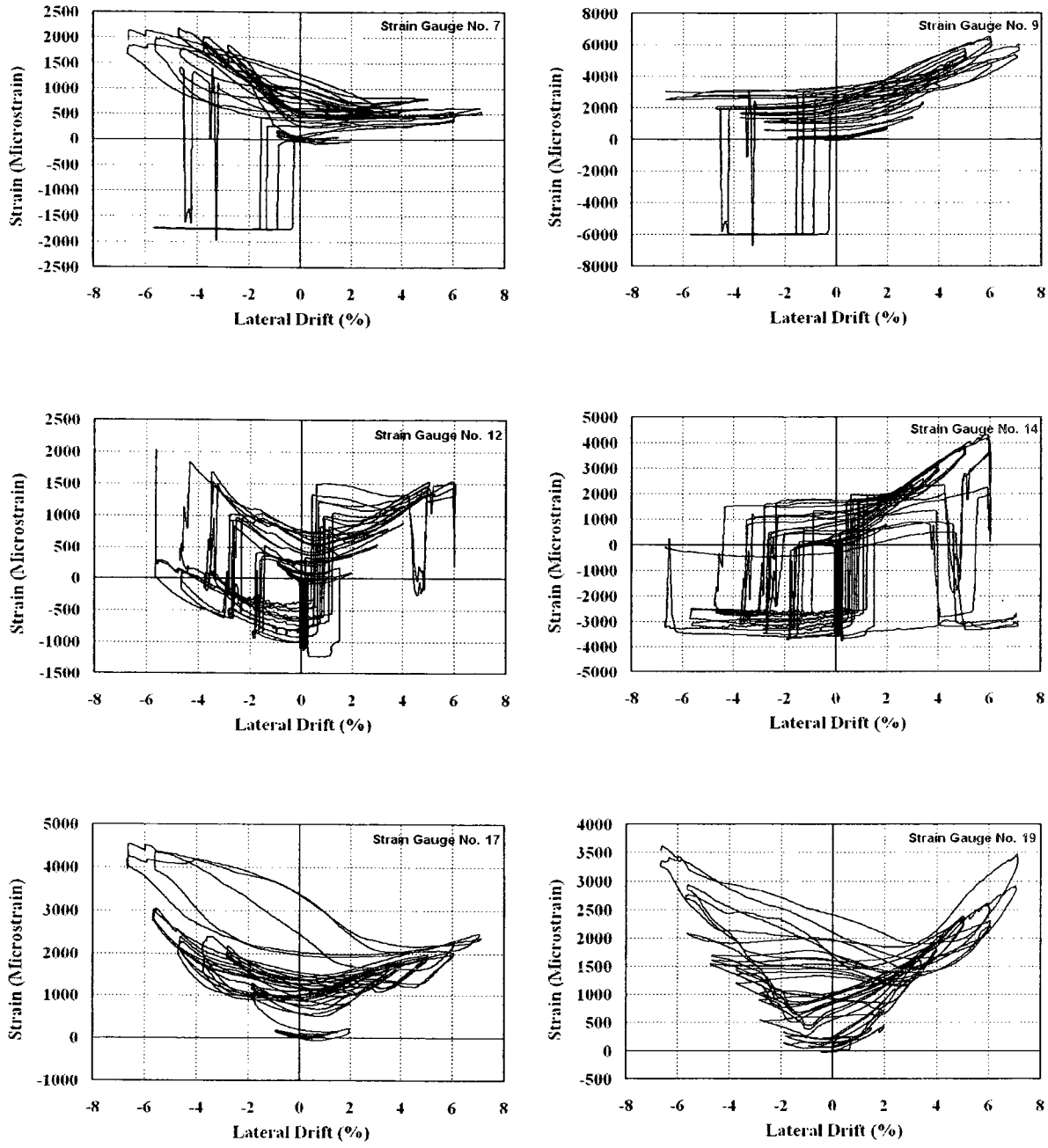

Figure A.2: Tire Strains in Column TC-7, Measured on Treads

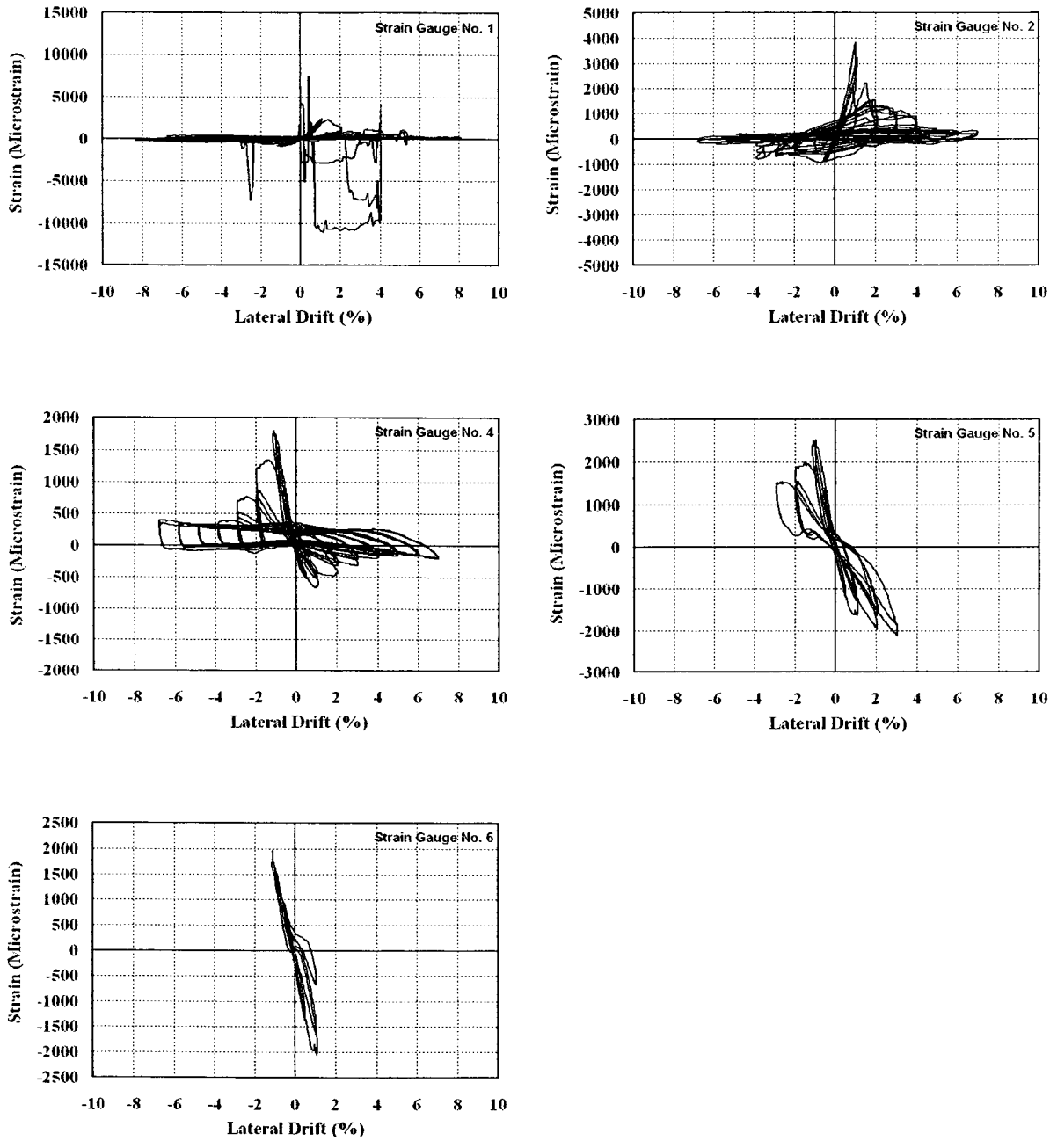

a) Starter Bars Strain Gauge Data in Column TC-8

Figure A.3: Strain Gauge Data for Longitudinal Reinforcement in Column TC-8

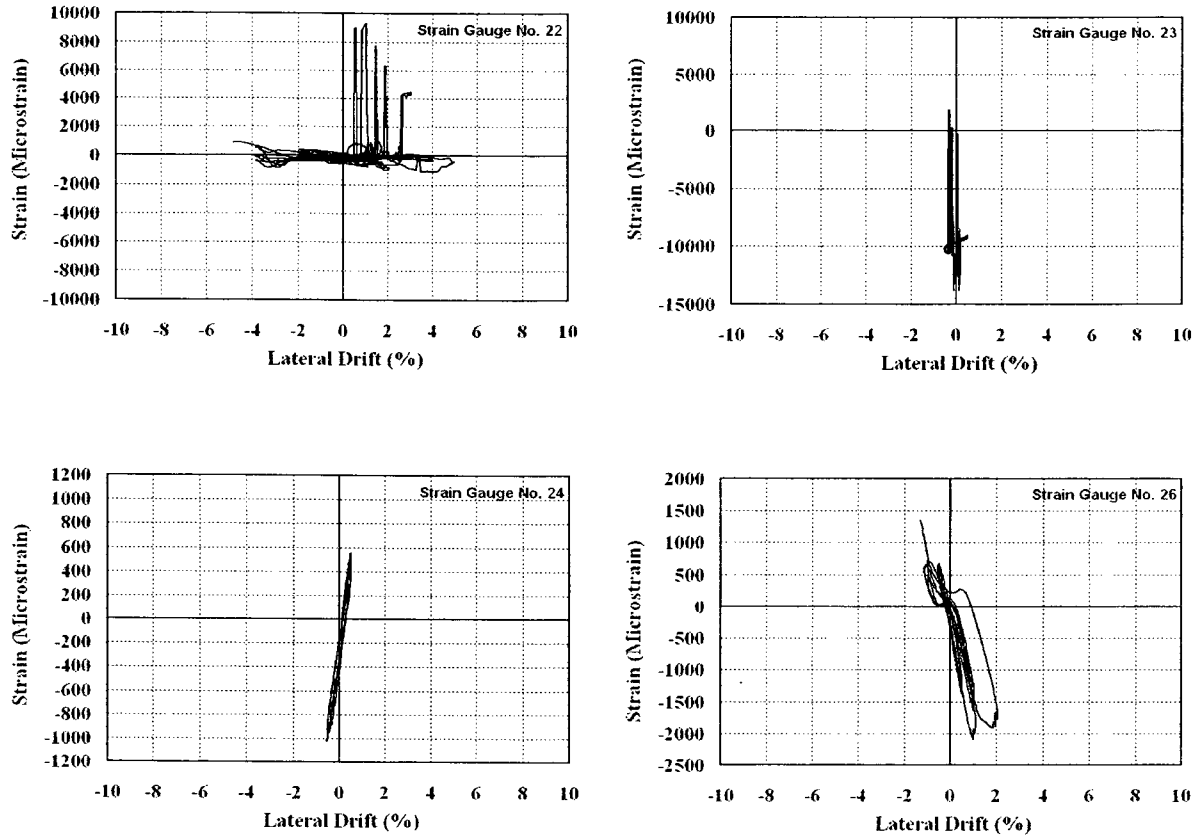

b) Longitudinal Reinforcement Strain Gauge Data in Column TC-8

Figure A.3 (Cont'd): Strain Gauge Data for Longitudinal Reinforcement in Column TC-8

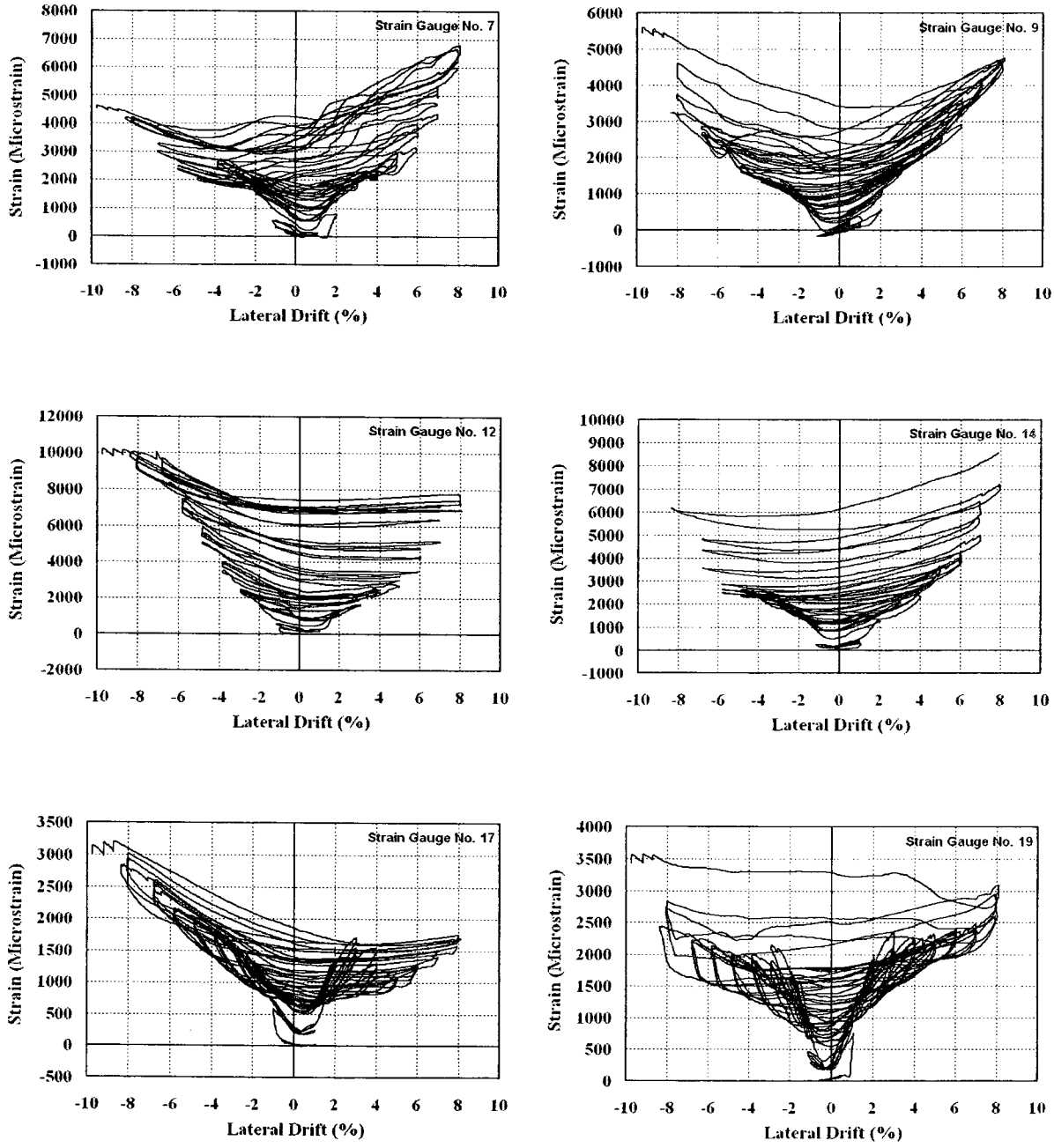

Figure A.4: Tire Strains in Column TC-8, Measured on Treads

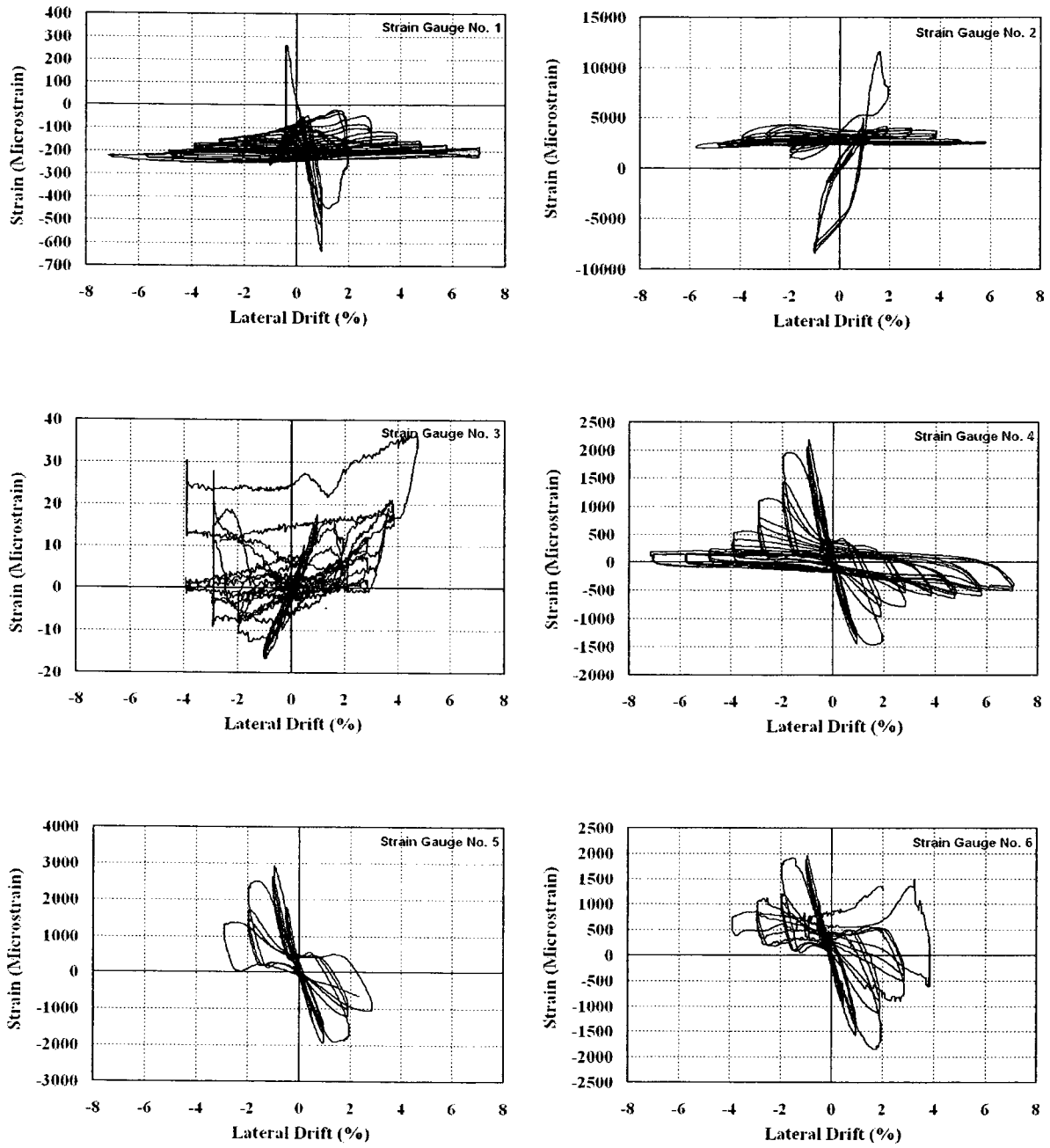

a) Starter Bars Strain Gauge Data in Column TC-9

Figure A.5: Strain Gauge Data for Longitudinal Reinforcement in Column TC-9

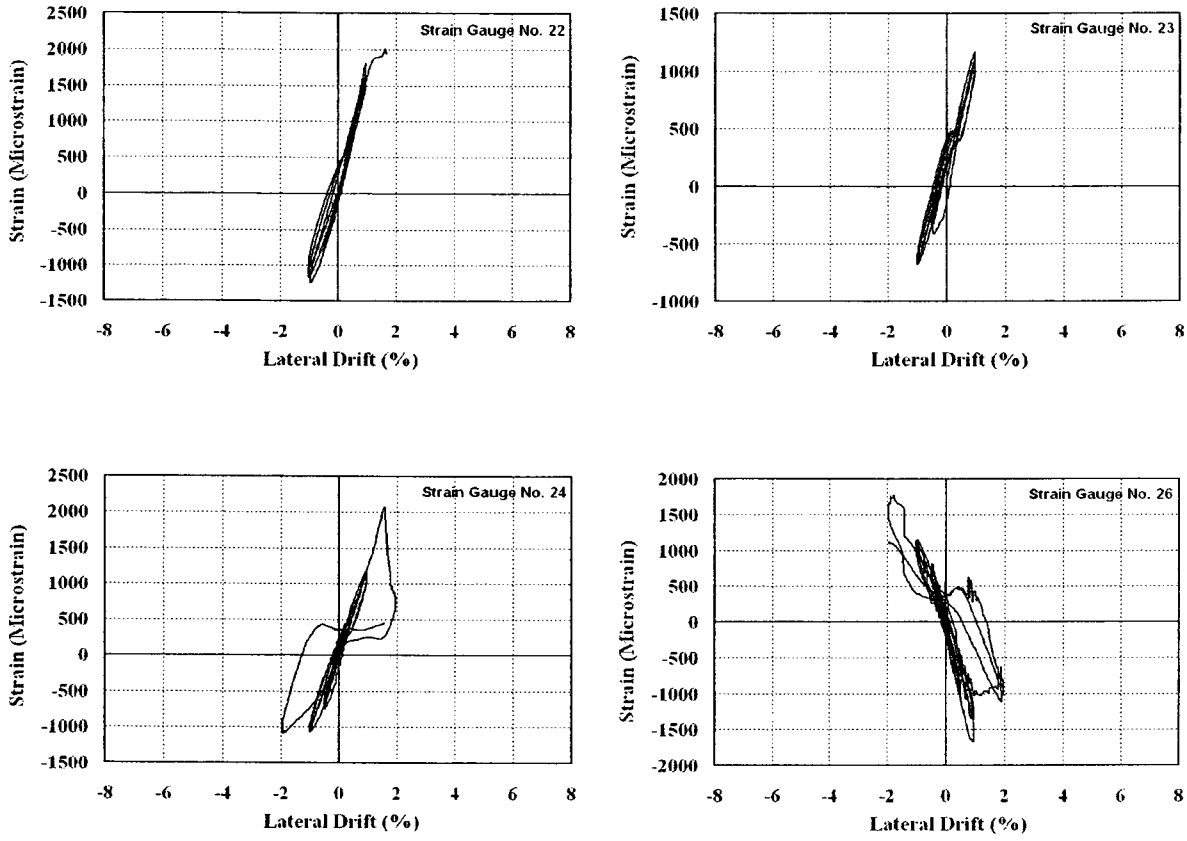

b) Longitudinal Reinforcement Strain Gauge Data in Column TC-9

Figure A.5 (Cont'd): Strain Gauge Data for Longitudinal Reinforcement in Column TC-9

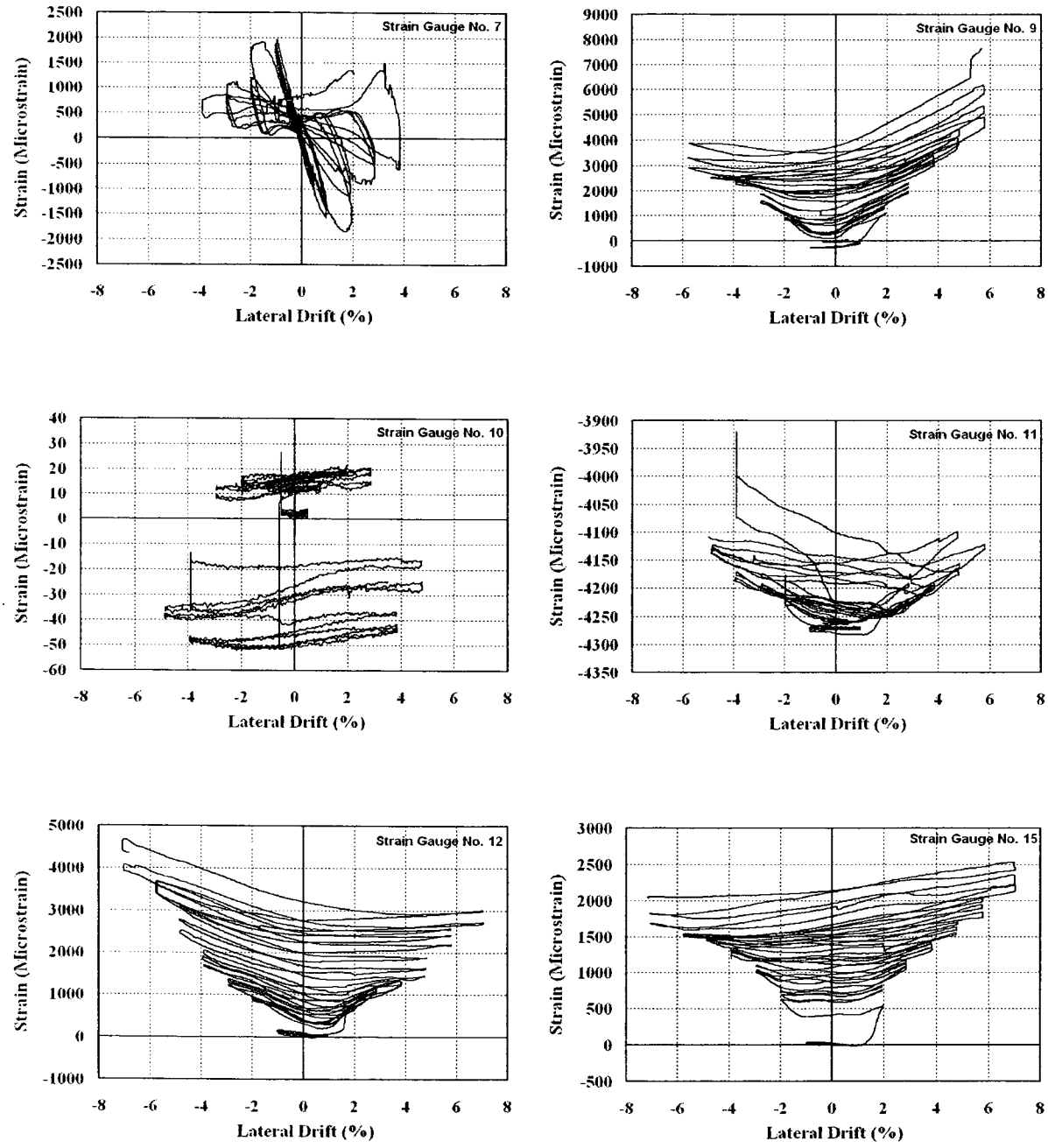

Figure A.6: Tire Strains in Column TC-9, Measured on Treads

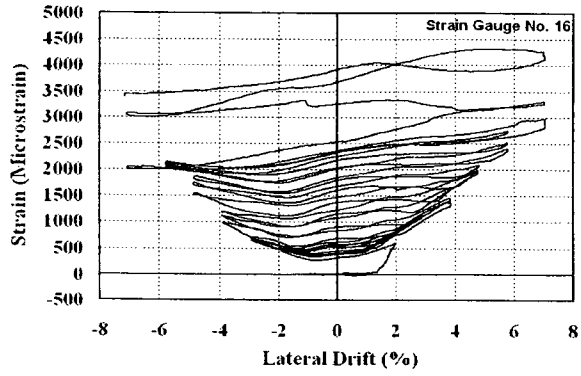

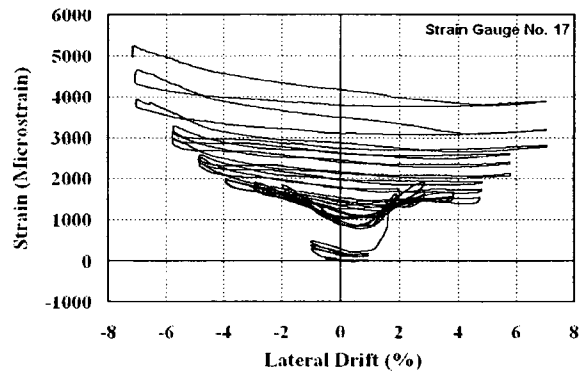

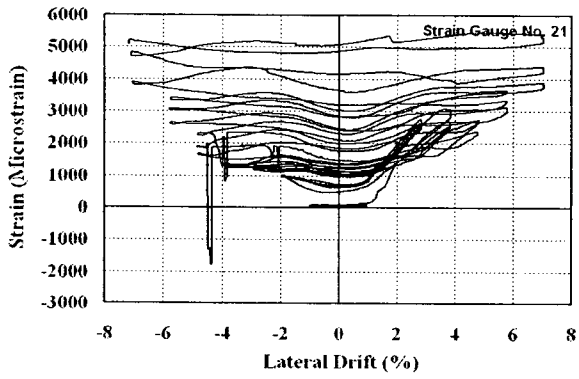

Figure A.6 (Cont'd): Tire Strains in Column TC-9, Measured on Treads

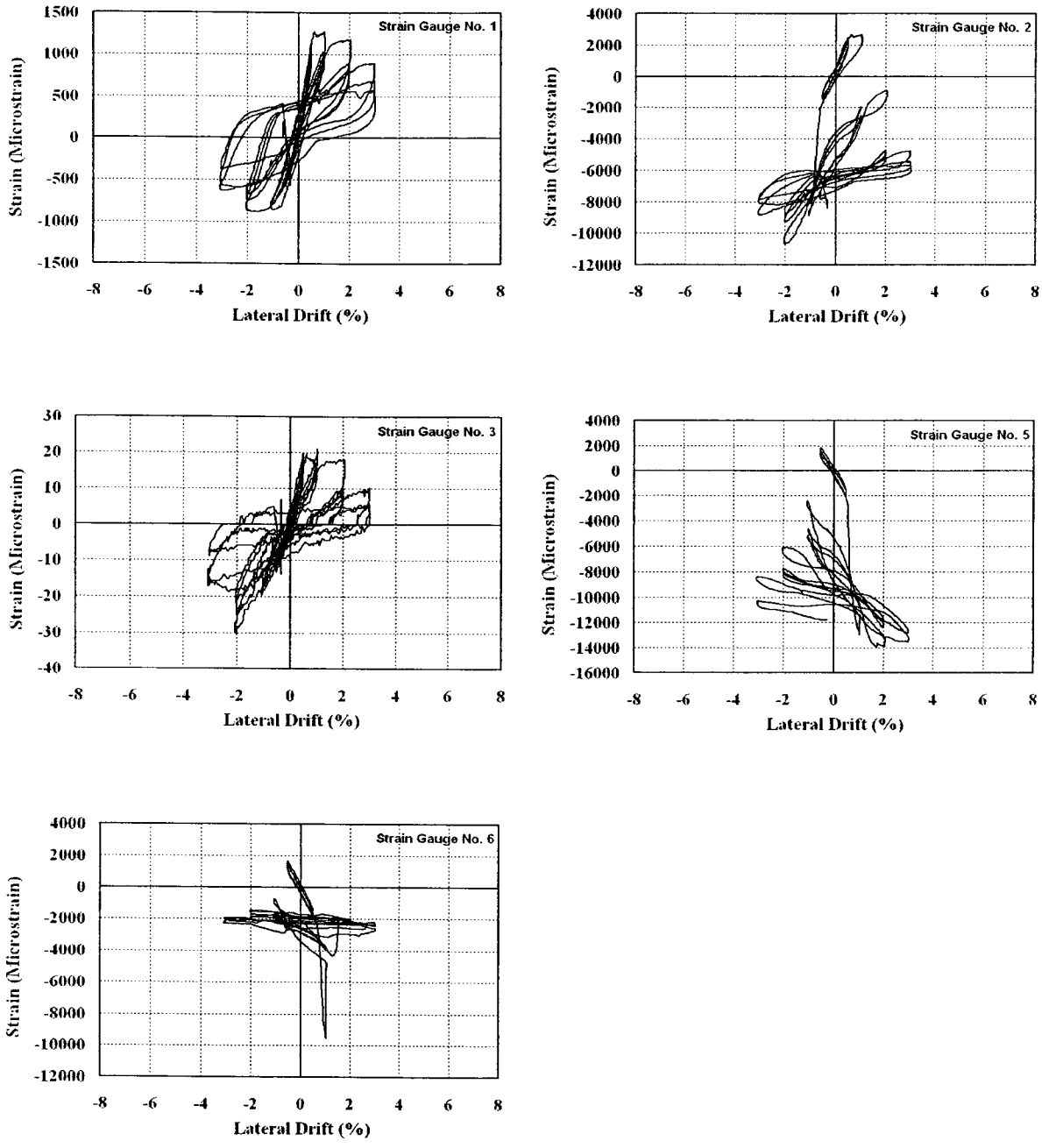

Figure A.7: Strain Gauge Data for Longitudinal Reinforcement in Column TC-10

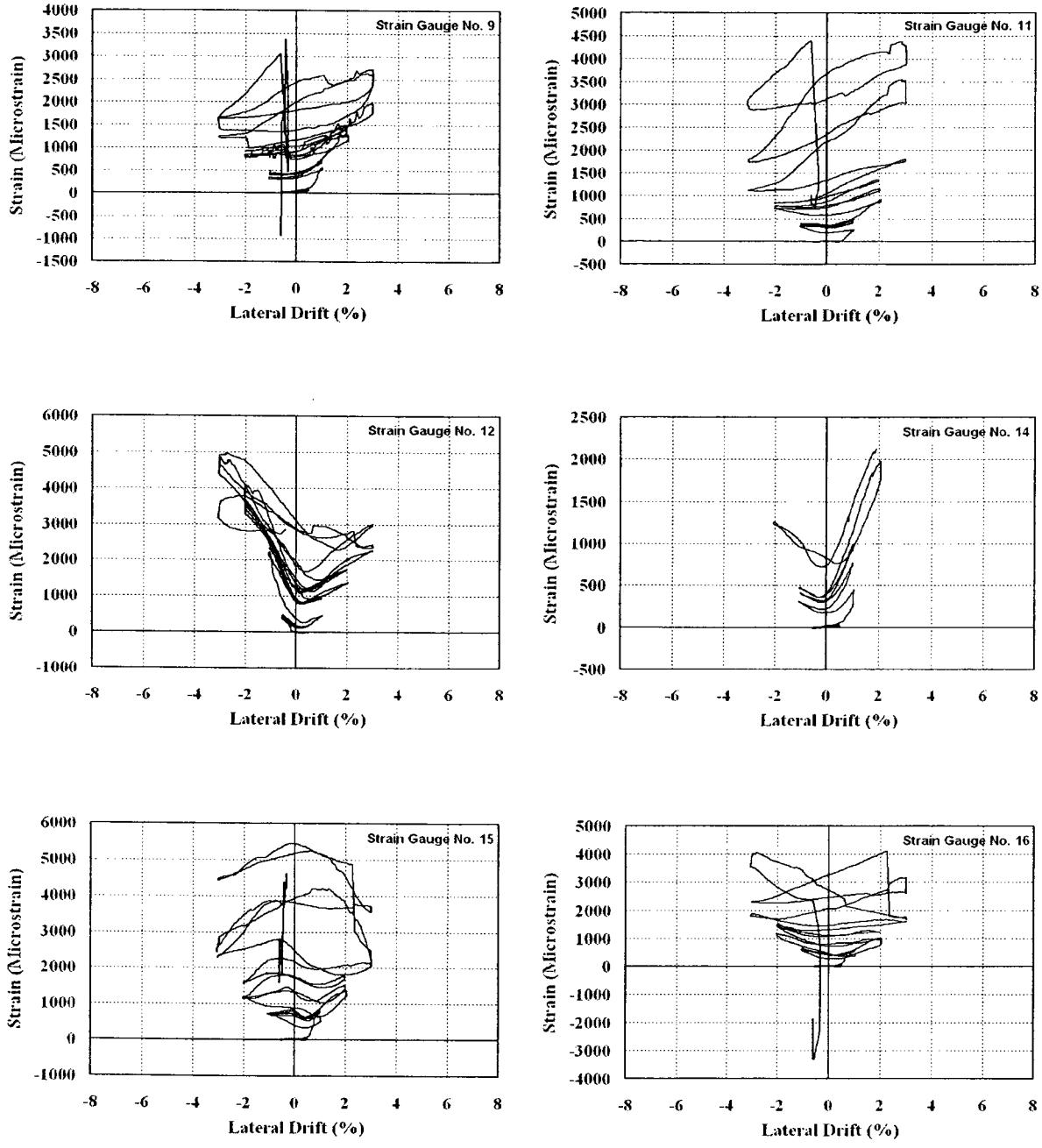

Figure A.8: Tire Strains in Column TC-10, Measured on Treads

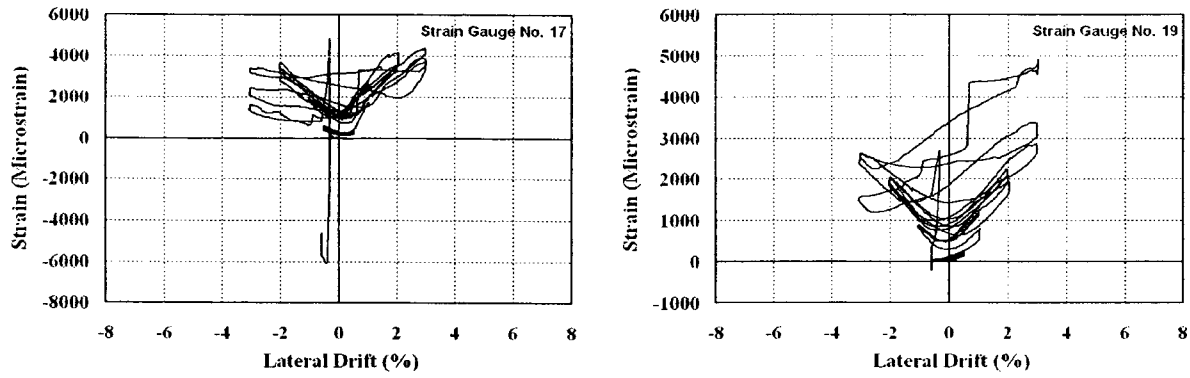

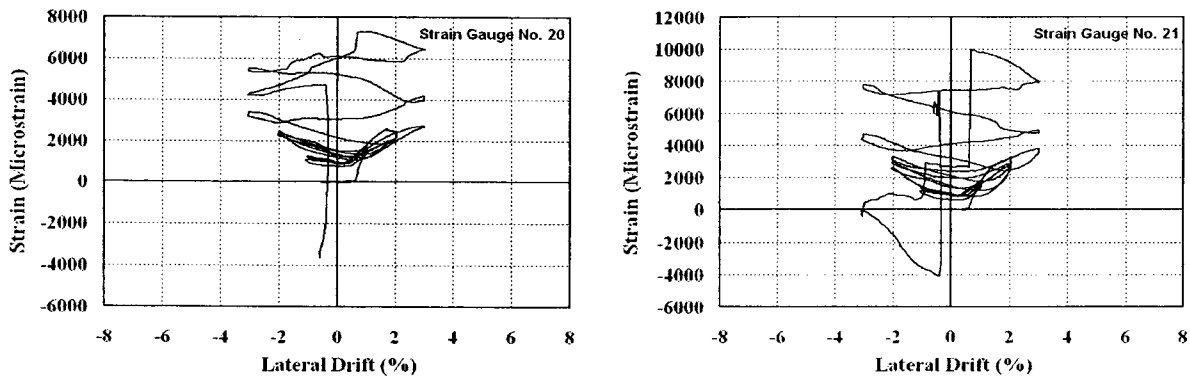

Figure A.8 (Cont'd): Tire Strains in Column TC-10, Measured on Treads

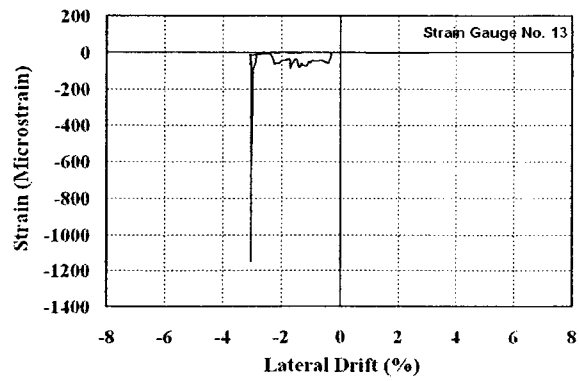

Figure A.8 (Cont'd): Tire Strains in Column TC-10, Measured on Rims

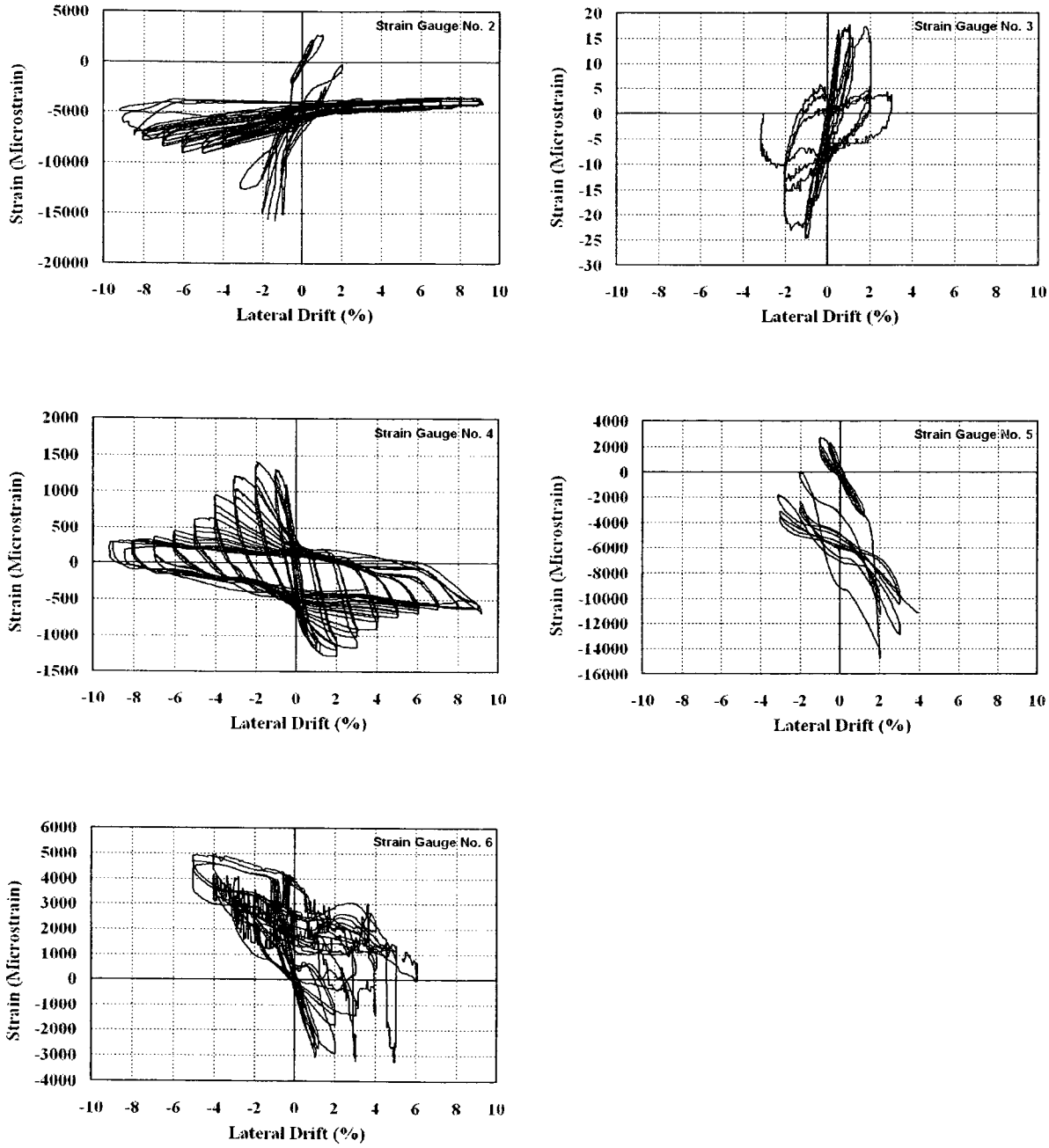

Figure A.9: Strain Gauge Data for Longitudinal Reinforcement in Column TC-11

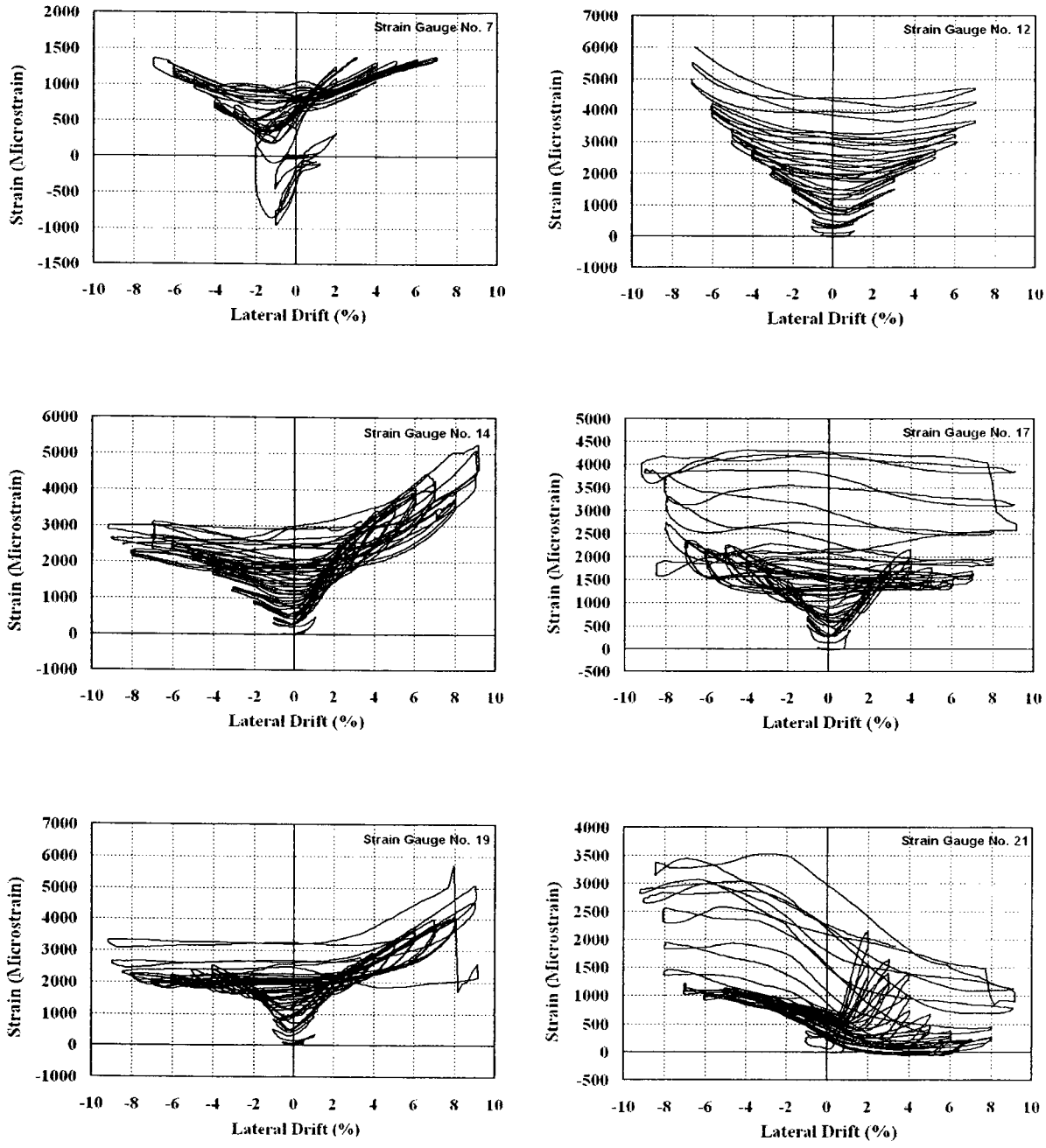

Figure A.10: Tire Strains in Column TC-11, Measured on Treads

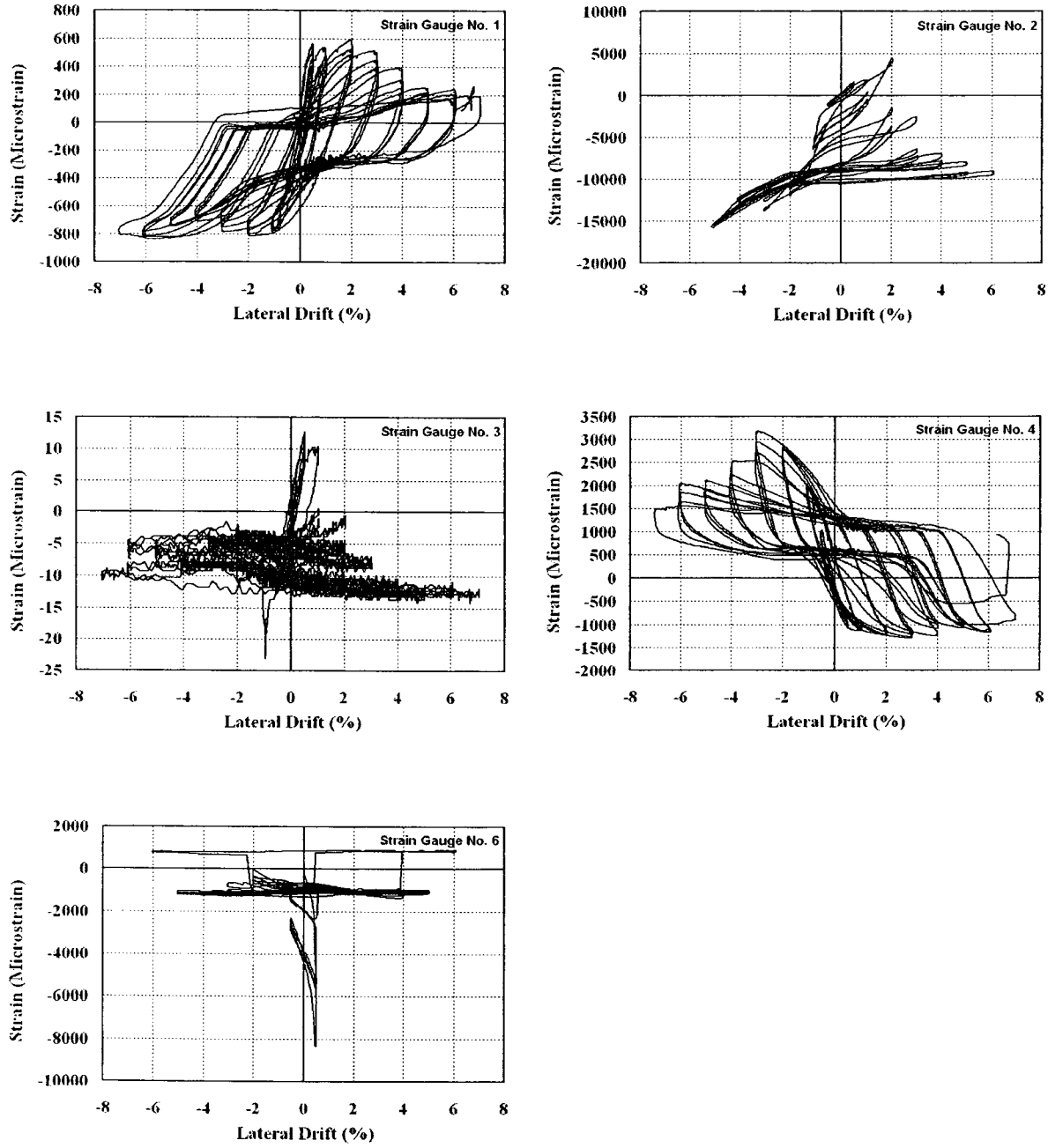

Figure A.11: Strain Gauge Data for Longitudinal Reinforcement in Column TC-12

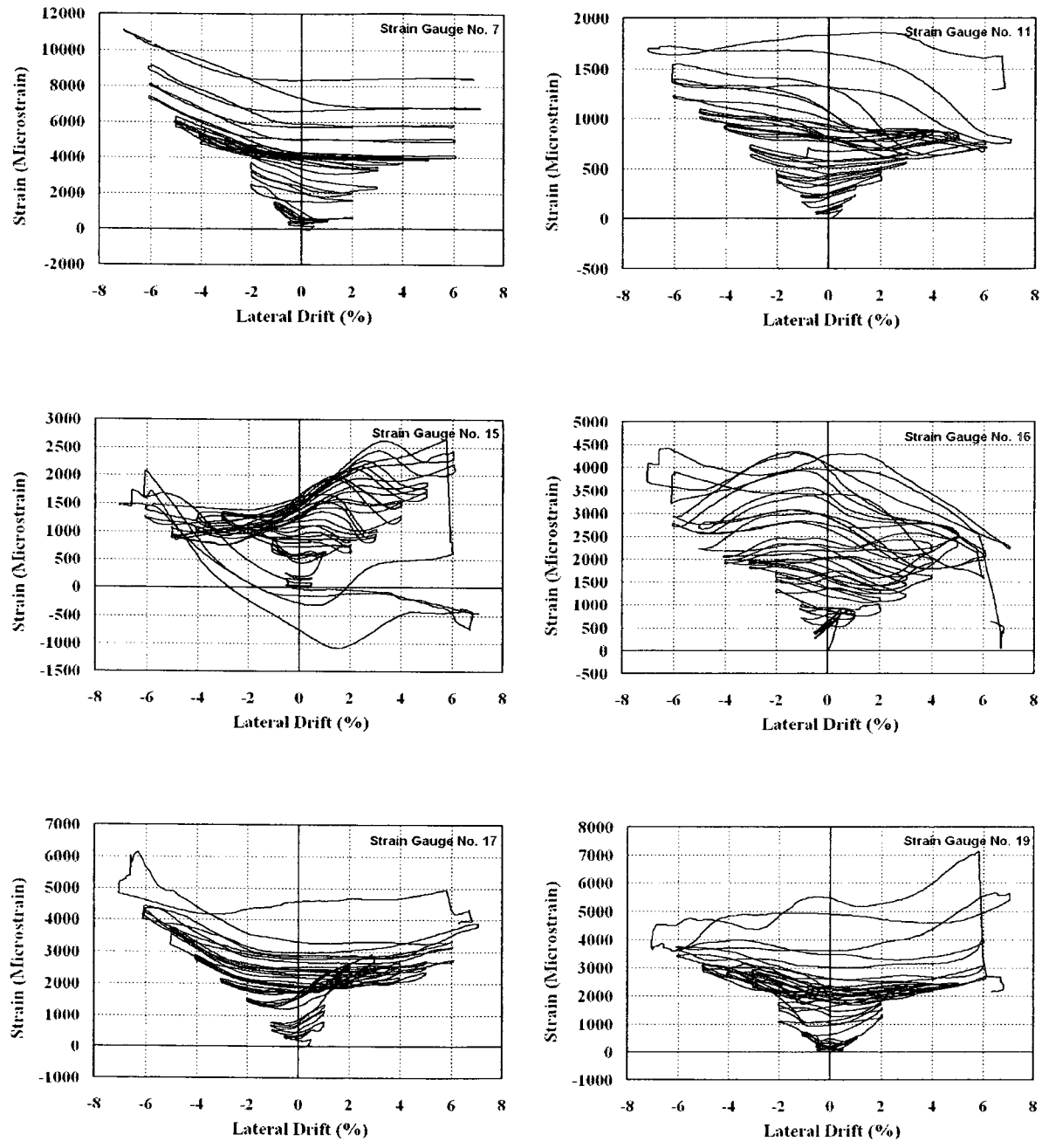

Figure A.12: Tire Strains in Column TC-12, Measured on Treads

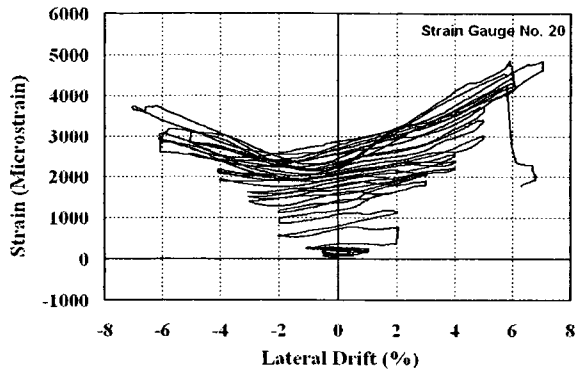

Figure A.12 (Cont'd): Tire Strains in Column TC-12, Measured on Treads